The Past, Present and Future of the El Niño/Southern Oscillation

by

Samantha Stevenson

B.A., Western Connecticut State University, 2000

M.A., Wesleyan University, 2003

M.S., University of Colorado, 2009

A thesis submitted to the Faculty of the Graduate School of the University of Colorado in partial fulfillment of the requirement for the degree of Doctor of Philosophy

Department of Atmospheric & Oceanic Sciences

2011

Thesis Advisor: Baylor Fox-Kemper

Committee: Antonietta Capotondi, Weiqing Han, Markus Jochum, Balaji Rajagopalan

This thesis entitled:

The Past, Present and Future of the El Niño/Southern Oscillation

written by Samantha Stevenson

has been approved for the Department of Atmospheric & Oceanic Sciences

Baylor Fox-Kemper

Balaji Rajagopalan

The final copy of this thesis has been examined by the signatories, and we find that both the content and the form meet acceptable presentation standards of scholarly work in the above mentioned discipline.

Abstract

Stevenson, Samantha (PhD, Atmospheric & Oceanic Sciences)
The Past, Present and Future of the El Niño/Southern Oscillation
Thesis directed by Assistant Professor Baylor Fox-Kemper

Predicting how the strength and character of the El Niño/Southern Oscillation (ENSO) will change as the climate warms is crucial for a number of societal impacts, yet there are fundamental limitations to our understanding of ENSO dynamics. The major obstacles are related to sampling length, physical adjustments to climate changes, errors in model physics and uncertainties in forcing projections. This dissertation uses these issues to assess what we currently can and cannot say about future ENSO variability.

The temporal extent of modern observations is too short to properly measure natural ENSO variations: averaging together at least 200 years is required to obtain robust ENSO statistics in a stable climate. Using paleoclimate 'proxies' to extend the observational record is another option, but is complicated by the uncertainties involved in translating between model and proxy signals. Coral oxygen isotopes, the most commonly used ENSO proxy, are shown to be governed by nonlinear dynamics: a more accurate 'forward model' for coral $\delta^{18}O$ is needed. Even using such a model, at least 4-5 contemporaneous records will be required for accurate ENSO amplitude estimation.

Simulations using several IPCC-class general circulation models (GCMs) are used to demonstrate that the adjustment to climate change itself takes place over decadal timescales, meaning that ENSO response is not statistically significant during the 21st century. This implies that current model intercomparison experiments are insufficient to measure the true range of ENSO climate sensitivity. However, significant changes to atmospheric teleconnections may take place within the 21st century: the NCAR Community Climate System Model version 4 (CCSM4), for example, predicts harsher winters in the Southwestern US during La Niña and weaker Australian teleconnections during both El Niño and La Niña.

Stabilized CCSM3.5 simulations are then performed, which show that once the climate has equilibrated, the ENSO response to a CO_2 increase eventually does become significant. However, the details of that response are sensitive to small changes in model physics: the ENSO climate sensitivity in the CCSM3.5 and CCSM4 oppose one another, and the mechanisms for the difference are as yet unclear. Seasonal forcing, high-frequency wind stress variability, or other processes may be responsible, but a complete diagnosis requires longer CCSM4 simulations than are currently available.

Finally, an additional complication is discussed: future ENSO projections all rely on the standardized emissions scenarios from the IPCC. Projections of future emissions reductions may be overly optimistic, perhaps requiring attention to a wider range of CO_2 changes for accurate ENSO impacts studies.

Acknowledgments

I was supported by the CIRES graduate student fellowship and Innovative Research Program, as well as NASA's Earth and Space Science Fellowship, while pursuing this dissertation work.

I could not have done this without the guidance of my advisor, Baylor Fox-Kemper, who has been a tremendous help to me throughout my entire time at CU. Thank you for always being there to talk to me and helping me pursue my passions, even when they were scattered and vague. Thanks also to Markus Jochum for helping me with my model runs, for being an advocate for me at NCAR, and for many helpful discussions. Thanks go to Balaji Rajagopalan and Roger Pielke, Jr. for all of their help with projects that broadened the scope of my dissertation work, and to Antonietta Capotondi and Weiqing Han for always being willing to discuss research.

I also want to thank my amazing husband Steve for being so supportive and helping out with the rest of our life while I was busy working. You were always there to tell me not to worry so much, and I hope someday I will figure out how to listen.

Contents

List of Tables

List of Figures

Foreword

I would like to start this dissertation with some advice that I got from Brian Toon when I first began the PhD program at CU. He told our incoming class about the process of research, and pointed out that there is one key ability without which it is nearly impossible to successfully complete a research project. That is: the ability to state the purpose of your project in a single sentence... or ideally, as a single question. So I have included the underlying questions from each of the component projects that make up my dissertation as the titles of the corresponding chapters. But fundamentally, all of the work that has gone into all of the projects has been aimed at answering one single question:

How will anthropogenic climate change affect tropical climate variability?

And over the course of my PhD, I have realized that before answering that question, one has to think about an even more fundamental one that all too often goes both unasked and unanswered:

How well do we know what we think we know about the climate system?

For my PhD work, I have been focusing on tropical ocean dynamics and specifically the El Niño/Southern Oscillation, but I would like to continue to expand my research horizons over the course of my career. What I would really most like to know is:

How will anthropogenic climate change affect the world we live in?

I hope that this dissertation successfully explains what I have done so far and motivates what I would like to do in the future.

Chapter 1

Introduction

Contents

1.1 Historical Background

The phenomenon now known as the El Niño/Southern Oscillation (ENSO) has a long and interesting history. It was first noticed by fishermen in northern Peru, who named the abnormally warm current which arrived during the winter of certain years after 'El Niño', or the Christ child. During an El Niño, unusually warm waters led to enhanced precipitation along the South American coast, which affects both agriculture and the health of local ecosystems. Study of the El Niño phenomenon in Peru began in earnest during the late 1800s, when the Peruvian currents were documented and related to changes in local rainfall [Carranza 1891, Carillo 1892].

ENSO was originally named for an oceanic phenomenon, but we now know that it could not exist without communication with the atmosphere. The Southern Oscillation is the atmospheric component of ENSO, and is often measured using the difference in sea level pressure between Tahiti

and Darwin (northern Australia). Discovery of the Southern Oscillation took place around the same time as work on El Niño: the first identification of the Southern Oscillation was made by [Hildebrandsson 1897], who measured pressure differences between Sydney and Buenos Aires.

Sir Gilbert Walker was the first to provide a systematic analysis of sea level pressure variability across the Pacific: spatial correlations were mapped out for the first time in [Walker 1924]. The seminal papers by [Walker 1932, Walker 1937] built on the lag-correlations identified in [Walker 1924], in an effort to identify coherent patterns which would enable long-term predictability. This turned out to be much more difficult than anticipated, but the indices identified by Walker for the North Atlantic and North Pacific Oscillations are still in widespread use today.

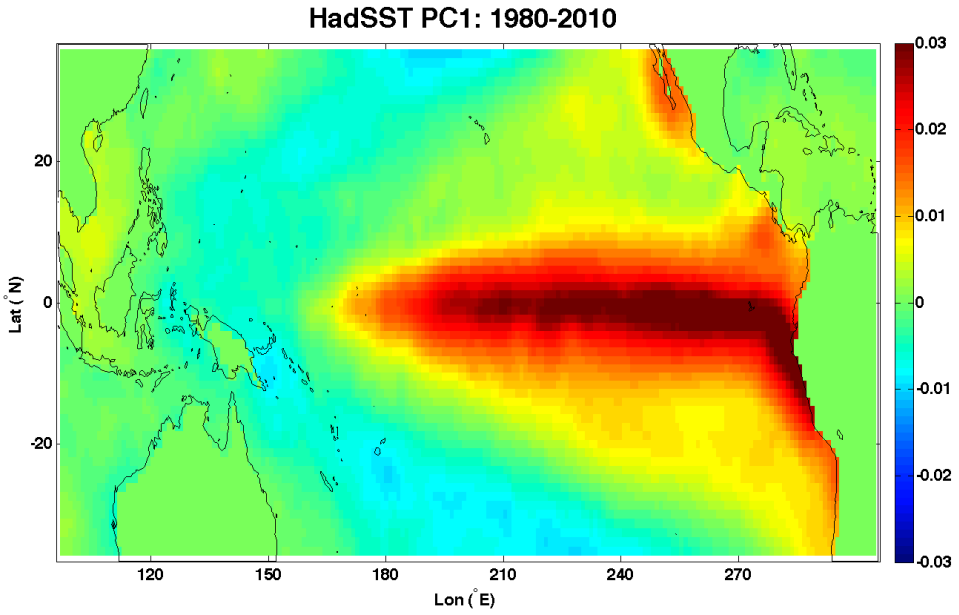

Figure 1.1: First principal component of SST variability between 1980-2010, generated using the HadSST2 dataset.

We now know that the Southern Oscillation's 'seesaw' in sea level pressure between the eastern and western Pacific is driven by large-scale changes in the tropical atmospheric circulation. But it was not until 1969 that a consistent physical explanation for this behavior was put forth, by

Jacob Bjerknes. Previous to this, a connection between SST and Pacific rainfall had been suggested [Leighly 1933] but did not receive much attention: the Bjerknes paper provided the physical insight necessary to tie everything together. Bjerknes proposed that anomalously warm sea surface temperatures (SSTs) in the central and eastern Pacific were a consequence of anomalously weak equatorial trade winds, which led to anomalously cold SSTs in the western Pacific. The weaker western Pacific convection then requires that the zonal flow aloft must weaken, as a consequence of continuity. Bjerknes named the overturning pathway the 'Walker Circulation' after Sir Gilbert (who had died roughly 10 years previously).

The trade wind-SST relation described above is often referred to as the 'Bjerknes feedback', which simply describes the tendency of an SST anomaly to lead to a wind stress anomaly which reinforces the initial disturbance. For example: an initial warm SST anomaly in the eastern Pacific weakens the Walker circulation [Gill 1980, Lindzen 1987] and is self-sustaining. Thus events can persist throughout the winter and into the following spring, as was the case for the strong El Niños observed during recent years [Rasmusson 1982]. The Bjerknes feedback, in other words, is what allows an El Niño event to grow.

The strong El Niño event of 1982-3 provided the impetus for establishing a moored observational network for monitoring ENSO. The size and persistence of the El Niño was not correctly predicted by any forecasting system at the time, nor was it even detected until months after the start of the event [McPhaden 1998]. The late detection was partly due to the neglect of real-time reports of extremely warm SST during the fall of 1982, which were ignored because the preconditioning thought to be essential for El Niño had not occurred. This included stronger-than-normal trade winds [Wyrtki 1975] and abnormal warming off the western coast of South America during boreal spring [Rasmusson 1982], neither of which were detected.

After the shock of the 1982-3 El Niño, the Tropical Ocean-Global Atmosphere (TOGA) program [WCRP 1995], already in the planning stages at the time, was given even higher priority by the scientific community. This program was designed to provide real-time, *in situ* observations of wind stresses, SST, and subsurface ocean conditions, and has proved to be one of the most successful

oceanographic observational campaigns ever conducted.

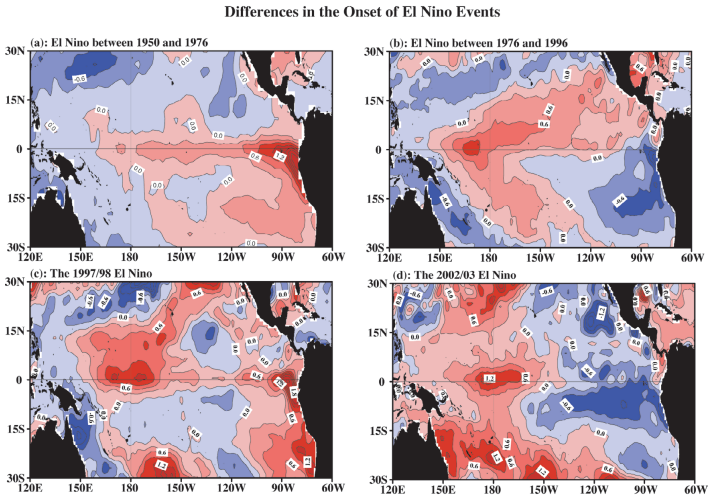

Figure 1.2: Plate 2 from [Wang 2004], showing variations in El Niño onset. a) Mean March-May anomaly during the El Niño years between 1950-1976; b) same as a) for 1976-1996; c) same as a) for the 1997-98 event; d) December 2001-February 2002 SST anomaly (onset of 2002-03 El Niño.)

Since the establishment of TOGA, the diversity of behavior among El Niño events has become clear: the same is true for La Niña, as the cold phase of the oscillation is now called. The overall 'shape' of ENSO is classically a horseshoe-like pattern in SST, with the strongest anomalies in the eastern equatorial Pacific. An example is shown in Figure 1.1, which depicts the first principal component of SST variability over the 1980-2010 period. The SST anomaly pattern for individual events, however, can differ markedly: for some El Niños, the anomalies form first in the eastern Pacific, and for others the warming begins in the central Pacific (Figure 1.2). The wind patterns associated with these events also change dramatically depending on the location and strength of the SST anomalies, which has important implications for the atmospheric impacts of individual events (see Section 1.3).

1.2 Overview of ENSO Dynamics

The major dynamical 'ingredients' for ENSO are:

1. A positive feedback between the trade winds and sea surface temperature

2. A negative feedback delayed in time from a developing SST anomaly

The first allows an El Niño/La Niña to grow; the second allows the oscillation to switch phases. As discussed previously, the positive SST/wind stress feedback is that of [Bjerknes 1969]: an increase in the Walker circulation increases trade wind strength and therefore creates a larger zonal SST gradient which further increases the Walker circulation. The discovery of a negative feedback to halt the developed event, however, took substantially longer: in fact, multiple negative feedbacks likely operate simultaneously.

Four major feedbacks have been proposed as part of theoretical 'oscillator' models for ENSO [Wang 2004]. Western boundary wave reflection is used in the delayed oscillator mechanism of [Battisti 1989, Suarez 1988]. Discharge of heat from the tropics is cited in the [Jin 1997] recharge oscillator. The western Pacific oscillator of [Weisberg 1997, Wang 1999] uses a wind-forced Kelvin wave initiated in the western Pacific warm pool. Finally, anomalous zonal advection was proposed as the negative feedback mechanism in [Picaut 1997]'s advective/reflective oscillator. In reality, these mechanisms are likely to be dynamically linked and are thus not truly independent [Picaut 2002], which was one reason for the development of the so-called 'unified oscillator' treatment by [Wang 2001]. The unified oscillator allows all four negative feedbacks to operate simultaneously, so that all of them contribute to the damping of an El Niño/La Niña event.

All of the oscillator models for ENSO have one thing in common: they assume that the dominant mode of variability is self-sustaining. For some model parameter values, a regular oscillation occurs at a single period: for others, chaotic behavior is observed [Wang 1996, Neelin 1993, Wang 2001]. In either case, the oscillation persists once it has begun. An alternative but equally valid approach is to view ENSO as a stochastic perturbation about a stable mean state. In the stochastic framework, events are triggered individually, and the maintenance of an oscillation is not guaranteed. This is the so-called 'series of events' framing [Kessler 2002].

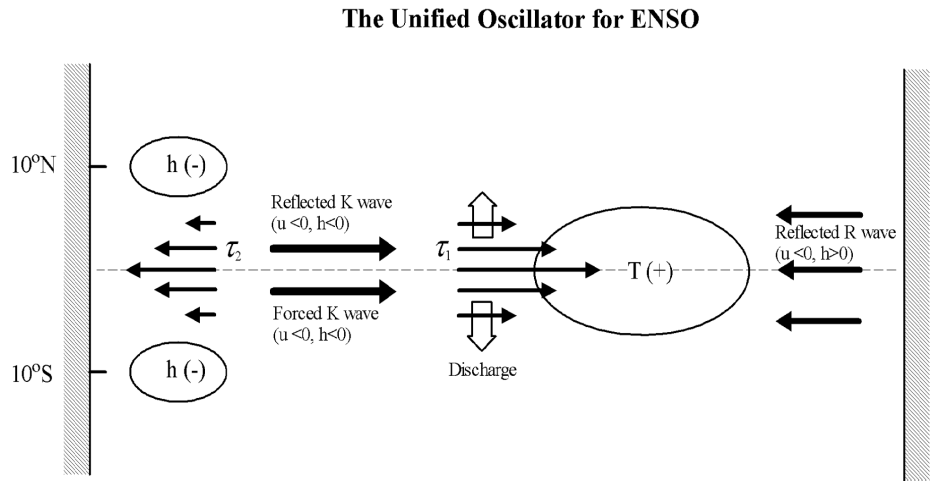

Figure 1.3: Figure 1 from [Wang 2004], illustrating the negative feedbacks which make up the unified oscillator. Pictured here are wave reflections at the eastern boundary [Picaut 1997] and the western boundary [Suarez 1988, Battisti 1989], leading to Rossby and Kelvin waves respectively; meridional heat transport due to anomalous Sverdrup transport [Jin 1997]; and wind-forced Kelvin waves in the western Pacific [Weisberg 1997, Wang 1999].

High-frequency atmospheric noise is a leading candidate for stochastic ENSO forcing. The 'SST mode' of [Neelin 1991] is one such mechanism, where events are generated by interaction between SST and the atmospheric boundary layer. Similar dynamics were described using observed SST anomalies [Penland 1995]: the 'optimal growth mode' for anomalies was diagnosed, in which atmospheric forcing creates an El Niño event by perturbing the SST gradient. The sources of atmospheric noise may be varied: the Madden-Julian Oscillation [Madden 1994], westerly wind bursts [Gebbie 2007, Tziperman 1997], or even the cumulative effect of a variety of perturbations [Kleeman 2006, Kleeman 2008] have all been proposed.

In reality it is likely that *both* stochastic 'SST' and subsurface 'oscillator' modes occur [Jin 1993, Neelin 1993]. Indeed, observations of ENSO events over the past few decades [McPhaden 2009, Wang 2002] have identified both types of dynamics through an investigation of the propagation direction of SST anomalies: thermocline-driven anomalies tend to propagate eastward as equatorial Kelvin waves [Fedorov 2001], while SST-driven anomalies propagate westward as a consequence of

the thermally induced wind stresses [Gill 1980].

The question of inter-event differences leads naturally to a consideration of decadal variability. This gained popularity as a result of the changes observed in 1976-7, now widely cited as a 'regime shift' [Ebbesmeyer 1991, Graham 1994, Hare 2000] where the behavior of ENSO changed significantly. Additional regime shifts have since been proposed at earlier times [Kondo 1988, Mantua 1997, Zhang 1997]. The extratropics are now invoked to explain regime shifts, and the 'North Pacific Oscillation' (NPO; [Gershunov 1998]) or 'Pacific Decadal Oscillation' (PDO; [Mantua 1997]) has since become widely accepted as a possible mechanism.

Reviews of mechanisms for extratropical ENSO influences are numerous [Latif 1998, Miller 2000, Minobe 2000, Mantua 2002, Wang 2004]. In the ocean, subduction of anomalously warm/cold water has been hypothesized to affect the equator [Deser 1996, Zhang 1998] through modulations of the subtropical cell [Gu 1997, McCreary 1994]. However, disagreement remains as to the importance of STCs to decadal variability [Schneider 1999b, Izumo 2002], since models indicate that tropical decadal variability is not controlled by transport from the subtropics [Schneider 1999a]. The *amount* of water transported into the thermocline may be more important [Kleeman 1999].

Finally, the role of the seasonal cycle should be discussed. The 'phase-locking' of ENSO to the boreal winter months has been well documented in both observations [Rasmusson 1982] and models [Xie 1995, Guilyardi 2006], and has been proposed as a source of ENSO's irregularity. Previous modeling studies [Chang 1995, Tziperman 1997, Jin 1994] showed that an interaction between the seasonal cycle and interannual variability could lead to a transition between periodic and chaotic regimes. The seasonal cycle has also been linked to El Niño initiation and termination through seasonal shifts in the equatorial trade winds [Lengaigne 2006] and corresponding effects on atmosphere/ocean feedbacks. Seasonal changes in the extratropical SST may also lead to the initiation of an El Niño/La Niña [Alexander 2002, Alexander 2010]: this is discussed in more detail in ([Stevenson 2011a]; Appendix 4).

1.3 Atmospheric Teleconnections

The societal impacts of ENSO are felt through indirectly forced variations in the atmosphere: outside the tropical Pacific, these impacts are referred to as teleconnections. The basic idea behind atmospheric teleconnections is that a tropical SST anomaly leads to changes in the tropical circulation, which in turn affects circulation in the extratropics [Lau 1997, Trenberth 1998, Hoerling 2002]. Anomalies in SLP and precipitation associated with El Niño in the extratropics have been summarized by [Ropelewski 1987] and are depicted graphically in Figure 1.4.

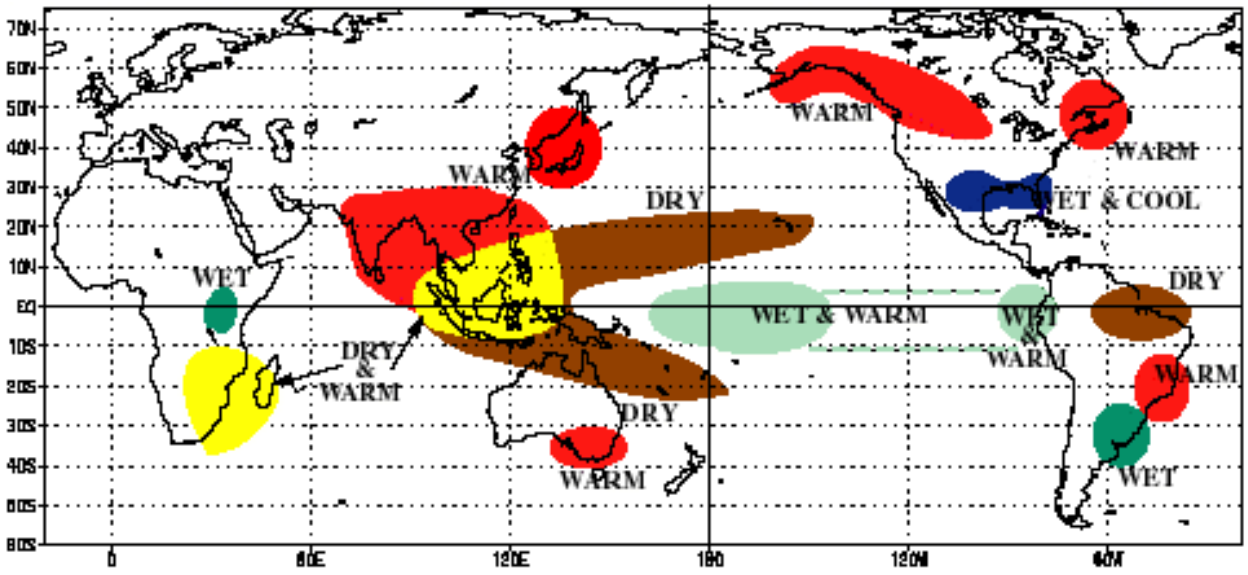

Figure 1.4: Wintertime teleconnections with El Niño (courtesy of the NOAA Climate Prediction Center). La Niña teleconnections generally are the reverse of El Niño, although the pattern is not perfectly symmetric.

The tropospheric response to ENSO has both a zonally symmetric and an asymmetric component. Zonal-mean surface air temperatures are warmer during the El Niño and colder during the La Niña phases of the oscillation [DeWeaver 2002]. For example, during El Niño when surface air temperatures are warmer, the upper troposphere is heated in the west Pacific due to the latent heat released from the additional convection; in the east Pacific, adiabatic heating from

increased subsidence takes place [Trenberth 1998, Horel 1981]. The zonal-mean surface air temperature anomalies in the subtropics are of opposite sign to the tropical anomalies, which combined with the corresponding geopotential height anomalies leads to an induced westerly anomaly aloft between 20-30°N [Clarke 2008].

Zonally asymmetric anomalies are created by extratropical Rossby wave activity [Trenberth 1998, Holton 2004, Horel 1981]. The anomalous convection associated with ENSO creates anomalous upper tropospheric divergence; the net effect is an alternating series of cyclones and anti-cyclones carrying energy to the extratropics (Figure 1.5). The wave train response has an impact on the position of the storm track; typically the track shifts southward during El Niño, which in turn influences precipitation over the United States. This effect has since been replicated with dynamical models [Branstator 1983, Hoskins 1981, Webster 1981].

Here I focus on teleconnections with three regions, which are important for later analyses: the North Pacific/western United States, Australasia, and the Southern Ocean.

North Pacific/United States. In the North Pacific, anomalies in SLP associated with ENSO are typically in the form of an unusually strong Aleutian Low during El Niño and a blocking high during La Niña [Hoerling 2002, Deser 1995]. The teleconnection (often referred to as the Pacific-North American, or PNA) is strongest during boreal winter when the event is at peak intensity. The primary mechanism for the PNA is the transport of energy between the tropical and extratropical eastern Pacific; this takes place through the action of Rossby waves. [Hoskins 1981] showed that the dispersion of energy from a barotropic quasi-stationary Rossby wave source should be primarily poleward and eastward of the source; in this case, the storm track. Since then, numerous other factors have been identified which are important for the PNA. The vertical structure of tropical heating anomalies influences their meridional propagation [Ting 1993]; the longitudinal position of heating can also be important for the midlatitudes [Simmons 1982, Webster 1988, Hoskins 1991]. The midlatitude jets themselves can also control the propagation of anomalies created in the tropics, 'guiding' anomalies into the eastern Pacific [Karoly 1983, Hoskins 1993].

Typically, El Niño events are associated with increased rainfall in the Southwest United States

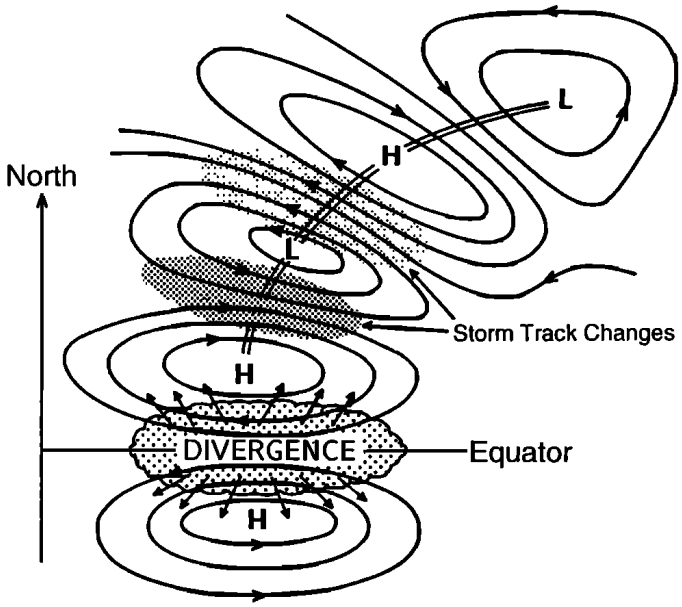

Figure 1.5: Reproduction of Figure 4 from [Trenberth 1998]. "Schematic view of the dominant changes in the upper troposphere, mainly in the northern hemisphere, in response to increases in SSTs, enhanced convection, and anomalous upper tropospheric divergence in the vicinity of the equator (scalloped region). Anomalous outflow into each hemisphere results in subtropical convergence and an anomalous anticyclone pair straddling the equator, as indicated by the streamlines. A wave train of alternating high and low geopotential and streamfunction anomalies results from the quasi-stationary Rossby wave response (linked by the double line). In turn, this typically produces a southward shift in the storm track associated with the subtropical jet stream, leading to enhanced storm track activity to the south (dark stipple) and diminished activity to the north (light stipple) of the first cyclonic center. Corresponding changes may occur in the southern hemisphere."

[Ropelewski 1996, Cayan 2010, Rasmusson 1982, Cayan 1992, Dettinger 2000, Gershunov 1998]. Teleconnections are more predictable over the Southwest (AZ/NM) than the Mountain West (CO/UT) states, due to the influence of the Rocky Mountain topography on the upper-level flow [Rasmusson 1982]. El Niño years generally see enhanced summer rainfall and larger snowpack in the northern Colorado River Basin, while La Niña winters can lead to enhanced snowpack in the southern Rockies. However, this influence is not perfectly symmetric between the El Niño and La Niña phases, and the effect on snowpack is dependent on the seasonal storage of snow from the previous year [Clark 2001]. This may have important implications for the future availability of water in the lower Colorado River Basin and associated reservoir storage levels as the climate warms [Rajagopalan 2009, McCabe 2007].

Australasia. Teleconnections with the Southern Hemisphere are generally weaker and more variable than their Northern Hemisphere counterparts [Trenberth 1998]. In Australia, La Niña is linked with extreme weather events like flooding and cyclone activity, while extreme droughts are often found during El Niño years [Nicholls 1996]. This is a consequence of the shifts in the Walker circulation and associated convection, with the eastward shift of the warm pool during El Niño bringing rains further from the Australian coast. El Niño-related droughts have led to increased interest in operational ENSO forecasting in the area [Power 1999, Kiem 2001, Zhang 1992, Simpson 1993], especially in the highly subscribed Murray Darling Basin [Smith 2010]. ENSO influences have also been observed on vegetation [Nicholls 1991, Holmgren 2006], as well as various types of animal life [Letnic 2005, Howden 2004, Holmgren 2001] and bushfire activity [Skidmore 1987, Lucas 2007].

The Walker cell's influence is strongest in tropical northern Australia. However in the extratropics, Rossby wave dynamics become important once again. The wave pattern equivalent to the PNA in the Southern Hemisphere is often referred to as the Pacific South American (PSA) pattern [Karoly 1989, Mo 1987], and is qualitatively similar to the PNA [Ghil 1991]. This pattern is believed to dominate due to the prevalence of upper-level westerlies near the equator which allow tropical divergence-induced heating to be carried by quasi-stationary Rossby waves [Cai 2011].

The Indian Ocean influences Australia as well. Rossby wave trains propagating eastward from

the Indian Ocean can impact Australian rainfall and temperature [Saji 2003] and are modulated by the Indian Ocean Dipole (IOD; [Ashok 2003, Risbey 2009]). The IOD connection implies a strong connection with ENSO activity, since the IOD is strongly correlated with ENSO [Saji 1999]. During the positive phase of the IOD, SSTs are cooler in the western Pacific, leading to suppressed convection over the Maritime Continent. The reverse is true during negative IOD periods, when convective activity is enhanced. Convective anomalies during the IOD function analogously to convection in the Pacific; a warm (cold) SST anomaly will lead to anomalous surface convergence (divergence) and to divergence (convergence) in the upper troposphere.

Thus far, less work has focused on the role of Indian Ocean diabatic heating anomalies in triggering teleconnected events than on the North American equivalent. However, recent work [Cai 2011] indicates that IOD-induced Rossby wave trains [Saji 2003] affect the baroclinic structure of the troposphere over the Maritime Continent via changes to the mean midlatitude westerlies. Orographic effects may influence the precise extent of these teleconnections [Hendon 2007], particularly in southeastern Australia. However, generally speaking a positive IOD can be associated with reduced rainfall across the southern part of the country due to the southward shift of the jet stream.

Southern Ocean. Finally, I briefly consider teleconnections with the high-latitude Southern Hemisphere, which are reviewed in [Turner 2004]. Once again, the communication between regions relies heavily on Rossby wave trains [Held 1989, Karoly 1989]: generally speaking, the southeastern Pacific experiences high (low) geopotential height anomalies during El Niño (La Niña). Figure 1.6 shows a schematic of Rossby wave trains propagating towards the Antarctic from the tropical Pacific; this structure can be generally understood as relating to the PSA through its interaction with the Antarctic Circumpolar Wave (ACW; [White 1996]). The PSA leads to subtropical SST anomalies in the South Pacific, which then propagate southwards and are eventually absorbed into the Antarctic Circumpolar Current (ACC; [Cai 2001]).

Sea ice cover near Antarctica is thought to be influenced by ENSO as well [Turner 2004], although the mechanisms of their interaction are complex. In the Ross Sea (south of New Zealand), wind forcing plays an important role in controlling sea ice extent. In the South Pacific, the PSA

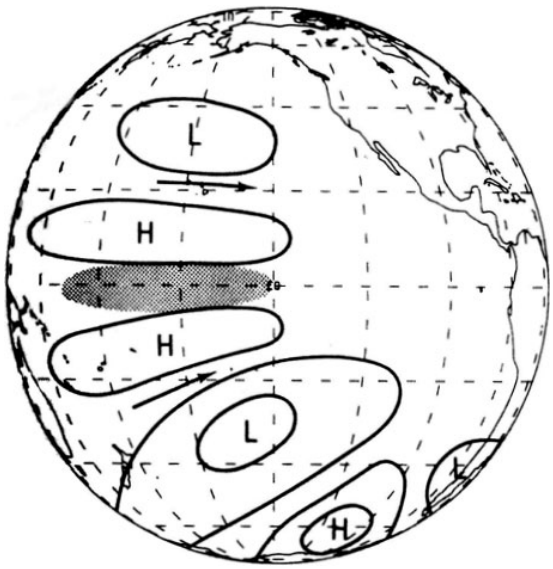

Figure 1.6: Reproduction of Figure 2 from [Turner 2004]. "Schematic illustration of the pattern of upper tropospheric height anomalies over the Pacific Ocean during the early stage of an ENSO event in the Southern Hemisphere winter (June-August). The stippling shows the region of enhanced convection over the central equatorial Pacific and the arrows indicate the westerly wind anomalies in the jet streams. From [Karoly 1989]"

teleconnection leads to anomalous southerly flow during El Niño, which leads to colder surface air temperatures; however, the pre-existing ice extent is also important in determining the magnitude of the ENSO influence [Weatherly 1991, Harangozo 2000].

Correlations between sea ice and tropical SST indicate that there is a quasi-periodic sea ice signal which may have a resonant relationship with NINO4 SST [Xie 1994a]. Later studies have since shown a link between surface air temperature and sea ice extent in the Amundsen-Bellingshausen Sea ($\approx 60°$S, $120 - 130°$E) with a lag time of 6 months [Yuan 2000, I. 1995]. The teleconnection patterns observed in the CCSM4 20th/21st century simulations seem to be consistent with these results, and will be documented in Chapter 4.

1.4 Modeling ENSO

The simple oscillator models of Section 1.2 do not capture stochastic forcing or extratropical teleconnections: fully coupled atmosphere-ocean models are required to correctly represent ENSO. The first such model (the 'Zebiak-Cane' model) was developed by [Zebiak 1987], which was able to reproduce the overall spatial structure, amplitude, and period of the oscillation. The Zebiak-Cane model is still often used for long-term ENSO studies due to its inexpensive computational setup: but it represents the tropics only, excluding potentially important extratropical processes. This model also relies on a prescribed annual cycle, which is not an accurate assumption since interaction between the seasonal cycle and ENSO can be quite important [Lengaigne 2006, Tziperman 1997, Neelin 2000, An 2001].

Representing the full spectrum of coupled atmosphere-ocean physics requires the use of a general circulation model (GCM), but ENSO representation in GCMs has historically been fairly poor. Previous to the Fourth Assessment Report of the intergovernmental Panel on Climate Change (IPCC), the majority of GCMs were not able to accurately reproduce ENSO-like oscillations [Meehl 1989, Sperber 1987, Meehl 1990], though some aspects of variability were captured. [Neelin 1992] summarized the state of the art in modeling ENSO at the time, including 'simple' models with a reduced set of atmospheric physics, atmospheric GCMs, and fully coupled GCMs.

There was a huge spread in the representation of tropical variability in the models: some showed SST anomalies propagating across the Pacific, while in others the anomalies developed in a single location. Some models exhibited very weak tropical SST variability, sometimes so weak that variability could not be classified. The differences between models could not be fully explained by those authors, but they concluded that model resolution and variations in climatological mean state were likely important.

Large improvements in model ENSO have been made since the 1990s. [AchutaRao 2002] reviewed model performance for the Coupled Model Intercomparison Project (CMIP2), and found that performance was substantially better, but that the models still had major problems. At this time, flux correction was still a common practice in GCM studies: top-of-atmosphere radiative fluxes were specified to prevent the model mean state from rapidly falling out of equilibrium. Roughly half the CMIP2 models employed flux correction, which improved the mean state biases but generally did not improve ENSO behavior. The majority of models also showed an overly rapid and regular ENSO. Some of these errors were attributed to poor representation of wind stress field [Davey 2002], which were proposed to lead to problems in SST. Also generally speaking, the CMIP2 models were unable to place ENSO-related variability in the correct location: variations were displaced to the west [Latif 2001].

The next generation of coupled GCMs (the CMIP3 models) shows improvement [AchutaRao 2006, Guilyardi 2009b, Meehl 2007a]. The CMIP3 models avoid flux correction for the most part, and are generally better at reproducing the overall ENSO frequency. The ENSO 'center of action' also generally moves eastward relative to the CMIP2 models, in better agreement with observations. However, there is a large scatter in the ENSO amplitude reported by the CMIP3 models, with many models showing much stronger or weaker variability than observations [Guilyardi 2009b]. The same is true of the mean state in the tropics: the equatorial wind stress is too strong, and tropical wind stress contained too close to the equator [Capotondi 2006]. The cold tongue also extends too far west and shows colder-than-observed SSTs [Reichler 2008].

The coarser-resolution CMIP3 models under-represent the strength of upwelling in coastal re-

gions, leading to a warm SST bias along the equator, as well as the coasts of Africa and North and South America. [Gent 2010] showed that increasing model resolution from 2° to 0.5° greatly reduced these biases, by allowing orographic effects to more strongly influence surface winds near the coasts. However, most models were run at 1-2° resolution, so these biases remain an issue.

The CMIP3 models also retain the 'double ITCZ' problem of previous model generations. The SPCZ extends too far east, with a precipitation excess over the majority of the tropics and a deficit along the equator. The mechanisms for the double ITCZ bias were investigated in the CMIP3 models by [Lin 2007], who found that atmospheric feedbacks were the dominant factor. Some combination of an overly strong Bjerknes feedback, an overly sensitive dependence of atmospheric humidity on SST (surface-latent heat flux feedback; [Wallace 1992]), and an overly weak dependence of cloud amount on precipitation (SST-surface shortwave heat flux feedback; [Ramanathan 1991]) was responsible. The biases toward strong equatorial trade winds and insufficient SST-stratus feedback also contribute.

The current generation of GCMs, developed for CMIP5, shows the best ENSO representation to date. For example, in the CCSM4 [Gent 2011], improvements in model resolution have allowed better representation of atmospheric convective processes [Neale 2008, Neale 2011b], which leads to improvements in teleconnections between ENSO and the extratropics [Deser 2011] as well as lengthening the ENSO period to a more realistic value [Jochum 2010, Neale 2011a]. As of this writing, the CMIP5 simulations have just been completed, and no comprehensive review of their performance is yet available. However, expectations are that CMIP5 should prove to be a significant advancement over CMIP3.

All ENSO model evaluations rest on comparing the model output with observations, but the complex nature of the oscillation makes it unclear which metric is the best to use. Is it more important to correctly capture the mean structure of tropical SST, or of the wind stress? What about the subsurface ocean? This is an ongoing debate in the community. Recent work by the CLIVAR Pacific panel addresses the issue of ENSO metrics; to compile the most accurate assessment of ENSO performance, a variety of observations are required. ENSO is typically defined using one

or more SST 'indices', being box-averages over a given region (*i.e.* NINO3, 5°S-5°N, 190-240°E); but this neglects measures of atmospheric variability. The western Pacific precipitation, mean zonal wind stress, surface heat fluxes, and SST annual cycle are all commonly used to evaluate model errors [Guilyardi 2009b].

A more comprehensive analysis of climate model metrics was performed by [Gleckler 2008], who compared the last 20 years of the CMIP3 20th century simulations to observational data from a variety of sources. Those authors found that no one model was systematically better than all others in every variable, and indeed the multi-model mean outperformed the individual models in most quantities examined. They also found little correlation between the accurate representation of the mean climate and of interannual variability: getting the mean state right is not enough to guarantee a good ENSO.

There is one final impediment to validating model ENSO: the impact of natural variability within the climate system. The observational record length is extremely short, especially for some atmospheric variables like heat fluxes and precipitation where accurate observations date only from the satellite era (*i.e.* CMAP; [Xie 1997]). Since numerical models become widely used, they have been put to work in constructing reanalyses to fill in the gaps between sparse measurement in a dynamically consistent way: the two most commonly used reanalysis products are the ERA40 [Uppala 2005] and the NCEP/NCAR [Kalnay 1996]. These are improvements in many ways over the instrumental data alone, but do suffer from some limitations, particularly when reconstructing earlier time periods.

Even if it were possible to create a completely accurate observational record extending back an arbitrary length of time, one would still need to know how long that record actually *needed* to be. This will be dependent on the application, of course: but for ENSO, we know that modulations occur even within the records we do have, suggesting that the available observations may not be long enough. Systematic investigations of ENSO convergence in GCMs are few: [Wittenberg 2009] showed that timescales of centuries are required, using the GFDL CM2.1. I have since been able to quantify the convergence rate more precisely, and find that 250 years typically provides sufficient

averaging time ([Stevenson 2010]; Appendix 2). This is described in Chapter 3.

1.5 Using Paleoclimate Information

To obtain measurements with baselines longer than a few decades, we must turn to paleoclimatic indicators. When combined with modern observations, proxies can dramatically increase the length of ENSO records; reviews of the topic may be found in [Cane 2005, Chiang 2009]. But the trouble with reconstructing ENSO (among other factors; see below) is the necessity for high-resolution proxy data. When working with proxies like lake/ocean sediments which have very slow deposition rates, it is most often impossible to resolve individual events.

Using low-temporal resolution proxies has has led to some debate over ENSO mean state versus variability in reconstructions: for example, [Cane 2001, Molnar 2002] suggested that permanent El Niño-like conditions may have existed during the Pliocene (3-2 Ma) [Ravelo 2006, Wara 2005], while GCM studies of the same period show no indication of an absence of variability [Fedorov 2006, Haywood 2007]. To some extent, this debate illustrates the difference between model validation for the mean state and the variance about the mean. Although proxy data provides an accurate assessment of quantities like mean surface temperature [Mann 2008, Mann 2009], the accuracy required to correctly capture the magnitude of *variability* may be much higher. In a sense, the problem of ENSO model validation is inherently quantitative.

Of all the proxies currently in use, coral records are best suited for ENSO reconstructions due to their tropical location and high temporal resolution. The majority of coral analyses focus on the oxygen isotopic composition of their aragonite skeletons (typically reported as δ^{18}O, the ratio of ^{18}O to ^{16}O abundance). δ^{18}O can be complicated to interpret due to the combined influence of temperature and salinity [Weber 1972, Leder 1996, Quinn 1993, Urban 2000, Linsley 2004, Felis 2003]. For corals located in the western Pacific warm pool, salinity can be the dominant contributor to the signal [Tudhope 2001], while locations in the central/eastern Pacific tend to be dominated by temperature changes [McGregor 2004]. Of course, knowing that a location experiences more or less

influence from salinity in the present climate is no guarantee that the same was true in the past, especially for more distant time periods such as the Last Glacial Maximum (LGM) when global conditions were dramatically different [McCulloch 2000, Guilderson 2001].

The true extent of processes controlling the coral δ^{18}O signal are likely quite complex, and local environmental influences most likely play a role [McGregor 2011a]. Many coral samples are collected from island locations, and although every effort is made to sample in such a way as to minimize local effects, this is not always possible. For example, corals on the Huon peninsula of Papua New Guinea feel effects from river runoff in certain locations [Tudhope 1995], and corals collected from microatoll environments on Kiritimati island in the central Pacific are subject to influences from lagoonal effects [McGregor 2011a, Woodroffe 2003]. The best way to minimize these complicating influences is to collect multiple corals from each location - then environmental factors may be controlled and hopefully subtracted from the signal [Lough 2010]. However, this is complicated to do in practice, since collecting live corals is expensive and it is often impossible to know whether fossil corals are contemporaneous until after they have been analyzed in the lab. The majority of locations from which coral δ^{18}O records have been obtained, therefore, have only one or two time series available. These are available through the NOAA Paleoclimatic Database, and to date roughly 20-30 high-quality records exist for tropical Pacific locations. Still, this network is very sparse by modern standards [Evans 1998] and the number of simultaneous records available for times before the 20th century is smaller still.

Because the coral network is so sparse, the use of climate models is essential to provide a dynamical framework within which to understand the coral signal. This has been done with some success by the Paleoclimate Modelling Intercomparison Project (PMIP; [Joussaume 2000]) which is currently in its third iteration. PMIP3 will perform modeling experiments for the last millennium, the mid-Holocene, and the Last Glacial Maximum (LGM) with all the CMIP5 models. But the majority of the PMIP models do not have the capacity to directly simulate proxy signals like coral δ^{18}O, making it difficult to compare model output to proxy records. An exception is the NASA Goddard Institute for Space Studies (GISS) model [Schmidt 2005, Schmidt 2006], which is able to

simulate seawater δ^{18}O but which suffers from poor ENSO representation [Guilyardi 2009b].

How important is it to directly represent δ^{18}O in climate models? This dissertation will argue that it is very important indeed. Currently the most common technique for quantitative model/proxy comparison is the use of linear 'pseudoproxies' (*i.e.* [Brown 2008, Thompson 2011]). I have performed a detailed investigation of the accuracy of such methods using modern corals ([Stevenson 2011c]; Appendix 1); I find that a linear representation is wholly inadequate to describe the relation between δ^{18}O and climate variables. Yet there are not many good model/proxy conversion methods available, which may be problematic for paleo-ENSO model validation. Results from this analysis are described in Chapter 2.

1.6 Implications for Climate Change

If the modern observational record is too short to constrain present-day ENSO, and the paleoclimate records are too uncertain to constrain past ENSO, then where does that leave us in terms of understanding changes to future ENSO? The issue of how climate change will affect ENSO dynamics is one of the most important topics in the field at the moment, and yet the tools available for looking at the problem are notorious for their lack of ability to make correct predictions. These, of course, are coupled GCMs.

The CMIP5 simulations are just beginning to show results at the time of this writing. This means that assessing the state of model ENSO representation must rely on CMIP3 results until the CMIP5 simulations have been completely analyzed. [Collins 2010] has published a review of the CMIP3 ENSO projections, and finds that there is a huge spread in future ENSO amplitude among models. Figure 1.7 illustrates this disagreement; here the models which perform best relative to observations are represented in bold. Interestingly, the 'best' models do not show any better agreement than the full set of models; this suggests that projected future ENSO amplitude changes have little to do with the overall performance of a given GCM.

There are certainly many well-understood responses to climate change, however, which are

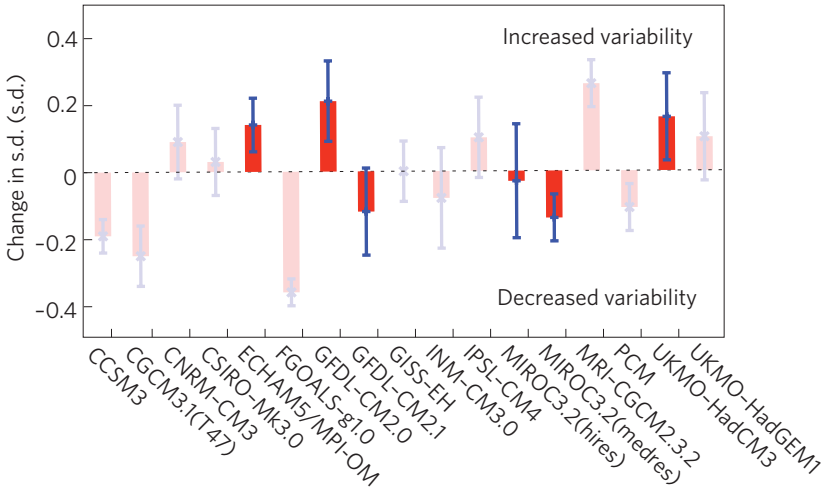

Figure 1.7: Figure 3 from [Collins 2010]. "Projected changes in the amplitude of ENSO variability, as a response to global warming, from the CMIP3 models. The measure is derived from the interannual standard deviation (s.d.) of a mean sea-level-pressure index, which is related to the strength of the Southern Oscillation variations. Positive changes indicate a strengthening of ENSO, and negative changes indicate a weakening. Statistical significance is assessed by the size of the blue bars, and the bars indicated in bold colours are from those CMIP3 CGCMs that are judged to have the best simulation of present-day ENSO characteristics and feedbacks."

generally well represented in GCMs. The mean-state response of the atmosphere and ocean to CO_2 increases is one of these. The robust mean-state responses identified in multiple coupled GCMs are: a decrease in the atmospheric overturning circulation, a decrease in the zonal SST gradient along the equator, an increase in the meridional SST gradient between the tropics and extratropics, an increase in vertical thermal stratification in the ocean, a weakening of the equatorial trade winds and an eastward shift of the Walker cell.

Weaker Walker circulation. As the climate warms, the mean saturation vapor pressure of the atmosphere should rise, in accordance with the Clausius-Clapeyron relationship:

$$\frac{dlne_s}{dT} = \frac{L}{RT^2} = \alpha(T) \tag{1.1}$$

([Held 2006] equation 1), which leads to an increase of roughly 6%/°K. [Held 2006] then compute the rate of increase in global mean precipitation with rising temperature, using the CMIP3 simulations for various models. Precipitation increases by only 2%/°K; this slower increase requires a compensating decrease in the convective mass flux. The rate of exchange of mass between the atmospheric boundary layer and the free troposphere must decrease, and the only way to accomplish this in a global-mean sense is to decrease the strength of the Walker circulation. This has been confirmed using both GCM studies and theoretical predictions [Vecchi 2007].

Weaker equatorial trade winds. As a direct consequence of the weaker Walker circulation, the strength of the equatorial trade winds should decrease with climate change. Once again, this has been diagnosed in coupled GCMs as well as 20th century observations [Vecchi 2006, Power 2007, Zhang 2006, Karnauskas 2009].

Eastward shift of the Walker cell. The shift of the Walker circulation is primarily to the east under climate change. As the trade winds weaken, warm water is 'piled up' in the western Pacific to a lesser degree, and waters in the central and eastern Pacific are now up to several degrees warmer

than the previous climatological average. A larger portion of these waters will now be sufficiently warm to create strong convective activity, thus enhancing convection in the central Pacific.

Decreased equatorial zonal SST gradient. The strength of the zonal SST gradient along the equator is set by the Walker circulation and by coupling with the atmospheric boundary layer. When the equatorial trades decrease, the Bjerknes feedback requires that the SST gradient decreases as well.

During the late 1990s, there was some disagreement over the direction of change of the zonal SST gradient in a warming climate. One school of thought predicted a decrease in SST gradient [Meehl 1996] since the formation of additional cloud cover over the warm western Pacific would lead to a 'shielding' effect and inhibit further warming. The other argued that the equatorial upwelling in the eastern Pacific would overcome the warming due to climate change, thus increasing the equatorial trades and opposing the changes to the Walker circulation. This 'dynamical thermostat' [Cane 1997] is not observed to dominate in the CMIP3 models; the improved representation of equatorial upwelling in the higher-resolution models allows us to conclude that upwelling is not, after all, more powerful than climate change.

Increased meridional SST gradient. In addition to the reduction of the Walker circulation strength, a corresponding weakening is seen in the Hadley circulation [Held 2006]. The weaker equatorward flow in both hemispheres should then lead to a differential reduction in the strength of the trade winds, with winds at higher latitudes experiencing a more pronounced weakening than lower latitudes as a result of the Coriolis force ([Stevenson 2011b]; Appendix 3). Since the transport in the subtropical cells is bound up with the curl of the wind stress [McCreary 1994, Liu 1995], the transport of warm water from the tropics to the subtropics should therefore decrease as a result of climate change. The net effect is a reduction in the divergence of heat flux away from the equator; more heat is built up at lower latitudes, and the meridional SST gradient therefore increases as the climate warms.

Increased oceanic thermal stratification. The surface-intensified warming in the tropics has been documented in many model studies [Timmermann 1999]. This is due to the larger surface heating created by CO_2 radiative forcing, which requires an increase in the vertical temperature gradient to compensate [Yeh 2009, Collins 2010].

Shifts in atmospheric teleconnections. This is less straightforward than the mean-state changes, but there is a body of literature on ENSO teleconnection response to climate change. The teleconnection response is thought to be caused by overall shifts in the general circulation [Meehl 1993, Meehl 2006]. [Meehl 2007b] used a six-member ensemble to show that the position of ENSO teleconnections shifts with climate change: the Aleutian Low anomaly, for example, shifts northeastward as the climate warms. Changes in the Australasian teleconnection, in contrast, are most likely connected with the IOD response to climate change [Cai 2009, Cai 2011].

The fact that the mean state response to ENSO is relatively well understood makes GCMs' inability to agree on a direction of future ENSO change all the more puzzling. The answer is thought to be related to differences in model physics; since ENSO is so sensitive to air-sea coupling strength, even a small change in feedback parameters could potentially spell the difference between a stronger or weaker oscillation in the future [Guilyardi 2009a]. The coupling parameters, additionally, may change under global warming even within a single model, as documented by [Philip 2006].

My contribution to the ENSO/climate change question has been published in ([Stevenson 2011b]; Appendix 3) and is described in Chapter 4. I certainly do not neglect the contributions of previous studies; but there is another possible explanation for the disagreements between CMIP models which has not been investigated to date. The 20th century, after all, is a period which is experiencing rapid changes to atmospheric forcing. These changes are imposed in a global-mean sense (since CO_2 is well mixed throughout the atmosphere) and lead to preferentially enhanced polar warming. This imposes an extratropical forcing which is communicated to the tropics on a relatively long timescale, on the order of decades [Boccaletti 2004]. Could it be that ENSO simply does not respond significantly to

climate change during such a short time period? This seems to be the case in at least four of the CMIP5 models, and most likely even more - which implies that our approach to studying future ENSO must change as a community.

If the 21st century truly is too short to diagnose a significant ENSO response to climate change, then this has another important implication. The CMIP5 experiments, in this case, are not a real test of the ENSO/climate change link, since they are comparing changes that are themselves insignificant. In other words, the underlying model ENSO sensitivity to climate change *remains an unknown*. We cannot claim to know what a quantity is, after all, until we have actually measured it! But interestingly, changes to teleconnections may become significant much faster than ocean dynamics (Chapter 4; ([Stevenson 2011b]; Appendix 3)) and the same may be true for El Niño event statistics (Chapter 5; ([Stevenson 2012b]; Appendix 5)). Thus, the required timescale depends on exactly what question you are asking - even as far as ENSO is concerned.

The last chapter of this dissertation is devoted to doing the problem 'right', in a sense: to examining the dynamical response of ENSO to CO_2 increases using a clean experimental setup. The only way to isolate the effects of CO_2 alone, in the absence of sampling issues or differences in model physics, is to run the same model for multiple centuries in an identical configuration changing nothing but CO_2 concentration. I have done this using the low-resolution version of the CCSM3.5 ([Stevenson 2011a]; Appendix 4), and discuss mechanisms for the amplitude increase in Chapter 6.

I conclude with a brief foray into science policy ([Stevenson 2012a]; Appendix 6). The entire investigation of the ENSO response to climate change relies on the use of standardized greenhouse gas predictions for the 21st century [Moss 2010]. Yet the contents of these scenarios are something of a 'black box' to the climate modeling community. How realistic are the assumptions which go into the creation of the CMIP5 scenarios - or as they are now called, the Representative Concentration Pathways? Are changes to those assumptions important enough to affect the answer to the ENSO question? Chapter 7 will show that the technological advances predicted in the 21st century may be dramatically overestimated, which has implications for every branch of climate science. It is my hope that this dissertation's results will help to underscore the need for better communication

between investigators of a variety of backgrounds.

Chapter 2

How Well Can Coral Oxygen Isotope Records Constrain Past ENSO Variability?

Contents

2.1 Motivation

Paleo-reconstructions of ENSO are useful for climate model validation in several respects - in addition to being interesting in their own right, of course. A model may represent modern climate correctly, but for the wrong reasons: the number of compensatory feedbacks within the climate system makes it relatively easy for errors to cancel one another out. Proxy reconstructions provide a test of model physics in climate regimes which might differ dramatically from those used to tune

the model initially: if a climate model is able to reproduce observations dating from very different epochs, then we can be more certain that the model physics are correctly represented.

For the most recent past, paleoclimate indicators are also useful for extending the modern instrumental record. As will be discussed in Chapter 3, the observations available from modern instruments are much too short to properly measure natural ENSO variability. The only way to extend the record farther back is to use naturally preserved proxies which record the climate at the time of their creation. A variety of proxies are commonly used, including tree rings, speleothems (stalactites/stalagmites), lake sediments and others. Here I focus on coral reefs since they are the most common proxy within the tropical Pacific. As noted in Section 1.5, the majority of coral analyses use the oxygen isotopic ratio of the aragonite skeletons (δ^{18}O) as a proxy for local climate variability.

The complexity of the coral δ^{18}O signal makes its interpretation in a given coral record difficult. Yet this is exactly what must be done, if one hopes to understand whether a climate model is correctly representing climate variability in that location. Towards that end, there has been a recent push towards 'forward modeling', or the inclusion of oxygen isotopes within a GCM to allow for a direct, 'apples to apples' comparison. But this represents an enormous investment in human resources and model infrastructure, and to date the vast majority of CMIP-class models do not incorporate oxygen isotopes. Even those which do offer isotope-enabled configurations (NASA GISS and NCAR CCSM) do not resolve processes on the appropriate spatial scale and do not directly simulate coral reefs, only going as far as computing the δ^{18}O of seawater. So is there anything that the climate community can do in the meantime to bridge the gap between coral δ^{18}O variability and model ENSO? Or are we doomed to wait until the technology improves?

In the no-forward-modeling limit, one is constrained to translate the models into the data 'language', the data to the models, or both the models and data to some other metric of interest. For ENSO, the metric of interest might be something like an estimate of NINO3.4 SST, the leading mode of SST variability, or another index which is sensitive to ENSO variability (for example: the Coupled ENSO Index of [Gergis 2005], the Multivariate ENSO Index of [Wolter 1998], or others.)

All ENSO metrics, however, require information from multiple locations to be combined to form an estimate of the total amplitude of variability. The options for model/proxy comparison are shown schematically in Figure 2.1. Here, conversions which take place after a model simulation is complete are referred to as pseudoproxies; conversions which rely on direct simulation of the proxy signal are termed forward models.

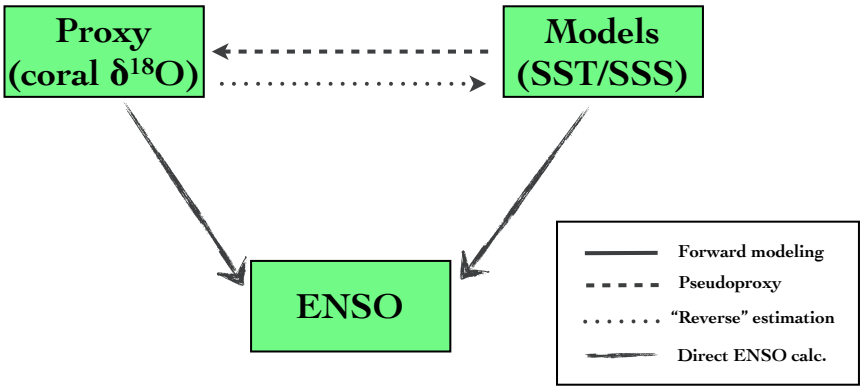

Figure 2.1: Schematic illustrating potential methods of ENSO model validation.

Leaving aside the question of converting between the model and proxy signals, some sources of error must be considered regardless. The major ones considered in this chapter are:

1. **Errors from age model estimation and/or local influences.** Since collecting coral records is a difficult, expensive, and time-consuming process, there is typically only one coral available from any given location. This leads to the possibility of undetected errors from local climatic influences. There is also the possibility of introducing errors through the process of estimating an age model: typically coral δ^{18}O records follow a sinusoidal pattern governed by the seasonal cycle, and this is exploited to assign exact calendar ages within a given year. The combined influence of local effects and age model uncertainty should lead to scatter between simultaneous δ^{18}O measurements from corals collected at a single location.

   A recent study by [McGregor 2011a] provides a unique look at age model/local uncertainty: multiple records are available for Kiritimati Island (pronounced 'Christmas') in the central

Pacific. The mean standard deviation between δ^{18}O time series is roughly 0.21‰, which is relatively small compared with δ^{18}O variability in most locations. As an illustration, see Figure 2.2 from [McGregor 2011a].

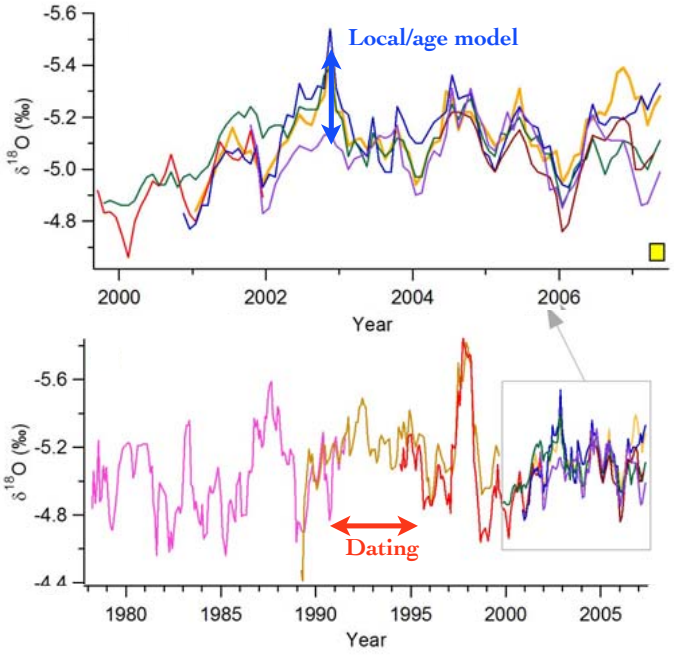

Figure 2.2: Figure 4 from [McGregor 2011a], showing various time series generated from living Kiritimati corals. Top: transects across the same coral at various angles to the growth direction. Bottom: δ^{18}O time series from various corals collected on Kiritimati.

2. **Effects of sample size.** As mentioned above, estimating ENSO amplitude requires data from multiple locations around the Pacific. But how many points are required? There is no consensus on this in the paleoclimate community. Typically studies are conducted using only one coral record at a time; however, some field reconstructions are available which cover the past few centuries [Evans 2002, Ault 2009, Wilson 2010, D'Arrigo 2005, D'Arrigo 2006]. The influence of sample size varies according to the ENSO reconstruction employed; details are provided in later sections.

3. **Dating uncertainty.** When collecting fossilized coral samples, one does not have the luxury

of using a calendar to get the date for a given measurement. In fact, collecting multiple coral records from the same time period is an extremely difficult process, since it is often not obvious whether two fossil corals are contemporaneous until *after* they have been sampled and taken back to the lab. Dating corals relies on radioactive decay of U-series elements. The typical accuracy of absolute dates on fossil corals is roughly 5-10 years [Cobb 2003]; this must be taken into account when looking at the combined signal from multiple records.

After the above sources of error have been accounted for, there still remains the question of introducing additional uncertainty from the model/proxy conversion. This is the subject of the remainder of this chapter.

2.2 Coral Data

Data from modern corals was obtained from the World Data Center for Paleoclimatology website (WDCP[1]), and from Helen McGregor at the University of Wollongong for the Kiritimati records [McGregor 2011a]. Requirements for inclusion of a given coral record in my dataset are: a location in the tropical Pacific (23°S-23°N, 60-300°E), at least 4 samples/year (seasonal resolution), and a statistically significant correlation between the coral δ^{18}O time series and NINO3.4 SST. This led to a set of 11 coral records from 10 different sites (two records are available from Nauru). The time period for analysis was chosen to be 1958-1990 so that information from all corals was available simultaneously.

The locations of each record are shown in Figure 2.4. All coral records were derived from samples taken from the massive *Porites* species (Figure 2.3) unless otherwise indicated.

Laing/Madang [Tudhope 2001]: (4.15°S, 144.9°E),(5.2°S, 145.8°E). Laing is located along the northeastern coast of Papua New Guinea; Madang Island is further down the coast. These samples were collected from living corals, and ages assigned on the basis of δ^{18}O and δ^{13}C seasonality

[1] http://www.ncdc.noaa.gov/paleo/paleo.html

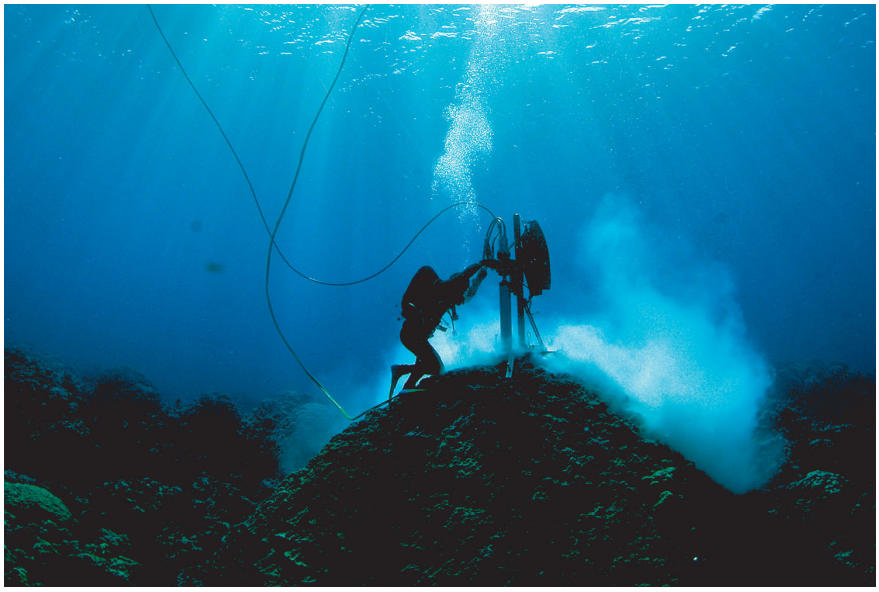

Figure 2.3: Reproduction of Figure 1 from [Lough 2010]: diver collecting sample from massive *Porites* coral.

and skeletal growth bands. These sites both experience substantial precipitative influences.

Tarawa Atoll [Cole 1993]: 1.0°N, 172.0°E. Tarawa Atoll is another western Pacific location: intense rainfall has been observed to radically alter sea surface salinity here, and Tarawa is therefore sometimes viewed as recording changes to convective activity in the western Pacific warm pool [Cole 1993]. This record was collected at 6.7m depth from a forereef site (seaward side of the atoll) and sampled 16x/year. Ages were determined through seasonal δ^{13}C variability, and δ^{13}C/δ^{18}O values interpolated to monthly resolution.

Palmyra [Cobb 2001]: 5.9°N, 197.9°E. Palmyra is an equatorial central Pacific site which experience both SST and SSS signals. The [Cobb 2001] record was generated from a coral collected at roughly 30' depth near the center of a large reef flat. Submonthly samples were possible due to the large coral growth rate, and intra-annual chronology established by fitting the δ^{18}O seasonal cycle. [Cobb 2001] estimate the dating error due to age model estimation at ≈4 months.

Maiana [Urban 2000]: 1.0°N, 173.0°E. Maiana is located in the central Pacific, near to Tarawa. Conditions are therefore similar in terms of the SST/SSS influences. The [Urban 2000] record was collected at 1mm resolution from a living coral and dated using X-ray imaging of the growth bands.

New Caledonia (Amedee) [Quinn 1998]: 22.5°S, 166.5°E. Amedee Island is located in the Coral Sea, and is part of the territory of New Caledonia. The region experiences strong influence from the seasonal motions of the Soth Pacific Convergence Zone [Morliere 1986] as well as the local currents [Quinn 1998]. This record was collected from a living coral in 3m of water, and was then sampled 12x/year.

Clipperton [Linsley 1999]: 10.3°N, 250.8°E. Clipperton Atoll is the easternmost atoll in the Pacific [Linsley 2000], 1100km off the coast of Mexico. Being at 10°N latitude, pronounced differences in δ^{18}O during different El Niño events can occur at Clipperton due to the position of equatorial rain bands [Deser 1990], which form more frequently during strong events. This record was collected from a carbonate terrace surrounding the atoll, and sampling performed at 12x/year.

Kiritimati [McGregor 2011a]: 1.9°N, 202.6°E. Kiritimati Atoll is located nearly at the center of the NINO3.4 region. As such it makes a sensitive recorder of ENSO variability, and for the most part δ^{18}O variability is dominated by SST signals. The record used here was spliced together from several different coral samples [Evans 1998, Woodroffe 2003] collected from *Porites* microatolls on the island. Microatolls are just that: small atolls which form in shallow-water lagoonal environments on the island. [McGregor 2011a] find that inter-colony reproducibility is greater for microatolls than other growh forms, which may potentially imply that the local/age model influences quoted above are lower limits on the true value for some locations. Here corals were sampled at roughly fortnightly resolution, then interpolated to 12 samples/year.

Secas [Linsley 1994]: 8.0°N, 280.0°E. Secas Island, off the coast of Panama, is extremely

close to Clipperton Atoll, and as such has a similar climate. The ITCZ plays an important role in the δ^{18}O signal [Linsley 1999]. The sample was collected from 3m depth, with a chronology developed based on X-rayed growth bands. 1mm sampling was performed, then interpolated to 10 samples/year. [Linsley 1994] use band counting to establish the chronology back to roughly 1800AD.

Nauru [Guilderson 1999]: 0.5°S, 166.0°E. Nauru Island is squarely within the western Pacific warm pool, and the semiannual cycle in SST is dominant due to the equatorial location of the island; overall variations in SST are relatively small, less than 2° [Guilderson 1999]. The variations in precipitation, however, can be dramatic: from nearly no rain to upwards of 4m annually [Baker 1995].

These corals were collected off the north shore of the island, at 14m depth. Density banding structures were not very pronounced, meaning that density-based dating was not possible. Instead, the age model was constructed using the seasonally varying δ^{13}C measurements, and the second coral ('Nauru 2') was mapped to the first coral ('Nauru 1') after the model was completed. Overall dating uncertainties are estimated at 2-3 months.

2.3 Linear Pseudoproxies

Next I consider errors due to pseudoproxy conversions. The simplest after-the-fact comparison of coral δ^{18}O and climate variables is the use of a linear regression:

$$\delta^{18}O = \beta_0 + \beta_1(SST) + \beta_2(SSS) + \varepsilon \tag{2.1}$$

where the regression coefficients β_n are obtained through least-squares error minimization and the error term ε is assumed to be normally distributed. (Note: this is not a good assumption, as many of the error PDFs actually show significant skewness. Details are available in the Supplemen-

tary Information to ([Stevenson 2011c]; Appendix 1).

Some previous studies have used basin-scale relationships to define common β_n for all coral records in a given basin [Thompson 2011]; this, however, does not lead to the optimal regression. I have therefore used a multivariate regression algorithm to fit each coral time series individually. Observational data is derived from the HadSST reconstruction and from SODA for SST and SSS, respectively.

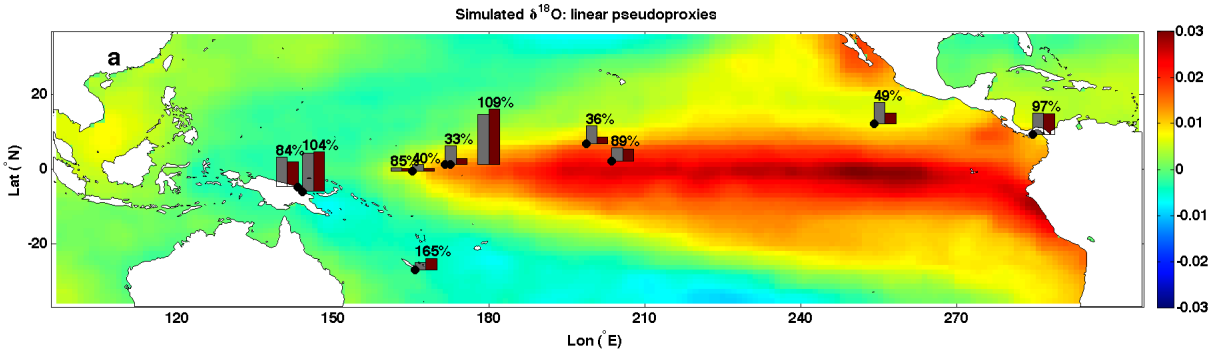

Figure 2.4: Figure 1a from [Stevenson 2011c], showing errors in linear pseudoproxy conversion. Background colors represent the leading PC of HadSST over 1958-1990; gray bars show the variance of δ^{18}O over the same time period, and red bars the variance of errors arising from the linear pseudoproxy estimation.

Sources of error from a linear pseudoproxy conversion are:

1. **Errors in regression coefficients.** This is a consequence of the least-squares regression algorithm. The errors for each coefficient can be modeled using a t distribution and the standard deviation returned from the fitting algorithm:

$$\sigma(\hat{\beta}_j) = \sqrt{\hat{\sigma}^2 C_{jj}}; \hat{\sigma}^2 = \frac{\sum_{i=1}^{n} \varepsilon_i^2}{n-3} \tag{2.2}$$

where n is the length of the time series, $\hat{\sigma}$ is the variance of the errors, and C_{jj} is the jth diagonal element of the covariance matrix [Montgomery 2007].

2. **Errors from fit residuals.** This is equivalent to the ε term from Equation 2.1, and turns out to be the largest contribution to pseudoproxy conversion error. I have modeled this for each fit using kernel density estimation (KDE) and simulate errors by sampling from the empirical distribution for each individual coral.

The details of the error fitting and resampling methods are given in ([Stevenson 2011c]; Appendix 1); Figure 2.4 is a reproduction of Figure 1 from that paper, which shows the magnitudes of the coral δ^{18}O errors thus simulated. The spatial structure of the first principal component of SST variability from HadSST is shown in color. Superimposed on this pattern are the $\delta^{18}O$ variance errors in red, next to the input δ^{18}O variance in black. Errors in the simulated δ^{18}O variance for each site are anywhere from 33%-185% of the input value, which is a strong argument for the inaccuracy of single-site estimation of δ^{18}O variability.

It remains to be seen whether the noise terms are able to drown out the covarying signal between the coral records. Indeed, this is what is most often done when sufficient coral data are available [Evans 1998]. To see whether the covarying δ^{18}O mode is captured in the instrumental record, I next compute δ^{18}O pseudoproxies from the instrumental SST and SSS using Equation 2.1, then calculate the first principal component between the simulated δ^{18}O time series. Principal components are calculated by singular value decomposition of the covariance matrix:

$$C = OO^T = U\Lambda V^T \tag{2.3}$$

where O is the matrix of coral δ^{18}O time series and C the covariance. The principal components are then given by $U\Lambda$, and take the form of a time series. I have included a figure illustrating the results below (Figure 2.6); this is Figure 2a from [Stevenson 2011c]. Now the only sources of error on the input coral δ^{18}O PC1 (Figure 2.6, red envelope) are local effects and age model estimation. These two sources of error are relatively small compared to the input spectrum, with the spectral peak remaining well-defined.

One important note when working with PCA is that the modes thus calculated are not necessarily

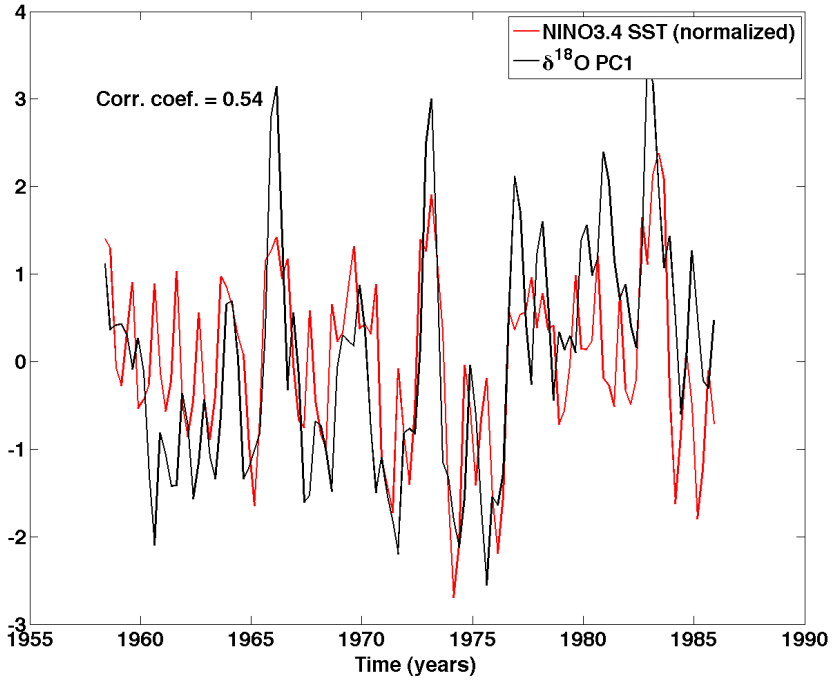

Figure 2.5: Verification that coral δ^{18}O PC1 contains ENSO-related variability. Time series of the first PC is shown in black, NINO3.4 SST in red.

representative of physically independent oscillations. I therefore confirm that the first principal component (PC1) is related to ENSO by correlating its time series with NINO3.4 SST: results are shown in Figure 2.5. The correlation is statistically significant, with a correlation coefficient of -0.54. Since this is much larger than the correlation between NINO3.4 and any other δ^{18}O principal component, I conclude that PC1 contains the majority of ENSO-related variability.

If the linear pseudoproxy noise does not contaminate the covarying mode, and ENSO is well represented in the first covarying mode, then the coral δ^{18}O PC1 should be replicable using the instrumental pseudoproxies. When the fir residual errors are applied to the pseudoproxies, the results (in Figure 2.6) are striking: the peak near 3 years is not captured at all. Additionally, the error envelope on the PC1 spectrum is enormous, with spectral power ranging from 0-200% of the mean value (from Equation 2.1) at any given frequency. I note that pseudoproxy PC1 still retains the highest correlation with NINO3.4 (not pictured), indicating that the spectral mismatch is not an artifact of 'bleeding' of ENSO variance between pseudoproxy modes.

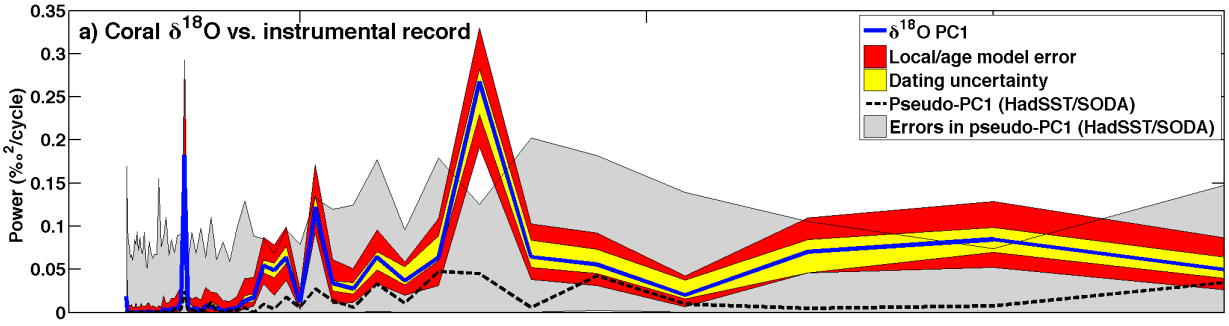

Figure 2.6: Figure 2a from [Stevenson 2011c], showing errors in coral δ^{18}O spectra from linear pseudoproxy estimation. Local (red) and dating (yellow) uncertainties are applied to the individual δ^{18}O time series before computing the first PC. Errors in pseudoproxies are calculated from Equation 2.1.

Using linear pseudoproxies to capture variability does not yield accurate ENSO spectral estimates, even when 11 different simultaneous coral records are available. This seems to be a rather discouraging result, as it implies that quantitative model ENSO validation is simply not possible.

Indeed, Figure 2.7 shows that errors in the pseudoproxies calculated from CCSM4 20th century SST and SSS overwhelm the input signal.

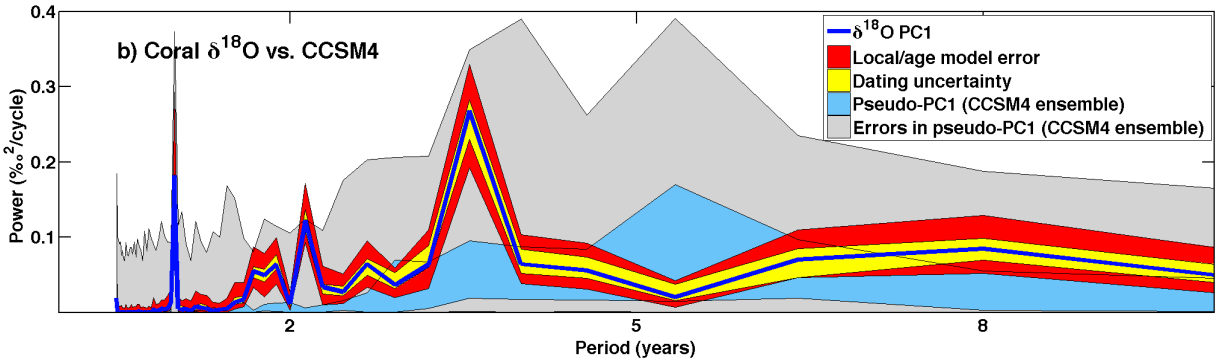

Figure 2.7: Figure 2b from [Stevenson 2011c], illustrating uncertainties in quantitative model ENSO validation using linear pseudoproxies. Here the pseudo-PC1 from each ensemble is shown in blue, and the associated errors in gray.

Although errors in linear pseudoproxies are very large, the situation is not as hopeless as it might seem: there are ways to mitigate the problem. One option is to improve our understanding of the processes controlling the δ^{18}O signal: but as the next section will show, this may prove to be extremely complicated.

2.4 Nonlinear Time Series Analysis

Given the limitations of the linear approach, the next challenge is to explain why exactly the linear pseudoproxy approximation yields such inaccurate results. If one plots coral δ^{18}O vs. local SST, the result is a simple scatter plot, as seen in many previous studies. But the bandpass-filtered time series show quite different behavior: Figure 2.8 shows the coral δ^{18}O vs. NINO3.4 SST, where both time series have been bandpassed over the 2-7 year period range. This plot bears a striking resemblance to high-order phase orbits: could it be that there really are predictable dynamics which govern coral δ^{18}O on interannual timescales, that are simply not well described by a linear approximation?

Some insight into coral δ^{18}O dynamics is possible using nonlinear techniques. For example,

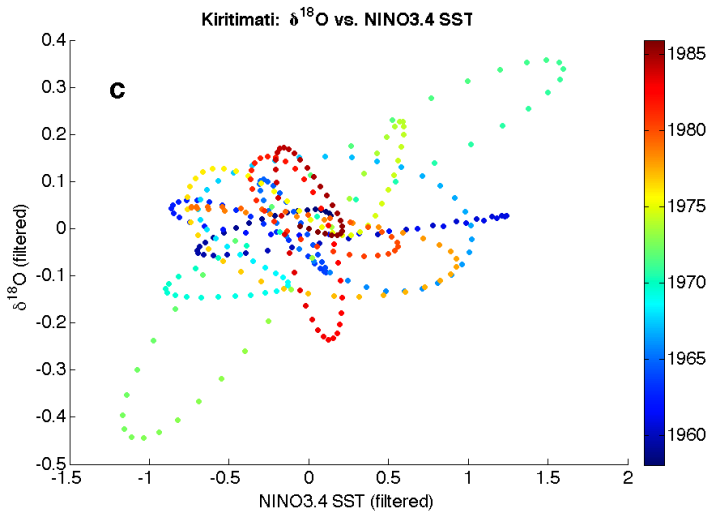

Figure 2.8: Figure 1c from [Stevenson 2011c], showing 2-7 year bandpass filtered δ^{18}O versus NINO3.4 SST for Kiritimati. Time is indicated by the color coding.

it is possible to estimate the number of independent variables required to describe δ^{18}O using the 'embedding dimension' [Sangoyomi 1996]. Full details of the calculations are described in the Supplementary Information to [Stevenson 2011c], but the basic idea of the calculation is this: the time series is represented in a 'pseudo-phase space' as a function of delayed versions of itself (the 'method of delays': [Takens 1981]).

$$\vec{x} = x(t), x(t-\tau), x(t-2\tau), ...x(t-(m-1)\tau) \tag{2.4}$$

where τ is the delay time, chosen to maximize the information about the phase trajectory included. Mutual information [Fraser 1986] is chosen as the method of optimizing τ, following [Sangoyomi 1996]:

$$MI = \sum\sum p(x(t), x(t-\tau))log(\frac{p(x(t), x(t-\tau))}{p(x(t))p(x(t-\tau))}) \tag{2.5}$$

where $p(x(t), x(t-\tau))$ is the joint probability distribution of the original and lagged time series,

and $p(x(t))$ and $p(x(t-\tau))$ the probability distributions of the original and lagged time series individually. The optimal lag τ minimizes the mutual information between lagged time series; this is equivalent to saying that τ is chosen such that the delayed time series are as independent of each other as possible.

After the pseudo-phase space representation is computed, the embedding dimension is calculated using the so-called 'false nearest neighbors' approach [Kennel 1992]. False nearest neighbors are defined as 'neighbors' within the time series, which appear when the series is projected into a dimensional space too small to fully describe its dynamics. The true embedding dimension, then, is the one which causes the false nearest neighbors to disappear. The embedding dimension threshold R_{tol} is the factor by which the Euclidean distance R_d increases when the dimension is increased by 1:

$$\frac{R_{d+1}^2(n,r) - R_d^2(n,r)}{R_d^2(n,r)} > R_{tol} \tag{2.6}$$

This is taken to be 15 in these calculations.

The embedding dimensions for each of the 2-7 year bandpass filtered coral δ^{18}O time series are shown in Figure 2.9 (Supplementary Figure 3 in [Stevenson 2011c]). The 'true' embedding dimension, here, is the value where the false nearest neighbors fall to 0: this happens at dimensions of 3-4 for all corals. The SST/SSS approximation may not be so bad in reality, but the true relationship with δ^{18}O may be more complex than the linear pseudoproxy approach would indicate.

Unfortunately, the embedding dimension calculation does not provide any information on what the independent variables needed to describe coral δ^{18}O might be, only on their number. It is entirely possible that the δ^{18}O value of seawater is one of these variables; this should experience interannual modulations, related to the transport of different water types past the coral sites. A full investigation of δ^{18}O dynamics, however, is left for future work.

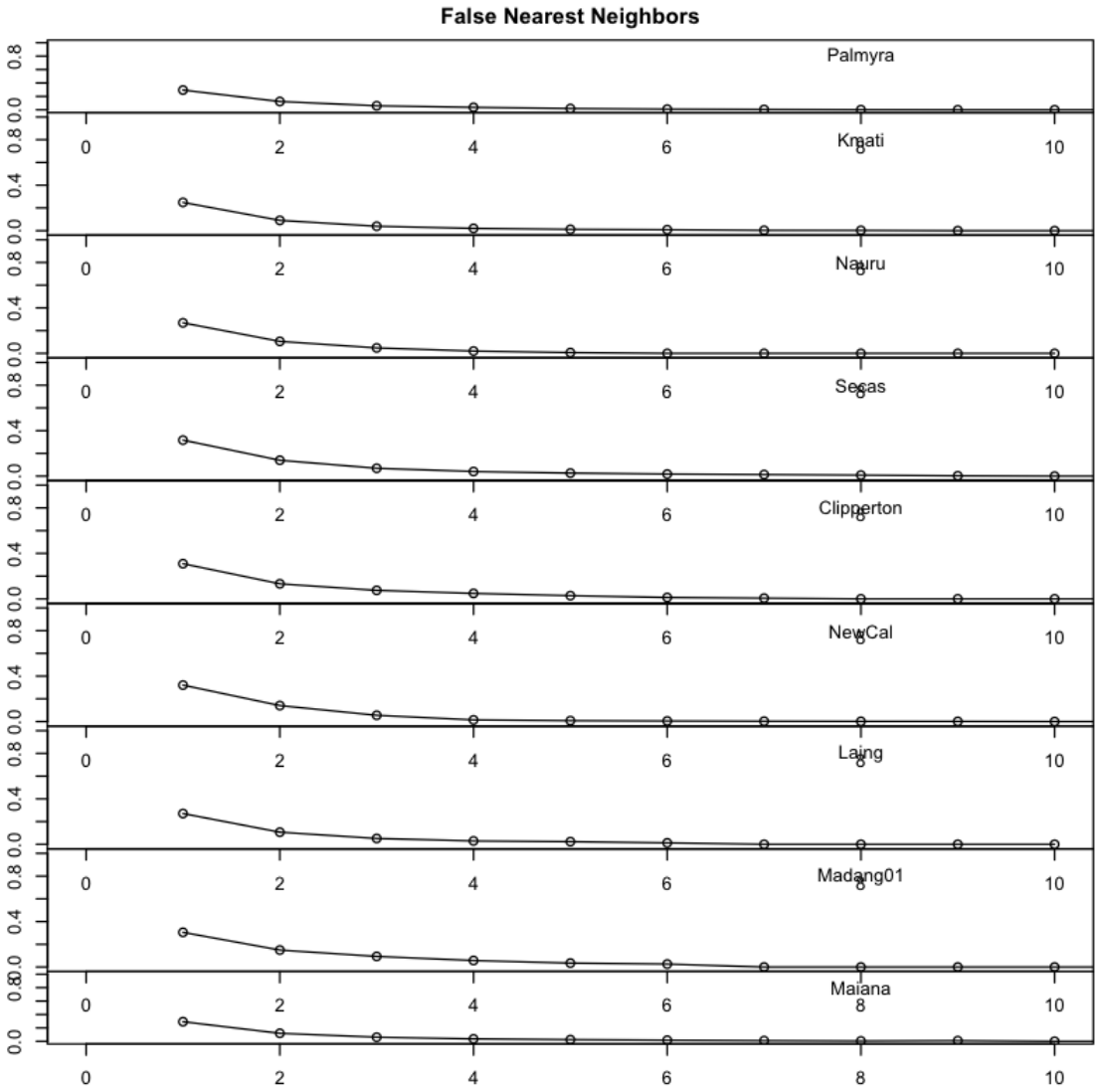

Figure 2.9: Fraction of false nearest neighbors as a function of embedding dimension, for all coral records.

2.5 Translation Using Climate Field Reconstruction

The previous section clearly indicates that a more sophisticated conversion between ENSO/δ^{18}O/climate model output is required. This chapter is not intended to provide an exhaustive look at every possible model/proxy conversion; but I have investigated one alternative method that seems to hold more promise than linear pseudoproxies. This is the application of climate field reconstruction (CFR) techniques to translate both model and proxy data into ENSO metrics. CFR is extremely popular in the hemispheric reconstruction community [Mann 2007, Mann 2008, Mann 2009, Emile-Geay 2011a, Emile-Geay 2011b], and provides highly accurate results of Northern Hemisphere mean temperatures over the modern epoch by exploiting covariances between known values to estimate the quantity of interest at the desired time.

A widely-used CFR technique at the moment is the so-called regularized expectation maximization algorithm, or RegEM [Schneider 2001]. Expectation maximization (EM) is a technique used to compute maximum-likelihood estimates for parameter values for statistical models, where the parameters are dependent on unknown variables; a full description is available in [Dempster 1977]. For this particular application, the parameters are the mean and covariance matrix.

The expectation step of EM uses an initial guess for the model parameters to compute the expectation value of the log-likelihood function, which is simply the logarithm of the likelihood L:

$$L(\theta|x) = f_\theta(x) \tag{2.7}$$

Here, L is the probability of a given model parameter θ given the observed dataset x and the assumed probability distribution function of θ, f_θ. In the second (maximization) step, this expectation value is used to find the model parameters which maximize the log-likelihood function.

The difference between EM and the regularized version of the algorithm is the fact that the treatment of [Dempster 1977] assumes the data follow a Gaussian distribution. For typical sets of climate data this is not the case; not only that, but the small number of data points available for typical climate variables often leads to a rank-deficient covariance matrix [Schneider 2001]. This

leads to an ill-conditioned maximum likelihood estimator, which can be remedied by using several different regularization techniques [Schneider 2001]. I have adopted truncated total least-squares regression (TTLS), following [Mann 2007]; this approach uses a truncated basis of principal components from the covariance matrix to compute the optimal regularization parameter, and was shown to have better performance than other regularization methods.

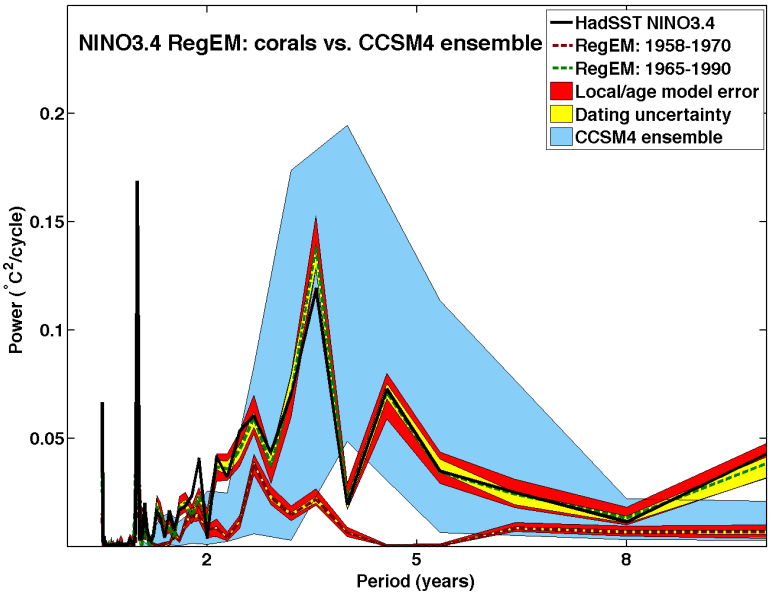

Figure 2.10: Figure 3 from [Stevenson 2011c]. Error analysis for estimation of NINO3.4 SST spectra using climate field reconstruction (RegEM). Errors are once again shown as envelopes: local/age model effects (yellow), dating uncertainties (red) and ensemble scatter from CCSM (purple). Here two different RegEM reconstructions are performed to illustrate the effects of varying the calibration interval: 1965-1990 (green) and 1958-1970 (red).

For this portion of the analysis, I have adopted the NINO3.4 SST as my ENSO metric of choice: both instrumental records and model output are converted to NINO3.4 SST, rather than using δ^{18}O PC1 as in Section 2.3. The results are shown in Figure 2.10, which is a representation of Figure 3 from ([Stevenson 2011c]; Appendix 1). Now that I am not applying a conversion method between proxies and model output, there is no need for simulation of regression errors *etc.*: but the local/age

model and dating uncertainty calculations have been applied as in Section 2.3, and appear as the envelopes surrounding the NINO3.4 estimates.

Using the RegEM algorithm requires the use of the covariances between known NINO3.4 and δ^{18}O values over a specified time interval, referred to as the 'calibration interval'. The choice of calibration interval is crucial, since the resulting spectrum is highly sensitive to changes in the input covariance matrix. When one is predicting values for NINO3.4 SST outside of the temporal range covered by that covariance matrix, there is a tendency for underprediction of the true variance. This is apparent in Figure 2.10, which shows the 1958-1990 NINO3.4 spectrum estimated using calibration intervals of 1965-1990 and 1958-1970. NINO3.4 is very well reproduced by coral δ^{18}O in the former case, and dramatically underestimated in the latter.

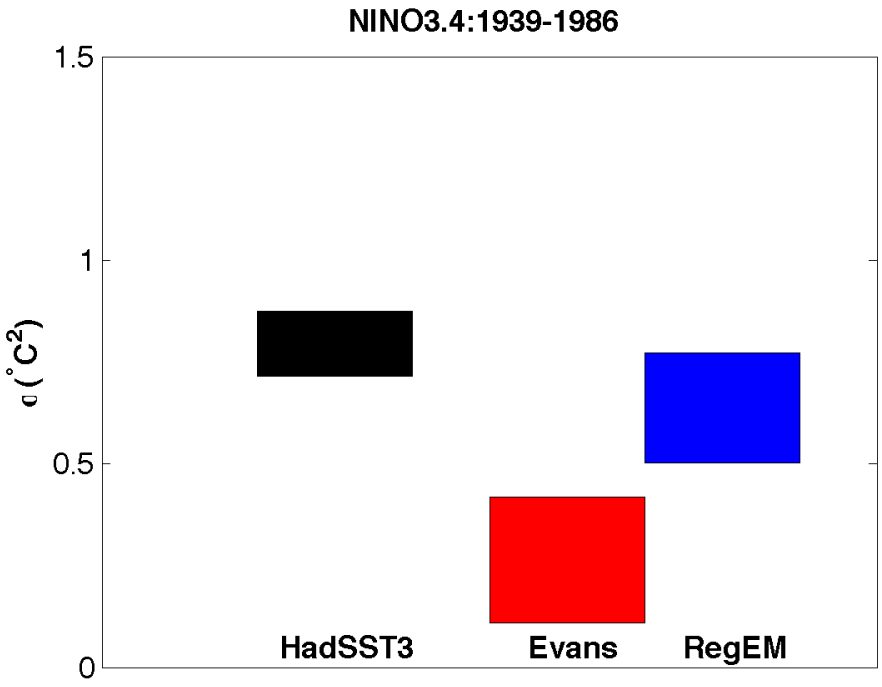

Figure 2.11: Comparison of NINO3.4 SST variances from different sources. Black: HadSST version 2. Red: Box-average over NINO3.4 of the SST field reconstruction of [Evans 2002]. Blue: Application of RegEM using a calibration interval from 1939-1986. Box height is equivalent to the bootstrap 90% confidence interval.

The underestimation of variance is evident in both spectral space and in total variance, and appears in pre-existing SST reconstruction products as well. This indicates that the problem is not unique to RegEM, but general to CFR approaches. An example is shown in Figure 2.11, where I have plotted the total variance in NINO3.4 SST over the time period 1939-1986 from HadSST. As a comparison, I then show the RegEM reconstructions over the same time period, and the NINO3.4 variance from the [Evans 2002] field reconstruction. The reconstruction technique in [Evans 2002] is a PCA-based approach, called reduced-space objective analysis [Kaplan 1997, Kaplan 1998, Kaplan 2000]. In both the [Evans 2002] and RegEM reconstructions, NINO3.4 variance is underestimated relative to HadSST.

Figures 2.10 and 2.11 demonstrate that even though climate field reconstructions are more accurate than linear pseudoproxies, they are still limited in their utility for past climates when there is no prior knowledge of the true covariance between coral sites and ENSO. In this case, we must rely on estimates from the modern climate; and the problem of variance underprediction becomes worse as the separation time from the calibration interval increases. This is not a huge problem when the goal is to reconstruct the mean of a given field [Mann 2009], but does present an issue when trying to reconstruct interannual variability.

2.6 Recommendations

Based on the results of the previous sections, I can now make some recommendations on what is required for quantitative model ENSO validation in past climates. Our understanding of the dynamics which govern the coral δ^{18}O signal is clearly incomplete; even still, using a bivariate linear pseudoproxy approximation is entirely inadequate. This approximation is so uncertain that even the dominant covarying mode between coral sites cannot be distinguished.

Given the shortcomings of the linear model, it seems that forward modeling of coral δ^{18}O is necessary to provide an accurate answer. In fact, the large embedding dimensions in Figure 2.9 suggest that a detailed process study may be required before coral δ^{18}O can be accurately

incorporated into GCMs. In the absence of this capacity, it would seem on the basis of Section 2.4 that at a minimum, a more sophisticated pseudoproxy is required to convert between model and proxy signals.

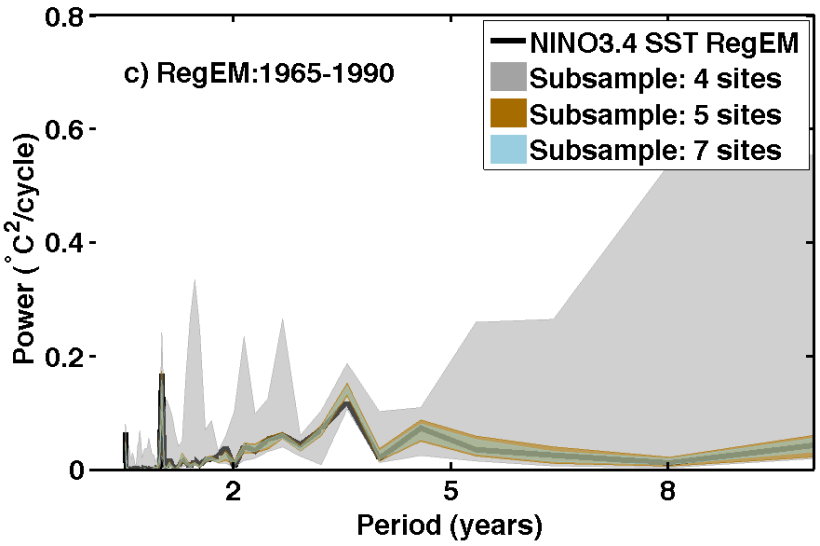

Figure 2.12: Figure 3a from [Stevenson 2011c], showing the influence of sampling error on RegEM reconstructions of NINO3.4 SST.

Another issue, of course, is data availability. All the results in this chapter thus far assume that 11 corals, measured more or less simultaneously, are available: far more than are normally available for coral paleoclimate research. I have therefore performed a preliminary investigation into the necessary sample size for identification of the covarying mode; results are shown in Figure 2.12. This figure was created by randomly selecting a subsample of specified size from the coral dataset, then rerunning the RegEM calculation. I find that the covariance matrix is insufficient to reproduce the NINO3.4 spectrum accurately if only 4 corals are used, especially at longer periods; moderate accuracy is achieved with 5 or more. This leads me to conclude that the optimal dataset for paleo-ENSO model validation consists of at least 5 corals, dated to within 10 years of one another (see [Stevenson 2011c] for the details of the dating uncertainty calculation).

Finally, the problem of variance underprediction remains. The current 'cutting edge' of field

reconstructions is the use of Bayesian techniques [Tingley 2010a, Tingley 2010b]; those authors found that Bayesian methods were superior to RegEM in retaining the variance of the original time series. I would ideally like to attempt such reconstruction methods in the future, to see whether the errors involved are still prohibitively large in comparison to the input values.

In conclusion, the problem of paleo-ENSO model validation is a difficult one, and the tools currently being used for the problem are too uncertain to provide an accurate answer. But this does not mean that the problem is intractable, only that more attention needs to be paid to the errors involved and the most appropriate ways to decrease their magnitudes.

Chapter 3

When Do Two ENSO Spectra Differ From One Another?

Contents

3.1 Motivation

The last chapter has demonstrated that reconstructing past ENSO variability using paleoclimate records is extremely difficult. But the issue of the too-short modern observational record still remains: this makes it quite difficult to determine when changes to ENSO are statistically significant in comparison to natural variability. In this chapter, I describe a new technique for isolating changes to a spectrum over time.

A great many significance tests already exist, designed for use with various types of distributions. Parametric tests are most commonly used, but the results are only valid if the underlying assumptions of the test have been satisfied. The most commonly used parametric tests are the

T-test and the F-test: these give the significance of differences between distribution means and variances, but require that the populations being compared are normally distributed.

To get around the distribution requirements of parametric tests, nonparametric approaches have been developed which can be applied to data of arbitrary distributions. One such method is the Kolmogorov-Smirnov (K-S) test, which measures changes to the cumulative distribution function (CDF) of two distributions, then determines whether those differences could have arisen by chance. Other nonparametric tests include the Wilcoxon rank-sum test and the Kruskal-Wallis test, which look at the distribution of the 'ranks' of relative magnitudes of values, as well as many others.

Are any of these tests suitable for measuring ENSO changes? Given their number, it seems that there should be no problem finding one. But natural ENSO changes are so large that they make the use of traditional testing methods nearly impossible. Consider NINO3.4 SST, one of the most commonly used ENSO metrics. The skewness of the NINO3.4 distribution has been well established in previous work [Kessler 2002, Burgers 1999, Okumura 2010], meaning that any test relying on the normality of distributions will not yield accurate results. Additionally, tests which measure changes to the mean of a distribution alone do not show whether the strength of variability has changed during a given period. This means that tests like the Wilcoxon rank-sum or other nonparametric tests for changes on the mean are of limited use as well. Even the K-S test does not work well, since it is actually *too* sensitive. Very small changes to the CDF are detected by the K-S test: changes that are easily created by natural variability within a single ENSO time series. This has been verified using the CCSM: when the K-S test is run on various combinations of centuries within a single long CCSM control simulation, a great many of them show up as different from one another.

Even more worrying are the results from the CCSM4 20th and 21st century ensemble simulations ([Stevenson 2011b]; Appendix 3). As part of my analysis of the ENSO response to climate change (see Chapter 4), I ran the K-S test on ensemble members versus one another. If this test really is picking up only changes due to real physical differences, one would expect that members of the same ensemble would show up as alike. The same radiative forcing applied to the same set of model physics should lead to the same simulated NINO3.4 SST distribution: but in fact, what happens is

that *every ensemble member differs from every other*. Once again, changes to the ENSO distribution due to natural variability are extremely large compared with typical applications of nonparametric tests. To accurately assess when two ENSO spectra differ from one another, a less sensitive test must be devised which takes into account the *expected* variations in the distribution with time.

What is the optimal way to measure changes to the ENSO distribution? One obvious consideration is the frequency of the signal: ENSO is characterized specifically by the interannual variability in the Pacific. A method of diagnosing ENSO changes must therefore be able to filter out low-frequency (decadal) signals, as well as higher-frequency seasonal and annual 'noise'. The metric used should also be able to measure ENSO-related variability localized in time, so that portions of a time series may be compared against one another. These characteristics are exactly those which define wavelets [Daubechies 1990], which are similar to the simpler windowed, or short-time, Fourier transform:

$$\hat{f}(\tau,\omega) = \int_{-\infty}^{\infty} f(t)g(t-\tau)e^{-j\omega}dt \tag{3.1}$$

Here g is the window function (typically a Gaussian) and τ is an imposed time delay. The wavelet transform also uses a function to filter the input signal in time and frequency: but this time, rather than applying a window of a given length in time/frequency, the size of the window is allowed to vary with frequency so that signals at higher frequencies are sampled at higher temporal resolution. Mathematically, this means that a wavelet basis function (h) of a given shape is adopted, then translated in both time(τ) and scale (s):

$$h(t) = |a|^{-\frac{1}{2}} h(\frac{t-\tau}{s}) \tag{3.2}$$

where a is an arbitrary amplitude. This approach is often referred to as the 'translation and dilation' approach [Daubechies 1990], and is what allows the wavelet transform to provide a higher-quality representation of the signal than a windowed Fourier transform. Wavelet basis functions may have many shapes, but are required to have zero mean and to be localized in both time and frequency

[Farge 1992].

The technique I have developed uses empirically derived distributions of the wavelet spectral power to diagnose changes to ENSO: I have named it wavelet probability analysis, or WPA. In this analysis, I make use of three major wavelet basis functions [Torrence 1998]: the Morlet, derivative-of-Gaussian (DOG) and Paul. The Morlet and Paul basis functions are complex, while the DOG is real-valued: this may lead to some differences in the sensitivity of each to small-scale features in the input signal, but does not affect the major results discussed here.

Table 3.1: Equations describing the wavelet basis functions used in this chapter. Equations are reproduced from Table 1 of [Torrence 1998]. For the Morlet and Paul wavelets, the integer m represents the order.

Morlet	$\pi^{-\frac{1}{4}} e^{i\omega_o \eta} e^{-\frac{\eta^2}{2}}$
Paul	$\frac{2^m i^m m!}{\sqrt{\pi(2m)!}} (1 - i\eta)^{-(m+1)}$
DOG	$\frac{(-1)^{m+1}}{\sqrt{\Gamma(m+\frac{1}{2})}} \frac{d^m}{d\eta^m} (e^{-\frac{\eta^2}{2}})$

3.2 Wavelet Probability Analysis: Conceptual Approach

An illustration of modeled ENSO variability is shown in Figure 3.1, within a control simulation performed using the CCSM3.5 ([Stevenson 2010], Figure 1). For comparison, the hindcast product of [Large 2008] (the Common Ocean-Ice Reference Experiment, or CORE) is shown as the white line, and the PDF of wavelet power at each scale value is plotted in color. Agreement between the model and observations is relatively good at some frequencies, and much worse at others (*i.e.* periods longer than ≈8 years). WPA is designed to distinguish times when natural variability can and cannot be invoked to explain data/model offsets.

I have defined a metric called the wavelet probability index (WPI) to provide a quantitative measure of data/model agreement. WPI is simply the integral of the joint probability distribution of the wavelet transform for two time series (Figure 3.2a). As such, it is constrained to have a value

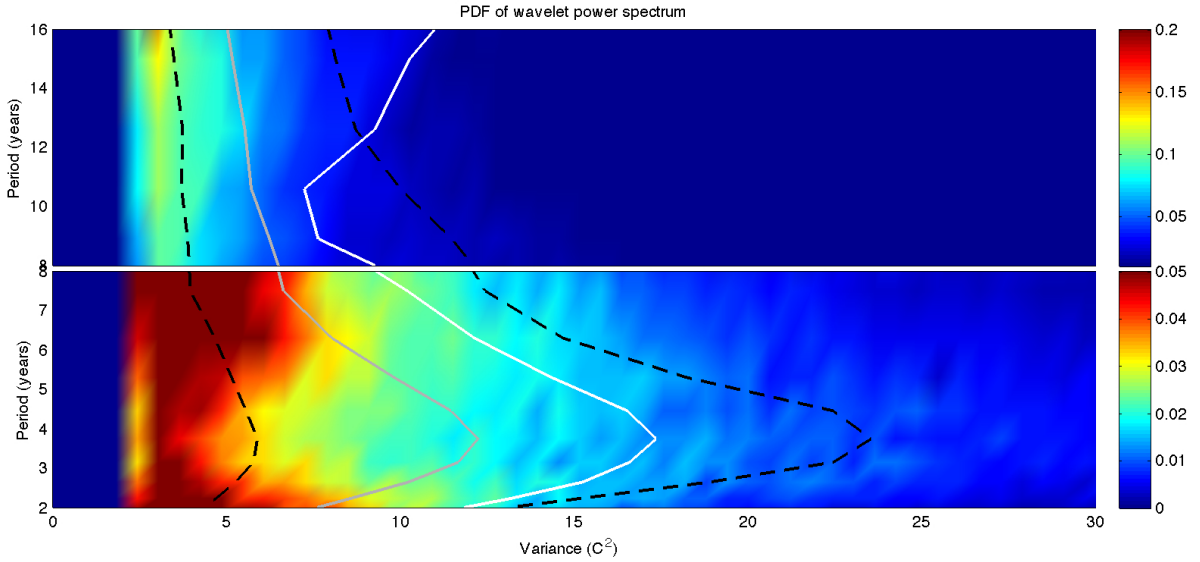

Figure 3.1: Figure 1 from ([Stevenson 2010]; Appendix 2). "Probability distribution functions for mean NINO3.4 wavelet power. The gray line represents the median value for the model simulation, while the white line is the mean value generated using the CORE hindcast. Dashed black lines correspond to the 25th and 75th percentile values for the model simulation (interquartile range)."

between 0 and 1, with higher values indicating that the similarity between the time series is larger. Mathematically, the WPI is defined as:

$$WPI(\nu) = \int_0^\infty F(\sigma, \nu) d\sigma = \int_0^\infty f_1(\sigma, \nu) f_2(\sigma, \nu) d\sigma \tag{3.3}$$

where $f_1(\sigma, \nu)$ and $f_2(\sigma, \nu)$ are two PDFs of wavelet power σ at frequency ν. The value of WPI relative to its distribution then becomes the statistic for testing differences between ENSO spectra, the equivalent of using the T and F distributions for the T and F tests. In those tests, however, the distribution of the test statistic was known, and the value computed for a given test used to derive statistical significance. Here the entire idea was not to specify an *a priori* distribution for the WPI, so this must be derived empirically for the application at hand. All possible non-overlapping subsets of the time series are compared, whose joint probability distributions yield various WPI values (a schematic is shown in Figure 3.2). This then forms the WPI distribution.

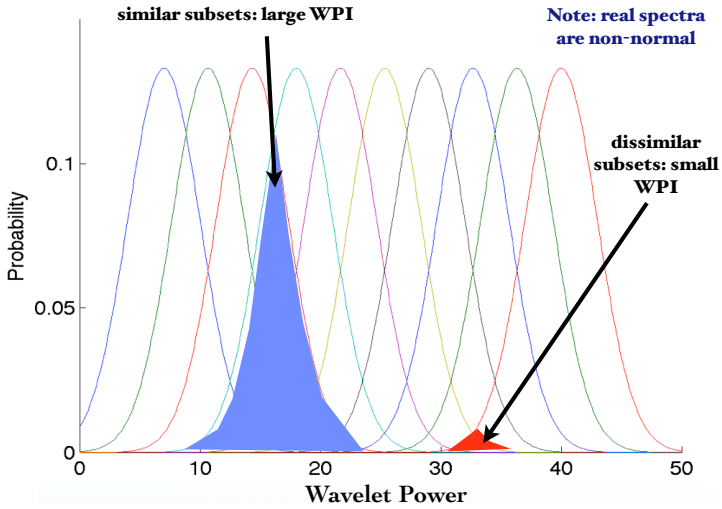

Figure 3.2: Schematic illustrating the calculation and distribution of the wavelet probability index. a) WPI value for a single comparison. b) generation of the WPI distribution; dissimilar (similar) subsamples have small (large) WPI.

The technique naturally lends itself to several different applications: one may compare the relative performance of two different climate models (Section 3.3), compare subsamples within a given time series (Section 3.5), or validate a model against observations (Section 3.4).

3.3 Comparing Model Performance

To compare the performance of two climate models using WPA, first what is needed is a 'reference' time series. This may be a control simulation if the goal is to diagnose responses to climate change (see Chapter 4), or it may be a set of observations if the goal is to find out which model has a better simulation of the 20th century. The reference time series provides a consistent dataset against which to measure changes in spectral behavior: it is compared with subsamples of each time series to form two WPI distributions. Then one may answer the question: Are subsets of one time series more similar to the reference than subsets of the other?

An example of WPI distributions used to diagnose the response to climate change in the CCSM4

([Stevenson 2011b]; Appendix 3) is shown in Figure 3.3, where the distributions have been smoothed using kernel density estimation. Here the reference time series is the 1300-year CCSM4 control simulation [Deser 2011] and the WPI distributions were created using subsamples of the 20th and 21st century ensembles. 90% confidence intervals on WPI are shown as the horizontal lines.

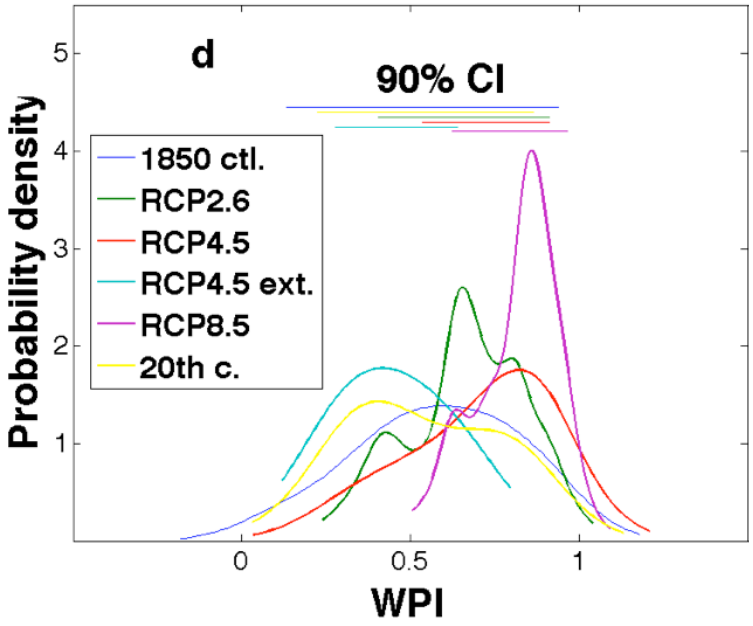

Figure 3.3: Figure 2d from [Stevenson 2011b], showing the WPI distributions generated from comparing subintervals of the CCSM4 20th and 21st century simulations with subintervals of the CCSM4 1850 control simulation. Here 30 years is used as the length for all sampling intervals.

The issue which must now be confronted is how to decide when changes to the WPI distributions are significant. The approach I have taken in ([Stevenson 2010]; Appendix 2)is to simply compute the confidence intervals and to see whether they overlap. The significance at level α is computed by finding the 1-α% confidence intervals and testing for overlap between them. Thus, differences at the 90% significance level ($\alpha = 0.1$) correspond to the situation where the 90% confidence intervals do not overlap. This is most likely not the most accurate way to diagnose the significance of changes, but in the absence of a less sensitive significance test is the best I have been able to do.

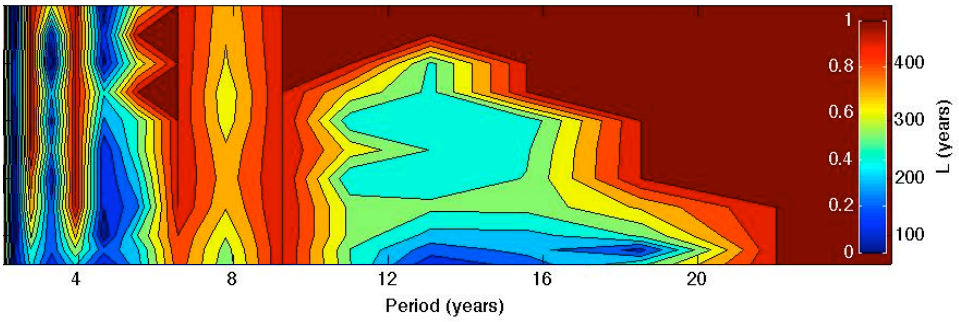

Figure 3.4: Selected panels from ([Stevenson 2010]; Appendix 2)Figure 3, showing the results of testing the CCSM3.5 and CM2.1 control simulations against one another using the CORE hindcast as a reference. In all panels, confidence levels plotted range from 0 (agreement) to 1 (disagreement).

The diagnosis of differences between models seems to work relatively well, in that the results are consistent with the qualitative assessments performed by previous researchers. As an example, see Figure 3.4, which is a reproduction of a panel from ([Stevenson 2010]; Appendix 2) Figure 3, showing the differences between a control simulation with the GFDL CM2.1 [Wittenberg 2009] and a control simulation with the NCAR CCSM3.5 ('PI' in Chapter 6). The models are broadly consistent with one another, but show some substantial differences at longer periods. Given the short extent of modern observations, diagnosing the sources of long-period offsets is difficult. However, the known biases in the GFDL CM2.1 ENSO-extratropical teleconnection patterns [Wittenberg 2006] may account for some of the differences seen in Figure 3.4.

3.4 Comparing a Model with Observations

The process for comparing a climate model with observations is nearly identical to that for comparing two models with one another. This time, the WPI distribution generated from comparing subintervals of a model simulation is tested against that generated from comparing subintervals of the simulation to observations (the reference). Figure 3.5 shows the results of performing such a comparison. Here the various horizontal lines indicate significance levels of 90%, 95% and 99%; differences between the CCSM and observations (again, the ocean hindcast product of [Large 2008])

are insignificant for the most part. Insignificance is denoted by a value for 1 - α_{max} of less than 0.9 in Figure 3.5.

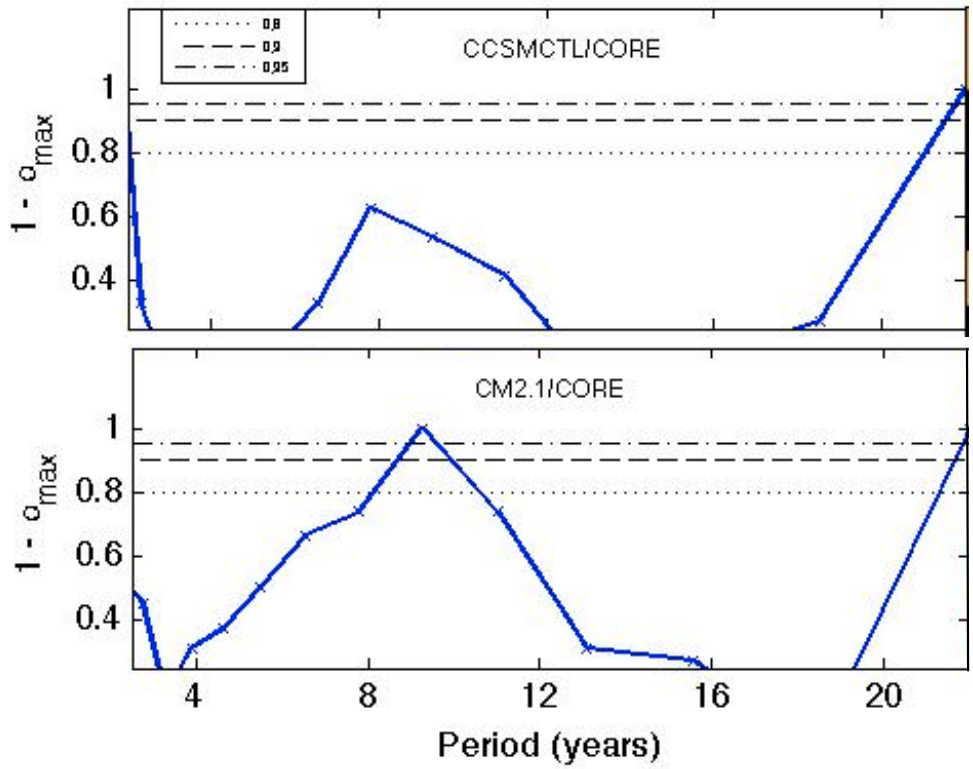

Figure 3.5: Selected panels from ([Stevenson 2010]; Appendix 2)Figure 3, showing the results of testing the CCSM3.5 and CM2.1 controls against observations (CORE hindcast). Subinterval length used here is 55 years.

Despite the insignificance of differences, there may nonetheless be a true offset between the model and observations (Figure 3.6). If the modeled and observed NINO3.4 SST values were truly generated from the same distribution, then one would expect that the upper bound of the 90% confidence interval would approach 1 as the subinterval length became longer: but this does not seem to be the case in Figure 3.6. This suggests that the WPI-based approach is detecting a real difference between the two time series, which is borne out by the fact that the upper limits for model subintervals compared with each other do approach 1 as their length increases.

Choosing larger 'chunks' of the model simulation results in differences with the ocean hindcast

Figure 3.6: Selected panels from ([Stevenson 2010]; Appendix 2)Figure 2, showing the 90% confidence intervals on WPI distributions generated from the CCSM3.5. Left: self-overlap calculations. Right: model/data distribution using the CORE hindcast.

which are significant at much higher levels than those in Figure 3.5 ([Stevenson 2010], not pictured). There may be sampling influences at play: the 1000-year CCSM3.5 simulation is able to represent a much larger degree of natural variability than is present in the 55-year hindcast. Some of this variability may or may not be consistent with the true extent of natural variability, but it is impossible to distinguish the two using such a short record.

3.5 ENSO Self-Convergence

What exactly *is* the length of time needed to observe ENSO before the full range of natural variability has been sampled? The limitations of paleoclimate indicators mean that this question cannot yet be answered precisely (Chapter 2), but model simulations can provide some insight. Comparing the WPI confidence intervals in Figure 3.6, it is clear that the width of the confidence interval decreases with subinterval length. When using WPI calculated from model subintervals compared to one another (hereafter the 'self-overlap' distribution), the decrease in 90% confidence interval

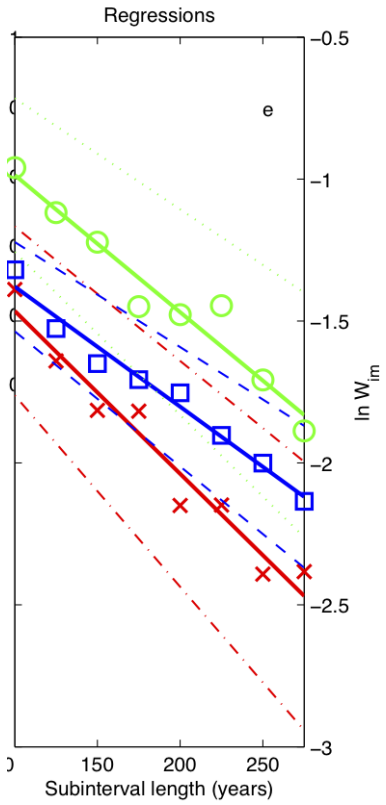

Figure 3.7: Figure 2 from ([Stevenson 2010]; Appendix 2), showing the regression of 90% confidence interval widths against subinterval length, for self-overlap calculations. CCSMcontrol (NCAR CCSM3.5) data appears as red X's, GFDL CM2.1 as blue squares and IPSL CM4 as green circles.

width with length is well fit by an exponential decay curve:

$$lnW_{90\%} = \beta_0 + \beta_1 L \tag{3.4}$$

where L is the subinterval length and $W_{90\%}$ the width of the self-overlap confidence interval.

The decay curve is plotted in Figure 3.7, for three different coupled climate models: the NCAR CCSM3.5, GFDL CM2.1 and IPSL CM4 (E. Guilyardi and M. Khodri, personal communication). What is remarkable about Figure 3.7 is that the decay rate is statistically identical between all three models, which were derived using very different model physics and have very different simulated ENSO behavior [Capotondi 2006]. This implies that there is something fundamental about the

ENSO spectrum which causes the decay rate to be so similar between models[1]. To test how the rate of WPI convergence compares with what one would get from simple noise, I ran tests using 1500-year time series of red and white noise processes. The results are shown in Figure 3.8. I note that the plots in Figure 3.8 use a significance level of 50% to exclude noise from the wavelet spectrum prior to the WPI calculation, rather than the 90% used in previous calculations. This was necessary to prevent the entirety of the AR(0)/AR(1) time series from being discarded.

I find that *both* the red and white noise spectra are able to reproduce the self-convergence behavior of the coupled climate models relatively well. This is a striking result, and may have implications in terms of how the long-term predictability of ENSO is understood. Oceanic variability is often modeled as a red-noise process, while atmospheric variability more closely resembles white noise [Hasselmann 1976, Frankignoul 1977]: in either case, the memory in the system may be contributing to the WPI convergence rate. Since these rates are roughly identical for both cases, it is not possible to distinguish between them on the basis of these results. However, the noise comparisons do indicate that the inter-model agreement likely represents more than sheer coincidence.

The stable rate of exponential decay in Figure 3.7 is convenient in the sense that it allows the necessary length of time for the oscillation to converge to be derived analytically. To do this for a particular model, the intercept β_0 must be estimated using a short integration of the model; then L, the required length for stable ENSO statistics, is the value at which the confidence interval width $W_{90\%} = 0.1$. This leads to estimates of roughly 250-370 years for the three models considered ([Stevenson 2010]; Appendix 2).

The derivation of the necessary run length for a given model is important since many of the control simulations currently used for climate change studies are much shorter than this. There is currently a push towards using longer control simulations, and some of the CMIP5 groups have adopted millennial-scale controls [Deser 2011, Wittenberg 2009], but this is not part of the official CMIP5 experimental design [Taylor 2009]. It is my hope that this work can start to motivate

[1]Note that although the regression slope β_1 is the same between models, the intercept β_0 does differ: this can be interpreted as a difference in the degree to which self-convergence is 'built in' to the particular model ([Stevenson 2010]; Appendix 2).

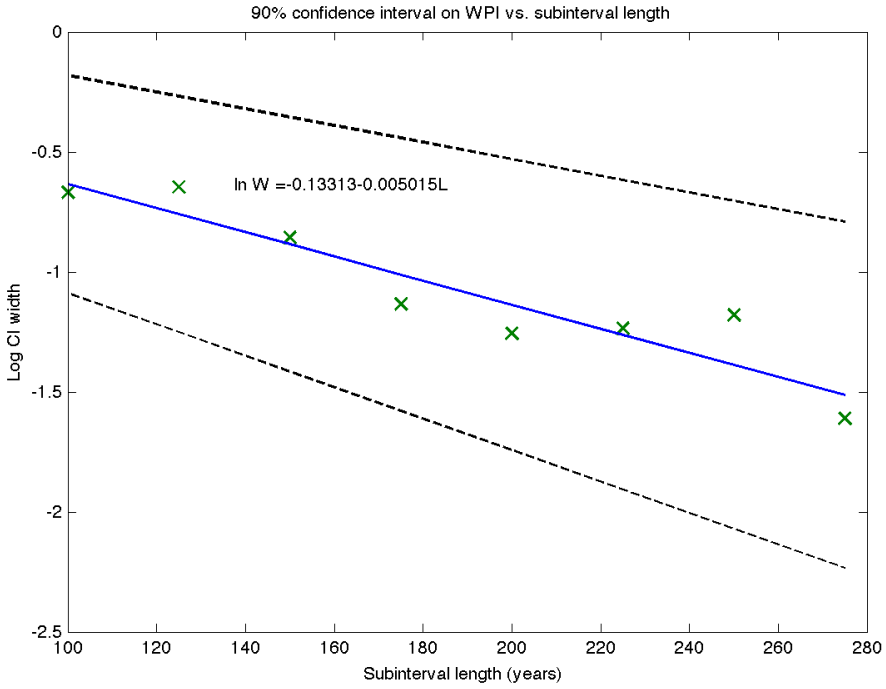

(a)

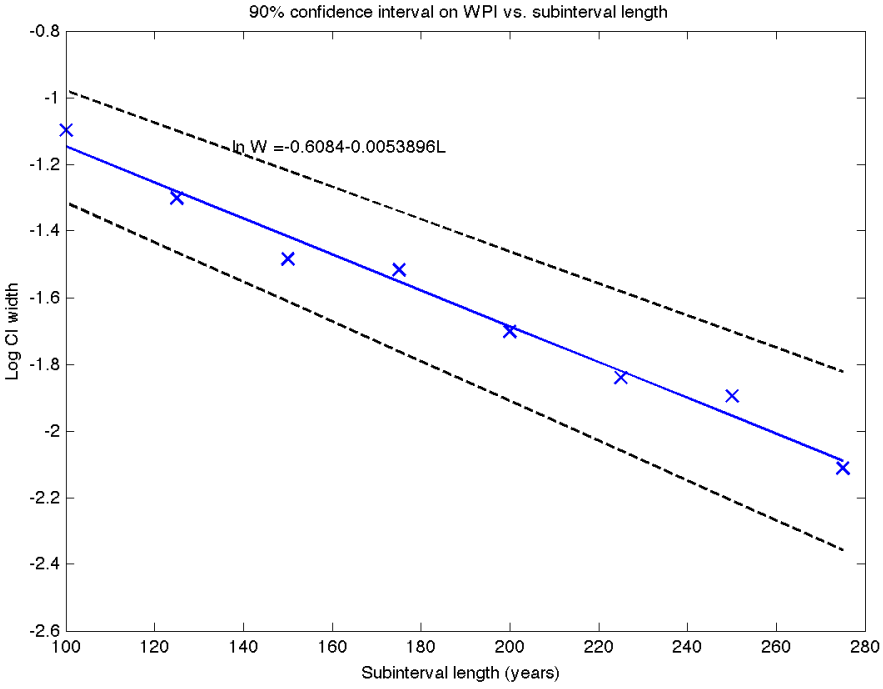

(b)

Figure 3.8: Self-overlap regressions for (a) red and (b) white noise spectra.

additional attention to longer stabilized control simulations (see also Chapter 6).

Table 3.2: Regression parameters for several test cases.

Time Series	β_0	β_1	$\Delta\beta_0$	$\Delta\beta_1$
White (AR(0))	-0.608	-0.0054	-0.720 - -0.497	-0.0060 - -0.0048
Red (AR(1))	-0.133	-0.0050	-0.433 - 0.167	-0.0065 - -0.0035
CCSMCTL	-0.891	-0.0057	-1.09 - -0.694	-0.0067 - -0.0047
GFDL CM2.1	-0.956	-0.0042	-1.06 - -0.852	-0.048 - -0.0037
IPSL CM4	-0.504	-0.0048	-0.683 - -0.324	-0.0057 - -0.0039

Chapter 4

Will There Be A Significant Change to El Niño in the 21st Century?

Contents

Climate changes within the 20th century have been well documented, and all indications are that changes will continue into the 21st century and beyond [Pachauri 2007]. As the climate warms, the circulation of the atmosphere and ocean are expected to change as well: along with these changes come potential influences on ENSO and its impacts.

Rather than considering individual events, what is usually done in GCM studies of ENSO and climate change is to consider the change to overall ENSO amplitude. Agreement between different models has historically been poor, however: as of CMIP3, roughly half of the models predicted an increase in ENSO amplitude with CO_2 increase, half a decrease, and some showed responses which were statistically identical to zero (Figure 1.7). Taken along with the results of the preceding chapters, this implies that we need to think carefully about the statistical significance associated with projections of 21st century ENSO changes.

Here I explore the effect of increasing ensemble size on the significance of ENSO response, and

examine some of the implications for GCM studies of ENSO more generally. The majority of these results have been published in ([Stevenson 2011b]; Appendix 3).

4.1 Simulations

The version of the model used in this study is the most recent incarnation of the NCAR Community Climate System Model (CCSM), version 4 [Gent 2011]. The CCSM4 does not include dynamic representations of the ecosystem, but represents a substantial advance in the representation of the physical climate system over the CCSM3. The differences are described in detail in [Gent 2011], but the most relevant changes for ENSO include ([Stevenson 2011b]; Appendix 3):

Changes to the atmospheric convection scheme. The convective parameterization developed by [Richter 2008] has been implemented, which includes the ability of convective plumes in the tropics to dilute and to transport momentum. These adjustments result in a substantial improvement in the representation of tropical climate in general [Neale 2011a], and ENSO in particular [Neale 2008]. The Madden-Julian Osscillation (MJO) is also improved in CCSM4 [Subramanian 2011].

Improved representation of the Equatorial Undercurrent (EUC). The tropical temperature bias in CCSM4 is much improved over CCSM3, and much of that improvement is thought to be due to the improved representation of the EUC [Large 2006]. Oceanic diffusion is now dependent on background stratification [Danabasoglu 2007], the vertical resolution has been increased from 40 to 60 levels, and the diapycnal diffusivity has a more realistic value [Jochum 2009].

Reduced bias in the equatorial cold tongue. As noted in Section 1.4, the equatorial cold tongue is typically too cold and extends too far west in GCMs; both biases were quite pronounced in CCSM3. The bias is much reduced in the CCSM4, which may be due in part to the sharper equatorial currents and corresponding improvements in simulating tropical instability waves [Jochum 2008].

Table 4.1: Table 1 from ([Stevenson 2011b]; Appendix 3). For transient simulations, the CO_2 value quoted is the approximate value at the end of the simulation period.

Simulation	Length (years)	Ensemble size	CO_2 (ppm)	Stable/transient
1850 control (PI)	1300	1	250	Stable
20th century	156	6	350	Transient
RCP 2.6	95	5	450	Transient
RCP 4.5	95	5	550	Transient
RCP 4.5 extension	200	1	550	Stable
RCP 8.5	95	1	1300	Transient

The simulations used in this chapter are summarized in Table 4.1; this is reproduced from Table 1 of ([Stevenson 2011b]; Appendix 3). I have referred to simulations with stabilized top-of-atmosphere radiative forcing as "Stable" and simulations representing climate change as "Transient". The "transient" simulations are the 20th and 21st century ensembles; these are each composed of 5-6 simulations. Also included here are the stable 1300-year 1850 CCSM4 control [Deser 2011] and the 'extension' run for RCP4.5, which simulates a stabilized climate at 4.5 W m^{-2} top-of-atmosphere radiative imbalance out to 2300.

4.2 Statistical Significance

Here I combine several different methods for measuring the significance of ENSO climate change responses, to make sure the results are robust against the choice of analysis technique. All rely primarily on diagnosing SST variability, since this is the most commonly used measure of ENSO amplitude. In ([Stevenson 2011b]; Appendix 3) I have looked at variability in both the eastern and western Pacific, but find that the results do not change substantially: significance tests therefore focus on NINO3 SST, where the majority of the 'action' takes place.

The spectrum of NINO3 variability is shown in Figure 4.2 for all ensembles, where spectra have been calculated using a Morlet wavelet decomposition. The 'envelopes' shown in this figure are calculated by taking the spectrum of each individual ensemble member, then finding the distance

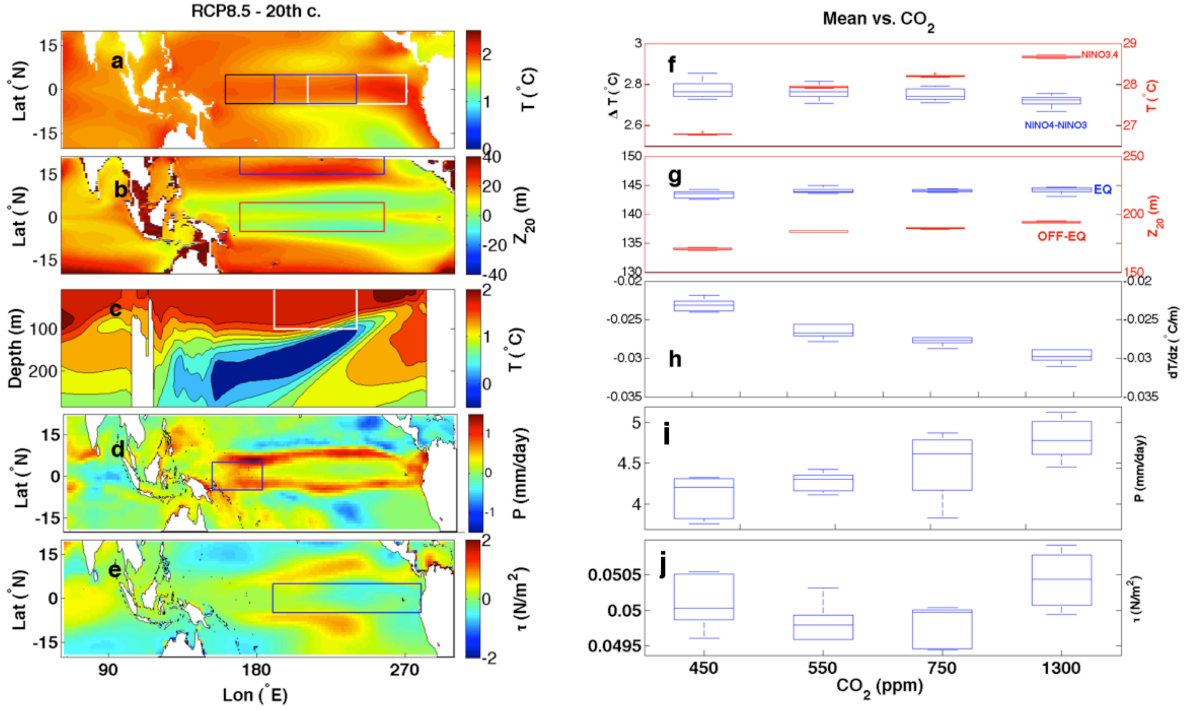

Figure 4.1: Figure 3 from ([Stevenson 2011b]; Appendix 3): "Summary of changes to the atmosphere/ocean mean state between CCSM4 ensembles. Lefthand column: ensemble-mean pattern of changes between RCP8.5 and the 20th century, with boxes indicating averaging regions. Righthand column: distribution of regionally-averaged diagnostics for each ensemble, corresponding to the quantity on the left, as a function of CO_2 stabilization level. (a) SST (°C); (b) Thermocline depth (Z_{20}); (c) Vertical temperature profile (°C); (d) Wind stress magnitude (N/m^2); (e) Precipitation (mm/day). Note that panel h shows the vertical temperature derivative dT/dz rather than the mean value of T(z); here z is positive downwards, and dT/dz has units of °C/m. In all righthand panels, the horizontal lines inside the boxes indicate the ensemble median, the extent of the boxes the distance between the 25th and 75th percentiles, and the whiskers the 2.5th and 97.5th percentiles. Where present, + symbols indicate outliers. All box averages on the right-hand side show the averages inside the boxes drawn on the lefthand panels: with the exception of panel h, which instead shows the vertical derivative of temperature averaged inside the box in panel c. "

between the minimum and maximum wavelet power. The most obvious feature in Figure 4.2 is the lack of change between ensembles, all of which overlap. Going from low CO_2 (20th century) to high (RCP 8.5), there does seem to be a tendency towards weaker ENSO amplitude, but based on the amount of overlap, one would intuitively tend to say that the decrease will not be statistically significant.

All significance tests agree with the intuitive expectation from Figure 4.2: as an example, see Figure 4.3 which shows not the spectrum, but the variance of NINO3 SST in the ENSO band (2-7 year periods). Confidence intervals are computed using a bootstrap randomization procedure applied by choosing subintervals of a given length. Here 'Full' refers to the use of the full ensemble member in each ensemble, and the other labels in Figure 4.2 to the appropriate subinterval length. The dependence of significance on subinterval length once again appears in Figure 4.3, where 30-year subsamples are unable to distinguish any ensemble from any other. More unexpected is the fact that using the full length of each ensemble member yields the same result.

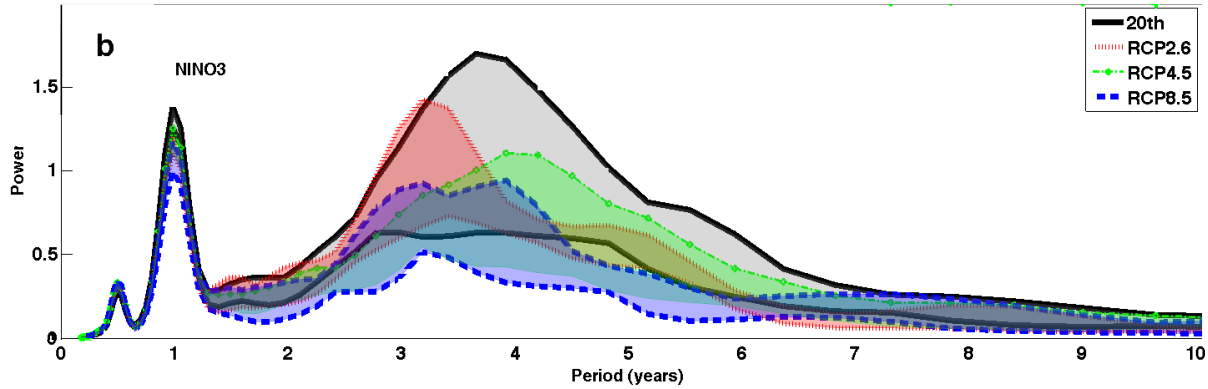

Figure 4.2: Figure 1b from ([Stevenson 2011b]; Appendix 3), showing spectral 'envelopes' for the NINO3 SST time series from the CCSM4 ensembles. Spectra are calculated using a Morlet wavelet transform of the SST timeseries. Envelopes for the ensembles are calculated by finding the maximum and minimum at each wavelet scale from spectra of each ensemble member.

Unfortunately, there does not exist a control run sufficiently long at high CO_2 to confirm that the weakening ENSO seen in the RCP simulations will eventually become significantly different from

PI. The RCP 4.5 extension run and PI are still statistically identical at 100-year sampling intervals (red bars in Figure 4.3), and the RCP4.5 extension is itself only 200 years long. In the absence of a longer control simulation, I can only speculate that CCSM4's ENSO will continue to weaken with sustained CO_2 increases.

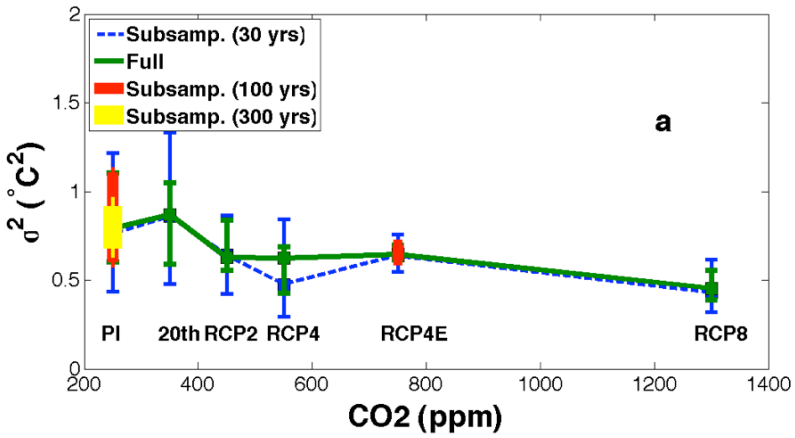

Figure 4.3: Figure 2a from [Stevenson 2011b], showing bandpassed NINO3 SST variance from the CCSM4 ensembles.

4.3 Oceanic Adjustment

The results of Section 4.2 seem straightforward in some sense, since they simply imply that the 20th century is too short to properly constrain ENSO statistics. The surprising aspect of these results is that what was analyzed in Section 4.2 was 5-6 separate realizations of the climate. In total, the 20th century ensemble has 936 model years and each of the RCP ensembles have 475; if simply having a given number of model years was sufficient to provide improvements to ENSO statistics, the CCSM4 ensembles should be well over the threshold. Given that even the ensemble means do not seem to differ (not pictured), what is causing the lack of statistical significance in the ENSO response to climate change?

The difference seems to be the delayed response of the ocean to the changes in radiative forcing

imposed by anthropogenic climate change; merely averaging together additional ensemble members, each of which experience the same change in greenhouse gas concentrations as a function of time, does not average out the effects of that change. Throughout the course of each simulation, the change in CO_2/greenhouse gas concentration changes the total heat content of the atmosphere: the effects of this heating tend to be amplified at high latitudes. The additional heat in the subtropical ocean then warms the water transported to the equator in the subtropical cell; eventually, a new equilibrium is reached. Communication between the subtropics and the tropics takes place on relatively long timescales: most models of the adjustment to an instantaneous temperature change show that the adjustment time is on the order of decades [Kessler 2006, Blanke 1997].

Shown in Figure 4.4 is the oceanic temperature and thermocline structure for RCP8.5; being the highest-CO_2 ensemble, the largest impact is seen here. Results for the other ensembles may be found in ([Stevenson 2011b]; Appendix 3). The difference between mean thermocline position during (2050-2100) and (2005-2050) are shown in the left-hand panel of Figure 4.4; as described above, the largest signal is seen in the extratropics. However, there is a large signal in the tropical temperature as well: see Figure 4.4, center panel, which shows the time-averaged vertical temperature profile for (2005-2050) and (2050-2100) in the 'equatorial', 'North', and 'South' boxes in the left-hand panel of Figure 4.4. There is a marked increase between the first and second halves of the simulation, due to the continuous rise in temperature throughout the course of the 21st century (Figure 4.4, right).

The large extratropical signals in Figure 4.4 support the hypothesis that the changes in tropical atmosphere/ocean mean state during the simulation period are driving variability within the 21st century which cannot be averaged out by increasing ensemble size. This means that in the real world, ascribing observed changes in ENSO to climate change may not become possible for a very long time.

The idea that the 21st century is too short to detect an ENSO response is further supported by results using other CMIP5 models. To date, the majority of modeling groups have run only one or two ensemble members for CMIP5: the exceptions to this are CanESM2, IPSL CM5 and CSIRO Mark 3.6. For these three models, therefore, I have reproduced the analysis for CCSM4 SST

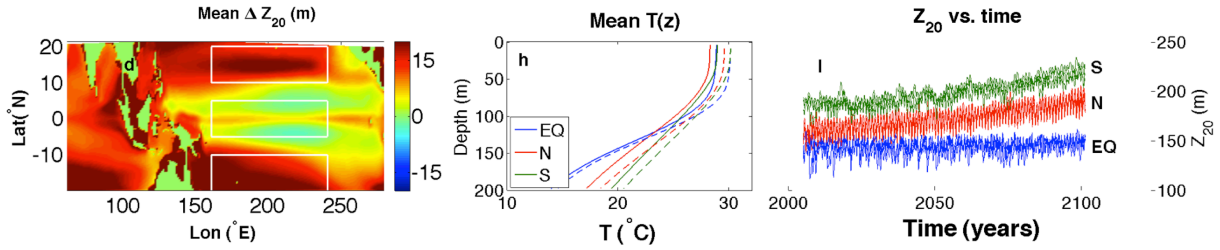

Figure 4.4: Figure 4 d,h,l from [Stevenson 2011b], showing the delayed response of the ocean to climate change in RCP 8.5. Lefthand panel shows difference maps taken between the first and second halves of the run: (2051-2100) - (2005-2050). Middle panel shows the vertical profiles of temperature averaged over the three boxes pictured at left: equatorial (EQ), northern (N) and southern (S). In these panels, the solid lines show the vertical profiles for the first half of the run and the dashed lines the profiles for the second. Righthand panel shows the time series of thermocline depth averaged over the same regions.

variability and find that the climate change response is also insignificant in all three (Figure 4.5).

4.4 Atmospheric Response

The response time of the atmosphere is much faster than that of the ocean. Perhaps this means that some of the atmospheric impacts of ENSO might show more rapid changes, even when the ocean response is insignificant.

My goal here is not to provide a comprehensive assessment of all possible ENSO teleconnections; I am only trying to provide a sense of whether it is *possible* for the atmospheric response to proceed on much faster timescales than the oceanic. As such, I have looked at some of the most commonly used diagnostics for atmospheric teleconnections. This analysis follows that used in [Deser 2006]: composites for El Niño and La Niña during DJF and JJA are constructed for each of the ensemble members. El Niño and La Niña events are defined as periods during which the DJF SST anomaly exceeded +/- 1 standard deviation, relative to a linearly detrended mean state. Figures 4.6-4.8 show the resulting composites: surface air temperatures are shown in colors and sea level pressure

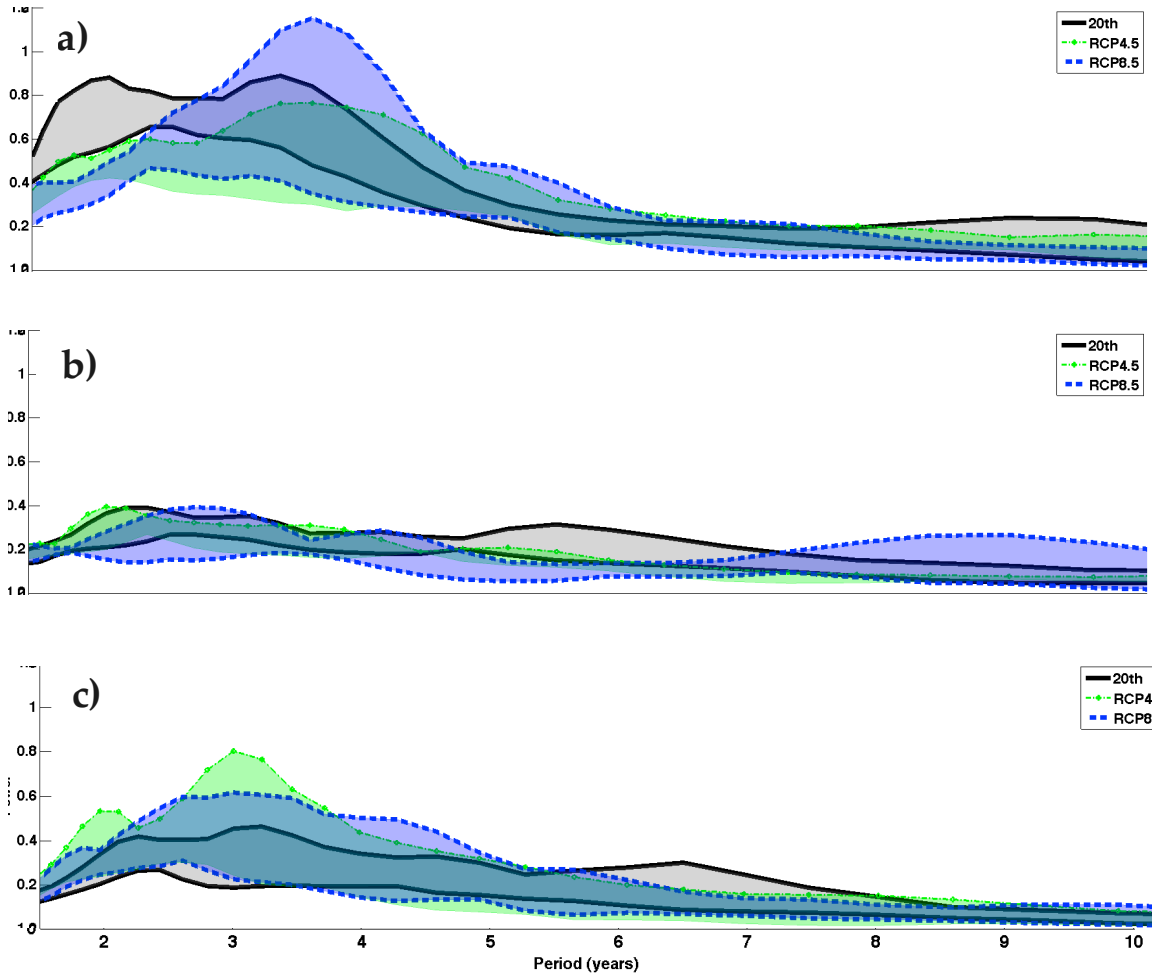

Figure 4.5: NINO3 spectra for the 20th century, RCP4.5 and RCP 8.5 ensembles using: a) the CanESM2, b) the IPSL CM5A, and c) the CSIRO Mark 3.6.

anomalies as contours. Changes to teleconnections are indeed statistically significant, but only during some seasons and only in certain regions. The largest changes are observed in the regions discussed in Section 1.3: south of the Aleutian Islands in the North Pacific, the western Pacific warm pool near Indonesia, and the Southern Ocean near 240°E.

In the North Pacific, the teleconnection changes are consistent with [Meehl 2007a], [Meehl 2007b]: the teleconnection pattern moves systematically to the north and east with CO_2. This is manifested during El Niño DJF as a negative SLP anomaly change over the northern US/Canada, and a positive one in the central Pacific just north of Hawaii (Figure 4.6). [Meehl 2007b] ascribe this change to a shift in the mean circulation, related to the development of an anomalous upper-tropospheric wave-5 response.

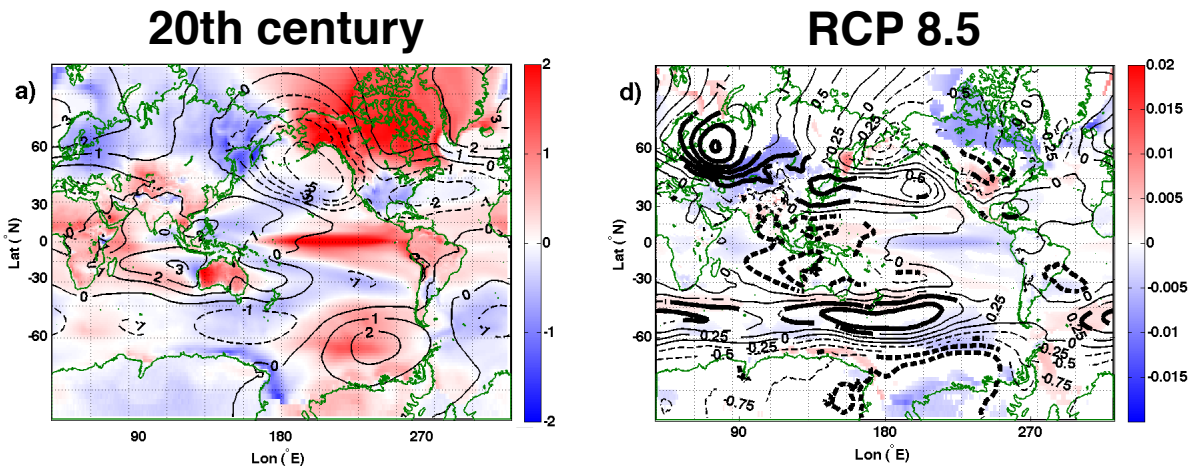

Figure 4.6: Panels a and d from Figure 5 in [Stevenson 2011b]: El Niño DJF. "a) Composite for 20th century ensemble. d) RCP 8.5 - 20th c. In all panels, surface air temperature (°C) is shown in color and sea level pressure (hPa) is shown in contours (contour interval 0.25 hPa). Negative anomalies are indicated as blue colors or dashed contours. In panel d, SLP anomalies significant at 90% are indicated by thicker contours, and only the significant surface air temperature values are plotted."

Australasian teleconnections seem to suggest an overall weakening of the ENSO influence with climate change. For example, the low pressure anomaly during El Niño DJF south of Tasmania

(30-40°S, 160-180°E) weakens with CO_2, as does the high over mainland Australia. This is shown in the right-hand panel of Figure 4.6 as a positive and negative anomaly in each of these regions, respectively. During La Niña DJF, the same pattern is seen, with opposite sign ([Stevenson 2011b]; Appendix 3). One might also view this as a weakening of the anomalous tropospheric convergence associated with warm SST anomalies in the region, which in turn might mitigate the associated reduction in rainfall. Perhaps droughts/flooding might become weaker in Australia during future El Niño/La Niñas?

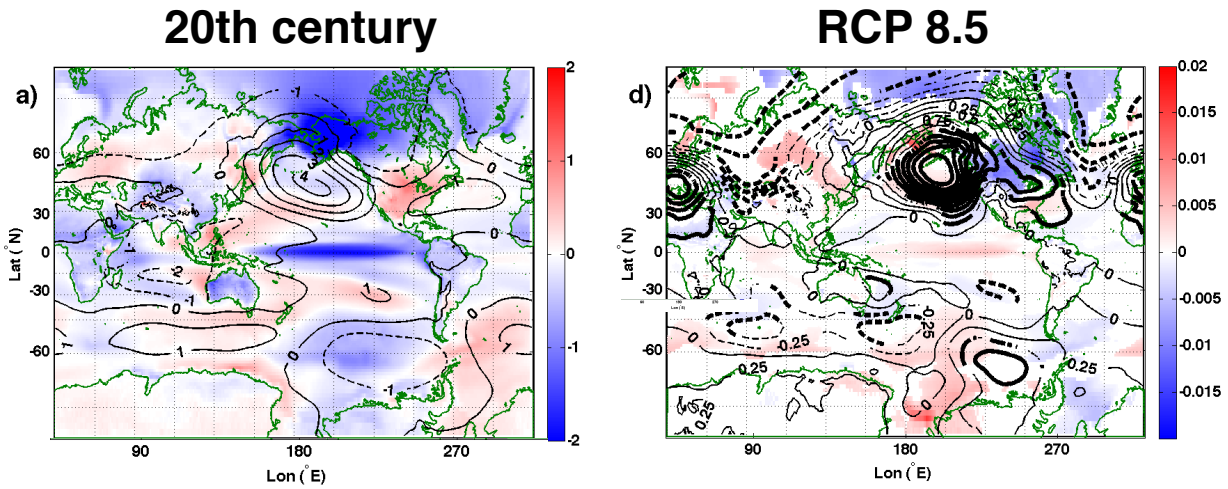

Figure 4.7: Panels a and d from Figure 5 in [Stevenson 2011b]: same as Figure 4.6 for La Niña DJF.

Finally, the teleconnection changes with the Southern Ocean become most apparent during JJA. I have included only the La Niña phase in this chapter (Figure 4.8), but the anomalies during El Niño are largely the reverse of this picture in the Southern Ocean ([Stevenson 2011b]; Appendix 3). Note that RCP 2.6 is included as the comparison case in Figure 4.8 rather than RCP 8.5; this is because RCP 2.6 shows the strongest change relative to the 20th century. I have not been able to identify an exact reason for the nonmonotonic behavior of this particular teleconnection, but can speculate that it may have to do with the fact that the TOA radiative forcing in RCP2.6 stabilizes more quickly than in either of the other two scenarios.

The low-pressure anomaly during La Niña JJA near 60°S, 240°E is apparent in the 20th century mean (Figure 4.8, left). This is consistent with the mean teleconnections described in [Turner 2004] (Section 1.3). However, looking at the RCP 2.6 anomaly a dipolar pattern of changes is visible, with a negative anomaly over the Amundsen-Bellingshausen Sea and a positive anomaly near the Drake Passage. This could be related to a shifting of the PSA pattern discussed in Chapter 1 - a northwestward shift of the PSA would be consistent with the expected slowdown of the Hadley circulation with climate change [Meehl 2007b], ([Stevenson 2011a]; Appendix 4).

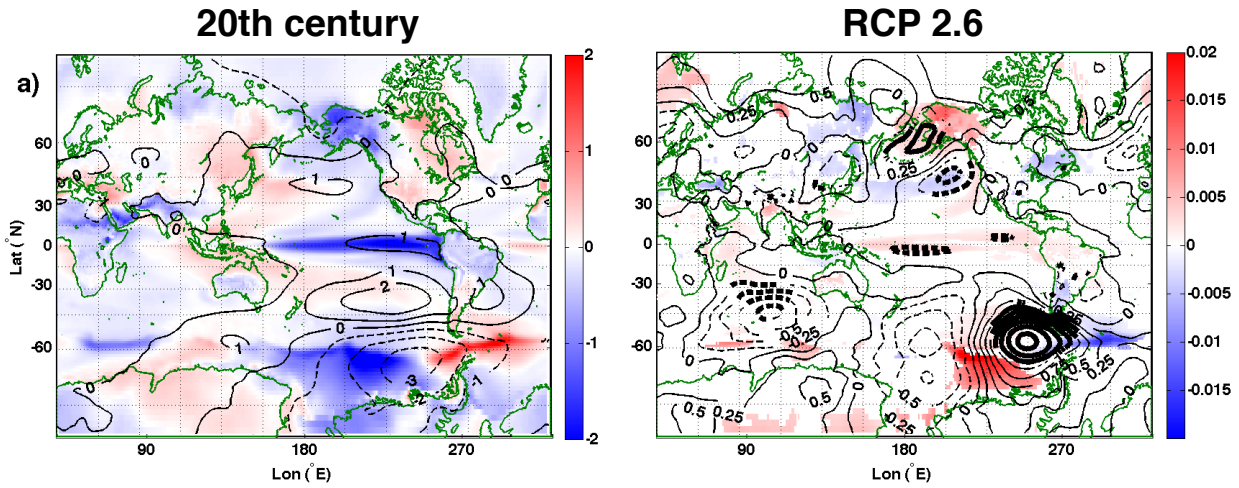

Figure 4.8: Panels a and d from Figure 5 in [Stevenson 2011b]: La Niña JJA.

Overall, the results of this chapter clearly demonstrate that changes to ENSO and to its teleconnections cannot be considered interchangeably, since the timescales for each are so different. Thus it may be possible to make predictions of societal impacts in the future, without knowing the details of how the oceanic dynamics may change.

Chapter 5

How Do El Niño/La Niña Characteristics Respond to Climate Change?

Contents

5.1 Event Characteristics

The previous chapter illustrates the potential importance of the different response times in the atmosphere and ocean. In a scenario when the oceanic ENSO response to climate change has not yet become significant, it is entirely possible that changes to atmospheric teleconnections may take place. This begs the question of whether the overall properties of El Niño/La Niña events may be distinguished from one another in such a scenario. Here I define event 'properties' as the magnitude and persistence of individual events. One may imagine that a given amount of SST variability may be created by El Niño/La Niña events with various combinations of magnitudes and lengths. Several very large events may cause the same amount of variance as many more smaller events. From Chapter 4, we know that the overall variability does not change significantly in the CCSM4 21st century ensemble. Does that necessarily mean the same thing for the events themselves?

The problem with considering event statistics in the CCSM4 ensembles is that their sizes are relatively small: the maximum ensemble size as of this writing was 6. But building up robust event statistics requires a much larger ensemble. In order to increase the effective ensemble size without spending many CPU hours re-running the CCSM4, one may build a statistical model conditioned on the CCSM4 ensembles, to generate additional time series having the same overall statistical properties. This provides a measure of the expected spread in event magnitude/persistence given a larger ensemble.

Many statistical models have been created for ENSO in the past; for instance, several forecasting models are used by the International Research Institute for Climate and Society (IRI) at Columbia University[1]. Notable examples include linear inverse models (LIMs; [Penland 1995, Penland 1993, Penland 1998]), canonical correlation analysis (CCA; [Barnston 1992, Barnett 1987]) and seasonal Markov modeling [Xue 2000, Xue 1994]. These, of course, are not the only statistical models in use: there are many more examples not discussed here [Tangang 1997, Clarke 2003, Landsea 2000, Mason 2002].

Generally speaking, the major limitation of statistical forecasting methods is that their results depend upon multivariate relationships observed in the past, and do not always account for the physical processes driving a particular event. For instance, LIM specifies a system using the empirically derived modes generated from the lagged covariance matrix, with stochastic perturbations applied to ensure that the dominant mode is robust against noise. The seasonal Markov model also uses the dominant covarying modes: in this case, EOFs are used to construct a seasonally varying Markov chain for forecasting.

To get away from the reliance of statistical models on the stationarity of past covariances, the use of coupled GCMs has risen in popularity as the representation of ENSO-relevant physics improves [Jin 2008]. A wide variety of GCMs are typically used in the production of operational ENSO forecasts, though this does not eliminate the influence of systematic model bias [Rosati 1997, Schneider 2003, Kug 2007, Kug 2008, Latif 1998]. Given the strengths and weak-

[1] http://portal.iri.columbia.edu/portal/server.pt?

nesses of the statistical and dynamical approaches, some combination of both seems to be the best bet for simulating the spread in El Niño/La Niña characteristics with climate change. This chapter presents an attempt to do just that.

5.2 Markov GLM methods

I have developed my own statistical model for predicting NINO3.4 SST, which relies on the combination of a Markov chain and a generalized linear model (GLM). The Markov approach allows the system state (El Niño, neutral or La Niña) during the previous seasons, as well as the probability of transitioning into a different state in the current season, to be taken into account. The GLM allows additional predictors containing physical information about the system to be included.

A generalized linear model is exactly what the name indicates: an extension of the 'classical' linear regression to more complex relationships, where the distribution of the variable involved need not be normal and the variables themselves need not be continuous [Dobson 2002]. In general, the prediction given by the regression model can be viewed as the expected value of the dependent variable (for example, NINO3.4 SST) given the independent variable (for example, mean zonal wind stress). The univariate linear regression of y on x can then be viewed as:

$$E(Y) = \mu = \beta_0 + \beta_1 x \tag{5.1}$$

More generally, given a set $\tilde{\mathbf{x}}$ of independent variables, a multivariate linear regression at timestep i yields a prediction for Y of

$$E(Y_i) = \tilde{\mathbf{x}}_i^T \beta \tag{5.2}$$

This formulation assumes that Y is normally distributed. However, the same approach can be used in the case where Y follows any of a class of exponential distributions

$$f(y|\theta) = exp[a(y)b(\theta) + c(\theta)d(y)] \tag{5.3}$$

where θ is a single parameter specifying the distribution [Dobson 2002].

The other strength of the GLM framework is that both continuous and categorical variables may be included. For a categorical variable (*i.e.* El Niño/La Niña state), the variable is transformed using a function called the link function, which has a specified form for any given member of the exponential distribution family. In general, the link function g relates the predicted mean value of the dependent variable y to the (categorical) covariate x:

$$g(\mu_i) = \tilde{\mathbf{x}}_i^T \beta \tag{5.4}$$

For this particular problem, the system states are the only categorical variables: these follow a multinomial distribution. The link function in this case becomes the expression for the transition probability between states:

$$p = \frac{exp(\tilde{\mathbf{x}}^{\mathbf{T}} \beta_{\mathbf{j}})}{1 + \sum_{j=1}^{N_j} \tilde{\mathbf{x}}_{\mathbf{j}}^{\mathbf{T}} \beta_{\mathbf{j}}} \tag{5.5}$$

where j is the index for a given state. The regression is then performed using an algorithm written in R, and the set of best predictors obtained (see Section 5.3).

The model was validated against the 20th century ensemble to be sure that it correctly represented the majority of the statistics from the input time series: the overall performance is quite good. A sample of model diagnostics are shown in Figure 5.1, which gives selected panels from ([Stevenson 2012b]; Appendix 5) Figure 1. The seasonal variance is well captured by the model, and the magnitude of individual events is accurately represented. Not shown are the PDFs of El Niño and La Niña, which are also generally well represented ([Stevenson 2012b]; Appendix 5). This lends credence to the use of the model for generation of additional 21st century time series.

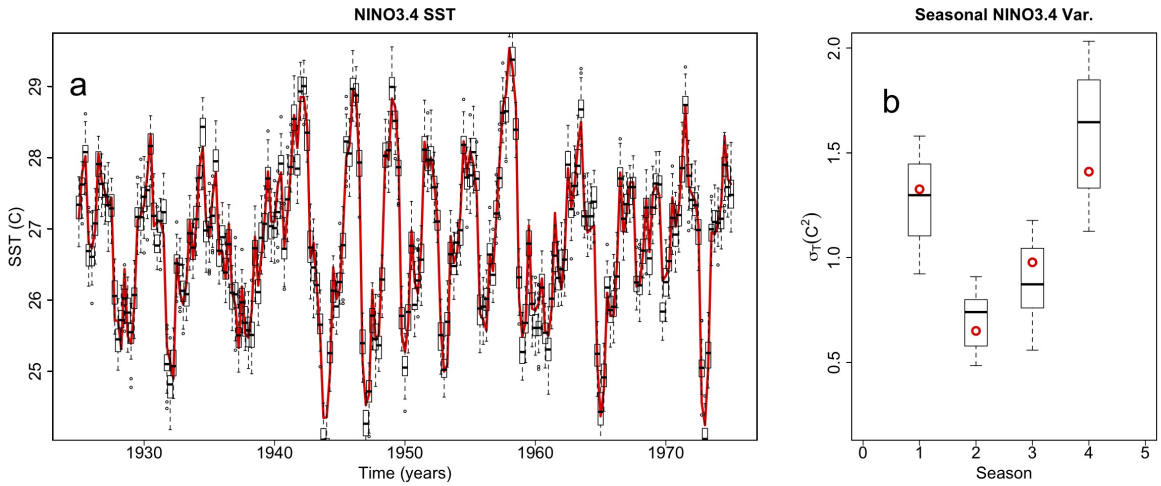

Figure 5.1: Figure 1a,b from ([Stevenson 2012b]; Appendix 5), showing a) the simulated NINO3.4 time series and b) the seasonal variance from the Markov GLM model.

5.3 Set of best predictors

One of the advantages of using a statistical model is the ability to study changes in the dependency of NINO3.4 SST on various physical parameters. But which variables are potentially the most important to begin with? This depends on the dynamics of the system being modeled.

I refer back to the oscillator models discussed in Section 1.2 for some general guidance, and choose to model a subset of the possible physical processes contributing to ENSO. Some measure of the development of SST anomalies will be necessary: thus I include the NINO3.4 SST during previous seasons. There will most likely be contributions from subsurface disturbances: the thermocline depth must be included. The zonal wind stress on and off the equator is related to changes in ocean heat content (Section 1.2), so this is included as well. Finally, the variance of the zonal wind stress in the western Pacific may trigger El Niño events: so this makes up the final set of predictors.

Variables are generated from box-averages of the relevant field, within regions chosen to maximize their correlation with the NINO3.4 SST. A schematic of the resulting predictors is shown in Figure 5.2. Thermocline regions are chosen along the equator and near 10°N/S to capture Kelvin and

Rossby wave excitation. Interestingly, these latter two regions are very similar to the Rossby wave pathways seen in a previous version of the CCSM, and the correlations in the Northern and Southern Hemispheres are out of phase with one another: this points to a potential role of the seasonal cycle in the generation of El Niño/La Niña events ([Stevenson 2011a]; Appendix 4).

The zonal wind stress predictors are averaged in the north central Pacific, the Indian Ocean, and the equatorial central Pacific (Figure 5.2c). The equatorial correlation is a simple consequence of the [Bjerknes 1969] feedback. The North Pacific region likely comes into play during the generation of anomalous Sverdrup transport [Jin 1997]. Finally, the Indian Ocean anomalies are related to the shift in position of the mean convective center over the western Pacific warm pool during El Niño/La Niña.

The triggering of El Niño events by stochastic wind variability is a topic of much debate, as discussed in Chapter 1. There have been some efforts to catalog westerly wind burst activity by the region of wind variability, with the warm pool subdivided into as many as 8-10 regions [Harrison 1997]. I have not used such a complex system here, since the zonal wind stress variance is not a very important predictor of NINO3.4 SST (note the low correlations of variance with NINO3.4 in Figure 5.2d). Instead, I average the variance over the western Pacific warm pool and over the eastern Indian Ocean, for a rough idea of the efficiency of high-frequency wind variability in triggering ENSO events.

The choice of predictors is done using a stepwise regression algorithm, where successive subsets of the initially input regression parameters are taken until a 'best' prediction is achieved. Here I minimize the 'Bayesian information criterion', or BIC [Sakamoto 1986], to determine the best fit:

$$BIC = -2ln(L) + kln(N) \tag{5.6}$$

where L is the maximized value of the likelihood function for the model, k is the number of regressors, and N the length of the time series. For the exponential distribution,

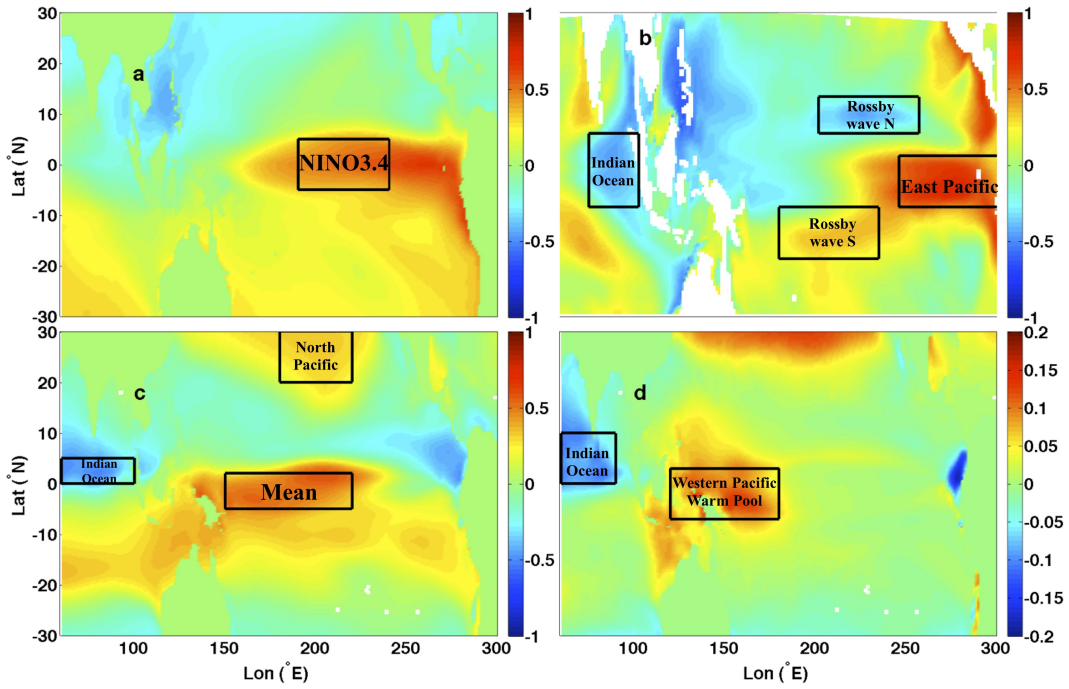

Figure 5.2: Figure 3 from ([Stevenson 2012b]; Appendix 5). "Lag-correlation maps with NINO3.4 SST, lag 3 months. a) SST, b) thermocline depth, c) zonal wind stress, d) submonthly zonal wind stress variance. Black boxes indicate the positions of the averaging regions used to generate the Markov GLM predictors, which are labeled according to the naming conventions in Table 5.1. Note that panel d uses a different color scale than panels a-c, owing to the much smaller correlations with wind stress variance."

$$L = \prod_{i=1}^{N} \lambda e^{-\lambda x_i} \tag{5.7}$$

The BIC penalizes models with larger numbers of regressors and is, as such, more parsimonious than other commonly used criteria [Akaike 1974]. Although not a guarantee that the regressors included in the model will be physically meaningful, using BIC nonetheless gives an idea of the true importance of a given predictor.

For each ensemble, time series of NINO3.4 and the predictors from each ensemble member are concatenated together and the GLM fit calculated for the full ensemble simultaneously. The set of best predictors for each ensemble is shown in Table 5.1: full details of the regression procedure are found in ([Stevenson 2012b]; Appendix 5).

Table 5.1: Table 3 from ([Stevenson 2012b]; Appendix 5). "Set of best predictors for the CCSM4 ensembles. Numbers indicate the value of regression coefficients for each ensemble/variable combination."

Predictor	20th c.	RCP 2.6	RCP 4.5	RCP 8.5
Lag-1 state	-0.119	-0.0404	-0.133	-0.117
Lag-2 state	0.587	0.430	0.588	0.527
Lag-3 state	-0.227	-0.203	-0.256	-0.165
Lag-1 value	0.114	0.083	0.149	0.108
RW path Z (N)	-8.99×10^{-5}	-7.56×10^{-5}	-1.03×10^{-4}	-6.58×10^{-5}
RW path Z (S)	9.24×10^{-5}	2.77×10^{-5}	1.48×10^{-4}	4.83×10^{-5}
Ind. Ocn. Z	1.12×10^{-4}	1.11×10^{-4}	4.84×10^{-5}	2.86×10^{-4}
E. Pac. Z	2.06×10^{4}	1.83×10^{-4}	6.59×10^{-5}	3.49×10^{-4}
Mean Taux	3.90	4.74	4.96	3.34
Ind. Ocn. Taux	-0.208	-0.474	-0.899	
N. Pac. Taux	0.0826			
WPWP Taux var.	-1.86	-1.39	-1.55	-1.37
Ind. Ocn. Taux var	-0.325		-0.496	
Sin	0.127	0.0833	0.105	
Cos	-0.153	-0.142	-0.0706	-0.0817

For the most part, the set of best predictors is relatively similar between ensembles. However, there may be a tendency for wind stress variables to become less important with increased CO_2.

For example, the North Pacific zonal wind stress disappears from the predictor set in the RCPs, and the Indian Ocean wind stress is not included in the RCP8.5 predictor set. Indian Ocean wind stress variance shows nonmonotonic behavior, appearing in the 20th century and RCP4.5.

The magnitudes of the regression coefficients do not show strong CO_2 dependencies: I therefore try not to draw too many conclusions from coefficient changes. I do note, however, that the changes are consistent overall with the known shifts in the Walker circulation: the convective cell moves east with CO_2 in the CCSM4 (Chapter 4), which one might expect to cause the western Pacific and Indian Oceans to become less important in initiating El Niño events.

5.4 El Niño/La Niña event statistics

I next examine the statistics of individual events. I have simulated each CCSM4 ensemble 1000 times using the Markov GLM, and present the resulting PDFs in Figure 5.3 (Figure 2 from ([Stevenson 2012b]; Appendix 5)). Here, magnitudes are calculated for each event as the mean NINO3.4 SST over the time during which the system was in the appropriate state. All of the RCP ensembles show a tendency towards narrowing of the La Niña magnitude PDF and a shortening of the high-power El Niño PDF tail (Figure 5.3a-c), relative to the 20th century.

There is a reduction in El Niño persistence in the RCP ensembles, especially in RCP2.6 (Figure 5.3d-f, g-i). For La Niña, in contrast, the changes in persistence PDF seem not to be as large; the RCP4.5 and 8.5 results in particular show that the interquartile range (IQR) for the simulated time series brackets the 20th century PDF (Figure 5.3h,i). In short: El Niño events tend to weaken and become less persistent with CO_2, while La Niña events weaken but do not change much in length.

The combined weakening of El Niño and La Niña events will lead to an overall weakening of the ENSO amplitude; this is completely consistent with the results from Chapter 4. The persistence results are somewhat surprising, and suggest that perhaps a portion of the ENSO weakening in the 21st century is caused by less persistent El Niños. I will also note here that even though the changes seen in magnitude and persistence make intuitive sense, they are not statistically significant given

that the IQR for the simulated time series so often covers the 20th century La Niña values.

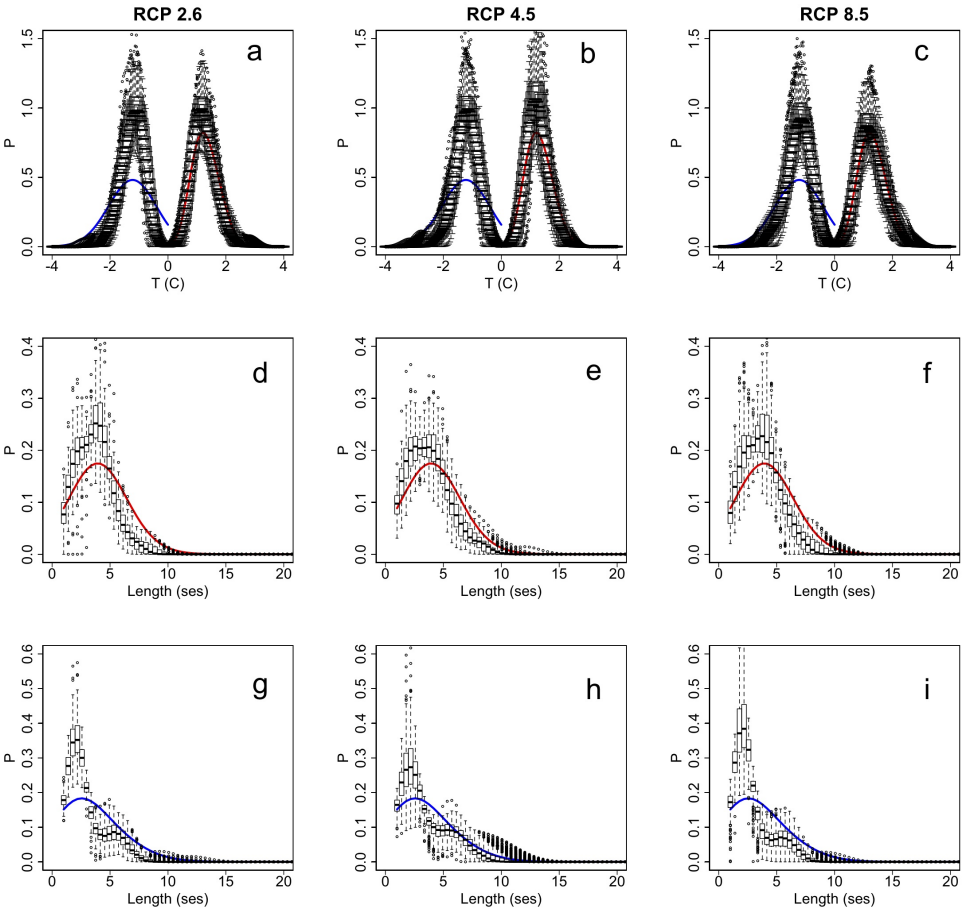

Figure 5.3: Figure 2 from ([Stevenson 2012b]; Appendix 5). "El Niño/La Niña statistics for the 21st century ensembles, simulated using the Markov GLM. Solid lines indicate the PDF for the 20th century, with red and blue indicating El Niño and La Niña, respectively. Event magnitudes appear in panels a-c; El Niño persistence in d-f; and La Niña persistence in g-i."

Finally, I consider the implications of these results for protracted El Niño and La Niña events. When one ENSO phase lasts longer than a few years, it can have profound implications for certain regions. In particular, El Niños longer than 5 years have been the subject of some debate, since estimating their expected return period under climate change is extremely difficult using the short instrumental record [Rajagopalan 1997, Trenberth 1996]. The large ensemble size and physically-based prediction method makes the Markov GLM an ideal candidate for repeating the calculation;

expected return periods for 5-year (20 season) El Niño and La Niña events are given in Table 5.2. Calculations are performed using the transition probabilities determined from the simulated NINO3.4 index:

$$R_{5yr} = p^{-N} \tag{5.8}$$

where N = 20 seasons and p represents the (El Niño-El Niño) or (La Niña-La Niña) transition probability calculated from that particular simulated time series.

Table 5.2: Table 2 from ([Stevenson 2012b]; Appendix 5). "Return periods for 5-year El Niño and La Niña events (units of years)."

Ensemble	10%, EN	Median, EN	90%, EN	10%, LN	Median, LN	90%, LN
20th c.	1,078	3,325	41,337	3,905	7,718	17,388
RCP 4.5	6,041	20,872	104,388	827	5,449	21,938
RCP 8.5	9,504	34,872	155,864	12,870	55,475	342,005

Table 5.2 shows that the median return periods for El Niño increase monotonically: protracted El Niños become less common with climate change. However, Table 5.2 also shows that the 90% confidence intervals on the return periods overlap: the return periods are statistically indistinguishable from one another. Likewise, the 90% confidence intervals for the return period of 5-year La Niña events also overlap between ensembles, despite the fact that the change in the median return period is no longer monotonic.

The overall conclusions that I draw from this analysis are that the characteristics of individual events change in ways that are reflective of the changes in overall ENSO strength in the CCSM4. The amplitude of ENSO tends to weaken with CO_2, due preferentially to a weakening of El Niño, with some La Niña weakening as well. Very strong events become less frequent with CO_2, and the El Niño events which do occur tend to be less persistent. This means that we can expect ENSO in the future to be both weaker and possibly more predictable overall... at least, if the results from CCSM4 are representative of the real climate. But even still, if the quantity of interest is the

appearance of El Niño/La Niña events which last for 5 years or longer, detecting any change to the frequency of those events will be basically impossible given observations of the 21st century alone.

Chapter 6

How Does CO_2 Affect ENSO Dynamics in a Stable Mean Climate?

Contents

6.1 Importance of An Equilibrated Mean State

Based on the results of the previous chapters, it becomes relatively simple to summarize the limitations of our ability to measure ENSO climate sensitivity ([Stevenson 2011a]; Appendix 4):

1. Sampling effects from using an insufficiently long record
2. Long-term background state shifts due to changes in the radiative forcing imposed on the ocean
3. Errors in model physics

I will not spend too much time addressing the last point since issues of model bias require a large sample of multi-century simulations with different GCMs, which currently do not exist (see Section 8.5.1). However, it is important to bear in mind that all of the model results in this dissertation will be subject to potential model biases. That said, the results of the last two chapters lead to a single conclusion. In order to understand the sensitivity of model ENSO to CO_2 increases, a series of model experiments is necessary where the *same* GCM is run for multiple centuries, changing nothing except the CO_2 concentration. I have conducted three such simulations with the CCSM3.5, a slightly older version of the CCSM4 which does not include some of the newest physical parameterizations. These experiments are constructed such that the mean climate in each simulation is stable, allowing influences from background heat content anomalies to be ruled out as potential drivers for dynamical change. Of course, this experimental design does not show the response to a time-varying forcing, which is the relevant question for climate change. Still, it provides mechanistic insight into the CO_2 response, which can then be used to understand the results of further climate change studies.

6.2 Simulations

The configuration of the model used in this chapter is discussed in ([Stevenson 2011a]; Appendix 4). I have used a low-resolution version of the CCSM3.5 called the T31x3, which uses T31 spectral truncation in the atmosphere (roughly 3.75° resolution) and a spatially varying resolution in the ocean. The ocean model places the north pole over Greenland, and the resolution in that region is roughly 40km x 40km. Zonal resolution in the ocean is larger at the equator (340km), and meridional resolution varies as well: 70km in the equatorial region and 350km in the North Pacific. This grid configuration is designed to provide the best possible representation of deep convection in the Arctic and upwelling/heat uptake along the equator.

The T31x3 was designed to run efficiently for long periods of time, and was primarily intended for paleoclimate applications. A description of the T31x3 CCSM3 is available in [Yeager 2006]: the present configuration differs from that setup in several ways. In the atmosphere, the most

important difference is the use of the new convection scheme described in [Neale 2008]. In the ocean, changes were made to the thickness diffusivity [Danabasoglu 2007], which is now a function of ocean stratification, and to the diapycnal diffusivity [Jochum 2009]. The ocean viscosity was also reduced to a more realistic value [Jochum 2008]. These changes are similar to those implemented in the CCSM4, and the ENSO representation in the T31x3 CCSM3.5 is as good as the CCSM4, if not better [Neale 2008, Deser 2011].

The three simulations I conducted were all begun at the same initial condition: the climatology of [Levitus 1998]. CO_2 was then set to one of three values, and the model integrated for 1000 years. Each model reached equilibrium after about 200 years, and no additional external forcing was applied. Model years 200-1000 were used in the analysis to prevent contamination from ramp-up effects. CO_2 values were chosen to span the range of observed CO_2 concentrations over the past 100 years, and some of the range expected in the future: values are 255, 355 and 455ppm. Hereafter, the simulations are referred to as 'pre-industrial' (PI; 255ppm), 'present-day' (PD; 355ppm) and 'high-CO_2' (HC; 455ppm).

6.3 Statistical Significance

The assessment of statistical significance in the CCSM3.5 runs is very similar to the analysis performed in ([Stevenson 2011b]; Appendix 3) for the CCSM4 simulations. A full description is available in ([Stevenson 2011a]; Appendix 4).

The spectrum of NINO3 SST is presented in Figure 6.1. Here, the scatter between 100-year subsamples is used to construct 'envelopes' of variability: subsamples were randomly chosen from the simulation period, and the wavelet spectrum recomputed for each according to the wavelet toolkit of [Torrence 1998]. As in Chapter 4, the Morlet wavelet basis function was used, and the bias correction of [Liu 2007] applied to prevent the artificial enhancement of wavelet power at large periods.

The most notable result in Figure 6.1 is the increase in spectral power at 2-5 year periods as

CO_2 increases. The increase between PI and PD is small, and there is some overlap between the envelopes. Changes in HC are larger: this simulation shows a substantial increase in power over both of the other two. I also note that this increase is seen using 100-year intervals, which are expected to experience substantial natural variability (Chapter 3; ([Stevenson 2010]; Appendix 2)). This is therefore an indication that the ENSO amplitude is quite sensitive to CO_2.

Changes at other periods are also interesting. There is a definite enhancement with CO_2 in the power between 6-18 month periods in Figure 6.1. Longer periods, however, seem to be less sensitive to CO_2: the spectral envelopes in Figure 6.1 are indistinguishable at periods longer than 5 years, which in itself is an interesting result. More details on longer-period variability may be found in Section 6.7.

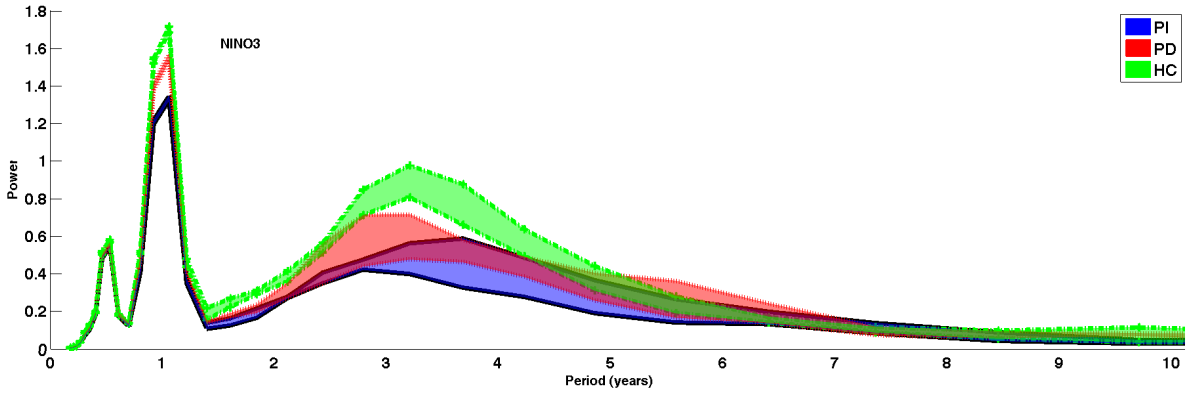

Figure 6.1: Figure 1a from ([Stevenson 2011a]; Appendix 4), showing the variability of the NINO3 SST. Spectra for 100-year subsamples of each simulation are calculated using the Morlet wavelet transform, and envelopes represent the scatter between them.

To confirm that the spectral results in Figure 6.1 are not an artifact of the wavelet decomposition, I next show the variance of NINO3 SST, bandpass filtered to lie within 2-4 and 5-7 year periods (Figure 2a,b from ([Stevenson 2011a]; Appendix 4)). Confidence intervals in Figure 6.2 are computed using a bootstrapping procedure, where subsamples of a particular length are selected randomly and the variance for each computed. This leads to a dependence of the 90% confidence

interval on the subsampling length, as would be expected. For 30-year subsamples, the variability is indistinguishable between all simulations. However, using 400-year subsamples it becomes possible to tell the difference between simulations: most likely the differences become significant at sampling intervals shorter than this. As for the spectra, an overall increase in 2-4 variance is observed, but the 5-7 year variance does not change significantly between any of the simulations.

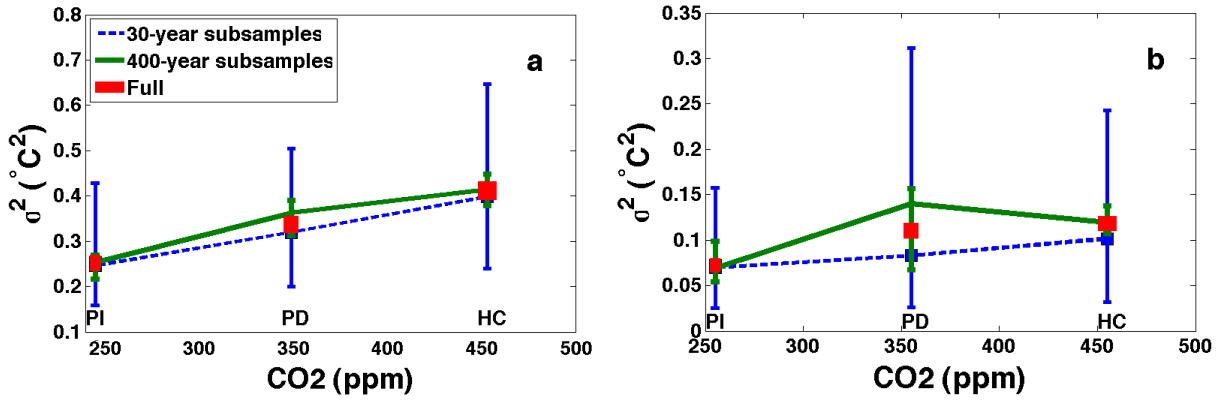

Figure 6.2: Figure 2a,b from ([Stevenson 2011a]; Appendix 4), showing bandpassed NINO3 SST variances bandpassed between a) 2-4 years and b) 5-7 years.

6.4 Circulation Changes

Changes to the mean state of the atmosphere are shown in Figure 6.3; here I have reproduced only the panels of Figure 3 in [Stevenson 2011a] which show the PD-PI differences[1] for wind stress, precipitation and vertical pressure velocity ω. The overall subtropical wind stress anomalies are primarily meridional, with northerly anomalies in the Southern Hemisphere and southerly anomalies in the Northern: this is consistent with a slowdown of the Hadley circulation. Anomalies along the equator have a stronger zonal component, tending towards weakening of the trade winds and therefore a weakening of the Walker circulation. The precipitation anomalies in the center panel of

[1]The shape of the HC-PD differences is largely the same as PD-PI: ([Stevenson 2011a]; Appendix 4).

Figure 6.3 are consistent with this picture: the eastward shift and weakening of the Walker cell is reflected in the negative anomalies in the Indian Ocean and positive anomalies in the central/eastern Pacific. Likewise, the equatorial ω anomalies show a similar pattern: the tendency is towards higher ω (weaker ascent) over the Indian Ocean and lower ω (weaker subsidence) in the central/eastern Pacific.

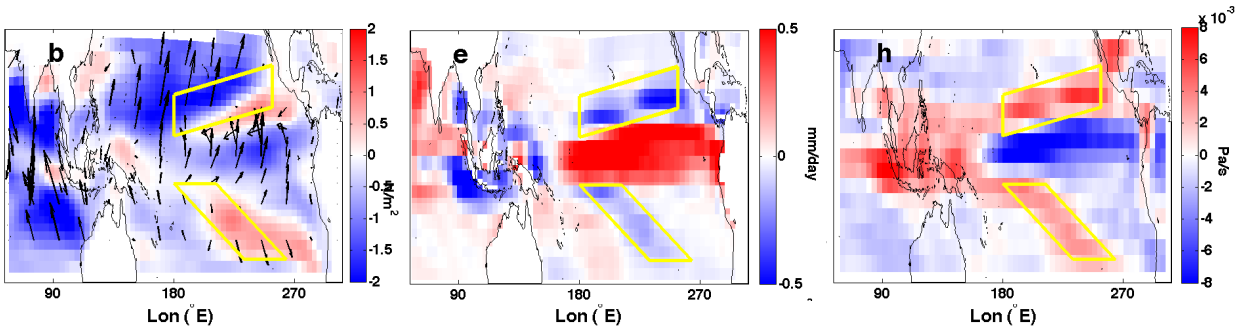

Figure 6.3: Figure 3b,e,h from ([Stevenson 2011a]; Appendix 4), showing changes in the mean atmospheric state between PD and PI. b: Wind stress magnitude (colors) and direction (arrows). e: Precipitation. h: Vertical pressure velocity ω. Yellow boxes show the approximate positions of the Rossby wave pathways active in the SFM-like mechanism discussed in the text.

The features highlighted in the yellow boxes of Figure 6.3 are quite interesting: here there is anomalous convergence in the Northern Hemisphere, and anomalous divergence in the Southern Hemisphere. In both regions, the mean changes to ω are positive and are just poleward of the main anomaly: these 'pathways' coincide with the regions previously identified as important for seasonal forcing [Alexander 2002, Vimont 2003] and are locations where Rossby waves tend to be active. The role of seasonal forcing will be discussed in more detail in Section 6.6.

The changes to the mean circulation of the atmosphere drive corresponding changes in the ocean. Generally speaking, the changes to the oceanic mean state in CCSM3.5 (not pictured) are in the same direction as the changes observed in CCSM4 ([Stevenson 2011a]; Appendix 4). The zonal SST gradient along the equator is reduced owing to enhanced warming in the eastern Pacific, and the vertical thermal and density stratifications increase as well. Transport in the subtropical cell (STC)

is reduced with CO_2 (Figure 6.4): changes typically range from 5-10%, and the majority tend to decrease the existing circulation. The exception is the surface region in the Northern Hemisphere near 5°N, where circulation increases slightly. This may be a locally driven circulation caused by the increased convergence near 5-10°N, which would tend to enhance the existing subduction in the northern branch of the STC.

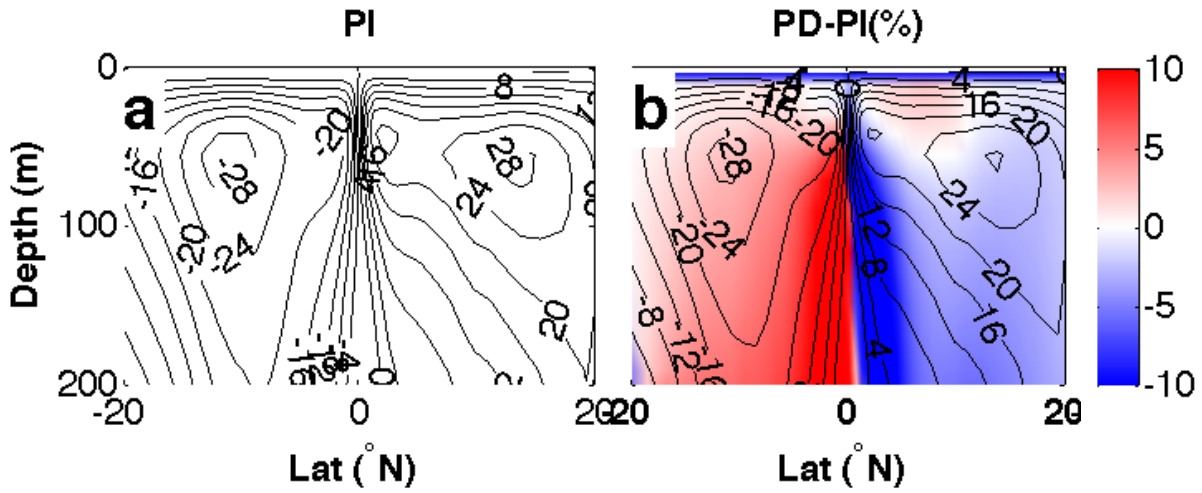

Figure 6.4: Figure 5a,b from [Stevenson 2011a], showing the mean changes to the circulation in the STC between PD and PI (units of Sv).

6.5 2-4 Year Variability

I next investigate the cause of the 2-4 year variability increase. A variety of possible diagnostics exist, including compositing [Deser 2006], analysis of the dominant modes of oceanic variability [Capotondi 2006], measurement of coupling between various regions [Philip 2006], heat budgeting [DiNezio 2010], measurement of the magnitude of variability in ENSO-sensitive regions [Collins 2010], and many more. This means that choosing a single set of metrics by which to measure ENSO changes can be a bewildering prospect: indeed, there is no one standard measure

for ENSO [Guilyardi 2009b].

I begin by asking the question: Can changes to the 2-4 year NINO3.4 variance in the CCSM3.5 be ascribed to changes in the excitation of a mode similar to one of the theoretical oscillators described in Chapter 1? For example, does the delayed oscillator mode become more or less active with CO_2? This type of thinking must be done with care, since the various oscillators involve processes which strongly covary (Section 1.2, cf. [Wang 2001]). Nonetheless, it provides a useful conceptual framework.

If a delayed oscillator-like mechanism is responsible for the majority of the ENSO climate response, then one or more of the following characteristics is likely to change with CO_2:

1. The excitation of off-equatorial Rossby waves
2. Wave reflection at the western boundary of the Pacific
3. The propagation of anomalies from the western boundary to the eastern Pacific

First I consider the growth of eastern Pacific SST anomalies. The most straightforward consequence of an increase in oceanic thermal stratification is an increase in the SST anomalies associated with a given displacement of the thermocline. Figure 6.5 shows the standard deviations of SST and thermocline depth: an increase is seen with CO_2 in both. In the SST panel (left), the majority of the changes happen near the equator, where there is a net decrease in variability in the western Pacific and a net increase in the central/eastern Pacific. This is what one might expect if the generation of El Niño events was taking place near the eastern boundary of the warm pool, for example.

The thermocline variability in Figure 6.5 does appear to represent an enhanced excitation of equatorial Kelvin waves with CO_2. The 'lobes' of variability near 5°S/N are qualitatively consistent with an increase in excitation of subsurface variability in this region; some of that increase in energy is then transmitted to the Kelvin wave mode, which accounts for the enhanced variability along the equator and at the eastern boundary of the basin. The off-equatorial signal is not very large, suggesting that transmission of subsurface variability from the subtropics to the tropics *via* delayed

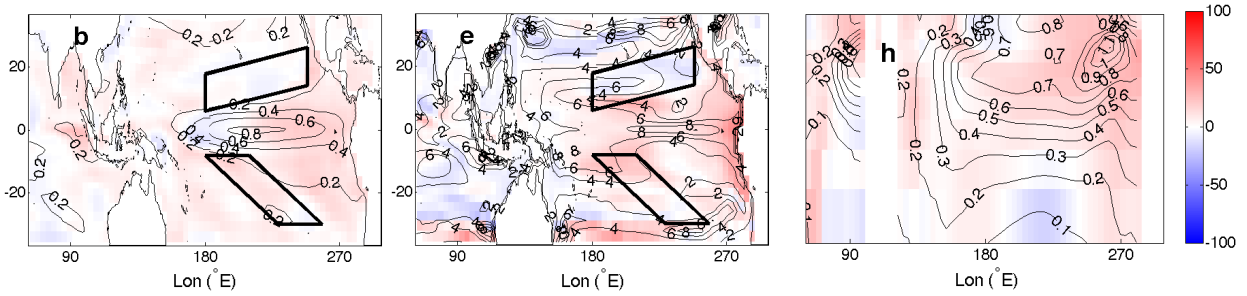

Figure 6.5: Panels b,e,h from ([Stevenson 2011a]; Appendix 4)Figure 7, illustrating the oceanic variability in the 2-4 year band in PD. Left: SST. Middle: Thermocline depth ($Z_{20.5}$). Right: Subsurface ocean temperature. In all panels, PD values are given in contours and the % difference from PI in color shading.

oscillator-like reflection at the eastern and western boundaries is not a dominant mechanism in this model.

The subsurface temperature variability shows some interesting structure (Figure 6.5, right). There appears to be a 'center' of variability along the main thermocline, near 100m depth in the central Pacific. Two other regions of large variability are also visible: one centered in the eastern/central Pacific surface layer, and another at the eastern boundary. All three centers strengthen with CO_2.

Thus far, the CO_2-induced changes seem relatively straightforward. The increase in vertical stratification leads to enhanced SST variability, and the eastward expansion of the warm pool aids in the growth of SST anomalies. The slackened equatorial easterlies also contribute to the ease with which SST anomalies propagate across the basin as Kelvin waves and grow into full-fledged El Niño events. This is not exactly the same formulation as the delayed oscillator, since the role of wave reflection seems to be relatively minimal, but nonetheless relies on relatively well-understood equatorial wave dynamics.

There is another complicating factor, however, which must be considered: the pronounced hemispheric asymmetry in CO_2 sensitivity, which is not easily explainable by a meridionally symmetric model like the delayed oscillator. The point is illustrated in Figure 6.6, which shows the vertical

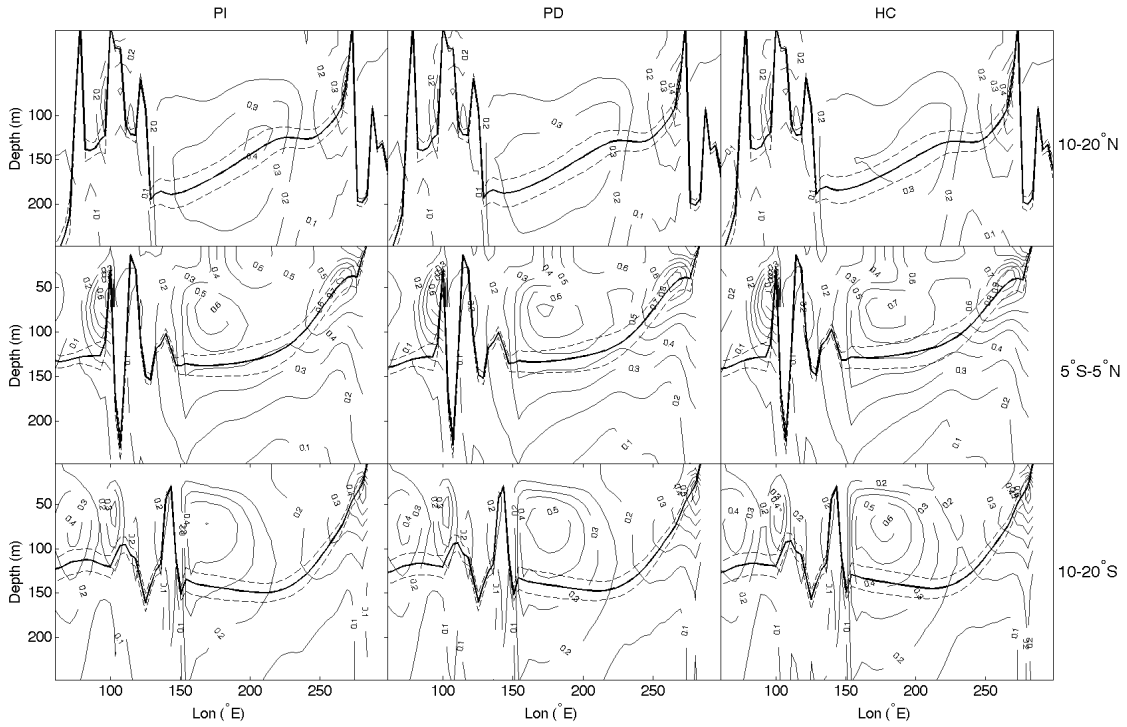

Figure 6.6: Reproduction of Figure 8 from ([Stevenson 2011a]; Appendix 4). Variability in subsurface ocean temperature (variance of gridpoint time series, bandpass filtered with 3dB points at 2 and 4 years). Thick solid lines indicate the mean position of the thermocline; dashed lines show the $\pm 1\sigma$ uncertainty on the mean thermocline position.

profile of subsurface temperature variability at 5°S-5°S as well as 10-20°N and S. The changes to variance between hemispheres are strikingly different: there is a decrease in variability in the Northern Hemisphere (Figure 6.6, top row) and an increase in the Southern (Figure 6.6, bottom row). Thus a hemispherically asymmetric mechanism is required to explain these changes.

6.6 Role of Seasonal Forcing

The presence of seasonal footprinting-like pathways in Figure 6.3 provides an indication that changes to the seasonal cycle might provide the necessary asymmetric driver: thus the seasonal influence on ocean dynamics is next considered.

It is first necessary to understand a fundamental feedback: the 'Wind-Evaporation-SST', or 'WES', feedback [Xie 1994b]. A schematic illustration of WES feedback near the equator is provided in Figure 6.7: an initial warm anomaly slightly to the north of the equator will lead to an SLP gradient driving northward flow. Then the Coriolis force accelerates the anomalous wind to the west (east) in the Southern (Northern) Hemisphere, which tends to increase (decrease) evaporation and creates a cold (warm) anomaly in SST. This is the mechanism often cited for the northward displacement of the ITCZ [Xie 2004], and will operate in the CCSM3.5 as well.

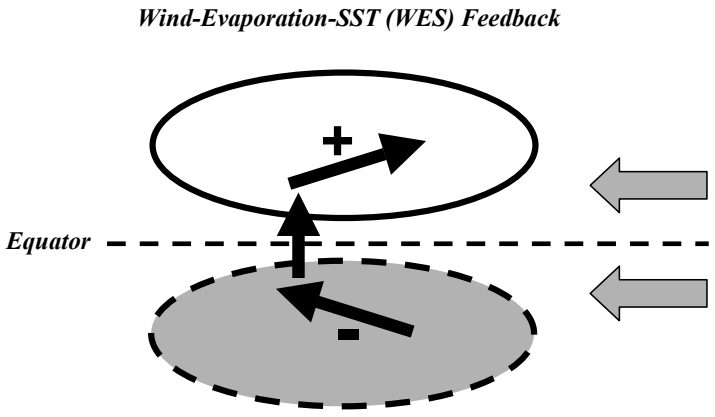

Figure 6.7: Figure 4-5 from [Xie 2004], a schematic illustrating the WES feedback.

The WES feedback occurs in any region where air-sea coupling takes place. In the Northern Hemisphere extratropics, for example, a warm SST anomaly will drive an anticyclonic circulation which interacts with the westerly trades to induce a cold (warm) anomaly to its north (south). The reverse is true in the Southern Hemisphere: the corresponding tendencies are for anomalies to propagate to the southwest in the Northern Hemisphere and to the northwest in the Southern Hemisphere.

In the seasonal footprinting mechanism of [Vimont 2003, Alexander 2002], the WES feedback is the dominant process. The initial disturbance there is generated by PDO-like variability centered near the Aleutian Islands. An initial positive SST anomaly eventually generates an El Niño event during the following winter: likewise, a cold SST anomaly leads to a La Niña event. Modeling experiments have since confirmed that both El Niño and La Niña may be triggered by this mechanism [Alexander 2010].

Here, I primarily focus on the tropics rather than invoking the PDO; nonetheless, the physical mechanism is the same. My hypothesis is that the interaction between the seasonal cycle of the Hadley cell with the ocean via the WES feedback is responsible for driving the weakening/strengthening of variability in the Northern/Southern Hemisphere. This seems to be due to the overall enhancement of the seasonal cycle in the eastern Pacific with CO_2.

A strengthening of the SST seasonal cycle in the NINO3 region means that during boreal summer when the meridional temperature gradient is at its climatological maximum, the overall magnitude of that gradient will be larger. A larger meridional temperature gradient will lead to a larger mean cross-equatorial flow, and therefore to larger hemispheric asymmetries in wind structure due to the WES feedback. Specifically, this will lead to increased convergence (divergence) in the Northern (Southern) Hemispheres. The influence on Ekman pumping will be towards strengthening (weakening) of the mean subduction near 5-10°.

If this seasonal influence is indeed important, then there should be evidence for a hemispherically asymmetric change in seasonally forced wind stress variability. Figure 6.8 shows the bandpassed variance of the zonal wind stress between 2 months-2 years, chosen to cover the semi-annual and

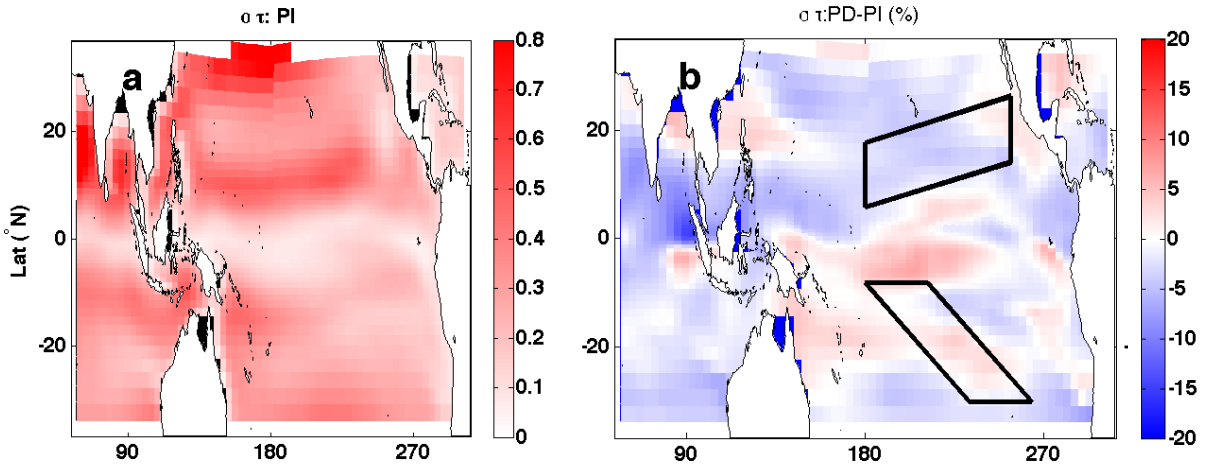

Figure 6.8: Figure 9 from ([Stevenson 2011a]; Appendix 4), showing the 2 month - 2 year bandpassed variance in zonal wind stress. "a) Zonal wind stress variance σ_τ for PI (N^2/m^4). b) % change in σ_τ between PD and PI. Black boxes indicate the position of the SFM-like pathways, and are identical to the regions defined in Figure 6.3."

annual cycle. The boxes in Figure 6.8 are identical with the boxes in other figures, and show that there is in fact a decrease in variability in the Northern and increased variability in the Southern Hemisphere near 5-10° in the eastern Pacific.

Communication between the atmosphere and ocean takes place through Ekman pumping. Figure 6.9 measures the correlation between the wind stress curl and thermocline depth, a direct proxy for the strength of Ekman pumping anomalies. And indeed, it is not only the overall variability on seasonal timescales which varies asymmetrically, but the Ekman pumping itself. This will tend to generate subsurface disturbances in the ocean, which will then propagate toward the tropics as Rossby waves.

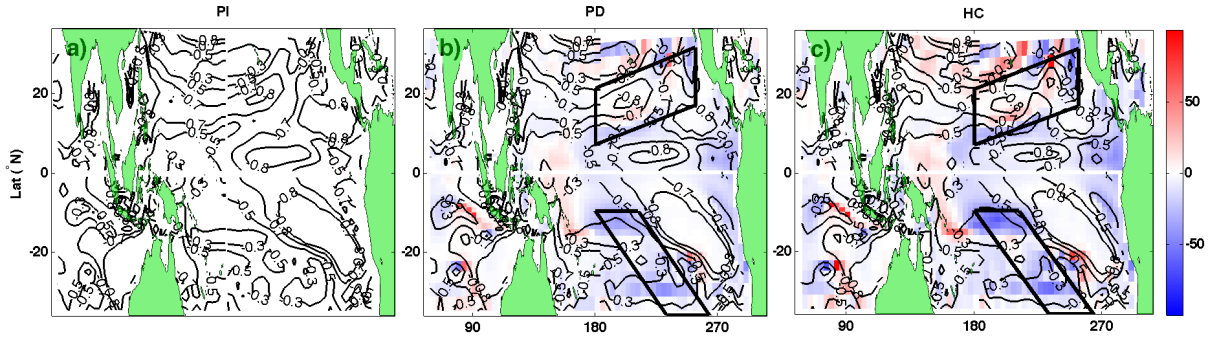

Figure 6.9: Figure 9 from ([Stevenson 2011a]; Appendix 4): Lag-correlations between the curl of the wind stress and thermocline depth at zero lag. Correlations for PI are shown as contours in panel a); in panels b-c contours indicate the values of the lag-correlations, while colors show the percentage change from PI. Black boxes are identical to those in Figure 6.3.

Figure 6.9 is somewhat incomplete since it does not show the phase of Ekman pumping in relation to the seasonal cycle. If one examines the phases of variability in each location (([Stevenson 2011a]; Appendix 4) Figures 11 and 12, not pictured), it becomes clear that Ekman pumping anomalies are strongest during boreal summer in the Northern Hemisphere and boreal winter in the Southern. This tends to lead to the initiation of El Niño/La Niña events due to Northern Hemisphere anomalies, whereas their termination is tied more directly to Southern Hemisphere anomalies. The shift toward

enhanced Southern Hemisphere variability thus leads to more efficient event termination. Combined with the larger equatorial event generation via Kelvin waves, this contributes to the larger amplitude of ENSO variability.

These results provide an interesting comparison with the analysis of [Philander 2003], who hypothesized that a deeper thermocline and weaker trade winds would lead to a weaker ENSO. Their mechanism was a weakening of the air-sea coupling and a warming of the waters upwelled to the surface in the eastern Pacific. This result built on stability analysis of a linearized atmosphere-ocean system [Fedorov 2001]. Mean changes in the CCSM3.5 seem consistent with the [Philander 2003] picture at first glance: the trade winds do weaken with CO_2, and the depth of the 20°C isotherm increases in the equatorial Pacific. All else being equal, this would seem to be conducive to a weakening of ENSO. However, the thermal stratification also increases, and the depth of the maximum vertical temperature gradient becomes shallower - changes which are more favorable to ENSO strengthening. To make things more complicated, the *same* mean-state changes in CCSM4 lead to a *weaker* ENSO ([Stevenson 2011b]; Appendix 3), so the mean state change alone is clearly insufficient to determine the ENSO response. All in all, it is not surprising that a simplified analysis like [Philander 2003] does not capture the full ENSO response - a more complete consideration of coupled processes is necessary.

6.7 5-7 Year Variability

I conclude with a brief investigation of the longer-period variability (P $\geq$5 years) in PI, PD and HC. Although changes to the tropical SST signal are insignificant here, there still may be interesting changes to the dynamics: a full exploration is beyond the scope of this dissertation, however.

I have performed an analysis of the bandpassed standard deviations of wind stress and thermocline depth. If the delayed oscillator or a similar mechanism is the dominant source of variability at these frequencies, one would expect to see changes similar to those at 2-4 year periods. Consistent with such a hypothesis, the thermocline depth changes between PD and PI (Figure 6.10) are

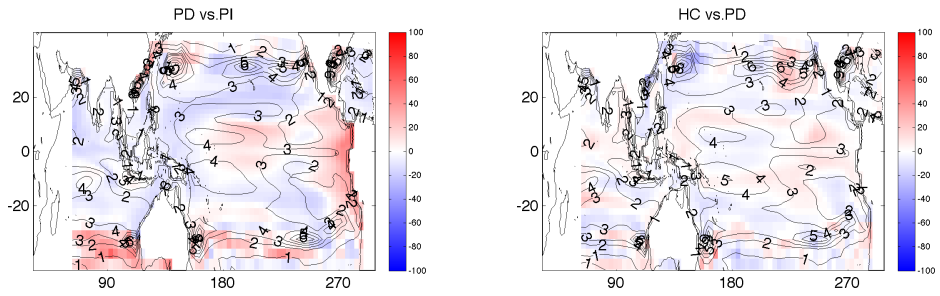

Figure 6.10: Bandpassed standard deviations of thermocline depth, with 3dB points at 5 and 7 year periods. Contours indicate the magnitude of the standard deviation (m^2), and colors show the percentage change relative to the lower-CO_2 end member in each comparison. These correspond to (PD-PI)/PI (left) and (HC-PD)/PD (right).

qualitatively similar to Figure 6.5, with enhanced excitation of the equatorial Kelvin wave mode creating larger variations in the eastern Pacific. However, the pattern of HC-PD changes is very different, appearing in many ways as a mirror image of the PD-PI panel. Variability strengthens (weakens) along the western boundary (central Pacific) in HC-PD, while the opposite is true in PD-PI. Likewise, variability near 250°E is enhanced in HC-PD and suppressed in PD-PI. I hypothesize that this represents a shift in the location of Kelvin wave generation by westerly wind bursts near the edge of the western Pacific warm pool [**?**]. It is possible that the enhanced variability in PI may represent a balance between two competing influences: the increased stratification in the eastern Pacific and the reduced equatorial trade winds. The former tends to favor wave generation, the latter to suppress it. However, testing this hypothesis definitively is left to future work.

Extratropical influences may also be expected to become important at these periods, and the variability in wind stress is therefore considered out to latitudes of 60°N and S in the upper panels of Figure 6.11. A lobe of variability can be seen off the Aleutian Islands in both panels, which may be associated with PDO-like dynamics. This lobe shifts southward substantially in PD relative to PI, as evidenced by the deficit (excess) near 60°N (50°N). However, the shift between HC and PD is much smaller, only a few percent of the PD value. Thus there may be interesting nonlinearities

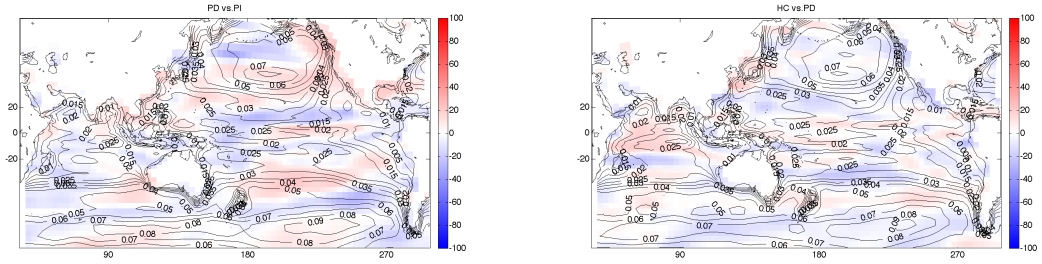

Figure 6.11: Bandpassed standard deviation of zonal wind stress, with 3dB points at 5 and 7 year periods. Contours and colors follow the same convention as Figure 6.10.

in wind-forced dynamics in the extratropics, which bear further investigation.

Chapter 7

How Realistic Are Emissions Scenarios to Begin With?

Contents

I have been interested in the connection of climate science with science policy for quite some time, since knowledge only truly benefits society if it is communicated to the people making decisions. During the course of my PhD, I have tried to understand how climate science and policy might interact, and how climate science research is viewed by the policy community, by participating in the CU graduate certificate program in science and technology policy. On a personal note, I found the experience completely fascinating in some respects and extremely frustrating in others: the other students often came from a political science or humanities background, and communication could sometimes be difficult. But one thing that I did learn is that we as climate scientists often take for granted some of the highly complex social and economic issues that have to be considered when dealing with the climate system. So I would like to use the last chapter of this dissertation to highlight one area that is treated as a 'black box' by the climate science community: namely, the AR5 'emissions scenarios'. In addition to being something that is important for climate scientists to understand when working with simulations of the 21st century, the emissions scenario issue

highlights the need for truly interdisciplinary collaboration.

As an introduction: I put emissions scenarios in quotations above because properly speaking, the AR5 does not use scenarios *per se*. Instead, the 'Representative Concentration Pathways', or RCPs, were developed specifically to be independent of socioeconomic development. This is a laudable goal, and represents a substantial advance over the previous generation of scenarios used in the AR4. However, as I will discuss in this chapter, there is a great deal of technological improvement which is implicitly built in to the AR5 pathways, as was the case for their predecessors. This does not necessarily mean that the mitigation goals set by the AR5 are impossible, but it may be substantially more difficult to achieve those goals than the IPCC lets on: having a realistic sense of the difficulty of the challenge is going to be crucial for developing policy strategies to deal with climate change.

7.1 Emissions Projections: AR4 vs. AR5

The defining feature of the RCPs, as noted above, is the fact that they are projections designed using a specified top-of-atmosphere radiative forcing, rather than specified profiles of greenhouse gas emissions. This represents a conceptual reversal from the previous generation of scenarios, described in the 'Special Report on Emissions Scenarios', or SRES [Nakicenovic 2000].

Table 7.1: Table 1 from ([Stevenson 2012a]; Appendix 6). SRES families and associated patterns of economic, population, and technological growth.

Family	Economic Growth	Population Growth	Technological Development
A1	rapid	peaks in mid-century, then declines	rapid introduction of new, efficient technologies
A2	fragmented, slow	continuous slow increase	
B1	transition to service /information economy	same as A1	clean, resource-efficient
B2	intermediate	continuous increase (slower than A2)	diverse, slower development

To provide some context for comparison, the four major SRES scenario 'families' are described in Table 7.1 (Table 1 from ([Stevenson 2012a]; Appendix 6)). The four families represent four different

philosophies of how social and economic systems will develop over the course of the 21st century. Generally the B families are more stringent mitigation pathways, and the A families represent more rapid growth with larger associated greenhouse gas emissions. The A1B scenario in particular is often used as the so-called 'business as usual' projection [Schneider 2001, Stroeve 2007]. That said, the past 10 years have shown even faster emissions growth than the A1B [Raupach 2007].

The four RCPs (RCP 2.6, 4.5, 6.0 and 8.5) cover a broadly similar range in climate projections as the SRES: projected CO_2 emissions and radiative forcing are shown for each in Figure 7.1. Each of the RCPs was constructed using a 'baseline' scenario from a different integrated assessment model, which combines economic and policy simulations with representations of the agricultural sector and a simplified version of the physical climate system. From this, combined with the desired stabilization top-of-atmosphere forcing, the emissions pathway is derived. Pathways are then replicated with a second model to ensure the reliability of the projection [Weyant 2009].

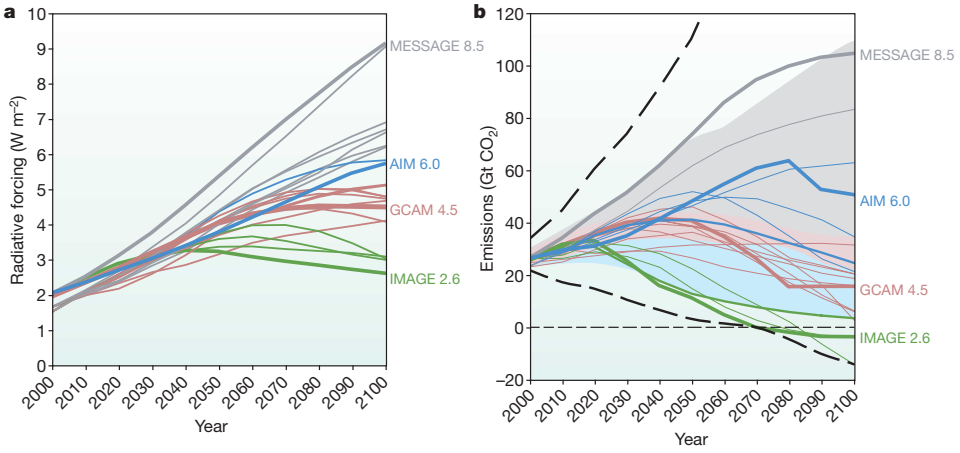

Figure 7.1: Figure 5 from [Moss 2010]. MESSAGE (RCP 8.5) is shown in gray, AIM (RCP 6.0) in blue, GCAM/MiniCAM (RCP 4.5) in pink and IMAGE (RCP 2.6) in green. (a) Top-of-atmosphere radiative forcing, W/m^2. (b) CO_2 emissions in gigatons.

Generally, the more stringent RCPs (2.6 and 4.5) most closely resemble the SRES B families; the less stringent (6.0 and 8.5) more closely resemble the SRES A families. Some of the similarities between the SRES and RCPs, in fact, go beyond the qualitative. For instance, the RCP2.6

[van Vuuren 2007, Van Vuuren 2006] was developed using a baseline emissions pathway derived from the SRES B2 [Weyant 2009] and modified to better fit the demographic trends from 2000-2010 by [van Vuuren 2007]. This is the lowest radiative forcing pathway, and has the notable feature of requiring *negative* emissions by 2100 (Figure 7.1).

The least stringent pathway, the RCP8.5 [Rao 2006, Riahi 2007], is also derived from a baseline projection which heavily draws on the SRES. The revisions made to the A2 scenarios in the derivation of RCP8.5 are discussed in [Riahi 2007], which mostly have to do with modification of population growth and technological development estimates to better fit UN projections. In this pathway, CO_2 levels rise well above 1000ppm, and continues to rise in 2100 and beyond (Figure 7.1b).

The two middle pathways, RCP 4.5 [Clarke 2007] and RCP 6.0 [Fujino 2006], were derived from baseline scenarios developed independently from the SRES. In the RCP4.5, technological improvements are assumed to result in large energy efficiency improvements over the course of the 21st century, with each dollar of 2100 gross domestic product (GDP) produced using only 25% as much energy as the equivalent in 2000 [Clarke 2007]. The RCP6.0 team derived their scenarios using data from the International Energy Association [Fujino 2006], and technological improvements in this scenario lie between the projections of the other groups. Both show CO_2 emissions stabilizing by the end of the 21st century (Figure 7.1b).

Table 7.2: Table 2 from ([Stevenson 2012a]; Appendix 6). "RCPs recommended for use in AR5. Modeling groups are: the Asia-Pacific Integrated Model (AIM), the Model for Energy Supply Strategy Alternatives and their General Environmental Impact (MESSAGE), the Mini-Climate Assessment Model (MiniCAM), and the Integrated Model to Assess the Global Environment (IMAGE)."

Name	Forcing (W/m^2)	CO_2 level	Modeling group	Country/region
RCP8.5	8.5	$\geq$ 1370	MESSAGE	Austria
RCP6	6.0	850	AIM	Japan
RCP4.5	4.5	650	MiniCAM	USA
RCP2.6	3.0	490	IMAGE	Netherlands

7.2 Decarbonization in the RCPs

Any effective climate change mitigation strategy must necessarily incorporate substantial reductions in world energy consumption [Hibbard 2007, Hoffert 1998, Hoffert 2002]. One of the more commonly used metrics is the decarbonization rate, defined simply as the rate of change of carbon emissions per unit of GDP. The decarbonization rate is the product of two quantities: the carbon intensity (CI) and energy intensity (EI). CI is a measure of the carbon emission required per unit of energy generated, while EI measures the amount of energy required to produce a unit of GDP.

Being the 'state of the art' in our knowledge of climate change, the scenarios used for the IPCC are often looked on as representing what is achievable given current economic realities. But this is not necessarily the case: for example, [Pielke Jr. 2008] calculated the projected decarbonization rates from the SRES scenarios. Using a 'frozen technology' baseline simulation, they show that the decarbonization in the AR4 simulations relies on 'automatic' efficiency improvements which account for a large fraction of CO_2 emissions reductions. This means that the effort required to achieve the SRES mitigation goals may be larger than anticipated.

The RCPs are designed to avoid being tied to a single possible socio-economic outcome - however, they still do require large decarbonization rates. To provide a 'ballpark' estimate of the degree of decarbonization required for the RCP stabilization targets, I have recreated Figure 2 from [Pielke Jr. 2008]. For RCP4.5 and 8.5, I have used the baseline scenario from which the projection was derived. This was not available for RCP2.6 and 6.0, so I used the GCAM 'replicate' simulation instead. Results are shown in Figure 7.2, using time periods of both 2000-2010 and 2010-2100. There is a notable lack of differences between the 2000-2010 and 2005-2020 RCP values; roughly the same range of carbon and energy intensities are covered by both groups of scenarios. Also interesting is the difference between the 2000-2010 and 2010-2100 results: particularly for RCP2.6, the required mean decrease in carbon intensity over the 21st century is much larger than that currently observed (Figure 7.2b, red star).

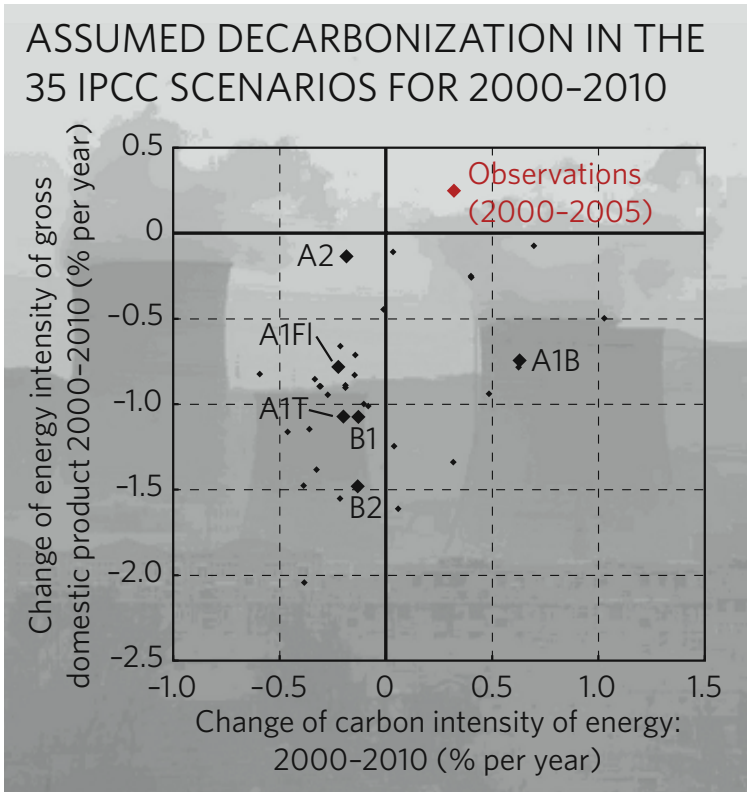
ASSUMED DECARBONIZATION IN THE
35 IPCC SCENARIOS FOR 2000–2010
Change of energy intensity of gross domestic product 2000–2010 (% per year)
Change of carbon intensity of energy: 2000–2010 (% per year)
Observations (2000–2005)
A2
A1FI
A1T
A1B
B1
B2
0.5
0
-0.5
-1.0
-1.5
-2.0
-2.5
-1.0
-0.5
0
0.5
1.0
1.5

a)

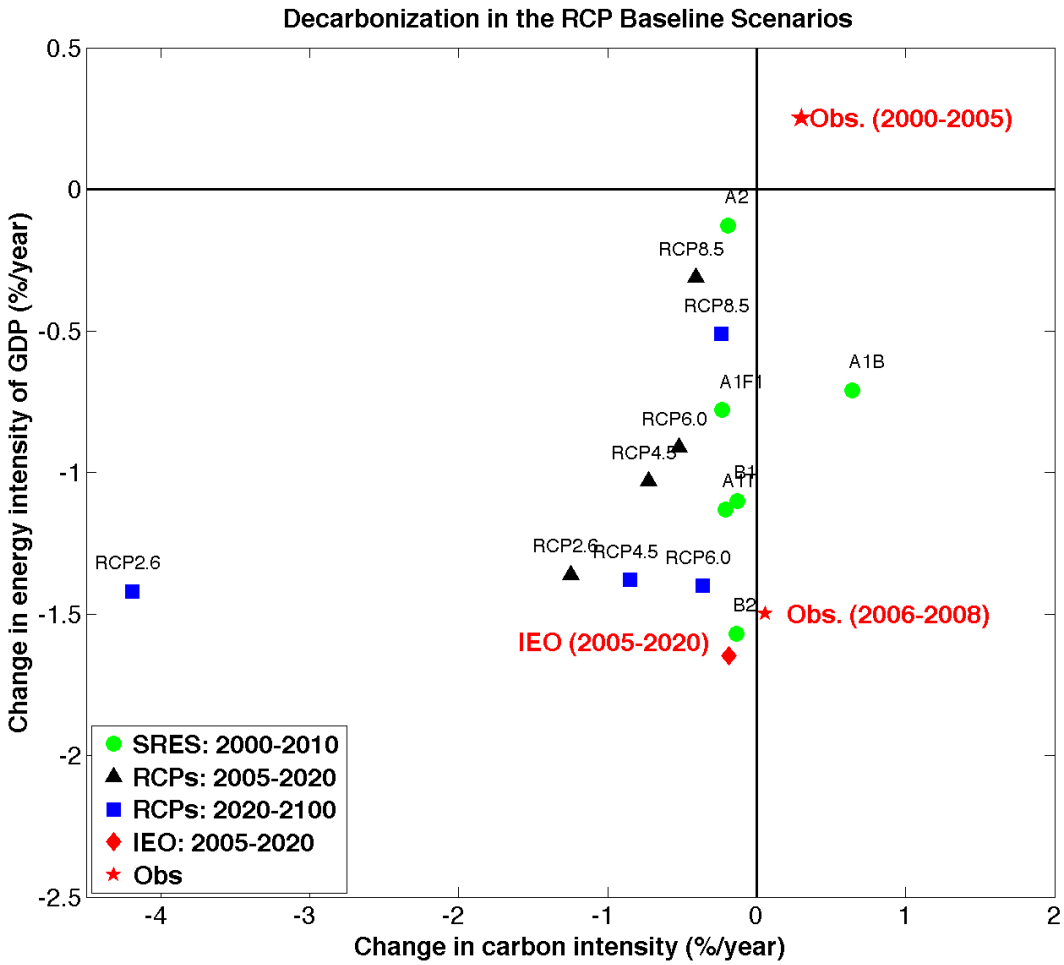
Decarbonization in the RCP Baseline Scenarios
Change in energy intensity of GDP (%/year)
Change in carbon intensity (%/year)
★Obs. (2000-2005)
★ Obs. (2006-2008)
IEO (2005-2020)
A2
RCP8.5
RCP8.5
A1B
A1FI
RCP6.0
RCP4.5
B1
A1T
RCP2.6
RCP2.6
RCP4.5
RCP6.0
B2
SRES: 2000-2010
RCPs: 2005-2020
RCPs: 2020-2100
IEO: 2005-2020
Obs
0.5
0
-0.5
-1
-1.5
-2
-2.5
-4
-3
-2
-1
0
1
2

b)

7.3 Energy Use in the RCPs

Figure 7.2 implies that despite the new approach to simulating 21st century economic development, the RCPs include some of the same built-in assumptions is leading to decarbonization predictions which might be extremely difficult to achieve in practice. This begs the question: where are we going wrong? Are the energy use projections in the RCPs completely unrealistic, or can we use them to make specific policy recommendations? A complete answer to these questions is beyond the scope of this dissertation, of course. However, to provide some perspective on the types of technologies the RCPs rely on most heavily, I have performed a brief overview of the literature on the subject.

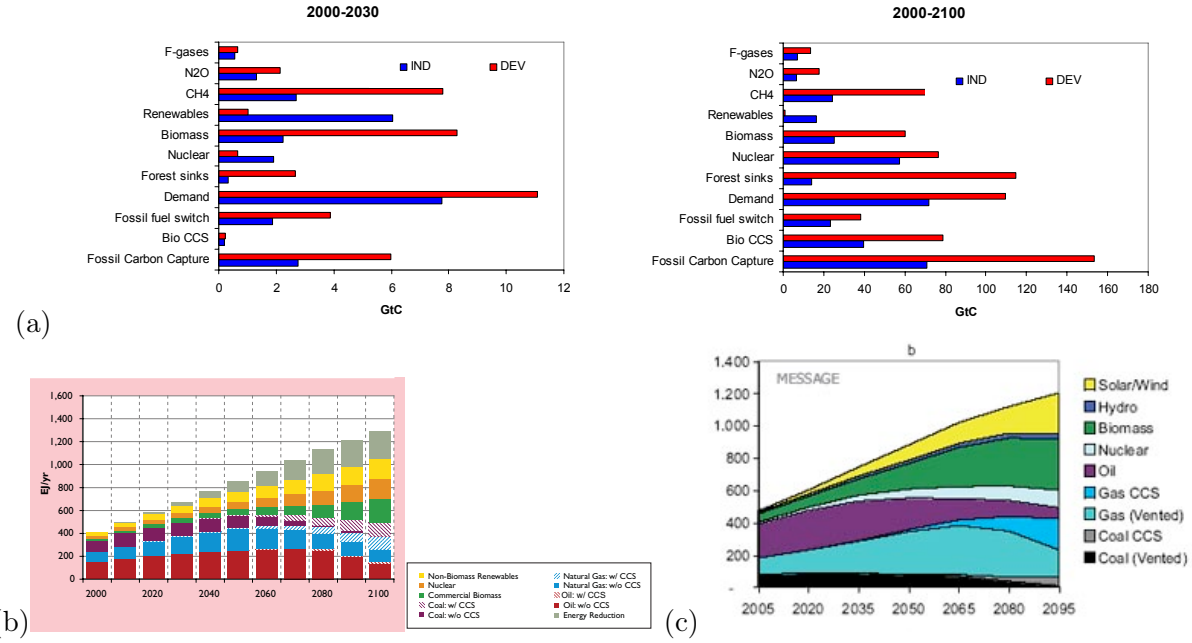

Figure 7.3: A reproduction of Figure 4 from ([Stevenson 2012a]; Appendix 6), showing figures from the literature on each RCP. "(a) Figure 3.7 from [Weyant 2009], showing the contribution to emissions reductions by fuel type for RCP2.6. Here 'IND' refers to the developed countries and 'DEV' to those in the developing world. (b) Figure 4.11 from [Clarke 2007], showing projected global energy emissions by fuel type for RCP4.5. Values shown are the differences between the RCP4.5 pathway and the GCAM 'reference' scenario. (c) Figure from the IPCC Special Report on Carbon Capture & Storage, showing energy use by fuel type for RCP8.5."

Figure 7.3 shows the distributions of energy use by sector over time in RCP2.6, 4.5 and 8.5. The overall picture is very clear: climate mitigation will require a drastic shift away from fossil fuels and toward more renewable sources of energy. This is done in all of the RCPs by some combination of energy efficiency improvements, reduction of oil and other fossil fuel consumption, adoption of solar/wind/biomass/hydrothermal technologies, and the capture and sequestration of associated carbon emissions.

Improvements to Energy Efficiency

Efficiency improvements are difficult to predict; [van Vuuren 2007] cites this as one of the largest uncertainties in future CO_2 projections in RCP2.6. The implementation will vary widely among world regions, with a range in RCP2.6 of 0.8% to 1.8%/year. In RCP8.5, efficiency becomes important as well: [Riahi 2007] find that this could account for up to 10-20% of the total greenhouse gas reductions.

The International Energy Association (IEA) has assessed our current ability to implement energy efficiency improvements, and find that improvements sufficient to stabilize the climate at 2.4°C above present will be difficult indeed [IEA 2008]. Efficiency improvements must be applied across every sector of society, but doing so requires dedicated action from governments. Once efficiency measures are implemented, however, the IEA finds that they could save up to 8.2 gigatons of CO_2/year [IEA 2008].

Use of Fossil Fuels

Fossil fuels are likely to remain a key source of energy throughout the 21st century: this is true in both the RCP projections and those of the World Energy Outlook [WEO 2009]. For example, coal is projected to account for up to 30% of total energy use in RCP4.5 [Clarke 2007]. 'Clean coal' technologies, which would reduce the associated CO_2 emissions, are being investigated at the moment [Chen 2010] but implementation is still at the testing stage[1]. Thus, the outcome of coal production on future CO_2 levels is currently unclear.

[1] http://fossil.energy.gov/programs/powersystems/cleancoal/publications/CCT_Program_Update_2009.pdf

Oil is also likely to remain in high demand [WEO 2009], although all the RCPs project that 'peak oil' will be achieved during the 21st century and production/use will therefore decline. Alternative sources such as tar sands and oil shales may come into play [Bartis 2005], but their feasibility is questionable at this point.

Nuclear Energy

All four RCPs project a large increase in nuclear energy production, since the technology is mature and has minimal associated greenhouse gas emissions. Despite the recent safety concerns raised by the disaster at the Fukushima plant in Japan [Christodouleas 2011], nuclear energy still has great potential for CO_2 emission mitigation. Currently Germany, Japan and Finland rely on nuclear energy for more than 25% of their energy [U.S. Dept. of Energy 2010] and China and India are currently making moves toward increasing their nuclear capacity.

Issues with nuclear power, in addition to safety, revolve around political/financial/logistical obstacles. Nuclear plants require a huge up-front cost, and waste disposal remains a controversial issue [Chapman 1987]. The adoption rate in the RCPs for nuclear technology may or may not be realistic; much will depend on the details of demographics and regional politics in the next few decades.

Use of Renewable Energy Technologies

In the RCPs renewables consist of a combination of wind, solar, hydroelectric and biomass technology. Interest in wind energy has been steadily growing for the past few decades, especially in Europe [EWEA 2009, Zarvos 2003] and the United States [NAS 2010, AWEA 2010]. The European and Australian wind power goals are 40% and 12% of energy production from wind by 2030, respectively [Fichaux 2009, AWEA 2010]. Even in the developing world, where coal is a larger contributor to total energy, there is interest in wind as well [GWEC 2008]. Recent assessments of the total capacity for wind power [Lu 2009, Archer 2005, Wiser 2011] suggest that the energy supply is plentiful; this makes wind energy an attractive option.

Biomass energy is a general term for energy from biological sources, including ethanol, biodiesel, or any other products burned for energy. The primary source of biomass energy, in terms of total energy production, comes from liquid fuels, and the projected contribution from biomass may be quite substantial (FIgure 7.3). However, there are unintended consequences of liquid biofuels which may complicate their widespread adoption. For example, ethanol production in the US can lead to an artificial increase in food prices elsewhere [Partnership 2009]; the influence is difficult to quantify [Mitchell 2008, Trostle 2008, CBO 2009] but must be considered when discussing the issue.

Use of Carbon Capture and Sequestration

Finally, carbon capture and sequestration (CCS; [Fisher 2007]) is a major contributor to greenhouse gas mitigation in the RCPs. When considered in the context of the current status of the technology, the amount of CCS assumed in the RCPs is worrying: up to 50% of the total CO_2 reductions by 2100 is achieved through CCS.

Given the potential for CCS to solve the climate crisis, it is naturally enough a subject of intense research [Hendriks 2002, van Alphen 2010]; a review of the efforts in the US is available in [Litynski 2008]. Sites for carbon storage have been identified in the US [Klara 2003, Klara 2002] and are being evaluated at the moment. In addition to the technical unknowns with CCS, unsolved issues include the economics of storage and local political and safety concerns [Hawkins 2009]. In short, a great deal more research is needed to evaluate whether CCS truly can provide a feasible reduction in atmospheric CO_2 content.

Investigating the details of the emissions scenarios and the RCPs was an eye-opening experience for me, since as a climate modeler one typically does not have much exposure to the social and economic issues that go into scenario development. But keeping in mind the fact that the RCPs may be underestimating the magnitude of climate change will most likely be very important as I move forward, since possibly it may be necessary to test ENSO sensitivity to a much wider range of CO_2 concentrations than is represented in the RCPs. This is probably true for many other impacts

studies as well, and also highlights the need for greater communication between the physical climate science and integrated assessment modeling/policy communities.

Chapter 8

Conclusions

Contents

If I had to summarize the results of my dissertation in just one sentence, I would say that what I have learned is: predicting future changes to ENSO behavior is a lot harder than I thought when I started. We don't have enough data to properly measure the extent of natural variability in the modern climate, and paleoclimatic ENSO proxies are so uncertain that using them to extend the instrumental record is extremely difficult. The adjustment to climate change takes place on decadal timescales, meaning that ENSO response may not really be statistically significant at all during the 21st century, but changes in the atmosphere may be felt sooner than that. We do know that once the climate has stabilized, ENSO responses will eventually become significant, and that changes to the mean atmospheric circulation as well as to high-frequency wind variability will be important in

determining that response. But we need to take the results from all the 21st century projections with a grain of salt, keeping in mind that in addition to the known problems with coupled climate models, the greenhouse gas emission projections used to drive the models may themselves be flawed.

It may sound a bit like this dissertation is aimed at trying to prevent firm conclusions from being drawn about ENSO: but actually this is just the opposite of my goal. It is my belief that science is best served when the limitations of any given analysis are well defined - even if that prevents the question one is interested in from being answered right away. I hope that the results of this dissertation will help advance our knowledge of projected future tropical climate variability.

8.1 Past ENSO

There are systematic issues with estimating the strength of past ENSO variability using coral δ^{18}O. The major errors which must be accounted for are age model estimation, local influences, sampling effects and uncertainty in absolute dating. In Chapter 2 I simulated these sources of error, and find that the majority are relatively small in comparison with the input variance. Age model and local influences were computed using a set of corals collected from Kiritimati island in the central Pacific: the typical uncertainty in total δ^{18}O variance is about 0.21‰, which for most coral locations is 10-20% of the input signal. For locations with weak variability, age model and local effects may become more of a concern; the most accurate results would ideally be obtained by a reproducibility study using corals collected from that particular location.

The major problems with ENSO estimation from proxies arise when trying to convert between proxy data and model output. Forward modeling is currently not a viable option, as even isotope-enabled models only simulate seawater δ^{18}O and not the signal expected in the reef itself; conversion must therefore be performed after the model is run. The most common method of after-the-fact conversion between coral δ^{18}O and ENSO variability is the use of a linear pseudoproxy, which assumes that δ^{18}O is a linear function of SST and SSS alone [Brown 2008, Thompson 2011]. I have calculated pseudoproxies using instrumental data from HadSST and SODA (Section 2.3), and use

a Monte Carlo simulation to estimate the magnitude of uncertainties in single-site δ^{18}O variance due to the fit residuals. This is much larger than local/age model uncertainty, and can be as large as 185% of the input variance. The errors are so large that they drown out the covarying mode between the modern coral sites as well; the PC1 of linear pseudoproxies calculated from HadSST and SODA bears little resemblance to that calculated from the δ^{18}O records themselves. This failure of the linear approach may be due to fundamental nonlinearities in the signal: calculating the required dimension to describe the δ^{18}O signal reveals that 3-4 independent variables will be needed. Alternatively, SST/SSS/seawater δ^{18}O might be sufficient to specify coral δ^{18}O, but only on local scales.

Given that a linear approach does not seem to work, I next attempt to investigate other methods of δ^{18}O-ENSO conversion. One possibility is the use of climate field reconstruction techniques; but all CFR methods make the assumption of a stationary covariance matrix between the coral sites and ENSO. I have performed example calculations using the regularized expectation maximization algorithm of [Schneider 2001], one of the most commonly used CFR methods. I find that if RegEM is used to predict the ENSO amplitude at a time when no covariance information is available, there is a systematic underprediction of variance. This is a known feature of CFR [Mann 2009], and makes it nearly impossible to correctly capture past ENSO magnitudes when no covariance information is available. It is possible that the effect may be mitigated by the implementation of Bayesian methods for imputing past δ^{18}O values [Tingley 2010a, Tingley 2010b]. Forward modeling, however, would provide the optimal solution, since then the coral and model output could be directly compared.

One encouraging aspect of the ([Stevenson 2011c]; Appendix 1) analysis was that the errors in absolute dating and the influence of a restricted sample size seem manageable. In particular, randomly assigning a dating error of $\pm$10 years to each coral did not lead to a large influence on the coral δ^{18}O PC1, suggesting that the covarying mode between fossilized corals might be robust against U-series dating uncertainties. The same is true for randomly selecting a subsample of the modern corals and re-computing δ^{18}O PC1, with the caveat that at least 5-6 corals seem to be required to detect the majority of the signal.

8.2 Present-Day ENSO

I have investigated the limitations of the modern observational record as well. Identifying epochs when differences between ENSO spectra are statistically significant is extremely difficult due to the large degree of natural variability in the system, and most commonly used statistical tests either make assumptions which are invalid for ENSO or are too sensitive to be useful. I have therefore developed a new, wavelet-based technique for identifying significant differences, and named it wavelet probability analysis (WPA). WPA functions by assessing changes to the distribution of the joint probability between subsets of a time series/pair of time series; this is referred to as the wavelet probability index (WPI) and adopted as the test statistic. Results are described in detail in ([Stevenson 2010]; Appendix 2) and summarized in Chapter 3.

I apply WPA to three different situations: comparison of the performance of two different climate models, validation of a climate model against observations, and determination of the necessary simulation length for accurate measurement of ENSO statistics. In all three cases, what is being compared are two different distributions of WPI generated from subsamples of the time series. The first instance compares the WPI from subsamples of two climate models, with a reference time series (in my case ocean observations from the CORE hindcast of [Large 2008]). The second compares WPI distribution from climate model subsamples *versus* the reference, to the WPI distribution from climate model subsamples *versus* each other.

Using three different GCMs, I find that the width of the 90% confidence interval on the WPI distribution declines with sampling length at an identical rate in several different models. Fitting an exponential curve to that decay leads to a required simulation length of somewhere between 270-370 years. This is long in comparison with many control simulations currently used for climate change applications, suggesting that perhaps a 'paradigm shift' in model experiment design may be required.

I find that the overall performance of CCSM3.5 relative to CORE is better than the performance of the GFDL CM2.1, which is consistent with previous assessments of the two models [Neale 2008,

Wittenberg 2006]. There do seem to be some offsets in both models relative to observations, but overall the CCSM3.5 reproduces observed NINO3.4 variability very well. However, the use of 55-year subsamples makes it difficult to say whether the observed model/data offsets are real or due to sampling error. This raises another interesting point: the WPI convergence relationship can just as easily be applied to instrumental data as to climate model output. When this is done, a similar answer results: an SST dataset must be roughly 170 years long to provide stable ENSO statistics! Clearly we do not have nearly enough observations of the real world, making the assessment of paleoclimate applications in Chapter 2 all the more relevant.

8.3 Future ENSO

The analysis of uncertainties in measuring past and present ENSO naturally leads one to wonder what the implications are for future ENSO. I was fortunate enough to work with the CCSM4 CMIP5 20th and 21st century simulations just before their release ([Stevenson 2011b]; Appendix 3), and found that the answer is not as straightforward as one might imagine. When the scatter between ensemble members is taken into account, the statistical significance of inter-ensemble changes is extremely low by several different measures. There does seem to be a slight tendency towards weaker ENSO with higher CO_2, but this should not be taken as definite by any means.

A null result like this one is always a bit unsatisfying, so I have investigated the possible reasons for the lack of significant signal between ensembles. Chapter 3 established that 100 years of data is not enough to distinguish climate change influences from natural variability, but each of the different 21st century scenarios has at least 5 100-year ensemble members, and the 20th century ensemble has 6. One might think that 500-600 years of model output would be sufficient to 'beat down' the statistical noise, but in fact all ensemble members are subject to the same imposed trends from anthropogenic forcing. This leads to a warming throughout the course of the simulation period which is particularly pronounced in the extratropics, and which is stronger in the higher-CO_2 ensembles. That extratropical influence then takes time to propagate down into the tropics; the timescale is

on the order of decades. That is, several decades *after* the external radiative forcing has stabilized are required for the tropics to come into equilibrium with the new mean climate. That point is where the 'clock' should start for obtaining the required 250-300 years of data to constrain ENSO behavior. All in all, it comes as little surprise that the significance of inter-ensemble changes is so low.

An insignificant response is also seen in the CanESM2, IPSL CM5A and CSIRO Mark 3.6: the result is robust across models. This has profound implications for climate change experiments like CMIP. The model simulations currently being performed as part of CMIP are not sufficiently long to provide a definite answer to the question of ENSO's response to climate change: model ENSO climate sensitivity is as yet *still an unknown*. We cannot rule out, on the basis of CMIP simulations, the possibility that inter-model differences are an artifact of sampling bias. Only very long model simulations at stabilized CO_2 can definitively show how ENSO amplitude may change in a given model.

I have been able to diagnose model ENSO climate sensitivity in the CCSM3.5. I conducted several 800-year simulations, each with identical model configurations varying only the atmospheric CO_2 concentration. Adopting values appropriate for 1850, 1990 and ≈2050 AD, I find that the amplitude change is indeed significant with CO_2, and that an increase in ENSO variability is seen. This is a striking contrast with the CCSM4's (slightly) weaker ENSO at high CO_2, since these are two members of the same model family. It would seem that it may be easy to get dramatic changes to model ENSO climate sensitivity, with only slight changes to model physics.

There are substantial changes to the mean state and circulation of the atmosphere and ocean in CCSM3.5 as CO_2 increases. An increase in vertical thermal stratification is seen, along with a weakening of the equatorial trades and an eastward extension of the warm pool. Enhanced equatorial Kelvin wave activity occurs at higher CO_2, excited in the central Pacific near the edge of the warm pool: this would tend to imply an increase in the excitation of El Niño and La Niña events, all else being held equal.

The enhanced wave activity certainly does play a role in the increased ENSO amplitude. But

there is also an interesting hemispheric asymmetry seen in CCSM3.5, along the equatorward edges of the subtropical gyres; variability in the Southern Hemisphere strengthens, while variability in the Northern Hemisphere weakens ([Stevenson 2011a]; Appendix 4). This occurs as the overall Hadley circulation migrates southward during boreal summer and the seasonal cycle in SST gets stronger overall. I have shown in Chapter 6 that an enhancement in Ekman pumping occurs during boreal winter in the Southern Hemisphere, and a weakening of Ekman pumping occurs during boreal summer in the Northern Hemisphere, along the pathways previously identified as important for excitation of El Niño events [Alexander 2002, Alexander 2010]. The Southern Hemisphere Rossby wave pathway appears to be more active than the Northern in terminating the El Niño/La Niña phase in CCSM3.5, because of the seasonality of the signal. Thus, an enhancement of the Southern Hemisphere forcing would lead to more efficient event termination, and when taken in combination with the enhanced excitation along the equator, a stronger ENSO amplitude overall.

8.4 El Niño/La Niña Events and Teleconnections

The climate change analysis of Chapter 4 also examined the different response times in the atmosphere and ocean. Despite the lack of significant changes to overall ENSO amplitude, I found that it was still possible for the atmospheric teleconnections during El Niño and La Niña to change significantly over the course of the 21st century (Section 4.4). I focused particularly on three regions, which seemed to show the largest changes with CO_2: the North Pacific, Australasia, and the far southern central Pacific.

The North Pacific is a highly studied region for teleconnections [Deser 2006, Meehl 2007a]; the influence of the Aleutian Low on the climate of the western United States and Canada makes understanding changes in that region important for North Americans. In the CCSM4, changes consistent with the predictions of [Meehl 2007b] are observed during El Niño DJF: the pattern of SLP and surface temperature shifts to the north and east as CO_2 increases. The strength of the blocking high during La Niña DJF increases, possibly indicating a tendency towards harsher La

Niña winters in the American Southwest.

In the western equatorial Pacific, changes are seen during El Niño/La Niña DJF as well. Changes are generally consistent with an overall weakening of the Australasian teleconnection: during El Niño, a positive anomaly is seen just south of Tasmania and a negative anomaly is seen over mainland Australia, which tend to oppose the prevailing teleconnection patterns. The reverse is seen during La Niña: taken together, these suggest that maybe the impacts of ENSO will not be felt as strongly in Australia during future climates.

In the Southern Ocean, changes are a bit more difficult to interpret. The shifts in teleconnections are nonmonotonic with CO_2, being strongest in RCP2.6: I speculate that this has something to do with the more stable climate in this scenario. The main feature in the Southern Ocean is seen during La Niña JJA, where the prevailing low weakens substantially between the 20th century and RCP 2.6. This may be related to a shift in the Pacific-South American teleconnection pattern, equivalent to the PNA shift seen in the Northern Hemisphere.

In addition to teleconnections, I also consider the possibility that the statistics of El Niño and La Niña events may change between ensembles; this issue is addressed in Chapter 5. The effective ensemble size for the CCSM4 20th and 21st centuries is enlarged by simulating the NINO3.4 SST time series for each ensemble, using a combined Markov chain/generalized linear model approach ([Stevenson 2012b]; Appendix 5). There appears to be a tendency for the wind stress and the seasonal cycle of SST to become less important in predicting NINO3.4 SST at higher CO_2, which may be related to the weakening of variability in both variables in CCSM4. In general, both El Niño and La Niña weaken with CO_2, and El Niño events become less persistent as well. The statistical significance of changes to magnitude and persistence are likely not very high, consistent with the results of Chapter 4; likewise, the return periods for 5-year events do not change significantly between ensembles.

8.5 Ideas and Future Directions

Working on the research for this dissertation has left me with at least as many questions as answers: I summarize a few of them below. These may serve as useful starting points for future investigations.

8.5.1 Diagnosing Differences Between Model ENSO Response

The stabilized CCSM3.5 simulations of ([Stevenson 2011a]; Appendix 4) showed a dramatically different ENSO response from the forced simulations in ([Stevenson 2011b]; Appendix 3). Unfortunately, as of this writing there do not exist CCSM4 simulations of sufficient length to allow me to understand the reasons for these differences. I suspect, however, that part of the difference has to do with changes to high-frequency wind stress variability; this is a triggering mechanism very often discussed for El Niño events [Gebbie 2007, Harrison 1997, Vecchi 2000]. I have taken a preliminary look at wind stress variability, by examining the 'highpass filtered' submonthly wind stress variance output from the CCSM ([Stevenson 2011a]; Appendix 4). If one assumes that all of this variability has to do with westerly wind bursts, then the results of Figure 8.1 would tend to indicate that WWBs strengthen in CCSM3.5 and weaken in CCSM4. If this is the case, then it would make intuitive sense that ENSO amplitude should respond accordingly; but there are other processes which must be taken into account for an accurate representation of the wind stress influence (*i.e.* the Madden-Julian Oscillation [Subramanian 2011]).

In reality, there are a large number of possible explanations for inter-model ENSO differences. However, in the absence of statistically significant changes to ENSO, one is constrained to ignore these processes for the most part. Thus one of the things I would like to see in the future is a series of very long, standardized simulations of stabilized climates, with a variety of GCMs. This seems to me to be a natural extension of CMIP, and allows for a much more meaningful investigation of tropical variability since sampling effects would no longer be a concern.

Although the signal is not yet significant, it would nonetheless be interesting to see whether the seasonally forced WES feedback mechanism described in ([Stevenson 2011a]; Appendix 4)operates

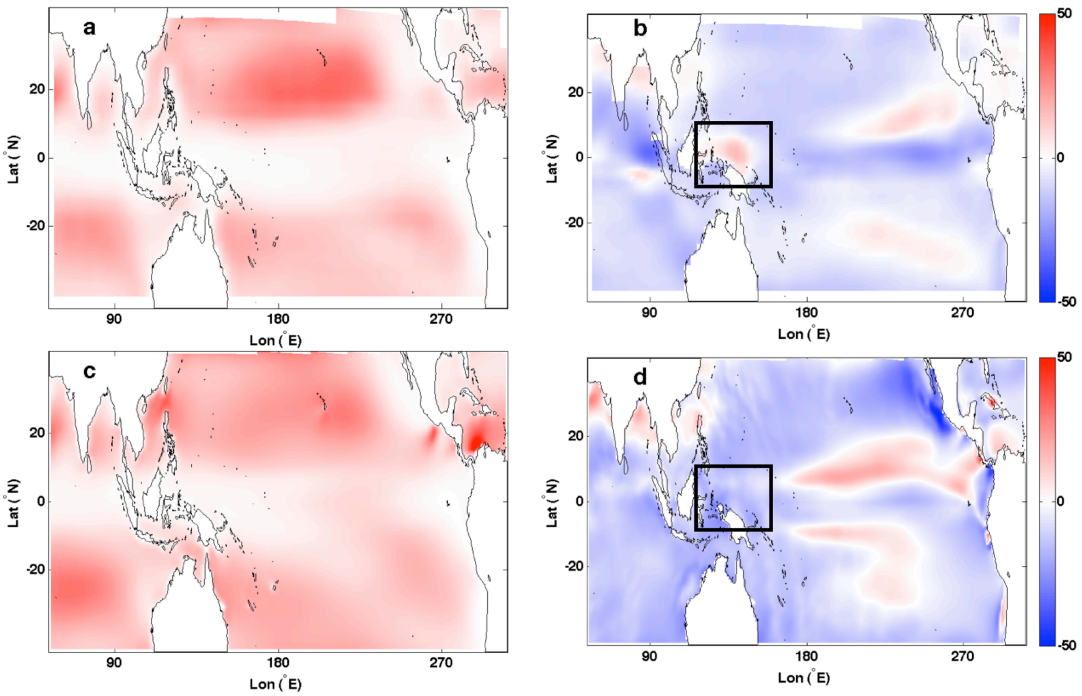

Figure 8.1: Reproduction of Figure 13 from ([Stevenson 2011a]; Appendix 4). Sub-monthly zonal wind stress variance (N^2/m^{-4}). a: Mean variance for PI (CCSM3.5), years 200-1000. b: Difference between HC and PI (CCSM3.5), years 200-1000 for both. c: Mean variance for RCP 4.5 (CCSM4), years 2250-2299. d: Difference between RCP4.5 and the CCSM4 1850 control (years 800-1299). Note that in panels b,d, the units are % (given relative to PI for panel b, CCSM4 1850 control for panel d).

in the CCSM4. The mean state changes in CCSM4 are in the same direction as in CCSM3.5, which might suggest a similar WES response, but the NINO3 SST seasonal cycle seems to weaken with CO_2 in CCSM4. Thus it is unclear how the WES feedback might respond in CCSM4, and the relationship between this change and the ENSO amplitude is also unknown. Answering this question will require reproducing the same diagnostics used in ([Stevenson 2011a]; Appendix 4), for the CMIP5 simulation ensembles.

Along the same lines, the interesting dynamical variations seen in the CCSM3.5 simulations at longer periods may bear further investigation. In particular, the role of the mean position of the warm pool in generating delayed oscillator-like variability may be quite interesting, as is the role of extratropical variability. It is possible that the interaction between ENSO and extratropical modes like the PDO responds nonlinearly to climate change, and the patterns of extratropical wind stress response change nonmonotonically in the CCSM3.5. A complete dynamical diagnosis, similar to the one for ENSO presented here, would be an interesting project in itself.

8.5.2 Response to Transient Atmospheric Forcing

Another issue I have run across during the course of this research is the question of the response to changing background forcing. All of the timescale estimates for ENSO statistical convergence presented in this dissertation ([Stevenson 2010]; Appendix 2) are only valid when the background state is stable. Yet one could perform a similar analysis on simulations where a time-varying radiative forcing is imposed. And in fact, this is the relevant situation for climate change applications. Some interesting questions then arise:

- Do the statistics of ENSO variability converge when there is a monotonic trend in tropical ocean heat content?
- If so, how does the convergence rate vary with the magnitude of the trend?
- What are the implications for atmospheric circulation and ENSO teleconnections?

- Are the dynamical changes seen in the time-varying case similar to those in the stable mean climate experiment?

Any of these would make an interesting topic for future investigation.

8.5.3 Improving Model/Proxy Comparisons

Another potentially rewarding area is improving comparisons between climate models and proxy data. This is a hot topic in the paleoclimate community at the moment [Phipps 2011], given the lack of forward modeling capacity in the current-generation CMIP models. The analysis in Chapter 2 focused on using coral δ^{18}O to reconstruct ENSO, but it is entirely possible that using additional proxies from other sources might improve the ENSO accuracy substantially [McGregor 2011b].

One obvious next step is to create a more detailed forward model for coral δ^{18}O. As noted in Chapter 2, the dimension of the coral δ^{18}O signal ranges from 6-8, and constructing a simplified mathematical model for δ^{18}O using local environmental variables would be a fascinating project in itself. Doing such a thing would require close interaction with experts in coral isotope analysis, and as such was not something I could complete within this dissertation. However, I hope to extend the collaborations I have formed in Australia and to continue this work over the course of the next few years.

I expect that there will be many potential issues with improving the δ^{18}O forward modeling capacity, which will have to be confronted. In particular, the questions which will need to be answered include:

- How big are local influences (*i.e.* runoff/lagoon effects) compared with variations in the large-scale (open ocean) environment?
- Is there a good way to predict the δ^{18}O of seawater based on open-ocean conditions?
- What is the proper mathematical form of the relation between coral δ^{18}O and local climate?

I anticipate that many more questions will arise during the course of this work.

8.6 Final Thoughts

I began this project as an attempt to identify the mechanisms for decadal variability of ENSO amplitude and the associated dynamics; but this was a question I never managed to answer. Instead, what I found was that there are fundamental gaps in our knowledge - and in the way most ENSO experiments are constructed - that prevent a straightforward diagnosis.

This dissertation has shown that it is possible to quantify the necessary length of time for ENSO behavior to 'settle down' statistically in a stable mean climate. The result obtained agrees well with previous qualitative assessments, and should provide motivation for lengthening the control simulations currently used for climate change studies. It also dovetails nicely with the experiments conducted with the CCSM3.5, which are the first comprehensive examination of CO_2-induced ENSO changes using millennial-scale GCM simulations.

The climate change simulations with CCSM4 have shown that the ENSO climate change response may take much longer than previously thought. This implies that the climate modeling community may need to rethink the entire approach to multi-model ENSO/climate change studies. It may make more sense to look in more detail at changing atmospheric teleconnections/regional impacts, rather than the slowly adjusting oceanic variability.

Now that I am able to examine my dissertation work with the benefit of hindsight, it is clear that looking at ENSO from a statistical perspective allowed me to take a somewhat 'holistic' approach to understanding the problem. I very much enjoyed the opportunity to think about past, present and future ENSO changes simultaneously, and the things I learned during each portion of the project helped to inform the questions I asked during the others. I would like to apply the same perspective to other problems in climate science in the future.

I have learned a great deal during the course of this work - I hope that it has been interesting to read about, as well.

Bibliography

[AchutaRao 2002] K. AchutaRao and K. R. Sperber. *Simulation of the El Niño Southern Oscillation: Results from the Coupled Model Intercomparison Project.* Climate Dynamics, vol. 19, pages 191–209, 2002. doi:10.1007/s00382-001-0221-9. (Cited on page 15.)

[AchutaRao 2006] K. AchutaRao and K. R. Sperber. *ENSO simulation in coupled ocean-atmosphere models: are the current models better?* Climate Dynamics, vol. 27, no. 1, pages 1–15, 2006. (Cited on page 15.)

[Akaike 1974] H. Akaike. *A new look at the statistical model identification.* IEEE Transactions on Automatic Control, vol. 19, no. 6, pages 716–723, 1974. (Cited on page 82.)

[Alexander 2002] Michael A. Alexander, Ileana Bladé, Matthew Newman, John R. Lanzante, Ngar-Cheung Lau and James D. Scott. *The Atmospheric Bridge: The Influence of ENSO Teleconnections on Air Sea Interaction over the Global Oceans.* Journal of Climate, vol. 15, pages 2205–2231, 2002. (Cited on pages 7, 92, 98 and 121.)

[Alexander 2010] M. A. Alexander, D. J. Vimont, P. Chang and J. D. Scott. *The Impact of Extratropical Atmospheric Variability on ENSO: Testing the Seasonal Footprinting Mechanism Using Coupled Model Experiments.* Journal of Climate, vol. 23, pages 2885–2901, 2010. (Cited on pages 7, 98 and 121.)

[An 2001] S.-I. An and B. Wang. *Mechanisms of Locking of the El Niño and La Niña Mature Phases to Boreal Winter.* Journal of Climate, vol. 14, pages 2164–2176, 2001. (Cited on page 14.)

[Archer 2005] C.L. Archer and M.Z. Jacobson. *Evaluation of global wind power.* Journal of Geophysical Research - Atmospheres, vol. 110, no. D12, page D12110, 2005. (Cited on page 112.)

[Ashok 2003] K. Ashok, Z. Guan and T. Yamagata. *Influence of the Indian Ocean Dipole on the Australian winter rainfall.* Geophysical Research Letters, vol. 30, page 1821, 2003. doi:10.1029/2003GL017926. (Cited on page 12.)

[Ault 2009] T. R. Ault, J. E. Cole, M. N. Evans, H. Barnett, N. J. Abram, A. w. Tudhope and B. K Linsley. *Intensified decadal variability in tropical climate during the late 19th century.* Geophysical Research Letters, vol. 36, page L08602, 2009. doi:10.1029/2008GL036924. (Cited on page 30.)

[AWEA 2010] AWEA. Wind energy assessment 2010. Australian Wind Energy Association, 2010. (Cited on page 112.)

[Baker 1995] C.B. Baker, J.K. Eischeid, T.R. Karl and H.F. Diaz. *The quality control of long-term climatological data using objective data analysis.* American Meteorological Society, Dallas, TX, Jan 15-20, 1995, 1995. Paper presented at AMS Ninth Conference on Applied Climatology. (Cited on page 34.)

[Barnett 1987] T. P. Barnett and R. Preisendorfer. *Origins and levels of monthly and seasonal forecast skill for United States surface air temperatures determined by canonical correlation analysis.* Mon. Wea. Rev., vol. 115, page 1825Ð1850, 1987. (Cited on page 76.)

[Barnston 1992] A. G. Barnston and C. F. Ropelewski. *Prediction of ENSO episodes using canonical correlation analysis.* Journal of Climate, vol. 5, pages 1316–1345, 1992. (Cited on page 76.)

[Bartis 2005] J.T. Bartis. Oil shale development in the United States: prospects and policy issues. RAND corporation, 2005. (Cited on page 112.)

[Battisti 1989] D. S. Battisti and A. C. Hirst. *Interannual variability in the tropical atmosphere/ocean system: influence of the basic state and ocean geometry.* Journal of the Atmospheric Sciences, vol. 46, pages 1687–1712, 1989. (Cited on pages viii, 5 and 6.)

[Bjerknes 1969] J. Bjerknes. *Atmospheric teleconnections from the equatorial Pacific.* Monthly Weather Review, vol. 97, pages 163–72, 1969. (Cited on pages 5 and 80.)

[Blanke 1997] B. Blanke and S. Raynaud. *Kinematics of the Pacific Equatorial Undercurrent: An Eulerian and Lagrangian Approach from GCM Results.* Journal of Physical Oceanography, vol. 27, pages 1038–1053, 1997. (Cited on page 69.)

[Boccaletti 2004] G. Boccaletti, R.C. Pacanowski, S.G.H. Philander and A.V. Fedorov. *The thermal structure of the upper ocean.* Journal of Physical Oceanography, vol. 34, pages 888–902, 2004. (Cited on page 24.)

[Branstator 1983] G. Branstator. *Horizontal energy propagation in a barotropic atmosphere with meridional and zonal structure.* Journal of the Atmospheric Sciences, vol. 40, page 1689Ð1708, 1983. (Cited on page 9.)

[Brown 2008] J. Brown, A. W. Tudhope, M. Collins and H. V. McGregor. *Mid-Holocene ENSO: Issues in quantitatve model-proxy data comparisons.* Paleoceanography, vol. 23, page PA3202, 2008. (Cited on pages 20 and 116.)

[Burgers 1999] G. Burgers and D. B. Stephenson. *The ÒnormalityÓ of El Niño.* Geophysical Research Letters, vol. 26, no. 8, page 1027Ð1030, 1999. doi:10.1029/1999GL900161. (Cited on page 50.)

[Cai 2001] W. Cai and P.G. Baines. *Forcing of the Antarctic circumpolar wave by El NiñoÐSouthern Sscillation teleconnections.* Journal of Geophysical ResearchÐOceans, vol. 106, page 9019Ð9038, 2001. (Cited on page 12.)

[Cai 2009] W. Cai, T. Cowan and A. Sullivan. *Recent unprecedented skew- ness towards positive Indian Ocean Dipole occurrences and its impact on Australian rainfall.* Geophysical Research Letters, vol. 36, page L11705, 2009. doi:10.1029/2009GL037604. (Cited on page 24.)

[Cai 2011] W. Cai, P. van Rensch, T. Cowan and H. H. Hendon. *Teleconnection Pathways of ENSO and the IOD and the Mechanisms for Impacts on Australian Rainfall.* Journal of Climate, vol. 24, pages 3910–3923, 2011. (Cited on pages 11, 12 and 24.)

[Cane 1997] M. A. Cane, A. C. Clement, A. Kaplan, Y. Kushnir, D. Pzdnyakov, R. Seager, S. E. Zebiak and R. Murtugudde. *Twentieth-century sea surface temperature trends.* Science, vol. 275, pages 957–960, 1997. (Cited on page 23.)

[Cane 2001] M. A. Cane and P. Molnar. *Closing of the Indonesian seaway as a precursor to east African aridification around 3∼4 million years ago.* Nature, vol. 411, pages 157–162, 2001. (Cited on page 18.)

[Cane 2005] M.A. Cane. *The evolution of El Niño, past and future.* Earth and Planetary Science Letters, vol. 230, page 227Ð240, 2005. (Cited on page 18.)

[Capotondi 2006] A. Capotondi, A. Wittenberg and S. Masina. *Spatial and temporal structure of Tropical Pacific interannual variability in 20th century coupled simulations.* Ocean Modelling, vol. 15, pages 274–298, 2006. (Cited on pages 15, 59 and 93.)

[Carillo 1892] C. N. Carillo. *Disertacion sobre las Corrientes Oceanicas y Estudias de la Corriente Peruana o de Humboldt.* Bol. Soc. Geogr. Lima, vol. 11, pages 52–110, 1892. Microficha. (Cited on page 1.)

[Carranza 1891] L. Carranza. *Contra-corriente maritima observada Piata y Pacasmayo.* Bol. Soc. Geogr. Lima, vol. 1, no. 9, pages 344–345, 1891. (Cited on page 1.)

[Cayan 1992] D. R. Cayan and R. H. Webb. *El Niño-Southern Oscillation and streamflow in the western United States.* In H. F. Diaz and V. Markgraf, editeurs, El Niño: Historical and Paleoclimatic Aspects of the Southern Oscillation, pages 29–68. Cambridge University Press, 1992. (Cited on page 11.)

[Cayan 2010] D.R. Cayan, T. Das, D. W. Pierce, T.P. Barnett, M. Tyree and A. Gershunov. *Future dryness in the southwest US and the hydrology of the early 21st century drought.* Proceedings of the National Academy of Sciences, vol. 107, pages 21271–21276, 2010. doi:10.1073/pnas.0912391107. (Cited on page 11.)

[CBO 2009] CBO. The Impact of Ethanol Use on Food Prices and Greenhouse Gas Emissions (online). US Congress, Congressional Budget Office, 2009. http://www.cbo.gov/ftpdocs/100xx/doc10057/04-08-Ethanol.pdf. (Cited on page 113.)

[Chang 1995] P. Chang, L. Ji, B. Wang and T. Li. *Interactions between the seasonal cycle and El NioÐSouthern Oscillation in an intermediate coupled oceanÐatmosphere model.* Journal of the Atmospheric Sciences, vol. 52, page 2353Ð2372, 1995. (Cited on page 7.)

[Chapman 1987] N.A. Chapman and I.G. McKinley. The geological disposal of nuclear waste. John Wiley & Sons, Inc., New York, N.Y., 1987. (Cited on page 112.)

[Chen 2010] W. Chen and R. Xu. *Clean coal technology development in China.* Energy Policy, vol. 38, pages 2123–2130, 2010. (Cited on page 111.)

[Chiang 2009] J. C. H. Chiang. *The Tropics in Paleoclimate.* Annu. Rev. Earth Planet. Sci., vol. 37, page 263Ð297, 2009. doi: 10.1146/annurev.earth.031208.100217. (Cited on page 18.)

[Christodouleas 2011] J. P. Christodouleas, R. D. Forrest, C. G. Ainsley, Z. Tochner, S. M. Hahn and E. Glatstein. *Short-Term and Long-Term Health Risks of Nuclear-Power-Plant Accidents.* The New England Journal of Medicine, vol. 364, pages 2334–2341, 2011. doi:10.1056/NEJMra1103676. (Cited on page 112.)

[Clark 2001] M.P. Clark, M.C. Serreze and G.J. McCabe. *Historical effects of El Nino and La Nina events on the seasonal evolution of the montane snowpack in the Columbia and Colorado River Basins.* Water Resources Research, vol. 37, no. 3, pages 741–757, 2001. (Cited on page 11.)

[Clarke 2003] A.J. Clarke and S. Van Gorder. *Improving El Niño prediction using a space-time integration of Indo-Pacific winds and equatorial Pacific upper ocean heat content.* . Geophysical Research Letters, vol. 30, no. 7, 2003. doi:10.1029/2002GL016673. (Cited on page 76.)

[Clarke 2007] L. Clarke, J. Edmonds, H. Jacoby, H. Pitcher, J. Reilly and R. Richels. *Scenarios of greenhouse gas emissions and atmospheric concentrations.* In Sub-report 2.1A of Synthesis and Assessment Product 2.1 by the U.S. Climate Change Science Program and the Subcommittee on Global Change Research, page 154 pp. Department of Energy, Office of Biological & Environmental Research, Washington, DC., 2007. (Cited on pages xiii, 107, 110 and 111.)

[Clarke 2008] A. Clarke. An introduction to the dynamics of El Niño and the Southern Oscillation. Academic Press, Elsevier, London, UK, 2008. (Cited on page 9.)

[Cobb 2001] K.M. Cobb, C.D. Charles and D.E. Hunter. *A central tropical Pacic coral demonstrates Pacic, Indian, and At- lantic decadal climate connections.* Geophysical Research Letters, vol. 28, pages 2209–2212, 2001. (Cited on page 32.)

[Cobb 2003] K. M. Cobb, C. D. Charles, R. L. Edwards, H. Cheng and M. Kastner. *U/Th-dating living and young fossil corals from the central tropical Pacific.* . Earth and Planetary Science Letters, vol. 210, pages 91–103, 2003. (Cited on page 31.)

[Cole 1993] J. E. Cole, R. G. Fairbanks and G. T. Shen. *Recent Variability in the Southern Oscillation: Isotopic Results from a Tarawa Atoll Coral.* Science, vol. 260, pages 1790–1793, 1993. (Cited on page 32.)

[Collins 2010] M. Collins, S.-I. An, W. Cai, A. Ganachaud, E. Guilyardi, F.-F. Jin, M. Jochum, M. Lengaigne, S. Power, A. Timmermann, G. Vecchi and A. Wittenberg. *The impact of global warming on the tropical Pacific Ocean and El Niño.* Nature Geoscience, vol. 3, pages 391–397, 2010. doi:10.1038/NGEO868. (Cited on pages ix, 20, 21, 24 and 93.)

[Danabasoglu 2007] G. Danabasoglu and J. Marshall. *Effects of vertical variations of thickness diffusivity in an ocean general circulation model.* Ocean Modelling, vol. 18, pages 122–141, 2007. (Cited on pages 64 and 89.)

[D'Arrigo 2005] R. D'Arrigo, R. Wilson, C. Deser, G. Wiles and E. Cook. *Tropical-North Pacific climate linkages over the past four centuries.* Journal of Climate, vol. 18, pages 5253–5365, 2005. (Cited on page 30.)

[D'Arrigo 2006] R. D'Arrigo, R. Wilson, J. Palmer, P. Krusic and et al. Curtis A. *The reconstructed Indonesian warm pool sea surface temperatures from tree rings and corals: linkages to Asian monsoon drought and El Niño- Southern Oscillation.* Paleoceanography, vol. 21, 2006. DOI:10.1029/2005 PA001256. (Cited on page 30.)

[Daubechies 1990] I. Daubechies. *The wavelet transform, time-frequency localization and signal analysis.* IEEE Trans. Inform. Theory, vol. 36, pages 961–1004, 1990. (Cited on page 51.)

[Davey 2002] M. Davey and Coauthors. *STOIC: A study of coupled model climatology and variability in tropical ocean regions.* Climate Dynamics, vol. 18, pages 403–420, 2002. (Cited on page 15.)

[Dempster 1977] A. P. Dempster, N. M. Laird and D. B. Rubin. *Maximum Likelihood from Incomplete Data via the EM Algorithm.* Journal of the Royal Statistical Society. Series B (Methodological), vol. 39, no. 1, pages 1–38, 1977. (Cited on page 43.)

[Deser 1990] C. Deser and J. M. Wallace. *Large-scale atmospheric circulation features of warm and cold episodes in the Tropical Pacific.* Journal of Climate, vol. 3, pages 1254–1281, 1990. (Cited on page 33.)

[Deser 1995] C. Deser and M. L. Blackmon. *On the relationship between Tropical and North Pacific sea surface temperature variations.* Journal of Climate, vol. 8, pages 1677–1680, 1995. (Cited on page 9.)

[Deser 1996] C. Deser, A. Alexander and M. S. Timlin. *Upper-ocean thermal variations in the North Pacific during 1970-1991.* Journal of Climate, vol. 9, pages 1840–1855, 1996. (Cited on page 7.)

[Deser 2006] C. Deser, A. Capotondi, R. Saravanan and A.S. Phillips. *Tropical Pacific and Atlantic Climate Variability in CCSM3.* Journal of Climate, vol. 19, no. 11, pages 2451–2481, 2006. (Cited on pages 70, 93 and 121.)

[Deser 2011] C. Deser, A. Capotondi and M. Alexander. *Tropical variability in the CCSM4.* Journal of Climate, 2011. submitted. (Cited on pages 16, 55, 60, 65 and 89.)

[Dettinger 2000] M. D. Dettinger, D. R. Cayan, G. J. McCabe and J. M. Marengo. *Multiscale streamflow variability associated with El Niño/Southern Oscillation.* In H. F. Diaz and V. Markgraf, editeurs, El Niño and the Southern Oscillation: Multiscale Variability and Global and Regional Impacts, pages 113–147. Cambridge University Press, 2000. (Cited on page 11.)

[DeWeaver 2002] E. DeWeaver and S. Nigam. *Linearity in ENSO's Atmospheric Response.* Journal of Climate, vol. 15, page 2446Ð2461, 2002. (Cited on page 8.)

[DiNezio 2010] P. N. DiNezio, A. C. Clement and G. A. Vecchi. *Reconciling Differing Views of Tropical Pacific Climate Change.* Eos, vol. 91, no. 16, pages 141–143, 2010. (Cited on page 93.)

[Dobson 2002] A. Dobson. Introduction to Generalized Linear Models (2nd edition). Chapman & Hall/CRC, 2002. ISBN 1-58488-165-8. (Cited on pages 77 and 78.)

[Ebbesmeyer 1991] C. C. Ebbesmeyer, D. R. Cayan, D. R. McLain, F. H. Nichols, D. H. Peterson and K. T. Redmond. *1976 step in the Pacific climate: forty environmental changes between 1968-1975 and 1977-1984.* In Proceedings of the Seventh annual Pacific Climate (PACLIM) Workshop : Asilomar, California – April, 1990. West Sacramento, CA, California Department

of Water Resources. Interagency Ecology Studies Program., pages 115–126. 1991. (California Department of Water Resources. Interagency Ecology Studies Program.Technical Report,26). (Cited on page 7.)

[Emile-Geay 2011a] J. Emile-Geay, K. M. Cobb, M. E. Mann and A. Wittenberg. *Estimating Tropical Pacific SST variability over the Past Millennium. Part 1: Methodology and Validation.* Journal of Climate, 2011. submitted. (Cited on page 43.)

[Emile-Geay 2011b] J. Emile-Geay, K. M. Cobb, M. E. Mann and A. Wittenberg. *Estimating Tropical Pacific SST variability over the Past Millennium. Part 2: Reconstructions and Uncertainties.* Journal of Climate, 2011. submitted. (Cited on page 43.)

[Evans 1998] M. N. Evans, A. Kaplan and M. A. Cane. *Optimal sites for coral-based reconstructions of global sea surface temperature.* Paleoceanography, vol. 13, no. 5, pages 502–516, 1998. (Cited on pages 19, 33 and 36.)

[Evans 2002] M. N. Evans, A. Kaplan and M. A. Cane. *Pacific sea surface temperature field reconstruction from coral $\delta^{18}O$ data using reduced space objective analysis.* Paleoceanography, vol. 17, no. 1, page 1007, 2002. doi:0.1029/2000PA000590. (Cited on pages x, 30, 45 and 46.)

[EWEA 2009] EWEA. Oceans of Opportunity: Harnessing Europe's largest domestic energy source. European Wind Energy Association, 2009. (Cited on page 112.)

[Farge 1992] M. Farge. *Wavelet transforms and their application to turbulence.* Annu. Rev. Fluid Mech., vol. 24, pages 395–457, 1992. (Cited on page 52.)

[Fedorov 2001] A. V. Fedorov and S. G. Philander. *A stability analysis of tropical ocean-atmosphere interactions: Bridging measurements and theory for El Niño.* Journal of Climate, vol. 14, pages 3086–3101, 2001. (Cited on pages 6 and 101.)

[Fedorov 2006] A. V. Fedorov, P. S. Dekens, M. McCarthy, A. C. Ravelo, P. B. deMenocal, M. Barreiro, R. C. Pacanowski and S. G. Philander. *The Pliocene Paradox (Mechanisms for a Permanent El Niño).* Science, vol. 312, pages 1485–1489, 2006. (Cited on page 18.)

[Felis 2003] T. Felis and J. Pätzold. *Climate records from corals.* In Marine Science Frontiers for Europe. Berlin Heidelberg: Springer- Verlag, 2003. (Cited on page 18.)

[Fichaux 2009] N. Fichaux and J. (eds) Wilkes. *Oceans of opportunity: Harnessing Europe's largest domestic energy resource.* European Wind Energy Association, page 69, 2009. (Cited on page 112.)

[Fisher 2007] B.S. Fisher, N. Nakicenovic, K. Alfsen, J. C. Morlot, F. de la Chesnaye, J.-Ch. Hourcade, K. Jiang, M. Kainuma, E. La Rovere, A. Matysek, A. Rana, K. Riahi, R. Richels, S. Rose, D. van Vuuren and R. Warren. *Issues related to mitigation in the long-term context.* In Metz., B. and Davidson, O.R. and Bosch, P.R. and Dave, R. and Meyer, L.A. [eds], editeur, Climate Change 2007: Mitigation. Contribution of Working Group III to the Fourth Assessment Report of the Inter-governmental Panel on Climate Change. Cambridge University Press, Cambridge, U.K., 2007. (Cited on page 113.)

[Frankignoul 1977] C. Frankignoul and K. Hasselmann. *Stochastic climate models. II: Application to sea surface temperature variability and thermocline variability.* Tellus, vol. 29, pages 284–305, 1977. (Cited on page 60.)

[Fraser 1986] A. M. Fraser and H. L. Swinney. *Independent coordinates for strange attractors from mutual information.* Phys. Rev. A, vol. 33, no. 2, pages 1134–1140, 1986. (Cited on page 40.)

[Fujino 2006] J. Fujino, R. Nair, M. Kainuma, T. Masui and M. Matsuoka. *Multigas mitigation analysis on stabilization scenarios using AIM global model.* Multigas Mitigation and Climate Policy: The Energy Journal Special Issue, pages 343–354, 2006. (Cited on page 107.)

[Gebbie 2007] G. Gebbie, I. Eisenman, A. Wittenberg and E. Tziperman. *Modulation of Westerly Wind Bursts by Sea Surface Temperature: A Semi-Stochastic Feedback for ENSO.* Journal of the Atmospheric Sciences, vol. 64, pages 3281–3295, 2007. (Cited on pages 6 and 123.)

[Gent 2010] P. R. Gent, S. G. Yeager, R. B. Neale, S. Levis and D. A. Bailey. *Improvements in a half degree atmosphere/land version of the CCSM.* Clim. Dyn., vol. 34, page 819Ð833, 2010. doi: 10.1007/ s00 382Ð009Ð0614Ð8. (Cited on page 16.)

[Gent 2011] P. R. Gent, G. Danabasoglu, L. J. Donner, M. M. Holland, E. C. Hunke, S. R. Jayne, D. M. Lawrence, R. B. Neale, P. J. Rasch, M. Vertenstein, P. H. Worley, Z. L. Yang and M. Zhang. *The Community Climate System Model version 4* . Journal of Climate, 2011. submitted. (Cited on pages 16 and 64.)

[Gergis 2005] J. L. Gergis and A. M. Fowler. *Classification of Synchronous Oceanic and Atmospheric El Niño-Southern Oscillation (ENSO) Events for Palaeoclimate Reconstruction.* International Journal of Climatology, vol. 25, pages 1541–1565, 2005. (Cited on page 28.)

[Gershunov 1998] A. Gershunov and T. Barnett. *Inter-decadal modulation of ENSO teleconnections.* Bulletin of the American Meteorological Society, vol. 79, pages 2715–2725, 1998. (Cited on pages 7 and 11.)

[Ghil 1991] M. Ghil and K. C. Mo. *Intraseasonal oscillations in the global atmosphere. Part II: Southern Hemisphere.* Journal of the Atmospheric Sciences, vol. 48, page 780Ð790, 1991. (Cited on page 11.)

[Gill 1980] A. E. Gill. *Some simple solutions for heat induced tropical circulation.* Q. J. R. Meteorol. Soc., vol. 106, pages 447–462, 1980. (Cited on pages 3 and 7.)

[Gleckler 2008] P.J. Gleckler, K.E. Taylor and C. Doutriaux. *Performance metrics for climate models.* Journal of Geophysical Research, vol. 113, page D06104, 2008. doi:10.1029/2007JD008972. (Cited on page 17.)

[Graham 1994] N.E. Graham. *Decadal-scale climate variability in the tropical and North Pacific during the 1970s and 1980s: observations and model results.* Clim. Dyn., vol. 10, pages 135–162, 1994. (Cited on page 7.)

[Gu 1997] D. Gu and S.G.H. Philander. *Interdecadal climate fluctuations that depend on exchanges between the tropics and the extratropics.* Science, vol. 275, pages 805–807, 1997. (Cited on page 7.)

[Guilderson 1999] T. P. Guilderson and D. P. Schrag. *Reliability of coral iso- tope records from the western Pacic warm pool: a compar- ison using age-optimized records.* Paleoceanography, vol. 14, pages 457–464, 1999. (Cited on page 34.)

[Guilderson 2001] T.P. Guilderson, R.G. Fairbanks and J.L. Rubenstone. *Tropical Atlantic coral oxygen isotopes: glacial-interglacial sea surface temperatures and climate change.* . Mar Geol, vol. 172, page 75Ð89, 2001. (Cited on page 19.)

[Guilyardi 2006] E. Guilyardi. *El Niño-mean state-seasonal cycle interactions in a multi-model ensemble.* Climate Dynamics, vol. 26, pages 329–348, 2006. (Cited on page 7.)

[Guilyardi 2009a] E. Guilyardi, P. Braconnot, F.-F. Jin, S.-T. Kim, M. Kolaskinski, T. Li and A. Musat. *Atmosphere Feedbacks during ENSO in a Coupled GCM with a Modified Atmospheric Convection Scheme.* Journal of Climate, vol. 22, pages 5698–5718, 2009. (Cited on page 24.)

[Guilyardi 2009b] E. Guilyardi, A. Wittenberg, A. Fedorov, M. Collins, C. Wang, A. Capotondi, G. Jan van Oldenborgh and T. Stockdale. *Understanding El Niño in Ocean-Atmosphere General Circulation Models: Progress and Challenges.* BAMS, pages 325–340, 2009. (Cited on pages 15, 17, 20 and 94.)

[GWEC 2008] GWEC. Global Wind Energy Outlook 2008. Global Wind Energy Council/Greenpeace, 2008. (Cited on page 112.)

[Harangozo 2000] S.A. Harangozo. *A search for ENSO teleconnections in the west Antarctic Peninsula climate in Austral winter.* International Journal of Climatology, vol. 20, page 663Ð679, 2000. (Cited on page 14.)

[Hare 2000] S.R. Hare and N.J. Mantua. *Empirical evidence for North Pacific regime shifts in Pacific North America.* Progress in Oceanography, vol. 47, pages 103–145, 2000. (Cited on page 7.)

[Harrison 1997] D. E. Harrison and G. A. Vecchi. *Westerly Wind Events in the Tropical Pacific, 1986-95.* Journal of Climate, vol. 10, pages 3131–3156, 1997. (Cited on pages 80 and 123.)

[Hasselmann 1976] K. Hasselmann. *Stochastic climate models. Part I: Theory.* Tellus, vol. 28, pages 473–485, 1976. (Cited on page 60.)

[Hawkins 2009] D. Hawkins, G. Peridas and J. Steelman. *Twelve years after Sleipner: moving CCS from hype to pipe.* Energy Procedia, vol. 1, page 4)40003?ÐÐ0404010, 2009. (Cited on page 113.)

[Haywood 2007] A. M. Haywood, P. J. Valdes and V. L. Peck. *A permanent El Niño-like state during the Pliocene?* Paleoceanography, vol. 22, page PA1213, 2007. doi:10.1029/2006PA001323. (Cited on page 18.)

[Held 1989] I.M. Held, S.W. Lyons and S. Nigam. *Transients and the extratropical response to El Niño.* Journal of the Atmospheric Sciences, vol. 46, page 163 Ð 174, 1989. (Cited on page 12.)

[Held 2006] I.M. Held and B.J. Soden. *Robust Responses of the Hydrological Cycle to Global Warming.* Journal of Climate, vol. 19, pages 5686–5699, 2006. (Cited on pages 22 and 23.)

[Hendon 2007] H. H. Hendon, D. W. J. Thompson and M. C. Wheeler. *Australian rainfall and surface temperature variations associated with the Southern Hemisphere Annular Mode.* Journal of Climate, vol. 20, page 2452Ð2467, 2007. (Cited on page 12.)

[Hendriks 2002] C. Hendriks, W. Graus and F. van Bergen. GLOBAL CARBON DIOXIDE STORAGE POTENTIAL AND COSTS. Ecofys, Utrecht, 2002. (Cited on page 113.)

[Hibbard 2007] K.A. Hibbard, G.A. Meehl, P.M. Cox and P. Friedlingstein. *A strategy for climate change stabilization experiments.* Eos, vol. 88, no. 20, pages 217,219,221, 2007. (Cited on page 108.)

[Hildebrandsson 1897] H. H. Hildebrandsson. *Quelques recherches sur les centres d'action de l'atmosphere. I-IV.* Kongl. Svenska Vetenskaps-Akademiens Handlingar, vol. 29, no. 3, page 36 pp., 1897. (Cited on page 2.)

[Hoerling 2002] M. P. Hoerling and A. Kumar. *Atmospheric Response Patterns Associated with Tropical Forcing.* Journal of Climate, vol. 15, pages 2184–2203, 2002. (Cited on pages 8 and 9.)

[Hoffert 1998] M.I. Hoffert, K. Caldeira, A.K. Jain, E.F. Haites, L.D. Danny Harvey, S.D. Potter, M.E. Schlesinger, S.H. Schneider, R.G. Watts, T.M.L. Wigley and D.J. Wuebbles. *Energy implications of future stabilization of atmospheric CO_2 content.* Nature, vol. 395, pages 881–884, 1998. (Cited on page 108.)

[Hoffert 2002] M.I. Hoffert, K. Caldeira, G. Benford, D.R. Criswell, C. Green, H. Herzong, A.K. Jain, H.S. Kheshgi, K.S. Leckner, J.S. Lewis, H.D. Lightfoot, W. Manheimer, J.C. Mankins, M.E. Mauel, J. Perkins, M.E. Schlesinger, T. Volk and T.M.L. Wigley. *Advanced technology paths to global climate stability: Energy for a greenhouse planet.* Science, vol. 298, pages 981–987, 2002. (Cited on page 108.)

[Holmgren 2001] M. Holmgren, M. Scheffer and E. et al. Ezcurra. *El Niño effects on the dynamics of terrestrial ecosystems.* Trends in Ecology and Evolution, vol. 16, page 89Ð94, 2001. (Cited on page 11.)

[Holmgren 2006] M. Holmgren, P. Stapp, C.R. Dickman, C. Gracia, S. Graham, J. R. Gutierrez, C. Hice, F. Jaksic, D. A. Kelt, M. Letnic, M. Lima, B. C. Lopez, P.L. Meserve, W.B. Milstead,

G.A. Polis, M.A. Previtali, M. Richter, S. Sabate and F. A. Squeo. *Extreme climatic events shape arid and semiarid ecosystems.* Frontiers in Ecology and the Environment, vol. 4, no. 2, pages 87–95, 2006. (Cited on page 11.)

[Holton 2004] J Holton. An Introduction to Dynamic Meteorology, Volume 88, Fourth Edition. International Geophysics series, Elsevier, London, UK, 2004. (Cited on page 9.)

[Horel 1981] J. D. Horel and J. M. Wallace. *Planetary scale atmospheric phenomena associated with the Southern Oscillation.* Mon. Wea. Rev., vol. 109, pages 813–829, 1981. (Cited on page 9.)

[Hoskins 1981] B. J. Hoskins and D. J. Karoly. *The Steady Linear Response of a Spherical Atmosphere to Thermal and Orographic Forcing.* Journal of the Atmospheric Sciences, vol. 38, pages 1179–1196, 1981. (Cited on page 9.)

[Hoskins 1991] B. J. Hoskins and F.-F. Jin. *Initial Value Problem for Tropical Perturbations to a Baroclinic Atmosphere.* Quart. J. Roy. Met. Soc., vol. 117, pages 299–317, 1991. (Cited on page 9.)

[Hoskins 1993] B. J. Hoskins and T. Ambrizzi. *Rossby wave propagation on a realistic longitudinally varying flow.* Journal of the Atmospheric Sciences, vol. 50, page 1661Ð1671, 1993. (Cited on page 9.)

[Howden 2004] S.M. Howden, S.E. Bruce and S. Graham. *Pasture cropping: the theory.* Grains Research Update - August 2004., 2004. (Cited on page 11.)

[I. 1995] Simmonds I. and TH. Jacka. *Relationships between the interannual variability of Antarctic sea ice and the Southern Oscillation.* Journal of Climate, vol. 8, page 637Ð647, 1995. (Cited on page 14.)

[IEA 2008] IEA. Towards A Sustainable Energy Future. International Energy Association, 2008. (Cited on page 111.)

[Izumo 2002] T. Izumo, J. Picaut and B. Blanke. *Tropical pathways, equatorial undercurrent variability and the 1998 La Niña.* Geophysical Research Letters, vol. 29, no. 22, page 2080, 2002. doi:10.1029/2002GL015073. (Cited on page 7.)

[Jin 1993] F.-F. Jin and J. D. Neelin. *Modes of interannual tropical ocean-atmosphere interaction - a unified view. Part I: numerical results.* Journal of the Atmospheric Sciences, 1993. (accepted). (Cited on page 6.)

[Jin 1994] F.-F. Jin, J. D. Neelin and M. Ghil. *El Niño on the devilÕs staircase: Annual subharmonic steps to chaos.* Science, vol. 264, pages 70–72, 1994. (Cited on page 7.)

[Jin 1997] F.-F. Jin. *A theory of interdecadal climate variability of the North Pacific Ocean-Atmosphere system.* Journal of Climate, vol. 10, pages 1821–1835, 1997. (Cited on pages viii, 5, 6 and 80.)

[Jin 2008] E. K. Jin, J. L. III Kinter, B. Wang, C.-K. Park, I.-S. Kang, B. P. Kirtman, J.-S. Kug, A. Kumar, J.-J. Luo, J. Schemm, J. Shukla and T. Yamagata. *Current status of ENSO prediction skill in coupled ocean-atmosphere models.* Climate Dynamics, vol. 31, pages 647–664, 2008. doi:10.1007/s00382-008-0397-3. (Cited on page 76.)

[Jochum 2008] M. Jochum, G. Danabasoglu, M. Holland, Kwon and W. Large. *Ocean Viscosity and Climate.* Journal of Geophysical Research, vol. 113, page C06017, 2008. doi:10.1029/2007JC004515. (Cited on pages 64 and 89.)

[Jochum 2009] M. Jochum, B. Fox-Kemper, P.H. Molnar and C. Shields. *Differences in the Indonesian seaway in a coupled climate model and their relevance to Pliocene climate and El Niño.* Paleoceanography, vol. 24, page PA1212, 2009. doi:10.1029/2008PA001678. (Cited on pages 64 and 89.)

[Jochum 2010] M. Jochum, S. Yeager, K. Lindsay, K. Moore and R. Murtugudde. *Quantification of the feedback between phytoplankton and ENSO in the Community Climate System Model.* Journal of Climate, vol. 23, no. 11, pages 2916–2925, 2010. (Cited on page 16.)

[Joussaume 2000] S. Joussaume and K.E. Taylor. *The Paleoclimate Modeling Intercomparison Project*. In Paleoclimate Modelling Intercomparison Project (PMIP). Proceedings of the Third PMIP workshop, La Huardiere, Canada, 4-8 October 1999, pages 9–25. WCRP, 2000. (Cited on page 19.)

[Kalnay 1996] E. Kalnay*et al.* *The NCEP/NCAR 40-year reanalysis project*. Bull. Am. Meteor. Soc., vol. 77, pages 437–471, 1996. (Cited on page 17.)

[Kaplan 1997] A. Kaplan, Y. Kushnir, M. A. Cane and M. B. Blumenthal. *Reduced space optimal analysis for historical data sets: 136 years of Atlantic sea surface temperatures*. Journal of Geophysical Research, vol. 102, pages 27835–27860, 1997. (Cited on page 46.)

[Kaplan 1998] A. Kaplan, M. A. Cane, Y. Kushnir, A. C. Clement, M. B. Blumenthal and B. Rajagopalan. *Analyses of global sea surface temperature: 1856-1991*. Journal of Geophysical Research, vol. 103, pages 18567–18589, 1998. (Cited on page 46.)

[Kaplan 2000] A. Kaplan, Y. Kushnir and M. A. Cane. *Analysis of historical sea level pressure 1854Ð 1992*. Journal of Climate, vol. 13, pages 2987–3002, 2000. (Cited on page 46.)

[Karnauskas 2009] K.B. Karnauskas, R. Seager, A. Kaplan, Y. Kushnir and M.A. Cane. *Observed Strengthening of the Zonal Sea Surface Temperature Gradient across the Equatorial Pacific Ocean*. Journal of Climate, vol. 22, pages 4316–4321, 2009. doi:10.1175/2009JCLI2936.1. (Cited on page 22.)

[Karoly 1983] D. J. Karoly. *Rossby-wave propagation in a barotropic atmosphere*. Dyn. Atmos. Oceans, vol. 7, page 111Ð125, 1983. (Cited on page 9.)

[Karoly 1989] D. J. Karoly. *Southern hemisphere circulation features associated with El Niño-Southern Oscillation events*. Journal of Climate, vol. 2, pages 1239–1252, 1989. (Cited on pages viii, 11, 12 and 13.)

[Kennel 1992] M. B. Kennel, R. Brown and H. D. I. Abarbanel. *Determining embedding dimension for phase-space reconstruction using a geometrical construction.* Phys. Rev. A, vol. 45, page 3403, 1992. (Cited on page 41.)

[Kessler 2002] W.S. Kessler. *Is ENSO a cycle or a series of events?* Geophysical Research Letters, vol. 29, no. 23, page 2125, 2002. doi:10:1029/2002GL015924. (Cited on pages 5 and 50.)

[Kessler 2006] W. S. Kessler. *The circulation of the eastern tropical Pacific: A review.* Progress In Oceanography, vol. 69, pages 181–217, 2006. doi:10.1016/j.pocean.2006.03.009. (Cited on page 69.)

[Kiem 2001] A.S. Kiem and S.W. Franks. *On the identiÞcation of ENSO-induced rainfall and runoff variability: a comparison of methods and indices.* Hydrological Sciences Journal, vol. 46, no. 5, page 715Ð727, 2001. (Cited on page 11.)

[Klara 2002] S.M. Klara and R.D. Srivastava. *Integrated collaborative technology development program for CO_2 separation and capture - U.S. Department of Energy R&D.* Environ. Prog., vol. 21, page 247, 2002. (Cited on page 113.)

[Klara 2003] S.M. Klara, R.D. Srivastava and H.G. McIlvried. *Integrated collaborative technology development program for CO_2 sequestration in geologic formations - United States Department of Energy R&D.* Energy Conversion & Management, vol. 44, pages 2699–2712, 2003. (Cited on page 113.)

[Kleeman 1999] R. Kleeman, J.P. McCreary and B.A. Klinger. *A mechanism for generating decadal ENSO variability.* Geophysical Research Letters, vol. 26, pages 1743–1746, 1999. (Cited on page 7.)

[Kleeman 2006] R. Kleeman. *Statistical predictability in the atmosphere and other dynamical systems.* Physica D, vol. 230, pages 65–71, 2006. (Cited on page 6.)

[Kleeman 2008] R. Kleeman. *Stochastic theories for the irregularity of ENSO.* Philosophical Transactions of the Royal Society, vol. 366, pages 2511–2526, 2008. (Cited on page 6.)

[Kondo 1988] J. Kondo. *Volcanic eruptions, cool summers and famines in the northeastern part of Japan.* Journal of Climate, vol. 1, page 775Ð788, 1988. (Cited on page 7.)

[Kug 2007] J.S. Kug, J.Y. Lee and I.S. Kang. *Global sea surface temperature prediction using a multi-model ensemble.* Mon Wea Rev, vol. 135, page 3239Ð3247, 2007. (Cited on page 76.)

[Kug 2008] J.S. Kug, I.S. Kang and D.H. Choi. *Seasonal climate predictability with tier-one and tier-two prediction Systems.* Clim Dyn., 2008. doi: 10.1007/s00382-007- 0264-7. (Cited on page 76.)

[Landsea 2000] C. W. Landsea and J. A. Knaff. *How much skill was there in forecasting the very strong 1997-98 El Nino?* Bull. Am. Meteor. Soc., vol. 81, pages 2107–2119, 2000. (Cited on page 76.)

[Large 2006] W. G. Large and G. Danabasoglu. *Attribution and Impacts of Upper-Ocean Biases in CCSM3.* Journal of Climate, vol. 19, pages 2325–2346, 2006. (Cited on page 64.)

[Large 2008] W. G. Large and S. G. Yeager. *The global climatology of an interannually varying air-sea flux data set.* Climate Dynamics, vol. 33, pages 341–364, 2008. (Cited on pages 52, 56 and 118.)

[Latif 1998] M. Latif, D. Anderson, T. Barnett, M. Cane, R. Kleeman, A. Leetmaa, J. O'Brien, A. Rosati and E. Schneider. *A review of the predictability and prediction of ENSO.* Journal of Geophysical Research, vol. 103, no. C7, pages 14375–14393, 1998. (Cited on pages 7 and 76.)

[Latif 2001] M. Latif, K. Sperber, J. Arblaster, P. Braconnot, D. Chen, A. Colman, U. Cubasch, C. Cooper, P. Delecluse, D. DeWitt, L. Fairhead, G. Flato, T. Hogan, M. Ji, M. Kimoto, A. Kitoh, T. Knutson, H. Le Treut, T. Li, S. Manabe, O. Marti, C. Mechoso, G. Meehl,

S. Power, E. Roeckner, J. Sirven, L. Terray, A. Vintzileos, R. Voβ, B. Wang, W. Washington, I. Yoshikawa, J. Yu and S. Zebiak. *ENSIP: the El Niño simulation intercomparison project.* Climate Dynamics, vol. 18, pages 255–276, 2001. (Cited on page 15.)

[Lau 1997] K. M. Lau, H.T. Wu and S. Bony. *The Role of Large Scale Atmospheric Circulation in the Relationship Between Tropical Convection and Sea Surface Temperature.* Journal of Climate, vol. 10, pages 381–392, 1997. (Cited on page 8.)

[Leder 1996] J. J. Leder, P. K. Swart, A. M. Szmant and R. E. Dodge. *The origin of variations in the isotopic record of scleractinian corals: I. Oxygen.* Geochimica et Cosmochimica Acta, vol. 60, pages 2857–2870, 1996. (Cited on page 18.)

[Leighly 1933] J. B. Leighly. *Marquesan meteorology.* Univ. Calif. Publ. Geogr., vol. 6, no. 4, pages 147–172, 1933. (Cited on page 3.)

[Lengaigne 2006] M. Lengaigne, J.-P. Boulanger, C. Menkes and H. Spencer. *Influence of the Seasonal Cycle on the Termination of El Niño Events in a Coupled General Circulation Model.* Journal of Climate, vol. 19, pages 1850–1868, 2006. (Cited on pages 7 and 14.)

[Letnic 2005] M. Letnic, C.R. Dickman and B. Tamayo. *The responses of mammals to La Nina (El Nino Southern Oscillation) - associated rainfall, predation and wildlfire in central Australia.* Journal of Mammalogy, vol. 86, pages 689–703, 2005. (Cited on page 11.)

[Levitus 1998] S.E. Levitus. World Ocean Data- base 1998, vol. 1, Introduction. NOAA Atlas NESDIS, vol. 18, NOAA, Silver Spring, Md., 1998. (Cited on page 89.)

[Lin 2007] J.-L. Lin. *The Double-ITCZ Problem in IPCC AR4 Coupled GCMs: Ocean-Atmosphere Feedback Analysis.* Journal of Climate, vol. 20, pages 4497–4525, 2007. (Cited on page 16.)

[Lindzen 1987] R. S. Lindzen and S. Nigam. *On the role of sea surface temperature gradients in forcing low-level winds and convergence in the tropics.* Journal of the Atmospheric Sciences, vol. 45, pages 2440–2458, 1987. (Cited on page 3.)

[Linsley 1994] B. K. Linsley, R. B. Dunbar, G. M. Wellington and D. A. Mucciarone. *A coral-based reconstruction of Intertropical Convergence Zone variability over Central America since 1707.* Journal of Geophysical Research, vol. 99, pages 9977–9994, 1994. (Cited on pages 33 and 34.)

[Linsley 1999] B. K. Linsley, R. G. Messier and R. B. Dunbar. *Assessing between-colony oxygen isotope variability in the coral Porites lobata at Clipperton Atoll.* Coral Reefs, vol. 18, pages 13–27, 1999. (Cited on pages 33 and 34.)

[Linsley 2000] B. K. Linsley, R. B. Dunbar and S. Howe. *El Niño/Southern Oscillation (ENSO) and decadal-scale climate variability at 10°N in the eastern Pacific from 1893 to 1994: a coral-based reconstruction from Clipperton Atoll.* Paleoceanography, vol. 15, pages 322–335, 2000. (Cited on page 33.)

[Linsley 2004] B.K. Linsley, G.M. Wellington, D.P. Schrag, L. Ren and M.J. et al. Salinger. *Geochemical evidence from corals for changes in the amplitude and spatial pattern of South Pacific interdecadal climate variability over the last 300 years.* Clim Dyn, vol. 22, page 1Ð11, 2004. (Cited on page 18.)

[Litynski 2008] J. T. Litynski, S. Plasynski, H.G. McIlvried, C. Mahoney and R.D. Srivastava. *The United States Department of Energy's Regional Carbon Sequestration Partnerships Program Validation Phase.* Environment international, vol. 34, pages 127–138, 2008. (Cited on page 113.)

[Liu 1995] Z. Liu and S.G.H. Philander. *How different wind stress patterns affect the tropical-subtropical circulations of the upper ocean.* Journal of Physical Oceanography, vol. 25, pages 449–462, 1995. (Cited on page 23.)

[Liu 2007] Y. Liu, X. S. Lian and R. H Weisberg. *Rectification of the Bias in the Wavelet Power Spectrum.* Journal of Atmospheric and Oceanic Technology, vol. 24, pages 2093–2102, 2007. (Cited on page 89.)

[Lough 2010] J. M. Lough. *Climate records from corals.* Wiley Interscience Reviews, vol. 1, pages 318–331, 2010. (Cited on pages ix, 19 and 32.)

[Lu 2009] X. Lu, M.B. McElroy and J. Kiviluoma. *Global potential for wind-generated electricity.* Proceedings of the National Academy of Sciences, vol. 106, no. 27, pages 10933–10938, 2009. (Cited on page 112.)

[Lucas 2007] C. Lucas, K. Hennessy, G. Mills and J. Bathols. Bushfire Weather in Southeast Australia: Recent Trends and Projected Climate Change Impacts. Bushfire CRC and Australian Bureau of Meteorology, 2007. Consultancy Report prepared for The Climate Institute of Australia. (Cited on page 11.)

[Madden 1994] R. A. Madden and P. R. Julian. *Observations of the 40Ð50-day tropical oscillation: a review.* Monthly Weather Review, vol. 122, pages 814–837, 1994. (Cited on page 6.)

[Mann 2007] M. E. Mann, S. Rutherford, E. Wahl and C. Ammann. *Robustness of proxy-based climate field reconstruction methods.* Journal of Geophysical Research, vol. 112, page D12109, 2007. doi:10.1029/2006JD008272. (Cited on pages 43 and 44.)

[Mann 2008] M. E. Mann, Z. Zhang, M. K. Hughes, R. S. Bradley, S. K. Miller, S. Rutherford and F. Ni. *Proxy-based reconstructions of hemispheric and global surface temperature variations over the past two millennia.* Proceedings of the National Academy of Sciences, vol. 105, no. 36, pages 13253–13257, 2008. (Cited on pages 18 and 43.)

[Mann 2009] M. E. Mann, Z. Zhang, S. Rutherford, R. S. Bradley, M. K. Hughes, D. Shindell, C. Ammann, G. Faluvegi and F. Ni. *Global Signatures and Dynamical Origins of the Little Ice Age and Medieval Climate Anomaly.* Science, vol. 326, pages 1256–1260, 2009. (Cited on pages 18, 43, 46 and 117.)

[Mantua 1997] N. J. Mantua, S. R. Hare, Y. Zhang, J. M. Wallace and R. C. Francis. *A Pacific interdecadal climate oscillation with impacts on salmon production.* Bull. Amer. Meteor. Soc., vol. 78, pages 1069–1079, 1997. (Cited on page 7.)

[Mantua 2002] N. J. Mantua and S. R Hare. *The Pacific Decadal Oscillation.* Journal of Oceanography, vol. 58, page 35Ð44, 2002. doi:10.1023/A:1015820616384. (Cited on page 7.)

[Mason 2002] S. J. Mason and G. M Mimmack. *Comparison of Some Statistical Methods of Probabilistic Forecasting of ENSO.* Journal of Climate, vol. 15, pages 8–29, 2002. (Cited on page 76.)

[McCabe 2007] G. J. McCabe and D. M. Wolock. *Warming may create substantial water supply shortages in the Colorado River basin.* Geophysical Research Letters, vol. 34, page L22708, 2007. doi:10.1029/2007GL031764. (Cited on page 11.)

[McCreary 1994] J. P. McCreary and P. Lu. *Interaction Between the Subtropical and Equatorial Ocean Circulations: The Subtropical Cell.* Journal of Physical Oceanography, vol. 24, pages 466–497, 1994. (Cited on pages 7 and 23.)

[McCulloch 2000] R.D. McCulloch, M.J. Bentley, R.S. Purves, D.E. Sugden and C.M. Clapperton. *Climatic inferences from glacial and palaeoecological evidence at the last glacial termination, southern South America.* Journal of Quaternary Science, vol. 15, pages 409–417, 2000. (Cited on page 19.)

[McGregor 2004] H. V. McGregor and M. K. Gagan. *Western Pacific coral $\delta^{18}O$ records of anomalous Holocene variability in the El Niño-Southern Oscillation.* Geophysical Research Letters, vol. 31, page L11204, 2004. (Cited on page 18.)

[McGregor 2011a] H. V. McGregor, M. J. Fischer, M. K. Gagan, D. Fink and C. D. Woodroffe. *Environmental control of the oxygen isotope composition of Porites coral microatolls.* Geochimica et Cosmochimica Acta, 2011. in press. (Cited on pages ix, 19, 29, 30, 31 and 33.)

[McGregor 2011b] S. McGregor and A. Timmermann. *The effect of explosive tropical volcanism on ENSO.* Journal of Climate, 2011. In press. doi: 10.1175/2010JCLI3990.1. (Cited on page 126.)

[McPhaden 1998] M. McPhaden, A. J. Busalacchi, R. Cheney, J-R. Donguy, K. S. Gage, D. Halpern, M. Ji, P. Julian, G. Meyers, G. T. Mitchum, P. P. Niiler, J. Picaut, R. W. Reynolds, N. Smith and K. Takeuchi. *The Tropical Ocean-Global Atmosphere observing system: A decade of progress.* Journal of Geophysical Research, vol. 103, pages 14169–14240, 1998. (Cited on page 3.)

[McPhaden 2009] M.J. McPhaden and X. Zhang. *Asymmetry in zonal phase propagation of ENSO sea surface temperature anomalies.* Geophysical Research Letters, vol. 36, page L13703, 2009. (Cited on page 6.)

[Meehl 1989] G.A. Meehl. *The coupled ocean-atmosphere modeling problem in the tropical Pacific and Asian monsoon region.* Journal of Climate, vol. 2, pages 1146–1163, 1989. (Cited on page 14.)

[Meehl 1990] G.A. Meehl. *Development of global coupled ocean-atmosphere general circulation models.* Clim. Dyn., vol. 5, pages 19–33, 1990. (Cited on page 14.)

[Meehl 1993] G. A. Meehl, G. W. Branstator and W. M. Washington. *Tropical Pacific Interannual Variability and CO_2 Climate Change.* Journal of Climate, vol. 6, pages 42–63, 1993. (Cited on page 24.)

[Meehl 1996] G. A. Meehl and W. M. Washington. *El Niño-like climate change in a model with increased atmospheric CO_2 concentrations.* Nature, vol. 382, page 56Ð60, 1996. (Cited on page 23.)

[Meehl 2006] G.A. Meehl, H. Teng and G. Branstator. *Future changes of El Niño in two global coupled climate models.* Climate Dynamics, vol. 26, pages 549–566, 2006. DOI:10.1007/s00382-005-0098-0. (Cited on page 24.)

[Meehl 2007a] G. A. Meehl, C. Tebaldi, H. Teng and T. C. Peterson. *Current and future U.S. weather extremes and El Niño.* Geophysical Research Letters, vol. 34, page L20704, 2007. doi:10.1029/2007GL031027. (Cited on pages 15, 72 and 121.)

[Meehl 2007b] G. A. Meehl and H. Teng. *Multi-model changes in El Niño teleconnections over North America in a future warmer climate.* Climate Dynamics, vol. 29, pages 779–790, 2007. doi:10.1007/s00382-007-0268-3. (Cited on pages 24, 72, 74 and 121.)

[Miller 2000] A. J. Miller and N. Schneider. *Interdecadal climate regime dynamics in the North Pacific Ocean: Theories, observations and ecosystem impacts.* Progress in Oceanography, vol. 47, pages 355–379, 2000. (Cited on page 7.)

[Minobe 2000] S. Minobe. *Spatio-temporal structure of the pentadecadal variability over the North Pacific.* Prog. Oceanogr., vol. 47, page 381Ð408, 2000. (Cited on page 7.)

[Mitchell 2008] D. Mitchell. A note on rising food prices. Policy Research Working Paper 4682, The World Bank, Development Prospects Group, April, 2008. (Cited on page 113.)

[Mo 1987] K.T. Mo and M. Ghil. *Statistics and Dynamics of Persistent Anomalies.* Journal of the Atmospheric Sciences, vol. 44, no. 5, pages 877–901, 1987. (Cited on page 11.)

[Molnar 2002] P. Molnar and M.A. Cane. *El Niño's tropical climate and teleconnections as a blueprint for pre-Ice Age climates.* Paleoceanography, vol. 17, no. 2, 2002. doi:10.1029/2001PA000663. (Cited on page 18.)

[Montgomery 2007] D. Montgomery and G. Runger. Applied statistics and probability for engineers. John Wiley & Sons, Inc., 2007. (Cited on page 35.)

[Morliere 1986] A. Morliere and J.P. Robert. *Rainfall shortage and El Niño-Southern Oscillation in New Caledonia, southwestern Pacific.* Mon. Weather Rev, vol. 114, pages 1131–1137, 1986. (Cited on page 33.)

[Moss 2010] R.H. Moss, J.A. Edmonds, K.A. Hibbard, M.R. Manning, S.K. Rose, D.P. van Vuuren, T.R. Carter, S. Emori, M. Kainuma, T. Kram, G.A. Meehl, J.F.B. Mitchell, N. Nakicenovic, K. Riahi, S.J. Smith, R.J. Stouffer, A.M. Thomson, J.P. Weyant and T.J Wilbanks. *The next*

generation of scenarios for climate change research and assessment. Nature, pages 747–756, 2010. Perspectives. (Cited on pages xiii, 25 and 106.)

[Nakicenovic 2000] N. et al. Nakicenovic. *Special Report on Emissions Scenarios: A Special Report of Working Group III of the Intergovernmental Panel on Climate Change.* page 599 pp. Cambridge University Press, Cambridge, U.K., 2000. (Cited on page 105.)

[NAS 2010] NAS. Electricity from Renewable Sources: Status, Prospects, and Impediments. The National Academies, 2010. (Cited on page 112.)

[Neale 2008] Richard B. Neale, Jadwiga H. Richter and Markus Jochum. *The Impact of Convection on ENSO: From a Delayed Oscillator to a Series of Events.* Journal of Climate, vol. 21, pages 5904–5924, 2008. (Cited on pages 16, 64, 89 and 119.)

[Neale 2011a] R. B. Neale, J. Caron, D. Coleman and J. Bacmeister. *The response of tropical atmospheric variability to deep convection changes in the Community Atmosphere Model, version 4 (CAM4).* Journal of Climate, 2011. to be submitted. (Cited on pages 16 and 64.)

[Neale 2011b] R. B. Neale, J. H. Richter, A. Park, S. J. Vavrus, P. J. Rasch and M. Zhang. *The mean atmospheric climate of the Community Atmosphere Model, version (CAM4) in forced SST and coupled experiments.* Journal of Climate, 2011. to be submitted. (Cited on page 16.)

[Neelin 1991] J. D. Neelin. *The slow sea surface temperature mode and the fast-wave limit: Analytic theory for tropical interannual oscillations and experiments in a hybrid coupled model.* Journal of the Atmospheric Sciences, vol. 48, pages 584–606, 1991. (Cited on page 6.)

[Neelin 1992] J. D. Neelin, M. Latif, M.A.F. Allaart, M.A. Cane, U.Cubasch, W.L. Gates, P.R. Gent, M. Ghil, C. Gordon, N.C. Lau, G.A. Meehl, C.R. Mechoso, J.M. Oberhuber, S.G.H. Philander, P.S. Schopf, K.R. Sperber, A. Sterl, T. Tokioka, J. Tribbia and S.E. Zebiak. *Tropical air-sea interaction in general circulation models.* Climate Dyn., vol. 7, pages 73–104, 1992. (Cited on page 14.)

[Neelin 1993] J. D. Neelin and F.-F. Jin. *Modes of interannual tropical ocean-atmosphere interaction —a unified view. Part II: Analytical results in the weak coupling limit.* Journal of the Atmospheric Sciences, vol. 50, pages 3504–3522, 1993. (Cited on pages 5 and 6.)

[Neelin 2000] J. D. Neelin, F.-F. Jin and H.-H. Syu. *Variations in ENSO Phase Locking.* Journal of Climate, vol. 13, pages 2570–2590, 2000. (Cited on page 14.)

[Nicholls 1991] N. Nicholls. *Teleconnections and health.* In M. H. Glantz, R. W. Katz and N. Nicholls, editeurs, Teleconnections Linking Worldwide Climate Anomalies: scientific basis and societal impact, pages 493–510. Cambridge University Press, 1991. (Cited on page 11.)

[Nicholls 1996] N. Nicholls, B. Lavery, C. Frederiksen and W. Drosdowsky. *Recent apparent changes in relationships between the El Niño-Southern Oscillation and Australian rainfall and temperature.* Geophysical Research Letters, vol. 23, no. 23, pages 3357–3360, 1996. (Cited on page 11.)

[Okumura 2010] Y. Okumura and C. Deser. *Asymmetry in the duration of El Niño and La Niña.* Journal of Climate, vol. 23, pages 5826–5843, 2010. doi:10.1175/2010JCLI3592.1. (Cited on page 50.)

[Pachauri 2007] R. Pachauri and A. (eds) Reisinger. Contribution of Working Groups I, II and III to the Fourth Assessment Report of the Intergovernmental Panel on Climate Change. Intergovernmental Panel on Climate Change, Geneva, Switzerland, 2007. (Cited on page 63.)

[Partnership 2009] Global Bioenergy Partnership. A review of the current state of bioenergy development in G8+5 Countries. Food and Agriculture Organisation, 2009. (Cited on page 113.)

[Penland 1993] C. Penland and T. Magorian. *Prediction of Nino 3 sea surface temperatures using linear inverse modeling.* Journal of Climate, vol. 6, pages 1067–1076, 1993. (Cited on page 76.)

[Penland 1995] C. Penland and P. Sardeshmukh. *The Optimal Growth of Sea Surface Temperature Anomalies.* Journal of Climate, vol. 8, pages 1999–2024, 1995. (Cited on pages 6 and 76.)

[Penland 1998] C. Penland and L. Matrosova. *Prediction of Tropical Atlantic Sea Surface Temperatures Using Linear Inverse Modeling.* Journal of Climate, vol. 11, pages 483–496, 1998. (Cited on page 76.)

[Philander 2003] S. G. Philander and A. V. Fedorov. *Role of tropics in changing the response to Milankovich forcing some three million years ago.* Paleoceanography, vol. 18, page 1045, 2003. doi:10.1029/2002PA000837. (Cited on page 101.)

[Philip 2006] S. Philip and G. van Oldenborgh. *Shifts in ENSO coupling processes under global warming.* Geophysical Research Letters, vol. 33, page L11704, 2006. (Cited on pages 24 and 93.)

[Phipps 2011] S. Phipps, D. Ackerley, J. Brown, M. Fischer, A. Gallant, J. Gergis, D. Lorrey, H. McGregor, S. Stevenson and T. van Ommen. *Palaeoclimate data-model integration: Concepts and application to the climate of the past 2,000 years.* Journal of Climate, 2011. Aus2K special issue, in preparation. (Cited on page 126.)

[Picaut 1997] J. Picaut, F. Masia and Y. du Penhoat. *An Advective-Reflective Conceptual Model for the Oscillatory Nature of the ENSO.* Science, vol. 277, pages 663–666, 1997. (Cited on pages viii, 5 and 6.)

[Picaut 2002] J. et al. Picaut. *Mechanisms of the 1997-98 El Niño-La Niña as inferred from space-based observations.* Journal of Geophysical Research, vol. 107, 2002. doi: 10.1029/2001JC000850. (Cited on page 5.)

[Pielke Jr. 2008] R. Pielke Jr., T. Wigley and C. Green. *Dangerous Assumptions.* Nature, vol. 452, 2008. Commentary. (Cited on pages xiii, 108 and 109.)

[Power 1999] S. Power, T. Casey, C. Folland, A. Colman and V. Mehta. *Interdecadal modulation of the impact of ENSO on Australia.* Climate Dynamics, vol. 15, pages 319–324, 1999. (Cited on page 11.)

[Power 2007] S.B. Power and I.N. Smith. *Weakening of the Walker Circulation and apparent dominance of El Niño both reach record levels, but has ENSO really changed?* Geophysical Research Letters, vol. 34, page L18702, 2007. (Cited on page 22.)

[Quinn 1993] T.M. Quinn, F.W. Taylor and T.J. Crowley. *A 173 year stable isotope record from a tropical south Pacific coral.* Quat Sci Rev, vol. 12, page 407Ð418, 1993. (Cited on page 18.)

[Quinn 1998] T. M. Quinn, T. J. Crowley, F. W. Taylor, C. Henin, P. Joannot and Y. Join. *A multicentury stable isotope record from a New Caledonia coral: interannual and decadal SST variability in the southwest Pacific since 1657.* Paleoceanography, vol. 13, pages 412–426, 1998. (Cited on page 33.)

[Rajagopalan 1997] B. Rajagopalan, U. Lall and M. A. Cane. *Anomalous ENSO Occurrences: An Alternate View.* Journal of Climate, vol. 10, pages 2351–2357, 1997. (Cited on page 84.)

[Rajagopalan 2009] B. Rajagopalan, K. Nowak, J. Prairie, M. Hoerling, B. Harding, J. Barsugli, A. Ray and B. Udall. *Water supply risk on the Colorado River: Can management mitigate?* Water Resources Research, vol. 45, page W08201, 2009. doi:10.1029/2008WR007652. (Cited on page 11.)

[Ramanathan 1991] V. Ramanathan and W. Collins. *Thermodynamic regulation of ocean warming by cirrus clouds deduced from observations of the 1987 El Niño.* Nature, vol. 351, page 27Ð32, 1991. (Cited on page 16.)

[Rao 2006] S. Rao and K. Riahi. *The role of non-CO_2 greenhouse gases in climate change mitigation: Long-term scenarios for the 21st century.* The Energy Journal, pages 177–200, 2006. (Cited on page 107.)

[Rasmusson 1982] E.M. Rasmusson and T.H. Carpenter. *Variations in tropical sea surface temperature and surface wind fields associated with the Southern Oscillation/El Niño.* Monthly Weather Review, vol. 110, pages 354–384, 1982. (Cited on pages 3, 7 and 11.)

[Raupach 2007] M. R. Raupach, G. Marland, P. Clais, C. Le Quere, J. G. Canadell, G. Klepper and C. B. Field. *Global and regional drivers of accelerating CO_2 emissions.* Proceedings of the National Academy of Sciences, vol. 104, no. 24, page 10288Ð10293, 2007. (Cited on page 106.)

[Ravelo 2006] A. C. Ravelo, P. S. Dekens and M. McCarthy. *Evidence for El Niño like conditions during the Pliocene.* GSM Today, vol. 16, pages 4–11, 2006. (Cited on page 18.)

[Reichler 2008] T. Reichler and J. Kim. *How Well Do Coupled Models Simulate Today's Climate?* Bulletin of the American Meteorological Society, vol. 89, pages 303–311, 2008. (Cited on page 15.)

[Riahi 2007] K. Riahi, A. Grubler and N. Nakicenovic. *Scenarios of long-term socio-economic and environmental development under climate stabilization.* Technological Forecasting & Social Change, vol. 74, pages 887–935, 2007. (Cited on pages 107 and 111.)

[Richter 2008] J. H. Richter and P. J. Rasch. *Effects of Convective Momentum Transport on the Atmospheric Circulation in the Community Atmosphere Model.* Journal of Climate, vol. 21, pages 1487–1499, 2008. doi: 10.1175/2007JCLI1789.1. (Cited on page 64.)

[Risbey 2009] J. S. Risbey, M.J. Pook, P.C. McIntosh, C. C. Ummenhofer and G. Meyers. *Characteristics and variability of synoptic features associated with cool season rainfall in southeastern Australia.* Int. J. Climatol., vol. 29, page 1595Ð1613, 2009. (Cited on page 12.)

[Ropelewski 1987] C. F. Ropelewski and M. S. Halpert. *Global and regional scale precipitation patterns associated with the El Niño/Southern Oscillation.* Monthly Weather Review, vol. 114, pages 2352–2362, 1987. (Cited on page 8.)

[Ropelewski 1996] C. F. Ropelewski and M. S. Halpert. *Quantifying Southern Oscillation-precipitation relationships.* Journal of Climate, vol. 9, page 1043 1059, 1996. (Cited on page 11.)

[Rosati 1997] A. Rosati, K. Miyakoda and R. Gudgel. *The impact of ocean initial conditions on ENSO forecasting with a coupled model.* Mon. Wea. Rev., vol. 125, page 752Ð772, 1997. (Cited on page 76.)

[Saji 1999] N. H. Saji, B. N. Goswami, P. N. Vinayachandran and T. Yamagata. *A dipole mode in the tropical Indian Ocean.* Nature, vol. 401, pages 360–363, 1999. (Cited on page 12.)

[Saji 2003] N. H. Saji and T. Yamagata. *Possible impacts of Indian Ocean Dipole mode events on global climate.* Climate Res., vol. 25, page 151Ð169, 2003. (Cited on page 12.)

[Sakamoto 1986] Y. Sakamoto, M. Ishiguro and G. Kitagawa. Akaike Information Criterion Statistics. D. Reidel Publishing Company, 1986. (Cited on page 80.)

[Sangoyomi 1996] T. B. Sangoyomi, U. Lall and H. D. I. Abarbanel. *Nonlinear dynamics of the Great Salt Lake: Dimension estimation.* Water Resources Research, vol. 32, no. 1, pages 149–159, 1996. (Cited on page 40.)

[Schmidt 2005] G.A. Schmidt, G. Hoffmann, D.T. Shindell and Y. Hu. *Modelling atmospheric stable water isotopes and the potential for constraining cloud processes and stratosphere-troposphere water exchange.* Journal of Geophysical Research, vol. 110, page D21314, 2005. doi:10.1029/2005JD005790. (Cited on page 19.)

[Schmidt 2006] G.A. Schmidt, R. Ruedy, J.E. Hansen, I. Aleinov, N. Bell, M. Bauer, S. Bauer, B. Cairns, V. Canuto, Y. Cheng, A. Del Genio, G. Faluvegi, A.D. Friend, T.M. Hall, Y. Hu, M. Kelley and N.Y. et al. Kiang. *Present day atmospheric simulations using GISS ModelE: Comparison to in-situ, satellite and reanalysis data.* Journal of Climate, vol. 19, pages 153–192, 2006. doi:10.1175/JCLI3612.1. (Cited on page 19.)

[Schneider 1999a] A. J. Schneider N.and Miller, M. A. Alexander and C. Deser. *Subduction of decadal North Pacific temperature anomalies: Observations and dynamics.* Journal of Physical Oceanography, vol. 29, pages 1056–1070, 1999. (Cited on page 7.)

[Schneider 1999b] N. Schneider, S. Venzke, A. J. Miller, D. W. Pierce, T. O. Barnett, C. Deser and M. Latif. *PaciÞc thermocline bridge revisited.* Geophysical Research Letters, vol. 26, pages 1329–1332, 1999. (Cited on page 7.)

[Schneider 2001] T. Schneider. *Analysis of Incomplete Climate Data: Estimation of Mean Values and Covariance Matrices and Imputation of Missing Values.* Journal of Climate, vol. 14, pages 853–871, 2001. (Cited on pages 43, 44, 106 and 117.)

[Schneider 2003] E.K. Schneider, D.G. DeWitt, A. Rosati, B.P. Kirtman, L. Ji and J.J. Tribbia. *Retrospective ENSO Forecasts: Sensitivity to Atmospheric Model and Ocean Resolution.* Monthly Weather Review, vol. 131, pages 3038–3060, 2003. (Cited on page 76.)

[Simmons 1982] A.J. Simmons. *The forcing of stationary wave motion by tropical diabatic heating.* Quart. J. R. Met. Soc., vol. 108, pages 503–534, 1982. (Cited on page 9.)

[Simpson 1993] H.J. Simpson, M.A. Cane, A.L. Herczeg, S.E. Zebiak and J.H. Simpson. *Annual river discharge in southeastern Australia related to El-Niño-Southern Oscillation forecasts of sea surface temperatures.* Water Resources Research, vol. 29, no. 11, page 3671Ð 3680, 1993. (Cited on page 11.)

[Skidmore 1987] A.K. Skidmore. *Predicting bushfire activity in Australia from El Niño/Southern Oscillation events.* Australian Forestry, vol. 50, no. 4, pages 231–235, 1987. (Cited on page 11.)

[Smith 2010] I. Smith and E. Chandler. *Refining rainfall projections for the Murray Darling Basin of south-east AustraliaÑthe effect of sampling model results based on performance.* Climatic Change, vol. 102, no. 3-4, pages 377–393, 2010. DOI: 10.1007/s10584-009-9757-1. (Cited on page 11.)

[Sperber 1987] K. R. Sperber, S. Hameed, W. L. Gates and G. L. Potter. *Southern oscillation simulated in a global climate model.* Nature, vol. 329, pages 140–142, 1987. (Cited on page 14.)

[Stevenson 2010] S. Stevenson, B. Fox-Kemper, M. Jochum, B. Rajagopalan and S. Yeager. *Model ENSO Validation Using Wavelet Probability Analysis.* Journal of Climate, vol. 23, pages 5540–5547, 2010. (Cited on pages x, 18, 52, 53, 55, 56, 57, 58, 59, 60, 90, 118, 125 and 194.)

[Stevenson 2011a] S. Stevenson, B. Fox-Kemper and M. Jochum. *Understanding the ENSO-CO_2 Link Using Stabilized Climate Simulations* . Journal of Climate, 2011. submitted. (Cited on pages xii, xiii, 7, 25, 74, 80, 87, 88, 89, 90, 91, 92, 93, 95, 96, 99, 100, 121, 123, 124, 125 and 195.)

[Stevenson 2011b] S. Stevenson, B. Fox-Kemper, M. Jochum, R. Neale, C. Deser and G. Meehl. *Will there be a significant change to El Niño in the 21st century?* Journal of Climate, 2011. In press: CCSM4 special issue. doi:10.1175/JCLI-D-11-00252.1. (Cited on pages vii, x, xi, 23, 24, 25, 50, 55, 64, 65, 66, 67, 68, 69, 70, 72, 73, 74, 89, 101, 119, 123 and 196.)

[Stevenson 2011c] S. Stevenson, H. V. McGregor, S. Phipps and B. Fox-Kemper. *Quantifying the Limitations of Paleo-ENSO Model Validation.* Geophysical Research Letters, 2011. in preparation. (Cited on pages ix, x, 20, 35, 36, 38, 39, 40, 41, 44, 47, 117 and 170.)

[Stevenson 2012a] S. Stevenson and R. Pielke Jr. *The Hidden Challenges of Climate Stabilization: Decarbonization and the IPCC AR5.* Wiley Interdisciplinary Reviews, 2012. in preparation. (Cited on pages vii, xiii, 25, 105, 107, 109, 110 and 243.)

[Stevenson 2012b] S. Stevenson and B. Rajagopalan. *ENSO Characteristics in the CCSM4 21st Century Projections.* Geophysical Research Letters, 2012. in preparation. (Cited on pages vii, xii, 25, 78, 79, 81, 82, 83, 84, 85, 122 and 231.)

[Stroeve 2007] J. Stroeve, M.M. Holland, W. Meier, T. Scambos and M. Serreze. *Arctic sea ice decline: Faster than forecast.* Geophysical Research Letters, vol. 34, no. L09501, 2007. (Cited on page 106.)

[Suarez 1988] M. J. Suarez and P. S. Schopf. *A delayed action oscillator for ENSO.* Journal of the Atmospheric Sciences, vol. 45, pages 3283–7, 1988. (Cited on pages viii, 5 and 6.)

[Subramanian 2011] A. Subramanian, M. Jochum, Miller, R. Murtugudde, R. Neale and Waliser. *The Madden-Julian Oscillation in CCSM4.* Journal of Climate, 2011. submitted. (Cited on pages 64 and 123.)

[Takens 1981] F. Takens. *Detecting strange attractors in turbulence.* In D. R. A. L. S. Young, editeur, Dynamical Systems and Turbulence, pages 366–381. Springer-Verlag, New York, 1981. (Cited on page 40.)

[Tangang 1997] F. T. Tangang, W. W. Hsieh and B. Tang. *Forecasting the equatorial sea surface tempuratures by neural network models.* Climate Dyn., vol. 13, page 135Ð147, 1997. (Cited on page 76.)

[Taylor 2009] K. E. Taylor, R. J. Stouffer and G. A. Meehl. *A summary of the CMIP5 experimental design.* CLIVAR report, pages 1–32, 2009. www.clivar.org/organization/wgcm/references/Taylor_CMIP5.pdf. (Cited on page 60.)

[Thompson 2011] D. M. Thompson, T. R. Ault, M. N. Evans, J. E. Cole and J. Emile-Geay. *Comparison of observed and simulated tropical climate trends using a forward model of coral $\delta^{18}O$.* Geophysical Research Letters, vol. 38, page L14706, 2011. doi:10.1029/2011GL048224. (Cited on pages 20, 35 and 116.)

[Timmermann 1999] A. Timmermann, J. Oberhuber, A. Bacher, M. Esch, M. Latif and E. Roeckner. *Increased El Niño frequency in a climate model forced by future greenhouse warming.* Nature, vol. 398, pages 694–697, 1999. (Cited on page 24.)

[Ting 1993] M. F. Ting and P. D. Sardeshmukh. *Factors Determining the Extratropical Response to Equatorial Diabatic Heating Anomalies.* Journal of the Atmospheric Sciences, vol. 50, no. 6, pages 907–918, 1993. (Cited on page 9.)

[Tingley 2010a] M. P. Tingley and P. Huybers. *A Bayesian Algorithm for Reconstructing Climate Anomalies in Space and Time. Part I: Development and Applications to Paleoclimate Reconstruction Problems.* Journal of Climate, vol. 23, pages 2759–2781, 2010. (Cited on pages 48 and 117.)

[Tingley 2010b] M. P. Tingley and P. Huybers. *A Bayesian Algorithm for Reconstructing Climate Anomalies in Space and Time. Part II: Comparison with the Regularized Expectation-Maximization Algorithm.* Journal of Climate, vol. 23, pages 2782–2800, 2010. (Cited on pages 48 and 117.)

[Torrence 1998] C. Torrence and G.P. Compo. *A Practical Guide to Wavelet Analysis.* Bull. Amer. Meteor. Soc., vol. 79, pages 61–78, 1998. (Cited on pages vii, 52 and 89.)

[Trenberth 1996] K.E. Trenberth and T. J. Hoar. *The 1990-1995 El Niño-Southern Oscillation event: Longest on record.* Geophys. Res. Lett., 1996. submitted. (Cited on page 84.)

[Trenberth 1998] K.E. Trenberth, G.W. Branstator, D. Karoly, A. Kumar, N.-C. Lau and C. Ropelewski. *Progress during TOGA in understanding and modeling global teleconnections associated with tropical sea surface temperatures.* Journal of Geophysical Research, vol. 103, no. C7, pages 14291–14324, 1998. (Cited on pages viii, 8, 9, 10 and 11.)

[Trostle 2008] R. Trostle. Global agricultural supply and demand: factors contributing to the recent increase in food commodity prices. Outlook Report No. WRS-0801 (Washington, DC: US Department of Agriculture Economic Research Service) May, 2008. (Cited on page 113.)

[Tudhope 1995] A.W. Tudhope, G.B. Shimmield, C.P. Chilcott, M. Jebb, A.E. Fallick and A.N. Dalgleish. *Recent changes in climate in the far western equatorial Pacific and their relationship to the Southern Oscillation; oxygen isotope records from massive corals, Papua New*

Guinea. Earth and Planetary Science Letters, vol. 136, pages 575–590, 1995. (Cited on page 19.)

[Tudhope 2001] A. W. et al. Tudhope. *Variability in the El Niño/Southern Oscillation through a glacial-interglacial cycle*. Science, vol. 291, pages 1511–1517, 2001. (Cited on pages 18 and 31.)

[Turner 2004] J. Turner. *The El Niño-Southern Oscillation and Antarctica*. International Journal of Climatology, vol. 24, pages 1–31, 2004. (Cited on pages viii, 12, 13 and 74.)

[Tziperman 1997] E. Tziperman, S. E. Zebiak and M. A. Cane. *Mechanisms of Seasonal-ENSO Interaction*. Journal of the Atmospheric Sciences, vol. 54, pages 61–71, 1997. (Cited on pages 6, 7 and 14.)

[Uppala 2005] S.M. Uppala, P.W. Kallberg, A.J. Simmons, U. Andrae, V. da Costa Bechtold, M. Fiorino, J.K. Gibson, J. Haseler, A. Hernandez, G.A. Kelly, X. Li, K. Onogi, S. Saarinen, N. Sokka, R.P. Allan, E. Andersson, K. Arpe, M.A. Balmaseda, A.C.M. Beljaars, L. van de Berg, J. Bidlot, N. Bormann, S. Caires, F. Chevallier, A. Dethof, M. Dragosavac, M. Fisher, M. Fuentes, S. Hagemann, E. Holm, B.J. Hoskins, L. Isaksen, P.A.E.M. Janssen, R. Jenne, A.P. McNally, J.-F. Mahfouf, J.-J. Morcrette, N.A. Rayner, R.W. Saunders, P. Simon, A. Sterl, K.E. Trenberth, m A. Untch, D. Vasiljevic, P. Viterbo and J. Woollen. *The ERA-40 re-analysis*. Quarterly Journal of the Royal Meteorological Society, vol. 131, pages 2961–3012, 2005. (Cited on page 17.)

[Urban 2000] F.E. Urban, J.E. Cole and J.T. Overpeck. *In£uence of mean climate change on climate variability from a 155- year tropical Pacic coral record*. Nature, vol. 407, pages 989–993, 2000. (Cited on pages 18 and 33.)

[U.S. Dept. of Energy 2010] U.S. Dept. of Energy. Annual energy outlook 2009, report no. DOE/EIA-0383. U.S. Energy Information Administration, Washington, DC, 2010. (Cited on page 112.)

[van Alphen 2010] K. van Alphen, P. M. Noothout, M.P. Hekkert and W.C. Turkenburg. *Evaluating the development of carbon capture and storage technologies in the United States.* Renewable and Sustainable Energy Reviews, vol. 14, page 971Ð986, 2010. (Cited on page 113.)

[Van Vuuren 2006] D.P. Van Vuuren, B. Eickhout, P.L. Lucas and M.G.J. den Elzen. *Long-term multi-gas scenarios to stabilize radiative forcing - Exploring costs and benefits within an integrated assessment framework.* The Energy Journal, pages 201–233, 2006. (Cited on page 107.)

[van Vuuren 2007] D.P. van Vuuren, M.G.J. den Elzen, P.L. Lucas, B. Eickhout, B.J. Strengers, B. van Ruijven, S. Wonink and R. van Houdt. *Stabilizing greenhouse gas concentrations at low levels: an assessment of reduction strategies and costs.* Climatic Change, vol. 81, pages 119–159, 2007. (Cited on pages 107 and 111.)

[Vecchi 2000] G. A. Vecchi and D. E. Harrison. *Tropical Pacific Sea Surface Temperature Anomalies, El Niño, and Equatorial Westerly Wind Events.* Journal of Climate, vol. 13, pages 1814–1830, 2000. (Cited on page 123.)

[Vecchi 2006] G.A. Vecchi, B.J. Soden, A.T. Wittenberg, I.M. Held, A. Leetmaa and M.J. Harrison. *Weakening of tropical Pacific atmospheric circulation due to anthropogenic forcing.* Nature, vol. 44, pages 72–75, 2006. doi:10.1038/nature04744. (Cited on page 22.)

[Vecchi 2007] G. Vecchi and B. Soden. *Global Warming and the Weakening of the Tropical Circulation.* Journal of Climate, vol. 20, pages 4316–4340, 2007. doi:10.1175/JCLI4258.1. (Cited on page 22.)

[Vimont 2003] D. J. Vimont, J. M. Wallace and D. S. Battisti. *The Seasonal Footprinting Mechanism in the Pacific: Implications for ENSO.* Journal of Climate, pages 2668–2675, 2003. (Cited on pages 92 and 98.)

[Walker 1924] G.T. Walker. *Correlation in seasonal variations of weather,IX: a further study of world weather.* Mem. India Meteorol. Dep 24 (Part 9), pages 275–332, 1924. (Cited on page 2.)

[Walker 1932] G.T. Walker and E.W. Bliss. *World Weather V.* Mem. R. Meteorol. Soc., vol. 4, no. 36, pages 53–84, 1932. (Cited on page 2.)

[Walker 1937] G.T. Walker and E.W. Bliss. *World Weather VI.* Mem. R. Meteorol. Soc., vol. 4, no. 39, pages 119–139, 1937. (Cited on page 2.)

[Wallace 1992] J. M. Wallace. *Effect of deep convection on the regulation of tropical sea surface temperature.* Nature, vol. 357, pages 230–231, 1992. (Cited on page 16.)

[Wang 1996] C. Wang and R. H. Weisberg. *Stability of equatorial modes in a simplified coupled ocean-atmosphere model.* Journal of Climate, vol. 9, pages 3132–3148, 1996. (Cited on page 5.)

[Wang 1999] C. Wang, R. H. Weisberg and J. I. Virmani. *Western Pacific interannual variability associated with the El Niño-Southern Oscillation.* Journal of Geophysical Research, vol. 104, pages 5131–5149, 1999. (Cited on pages viii, 5 and 6.)

[Wang 2001] C. Wang. *A unified oscillator model for the El Niño-Southern Oscillation.* Journal of Climate, vol. 14, pages 98–115, 2001. (Cited on pages 5 and 94.)

[Wang 2002] B. Wang and S.-I. An. *A mechanism for decadal changes of ENSO behavior: Roles of background wind changes.* Clim. Dyn., vol. 18, page 475Ð486, 2002. (Cited on page 6.)

[Wang 2004] C. Wang and J. Picaut. *Understanding ENSO Physics - A Review.* In C. Wang, S.-P. Xie and J. A. Carton, editeurs, Earth's Climate: the Ocean-Atmosphere Interaction, page 405. American Geophysical Union Monograph Series, 2004. (Cited on pages viii, 4, 5, 6 and 7.)

[Wara 2005] M. W. Wara, A. C. Ravelo and M. L. Delaney. *Permanent El Niño-like conditions during the Pliocene warm period.* Science, vol. 309, pages 758–761, 2005. (Cited on page 18.)

[WCRP 1995] World Climate Research Programme WCRP. Tech. Doc. WMO/TD-690 A Study of Climate Variability and Predictability. World Meteorological Organization, Geneva, Switzerland, 1995. (Cited on page 3.)

[Weatherly 1991] J.W. Weatherly, J.E. Walsh and H.J. Zwally. *Antarctic sea ice variations and seasonal air temperature relationships.* Journal of Geophysical Research, vol. 96, page 15119Ð15130, 1991. (Cited on page 14.)

[Weber 1972] J.N. Weber and P.M.J. Woodhead. *Temperaturedependence of oxygen-18 concentration in reef coral carbonates.* J Geophys Res, vol. 77, page 463Ð473, 1972. (Cited on page 18.)

[Webster 1981] P. J. Webster. *Mechanisms determining the atmospheric response to sea surface temperature anomalies.* Journal of the Atmospheric Sciences, vol. 38, pages 554–571, 1981. (Cited on page 9.)

[Webster 1988] P. J. Webster and H. R. Chang. *Energy Accumulation and Emanation Regions at Low Latitudes: Impacts of a Zonally Varying Basic State.* Journal of the Atmospheric Sciences, vol. 45, pages 803–829, 1988. (Cited on page 9.)

[Weisberg 1997] R. H. Weisberg and C. H. Wang. *A western Pacific oscillator paradigm for the El Niño-Southern Oscillation.* Geophysical Research Letters, vol. 24, pages 779–782, 1997. (Cited on pages viii, 5 and 6.)

[WEO 2009] WEO. World Energy Outlook 2009. International Energy Agency, 2009. (Cited on pages 111 and 112.)

[Weyant 2009] J. Weyant, C. Azar, M. Kainuma, J. Kejun, N. Nakicenovic, P.R. Shukla, E. La Rovere and G. Yohe. *Future IPCC Activities: New Scenarios.* Intergovernmental Panel on

Climate Change, Thirtieth Session: Antalya, 21-23 April 2009, vol. 1, pages 1–48, 2009. (Cited on pages xiii, 106, 107 and 110.)

[White 1996] W.B. White and R.G. Peterson. *An Antarctic circumpolar wave in surface pressure, wind, temperature and sea-ice extent.* Nature, vol. 380, page 699 Ð 702, 1996. (Cited on page 12.)

[Wilson 2010] R. Wilson, E. Cook, R. D'Arrigo, N. Riedwyl, M. N. Evans, A. Tudhope and R. Allan. *Reconstructing ENSO: the influence of method, proxy data, climate forcing and teleconnections.* Journal of Quaternary Science, vol. 25, no. 1, pages 62–78, 2010. (Cited on page 30.)

[Wiser 2011] R. Wiser, Z. Yang, M. Hand, O. Hohmeyer, D. Infield, P. H. Jensen, V. Nikolaev, M. O'Malley, G. Sinden and A. Zervos. *Wind Energy.* In O. Edenhofer, R. Pichs-Madruga, Y. Sokona, K. Seyboth, P. Matschoss, S. Kadner, T. Zwickel, P. Eickemeier, G. Hansen, S. Schlömer and C. von Stechow, editeurs, IPCC Special Report on Renewable Energy: Sources and Climate Change Mitigation. Cambridge University Press, Cambridge, United Kingdom and New York, NY USA, 2011. (Cited on page 112.)

[Wittenberg 2006] Andrew T. Wittenberg, Anthony Rosati, Ngar-Cheung Lau and Jeffrey J. Ploshay. *GFDLÕs CM2 Global Coupled Climate Models. Part III: Tropical Pacific Climate and ENSO.* Journal of Climate, vol. 19, pages 698–722, 2006. (Cited on pages 56 and 119.)

[Wittenberg 2009] A. T. Wittenberg. *Are historical records sufficient to constrain ENSO simulations?* Geophysical Research Letters, vol. 36, page L12702, 2009. (Cited on pages 17, 56 and 60.)

[Wolter 1998] K. Wolter and M. S. Timlin. *Measuring the strength of ENSO events - how does 1997/98 rank?* Weather, vol. 53, pages 315–324, 1998. (Cited on page 28.)

[Woodroffe 2003] C. D. Woodroffe, Beech M. R. and Gagan M. K. *Mid-late Holocene El Nio variability in the equatorial Pacific from coral microatolls.* Geophysical Research Letters, vol. 30, page 1358, 2003. doi:10.1029/2002GL015868. (Cited on pages 19 and 33.)

[Wyrtki 1975] K. Wyrtki. *El Niño – The dynamic response of the equatorial Pacific Ocean to atmospheric forcing.* J. Phys. Oceanogr., vol. 5, pages 572–84, 1975. (Cited on page 3.)

[Xie 1994a] S. Xie, C. Bao, Z. Xue, L. Zhang and C. Hao. *Interaction between Antarctic sea ice and ENSO events.* In Proceedings of NIPR Symposium on Polar Meteorology and Glaciology, page 95Ð110. 1994. (Cited on page 14.)

[Xie 1994b] S.-P. Xie and S.G.H. Philander. *A coupled ocean-atmosphere model of relevance to the ITCZ in the eastern Pacific.* Tellus, vol. 46A, pages 340–350, 1994. (Cited on page 97.)

[Xie 1995] S.-P. Xie. *Interaction between the annual and interannual variations in the equatorial Pacific.* Journal of Physical Oceanography, vol. 25, page 1930Ð1941, 1995. (Cited on page 7.)

[Xie 1997] S.-P. Xie and Arkin. *Global Precipitation: A 17-year monthly analysis based on gauge observations, satellite estimates, and numerical model outputs.* Bulletin of the American Meteorological Society, vol. 78, pages 2539–2558, 1997. (Cited on page 17.)

[Xie 2004] S.-P. Xie. *Chapter 4. The Shape of Continents, Air-Sea Interaction, and the Rising Branch of the Hadley Circulation.* In The Hadley Circulation: Present, Past and Future, page 121Ð152. 2004. (Cited on pages xii and 97.)

[Xue 1994] Y. Xue, M. A. Cane, S. E. Zebiak and B. Blumenthal. *On the prediction of ENSO: a study with a low-order Markov model.* Tellus, vol. 46A, pages 512–528, 1994. (Cited on page 76.)

[Xue 2000] Y. Xue, A. Leetmaa and M. Ji. *ENSO prediction with Markov model: The impact of sea level.* Journal of Climate, vol. 13, pages 849–871, 2000. (Cited on page 76.)

[Yeager 2006] S. G. Yeager, C. A. Shields, W. G. Large and J. J. Hack. *The low-resolution CCSM3.* Journal of Climate, vol. 19, pages 2545–2566, 2006. (Cited on page 88.)

[Yeh 2009] S.-W. Yeh, J.-S. Kug, B. Dewitte, M.-H. Kwon, B. P. Kirtman and F.-F. Jin. *El Niño in a changing climate.* Nature, vol. 461, pages 511–514, 2009. doi:10.1038/nature08316. (Cited on page 24.)

[Yuan 2000] X.J. Yuan and D.G. Martinson. *Antarctic sea ice extent variability and its global connectivity.* Journal of Climate, vol. 13, page 1697Ð1717, 2000. (Cited on page 14.)

[Zarvos 2003] A. Zarvos. *Developing Wind Energy to meet the Kyoto Targets in the European Union.* Wind Energy, vol. 6, pages 309–319, 2003. (Cited on page 112.)

[Zebiak 1987] S. E. Zebiak and M. A. Cane. *A model El Niño-Southern Oscillation.* Monthly Weather Review, vol. 115, pages 2262–2278, 1987. (Cited on page 14.)

[Zhang 1992] X.G. Zhang and T.M. Casey. *Long term variation in the Southern Oscillation and the relationship with rainfall in Australia.* Australian Meteorological Magazine, vol. 40, page 211Ð 225, 1992. (Cited on page 11.)

[Zhang 1997] Y. Zhang, J. M. Wallace and D. S. Battisti. *ENSO-like interdecadal variability: 1900-93.* Journal of Climate, vol. 10, pages 1004–1020, 1997. (Cited on page 7.)

[Zhang 1998] R.-H. Zhang, L. M. Rothstein and A. J. Busalacchi. *Origin of warming and El Niño change on decadal scales in the tropical PaciÞc Ocean.* Nature, vol. 391, pages 879–883, 1998. (Cited on page 7.)

[Zhang 2006] M. Zhang and H. Song. *Evidence of deceleration of atmospheric vertical overturning circulation over the tropical Pacific.* Geophysical Research Letters, vol. 33, page L12701, 2006. doi:10.1029/2006GL025942. (Cited on page 22.)

Appendix A

This appendix contains the text of [Stevenson 2011c], current as of November 22, 2011.

Quantifying the Limitations of Paleo-ENSO Model Validation

Samantha Stevenson, Helen McGregor, Steven Phipps

& Baylor Fox-Kemper

El Niño/Southern Oscillation (ENSO) dynamics show large centennial modulations, meaning that an accurate estimation of baseline ENSO variability requires the use of paleoclimate proxies to extend the modern observational record. Coral oxygen isotopes are the most commonly used ENSO proxy, but isotopic variations are not directly simulated in the majority of IPCC-class coupled climate models, necessitating a conversion between isotope and climate signals for quantitative comparisons. However, when errors from linear climate-δ^{18}O 'pseudoproxy' conversions are calculated, they are so large that they overwhelm the input signal, even when multiple coral sites are combined. Climate field reconstruction improves ENSO estimation, but suffers from chronic underprediction of variance when simulating times outside the calibration interval. However, an error analysis on modern corals shows that the dominant mode of variability is relatively insensitive to dating uncertainties between coral δ^{18}O records. Accurate, quantitative ENSO model validation will require the use of >4-5 contemporaneous fossil corals, in combination with either: isotope-enabled modeling, more accurate pseudoproxy calculations, or improved estimates of the covariance matrix between ENSO and all proxy locations during past climates.

The El Niño/Southern Oscillation (ENSO) is highly variable on long timescales, and previous

studies have shown that the 20th century observational record is too short to constrain ENSO statistics (Stevenson et al., 2010, 2011; Wittenberg, 2009). Coral oxygen isotopes (δ^{18}O) are often used to measure past ENSO variations, but δ^{18}O is influenced by both temperature and salinity, among other effects: additionally, most CMIP-class general circulation models do not provide direct simulations of the δ^{18}O signal ('forward modeling'). A quantitative comparison of modeled and observed ENSO amplitudes therefore requires some after-the-fact conversion between δ^{18}O , ENSO and climate variables.

Throughout this study, "ENSO variability" and "ENSO amplitude" will be taken as the *variance* of tropical Pacific surface waters. It will be compared to δ^{18}O and climate models variance in properties at varying locations. Often a power spectrum decomposition of the variance will be used so that the frequencies comprising the modeled variance are revealed.

Previous studies have used 'pseudoproxy' conversions to estimate model δ^{18}O time series (Thompson et al., 2011; Brown et al., 2008), where empirical relations (often linear regressions) are used to calculate δ^{18}O from instrumental data or climate model output. In this study, linear pseudoproxies are shown to be to uncertain to provide ENSO amplitude measures, even when many δ^{18}O time series are combined. Here, 11 sites spanning the tropical Pacific are chosen, such that records cover the 1959-1990 period at seasonal resolution ($>$ 4 samples/year; see Methods). The δ^{18}O time series is linearly regressed onto SST and SSS from HadSST (Rayner et al., 2006) and SODA (Carton and Giese, 2008) ($\delta^{18}\mathrm{O} = \beta_0 + \beta_1(SST) + \beta_2(SSS)$), and the resulting errors modeled using a Monte Carlo technique (see Supplementary Material). Errors from local influences and offsets in times assigned to δ^{18}O measurements (age models) are estimated from 5 contemporaneous modern corals from Kiritimati in the central Pacific (McGregor et al., 2011; Woodroffe et al., 2003;

Evans et al., 2000; Nurhati et al., 2009), and these errors are found to be relatively small (mean $\sigma = 0.253‰$). However, the residuals from the above regression gave error variances comparable to the input value in many cases (Figure 1a).

The large fit+residual error arises from the nonlinear dependence of the δ^{18}O signal on many variables. Figure 1c shows the relation between 2-7 year bandpassed δ^{18}O and SOI time series; a high-order phase orbit is apparent, and suggests that additional processes beyond SST/precipitation may be important. The 'embedding dimension', or number of independent variables needed to describe the signal (Sangoyomi et al., 1996), is ≈5-7 (see Methods, Supplementary Information for a complete description). The additional variables are as yet unknown; perhaps local influences, the δ^{18}O value of seawater, or trends in climate variables account for some of the signal. However, local SST and SSS alone can only partially predict the δ^{18}O variance at a given site.

ENSO amplitude estimates do not rely on a single location; rather, variability at multiple points is combined, in both modern and paleoclimatic contexts. Figure 2 shows the spectrum of the first principal component (PC1) for pseudo-δ^{18}O calculated using HadSST/SODA (see Methods). Once again, the errors due to linear fit residuals overwhelm the signal; even the dominant covarying mode between all 11 records cannot be captured by linear pseudoproxies. These large errors lead to an inability to distinguish model ENSO from proxies (Figure 2b), as demonstrated using pseudo-δ^{18}O calculated from the CCSM4 20th century ensemble (Gent et al., 2011). Without shrinking the error envelope, it is thus impossible to tell *whether*, much less *how*, to begin work on model improvements.

If a linear approach is not effective, what other options are available for after-the-fact model/δ^{18}O conversion? Climate field reconstructions (CFR) are commonly used to translate

proxy data into climate information; hemispheric temperature reconstructions are a notable example (Mann et al., 2008, 2009). These methods exploit the covariance between proxy locations to provide a robust reconstruction of the field of interest, and have been extremely successful in reproducing mean values for climate variables over long timescales. But can CFR provide a good estimate of interannual variability? Here, the regularized expectation maximization (RegEM; (Schneider, 2001)) algorithm is adopted as a representative example of CFR methods. RegEM uses an iterative estimation procedure to find the mean and covariance matrix between known (δ^{18}O) and unknown (NINO3.4 SST) values to reconstruct the NINO3.4 time series. The covariance matrix must be generated using measurements over some predetermined 'calibration interval'; Figure 3 shows RegEM reconstruction of the HadSST spectrum () for two example intervals, 1965-1990 and 1958-1970. Results are quite good in the former case, but a substantial underprediction of variance occurs in the latter. This is likely due to nonstationarity in the covariances between coral sites, and has strong implications for successful model validation. For instance, if RegEM were used to reconstruct the ENSO spectrum for a pre-instrumental period, where no information on the covariances between coral sites and ENSO was available, the resulting spectrum would tend to have too little variance compared with the 'real' answer: it would be impossible to say how much apparent model error was due to the limitations of the reconstruction algorithm in that case.

One might imagine that these problems would simply disappear when using forward modeling, since in that case a like-to-like comparison is possible. However, even if δ^{18}O were directly simulated, additional considerations remain (as well as bias in forward-modeled δ^{18}O). It is often difficult to collect multiple contemporaneous fossil corals, and absolute dating uncertainties may be on the order of 5-10 years or more (Cobb et al., 2003). The

effects of data sparsity and temporal offsets are therefore simulated using the modern corals (Methods; Figure 4): note that here no additional errors are included. Errors of up to 10 years in absolute age do not greatly affect the δ^{18}O PC1 spectrum (Figures 2, 3): good news for future fossil coral collection efforts. Note that this may not be true for other metrics; the power spectrum has the useful property of insensitivity to phase relationships between corals, and other measures of ENSO may experience larger phase-related influenced.

The number of corals in the sample has a much greater impact than the temporal offsets between coral records (Figure 4): here, the sample size is artificially reduced by selecting a random subsample of the modern corals. Using >5 corals retains most of the δ^{18}O variance, but for smaller samples much of the signal is lost. The same effect is seen using RegEM reconstructions (Figure 4b,c), where enormous error bars on NINO3.4 spectra appear for samples of 4 corals.

These findings suggest that quantitative ENSO model validation will be extremely challenging in the absence of the capacity for direct simulation of coral δ^{18}O . Figure 4 is a strong argument for using a large sample (>4-5) of fossil corals, contemporaneous to within 10 years of one another, for ENSO amplitude estimation. However, if the δ^{18}O signal cannot be computed accurately from climate models, then the question is moot: at a minimum, Figures 1 and 2 demonstrate that a more detailed pseudoproxy calculation which incorporates the nonlinearities in coral δ^{18}O is required. Unfortunately, using climate field reconstruction does not appear to improve the accuracy of ENSO amplitude estimation due to the underprediction of variance associated with changing the calibration interval for reconstruction. If better estimates of the ENSO/proxy site covariance were available, CFR techniques might prove to be a useful avenue. However, in the absence of this information we recommend additional efforts toward forward modeling of coral δ^{18}O within coupled climate models.

References

Brown, J., A. W. Tudhope, M. Collins, and H. V. McGregor, 2008: Mid-Holocene ENSO: Issues in quantitatve model-proxy data comparisons. *Paleoceanography*, **23**, PA3202.

Carton, J. A. and B. S. Giese, 2008: A Reanalysis of Ocean Climate Using Simple Ocean Data Assimilation. *Monthly Weather Review*, **136**, 2999–3017.

Cobb, K., C. Charles, H. Cheng, and R. Edwards, 2003: El Niño/Southern Oscillation and tropical Pacific climate during the last millennium. *Nature*, **424**, 271–276.

Evans, M. N., A. Kaplan, and M. A. Cane, 2000: Intercomparison of coral oxygen isotope data and historical sea surface temperature (SST): Potential for coral-based SST field reconstructions. *Paleoceanography*, **15 (5)**, 551–562.

Gent, P. R., et al., 2011: The Community Climate System Model version 4 . *Journal of Climate*, submitted.

Mann, M. E., Z. Zhang, M. K. Hughes, R. S. Bradley, S. K. Miller, S. Rutherford, and F. Ni, 2008: Proxy-based reconstructions of hemispheric and global surface temperature variations over the past two millennia. *Proceedings of the National Academy of Sciences*, **105 (36)**, 13 253–13 257.

Mann, M. E., et al., 2009: Global Signatures and Dynamical Origins of the Little Ice Age and Medieval Climate Anomaly. *Science*, **326**, 1256–1260.

McGregor, H. V., M. J. Fischer, M. K. Gagan, D. Fink, and C. D. Woodroffe, 2011: Environmental control of the oxygen isotope composition of *Porites* coral microatolls. *Geochimica et Cosmochimica Acta*, in press.

Nurhati, I., K. Cobb, C. Charles, and R. Dunbar, 2009: Late 20th century warming and freshening in the central tropical Pacific. *Geophysical Research Letters*, **36**, L21 606, doi:10.1029/2009GL040270.

Rayner, N., P.Brohan, D.E.Parker, C.F.Folland, J.J.Kennedy, M.Vanicek, T.Ansell, and S. Tett, 2006: Improved analyses of changes and uncertainties in sea surface temperature measured in situ since the mid-nineteenth century: the HadSST2 data set. *Journal of Climate*, **19 (3)**, 446–469.

Sangoyomi, T. B., U. Lall, and H. D. I. Abarbanel, 1996: Nonlinear dynamics of the Great Salt Lake: Dimension estimation. *Water Resources Research*, **32 (1)**, 149–159.

Schneider, T., 2001: Analysis of Incomplete Climate Data: Estimation of Mean Values and Covariance Matrices and Imputation of Missing Values. *Journal of Climate*, **14**, 853–871.

Stevenson, S., B. Fox-Kemper, M. Jochum, R. Neale, C. Deser, and G. Meehl, 2011: Will there be a significant change to El Niño in the 21st century? *Journal of Climate*, in press: CCSM4 special issue. doi:10.1175/JCLI-D-11-00252.1.

Stevenson, S., B. Fox-Kemper, M. Jochum, B. Rajagopalan, and S. Yeager, 2010: Model ENSO Validation Using Wavelet Probability Analysis. *Journal of Climate*, **23**, 5540–5547.

Thompson, D. M., T. R. Ault, M. N. Evans, J. E. Cole, and J. Emile-Geay, 2011: Comparison of observed and simulated tropical climate trends using a forward model of coral δ^{18}O. *Geophysical Research Letters*, **38**, L14 706, doi:10.1029/2011GL048224.

Wittenberg, A. T., 2009: Are historical records sufficient to constrain ENSO simulations? *Geophysical Research Letters*, **36**, L12 702.

Woodroffe, C. D., B. M. R., and G. M. K., 2003: Mid-late Holocene El Nio variability

in the equatorial Pacific from coral microatolls. *Geophysical Research Letters*, **30**, 1358, doi:10.1029/2002GL015868.

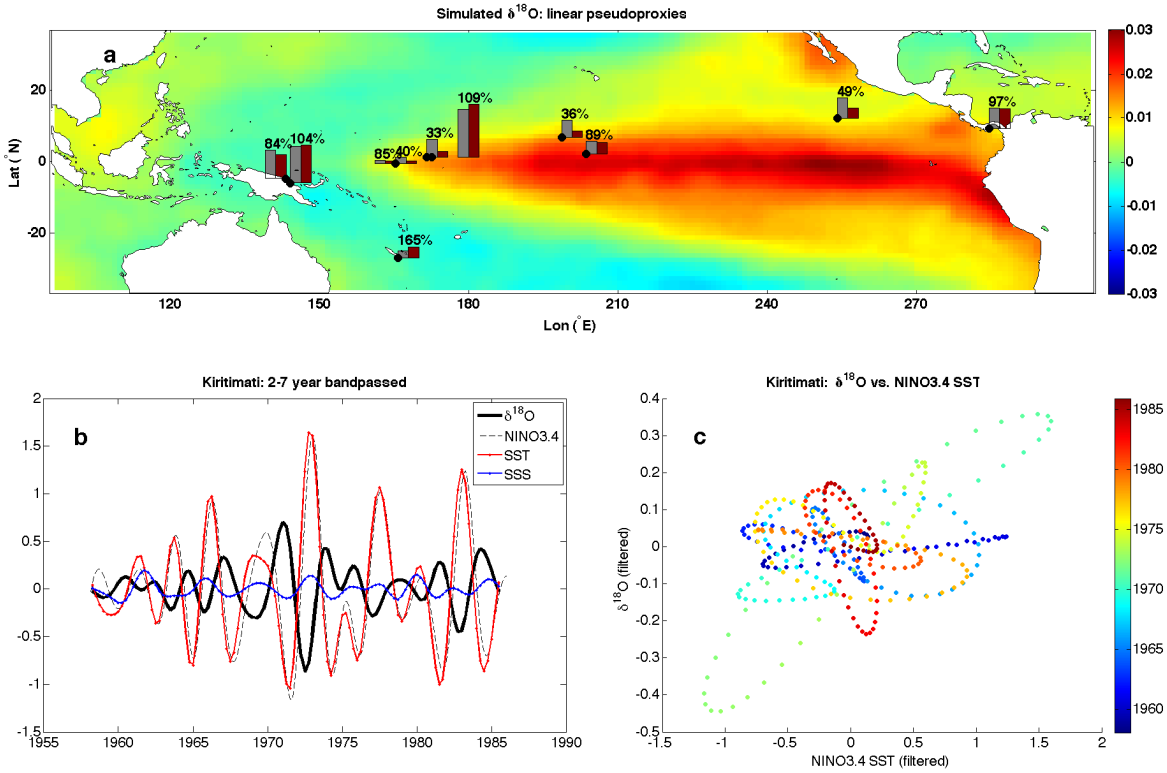

Figure 1: Error analysis for single-site estimation of δ^{18}O variance with linear pseudoproxies. a) Map of coral locations, showing the magnitude of δ^{18}O variance (normalized to the Kiritimati value) in gray and the error on the δ^{18}O variance in red. The percentage values indicate the proportion of the error on the δ^{18}O variance to the variance itself. Background colors correspond to the spatial pattern of the HadSST PC1; black circles show the positions of all coral sites. b) Time series of Kiritimati δ^{18}O from 1958-1986, along with NINO3.4 SST and local SST/SSS at the coral site. All time series have been bandpass filtered using a 10th order Butterworth filter with 3dB points at 2 and 7 year periods. c) Phase orbit of bandpass filtered δ^{18}O and NINO3.4 SST; colors indicate the time of each measurement.

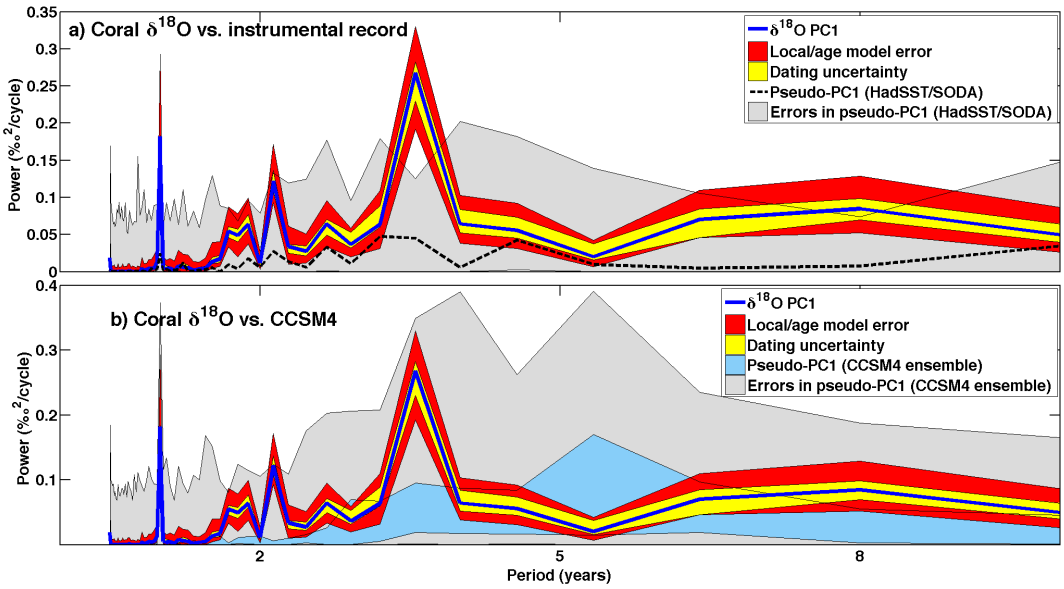

Figure 2: Error analysis for estimation of δ^{18}O PC1 spectra using linear pseudoproxies. a) Representation of $\delta^{18}O$ using instrumental records. HadSST and SODA SSS time series are used to create pseudo-$\delta^{18}O$ for all sites, from which PC1 is calculated. Errors from local/age model effects (yellow), dating uncertainties (red) and fit residuals (blue) are shown as envelopes. b) Representation of δ^{18}O using CCSM4 simulations. Errors from local/age model and dating effects are shown as in a); ensemble scatter appears in purple, and sampling errors from pseudoproxy fit residuals are shown in green.

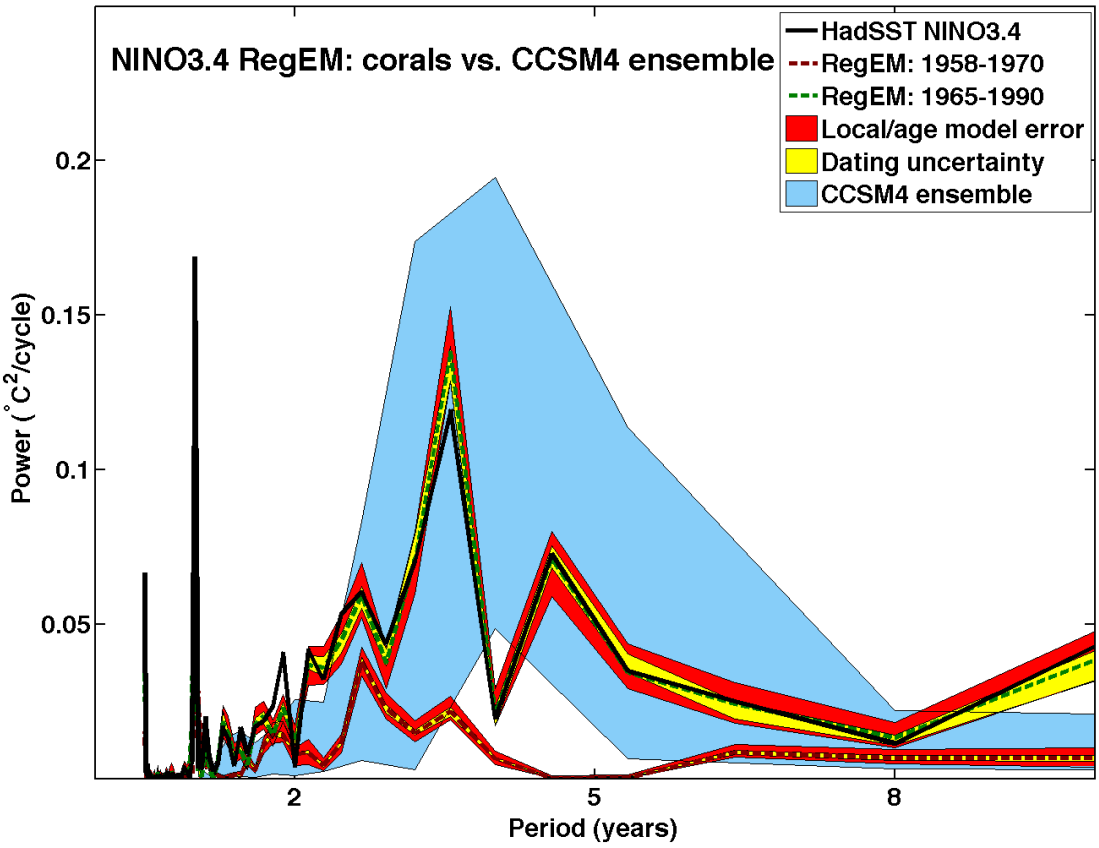

Figure 3: Error analysis for estimation of NINO3.4 SST spectra using climate field reconstruction (RegEM). Errors are once again shown as envelopes: local/age model effects (yellow), dating uncertainties (red) and ensemble scatter from CCSM (blue). Here two different RegEM reconstructions are performed to illustrate the effects of varying the calibration interval: 1965-1990 (green) and 1958-1970 (red).

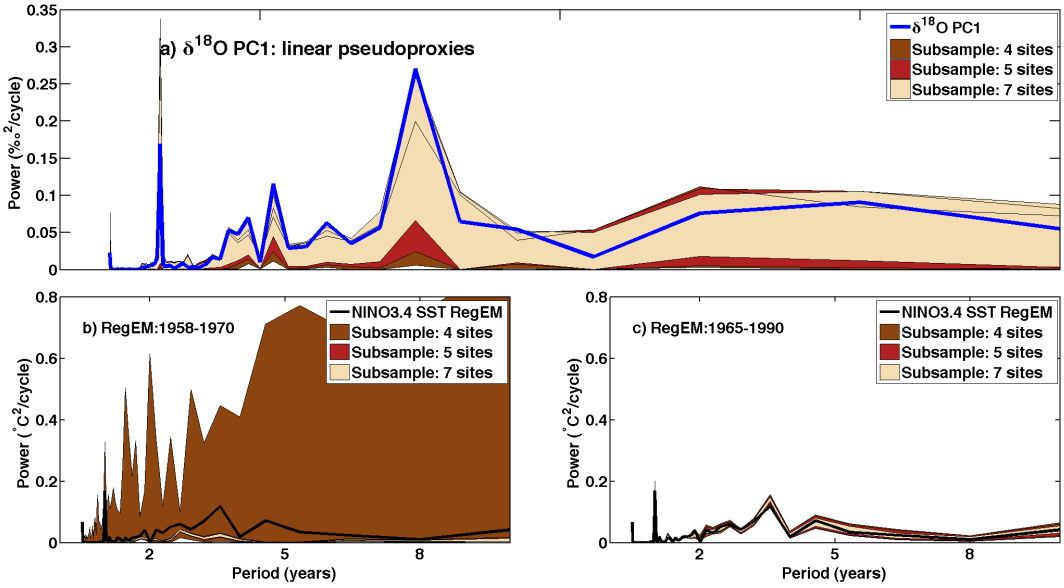

Figure 4: Contribution of sampling errors. a) Linear pseudoproxies. b) RegEM. In both cases, the sample size is artificially decreased by selecting a random sample (without replacement) of 4, 5, or 7 corals, then repeating the calculation. No additional errors are modeled here.

Supplementary Material for Stevenson et al. (2011)

The coral records selected for analysis, along with a brief description of the properties of each, is provided in Section 1. A description of the techniques used to model errors in the linear pseudoproxy time series is given in Section 2. Climate field reconstruction using RegEM is described in Section 3, and the nonlinear time series analysis algorithms used for the embedding dimension calculations are discussed in Section 4.

1 Coral Records

For the δ^{18}O pseudoproxy calculation and Monte Carlo error simulation, we have chosen all available coral records from the World Data Center for Paleoclimatology (WDCP) in the tropical Pacific for which the following criteria were met:

1. Temporal resolution of $\geq$4 records/year
2. Correlation with NINO3.4 SST significant at or above the 90% confidence level.

This led to the selection of 11 records from 10 locations, which are listed in Table 1. Note that two coral records are available for Nauru (Guilderson and Schrag, 1999).

Table 1: Basic information on modern (20th century) coral records used for Monte Carlo error estimation. Except for the McGregor et al. (2011) Kiritimati record, all coral data was downloaded from the WDCP at http://www.ncdc.noaa.gov/paleo/coral/coral_data.html.

Record	Citation	Time period
Clipperton	Linsley et al. (1994)	1707-1984
Kiritimati	McGregor et al. (2011)	1938-2004
Laing	Tudhope (2001)	1884-1993
Madang	Tudhope (2001)	1880-1993
Maiana	Urban et al. (2000)	1840-1994
New Caledonia	Quinn et al. (1998)	1657-1992
Nauru	Guilderson and Schrag (1999)	1891-1995
Palmyra	Cobb et al. (2001)	1886-1998
Secas	Linsley et al. (1994)	1894-1984
Tarawa	Cole et al. (1993)	1893-1989

2 Linear Pseudoproxies

Conversion to climatic variables in the linear pseudoproxy case is accomplished via a multivariate linear regression having the form

$$\delta^{18}O = \beta_0 + \beta_1 T + \beta_2 S + \epsilon \tag{1}$$

where T is the local SST, S the local SSS and ϵ the error in the fit. Data from 1958-1990 were used, to allow for the maximum time interval with simultaneous SST and SSS measurements. SST and SSS for all coral sites come from HadSST version 2 (Rayner et al., 2006) and the SODA reanalysis (Carton and Giese, 2008) datasets, respectively. Data from the two closest grid points are seasonally averaged to form the best-estimate time series, then linearly interpolated to match the coral age models.

The best-fit coefficients were calculated using a stepwise linear regression algorithm (Venables and Ripley, 2002), which selects those predictor variables best suited to represent the predictand according to a minimization of the Akaike information criterion (AIC; Akaike (1974)). Regression coefficients for both SST and SSS are given in Table 2: 5 sites show a significant dependence on both SST and SSS, 5 on SST only, and one (Laing; Tudhope (2001)) on SSS only.

Table 2: Fit statistics for conversion from climate variables to δ^{18}O. Fit parameters listed are the result of a stepwise regression of δ^{18}O on SST and SSS; the adjusted R^2 is listed in the last column. N/A indicates that a variable was not included in the best-fit regression.

Record	β_0	β_1	β_2	R^2 (adj.)
Palmyra	-11.60	-0.29	0.59	0.20
Tarawa	-33.52	-0.25	1.16	0.38
Nauru (1)	-7.81	-0.20	0.37	0.35
Nauru (3)	-3.71	-0.36	0.39	0.39
Kiritimati	6.01	-0.19	N/A	0.13
Secas	11.44	-0.44	N/A	0.11
Clipperton	5.95	-0.23	N/A	0.032
New Caledonia	0.52	-0.06	N/A	0.078
Laing	13.55	N/A	-0.42	0.018
Madang	13.08	-0.49	N/A	0.061
Maiana	-17.8	-0.55	0.93	0.22

2.1 Error Distributions

In order to estimate the errors ϵ expected due to local influences and age model uncertainties, we used data from Kiritimati: a complete analysis would benefit from examining multiple sites, but Kiritimati was the only location with sufficient sampling density. Six different coral records from Kiritimati were combined, each having slightly different temporal extent (Table 3). The standard deviation was calculated as a function of time, for each month having $\geq$2 measurements, and the mean value of that standard deviation was adopted in the Monte Carlo simulations.

Table 3: Kiritimati Island coral records used to estimate errors due to local effects/dating uncertainties.

Record	Citation	Time period
Evans 1	Evans et al. (1998)	1938-1993
Evans 2	Evans et al. (1998)	1981-1986
Nurhati	Nurhati et al. (2009)	1972-1998
McGregor	McGregor et al. (2011)	1994-2007
Woodroffe 1	Woodroffe and Gagan (2000)	1978-1991
Woodroffe 2	Woodroffe et al. (2003)	1989-1999

The remaining contributions to uncertainties are errors in the fitting process. We consider errors both from the fitted slope and from the residuals; the latter is calculated according to

$$R_i = \epsilon = \delta^{18}O - (\beta_0 + \beta_1 T + \beta_2 S) \tag{2}$$

Residual profiles for 100 Monte Carlo simulations are shown in Figure 1; they are approximately normal, with some skewness observed in some sites. We note that for each simulated time series, the slopes β_1 and β_2 were drawn from a normal distribution with mean equal to the best-fit β_i and standard deviation σ_β from the least-squares estimation procedure.

The use of fitted slope error distributions requires the recalculation of the regression intercept for each time series, which is done by minimizing the least-squares equations in the case where β_1 is constant:

$$\beta_0 = \frac{\sum \delta^{18}O - \sum \beta_1 T - \sum \beta_2 S}{N} \tag{3}$$

where N is the number of observations. ϵ was simulated using kernel density estimation to compute the probability distribution function (PDF) at each location, then sampling from

that distribution. The distributions in Figure 1 accordingly reflect contributions both from β_i and R.

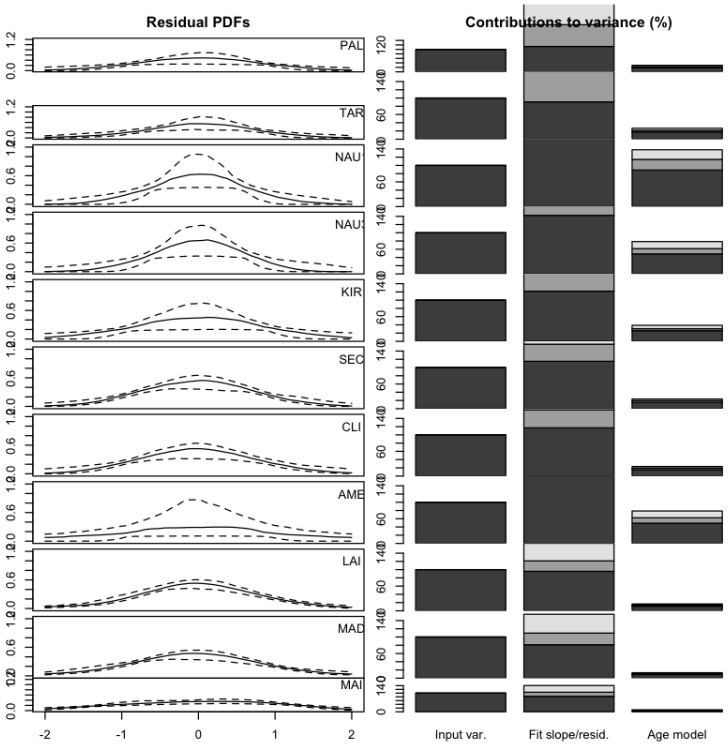

Figure 1: Errors in linear pseudoproxies. Lefthand column: PDFs of fit residuals generated using a Monte Carlo approach. Solid line indicates the median simulated error PDF, and the dashed lines the 90% confidence interval on the PDF. Righthand column: proportions of each source of error relative to the input $\sigma^2_{\delta 18O}$. Here the leftmost bar shows the 100% value (input variance) and the other two show the fit slope/residual and local/age model errors, respectively. Shaded portions of each bar indicate the 50, 75 and 90% levels for each source of error.

2.2 Confidence Intervals on δ^{18}O Variance

Applying the simulated errors as offsets to the input coral time series provides a good sense of the δ^{18}O uncertainty at any given time, but also results in an artificial inflation of the input variance since the errors are additive noise in this case. We therefore rely on error propagation to compute the uncertainty on δ^{18}O variance. Let σ be the standard deviation for any given measurement. Then the error on the variance, Σ, is given by

$$\Sigma = S[\frac{1}{N}\sum_{i=1}^{N}(x_i - \mu)^2] \tag{4}$$

$$= S[\frac{1}{N}\sum_{i=1}^{N} x_i^2 - 2\mu x_i + \mu^2 \tag{5}$$

$$= S[\frac{1}{N}(\sum_{i=1}^{N} x_i^2) - \mu^2] \tag{6}$$

where S(x) denotes the error on the quantity x. The overall sample variance is thus

$$\Sigma = 2|\mu|\sigma^2 - |\mu|\sigma^2 = |\mu|\sigma^2 \tag{7}$$

which is applied as the error bar on δ^{18}O variance, as seen in Figure 1 of the paper.

3 RegEM Calculations

The climate field reconstructions relied upon the regularized expectation maximization algorithm developed by Schneider (2001). We have made use of the Matlab suite available online at *http://www.meteo.psu.edu/ mann/Mann/tools/tools.html* and described in Mann et al. (2008, 2009).

The algorithm is an iterative method for estimating the mean and covariance of a missing portion of a data sample which has been adapted from the expectation maximization (EM) algorithm of Dempster et al. (1977) (see Little and Rubin (1987) for a review of the method). EM functions by finding the maximum-likelihood estimators of the model parameters (in the case of normally distributed data, these are the mean and covariance) given the observed data, then using the conditional expectation of these parameters to fill in values for the next iteration. This method works well in the case where the number of variables is small in comparison with the number of available records; but for climate datasets this is often not the case, resulting in an underdetermined system. RegEM applies a regularization parameter to the covariance matrix (Tikhonov and Arsenin, 1977), which allows a more accurate determination of the mean and covariance matrix, and therefore the missing values.

The regression model for missing values is

$$x_m = \mu_m + (x_a - \mu_a)B + \epsilon \tag{8}$$

where x_m are the missing values, x_a the available values, μ_m and μ_a the corresponding means, B the regression coefficients, and ϵ the regression error. In the particular case of estimating NINO3.4 SST from coral δ^{18}O, x_a are the coral time series and x_m the NINO3.4 time series. The EM algorithm calculates the matrix B using

$$B = \Sigma_{aa}^{-1}\Sigma_{ma} \tag{9}$$

where Σ_{aa} is the covariance matrix between available values and Σ_{ma} the covariance matrix between available and missing values. The difference between the EM and RegEM algorithms is in the calculation of B. RegEM regularizes Σ_{aa} through ridge regression, which inflates the diagonal components of Σ_{aa}:

$$\Sigma_{aa}^{-1} < -\Sigma_{aa}^{-1}(1 + h^2 D)^{-1} \tag{10}$$

Here the matrix D consists of the diagonal elements of Σ_{aa} and h is a regularization parameter estimating by minimizing the generalized cross-validation function (Golub et al., 1979; Hansen, 1997).

4 Nonlinear Time Series Analysis

The estimation of the 'embedding dimension' for nonlinear time series is quite complex. This quantity has been previously shown (Packard et al., 1980; Takens, 1981) to represent the number of state variables required to describe the behavior of a time series: so for example, if coral δ^{18}O is controlled solely by a combination of SST and precipitation, then the embedding dimension should be 2.

Here we follow the approach of Sangoyomi et al. (1996) in estimating the embedding dimension. The time series is represented in a 'pseudophase space' as in Takens (1981), where delayed versions of the time series form the state space. The 'delay vector' of pseudo-state variables is then given by

$$\vec{x} = x(t), x(t-\tau), x(t-2\tau), ...x(t-(m-1)\tau) \tag{11}$$

where τ is the assumed delay time. The choice of τ is somewhat arbitrary, but the goal is to choose τ so as to maximize the information about the trajectory included in the delay vector. Sangoyomi et al. (1996) discuss various methods for choosing τ, and conclude that the mutual information framework of Fraser and Swinney (1986) is optimal since it incorporates both linear and nonlinear autocorrelative effects. The mutual information is given by

$$MI = \sum \sum p(x(t), x(t-\tau)) log(\frac{p(x(t), x(t-\tau))}{p(x(t))p(x(t-\tau))}) \tag{12}$$

where $p(x(t), x(t-\tau))$ is the joint probability distribution of the original and lagged time series, and $p(x(t))$ and $p(x(t-\tau))$ the probability distributions of the original and lagged time series individually. For the embedding dimension calculation, we adopt the lag τ corresponding to the first local minimum in MI, which is typically between lags 4-10 for the coral records; this translates into roughly 4-18 months depending on the temporal resolution of the data (Figure 2).

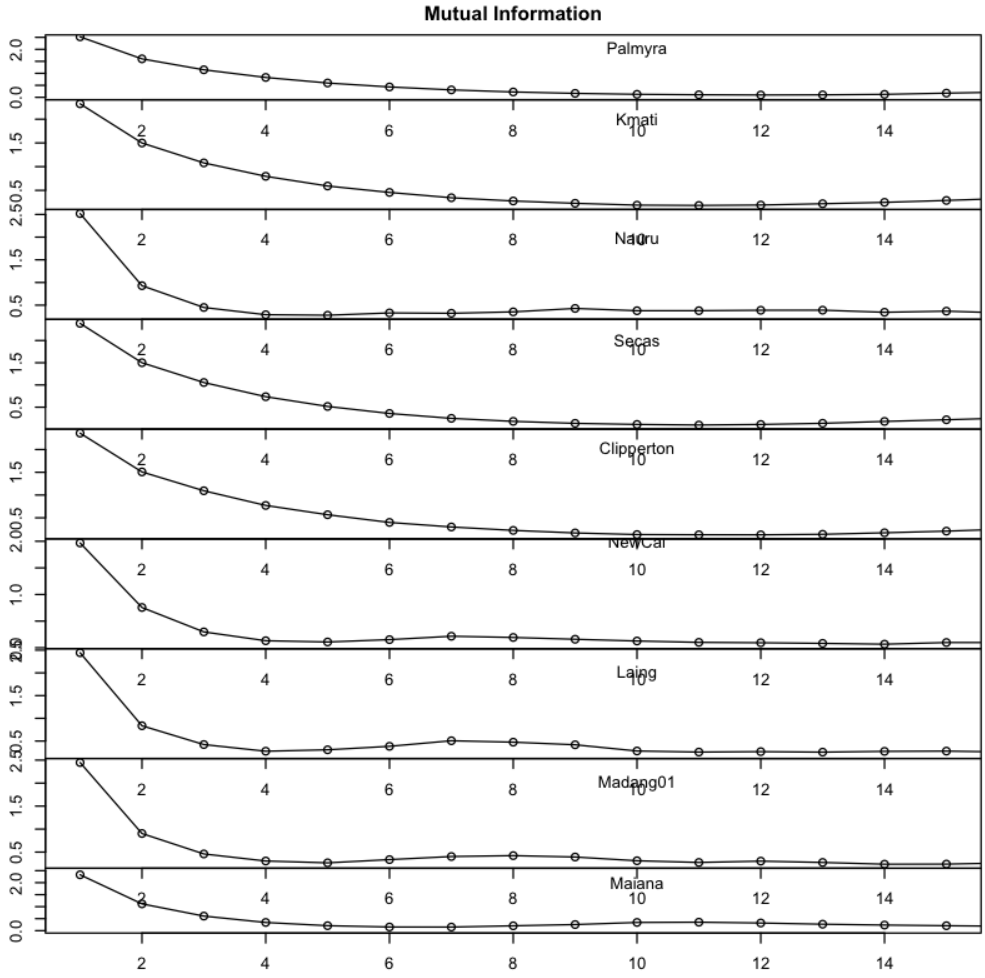

Figure 2: Mutual information as a function of lag τ for all coral records.

The delay is next used in the 'false nearest neighbors' algorithm of Kennel et al. (1992).

False nearest neighbors are points which appear as neighbors to a given point when the time series is projected into a dimension too low to uniquely describe the dynamics. In the case where the true embedding dimension n = 2, false nearest neighbors for the time series $x(t) = sin(t)$ might be calculated by projecting this unit circle onto a line. In general, the 'true' embedding dimension is estimated by finding the dimension for which the number of false nearest neighbors drops to 0. Mathematically, a false nearest neighbor is defined as one where the ratio of Euclidean distances R for dimension d+1 to dimension d is greater than some tolerance value R_{tol}:

$$\frac{R_{d+1}^2(n,r) - R_d^2(n,r)}{R_d^2(n,r)} > R_{tol} \tag{13}$$

False nearest neighbor calculation results are shown in Figure 3. Both this and the mutual information calculation were performed using algorithms in the TISEAN package (Hegger et al. (1999); R package 'tseriesChaos'). The embedding dimension thus estimated is roughly the same for all coral δ^{18}O time series - the false nearest neighbor plots cross 0 at dimensions between 6-8.

References

Akaike, H., 1974: A new look at the statistical model identification. *IEEE Transactions on Automatic Control*, **19 (6)**, 716–723.

Carton, J. A. and B. S. Giese, 2008: A Reanalysis of Ocean Climate Using Simple Ocean Data Assimilation. *Monthly Weather Review*, **136**, 2999–3017.

Cobb, K., C. Charles, and D. Hunter, 2001: A central tropical Pacic coral demonstrates Pacic, Indian, and At- lantic decadal climate connections. *Geophysical Research Letters*, **28**, 2209–2212.

Cole, J. E., R. G. Fairbanks, and G. T. Shen, 1993: Recent Variability in the Southern Oscillation: Isotopic Results from a Tarawa Atoll Coral. *Science*, **260**, 1790–1793.

Dempster, A. P., N. M. Laird, and D. B. Rubin, 1977: Maximum Likelihood from Incomplete Data via the EM Algorithm. *Journal of the Royal Statistical Society. Series B (Methodological)*, **39 (1)**, 1–38.

Evans, M. N., R. G. Fairbanks, and J. L. Rubenstone, 1998: Kiritimati Coral Isotope Data. *IGBP PAGES/World Data Center-A for Paleoclimatology Data Contribution Series*, 1998–035, nOAA/NGDC Paleoclimatology Program, Boulder CO, USA.

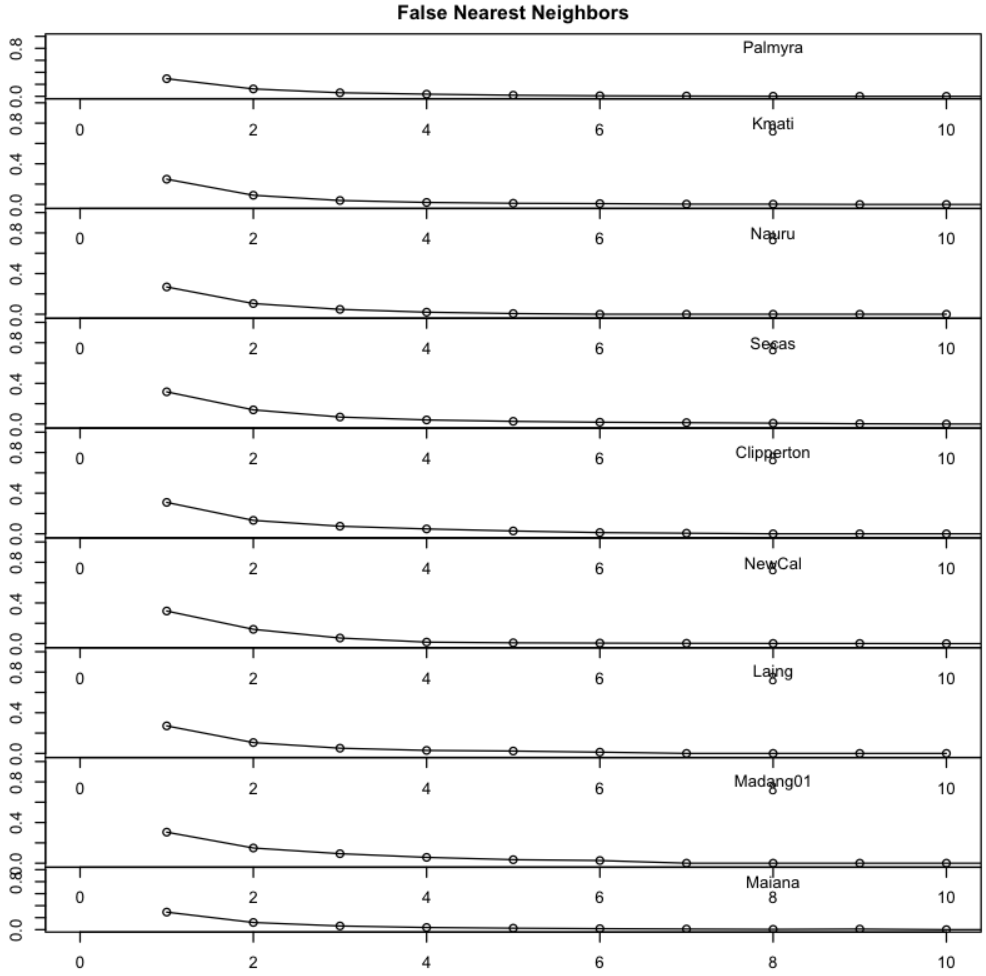

Figure 3: Fraction of false nearest neighbors as a function of embedding dimension, for all coral records.

Fraser, A. M. and H. L. Swinney, 1986: Independent coordinates for strange attractors from mutual information. *Phys. Rev. A*, **33 (2)**, 1134–1140.

Golub, G. H., M. T. Heath, and G. Wahba, 1979: Generalized cross-validation as a method for choosing a good ridge parameter. *Technometrics*, **21**, 215–223.

Guilderson, T. P. and D. P. Schrag, 1999: Reliability of coral iso- tope records from the western Pacic warm pool: a compar- ison using age-optimized records. *Paleoceanography*, **14**, 457–464.

Hansen, P., 1997: *Rank-deficient and Discrete Ill-posed Problems: Numerical Aspects of Linear Inversion*. SIAM Monograph on Mathematical Modeling and Computation, 247 pp.

Hegger, R., H. Kantz, and T. Schreiber, 1999: Practical implementation of nonlinear time series methods: The TISEAN package. *CHAOS*, **9**, 413–439.

Kennel, M. B., R. Brown, and H. D. I. Abarbanel, 1992: Determining embedding dimension for phase-space reconstruction using a geometrical construction. *Phys. Rev. A*, **45**, 3403.

Linsley, B. K., R. B. Dunbar, G. M. Wellington, and D. A. Mucciarone, 1994: A coral-based reconstruction of Intertropical Convergence Zone variability over Central America since 1707. *Journal of Geophysical Research*, **99**, 9977–9994.

Little, R. J. A. and D. B. Rubin, 1987: *Statistical Analysis with Missing Data. Series in Probability and Mathematical Statistics*. Wiley, 278 pp.

Mann, M. E., Z. Zhang, M. K. Hughes, R. S. Bradley, S. K. Miller, S. Rutherford, and F. Ni, 2008: Proxy-based reconstructions of hemispheric and global surface temperature variations over the past two millennia. *Proceedings of the National Academy of Sciences*, **105 (36)**, 13 253–13 257.

Mann, M. E., et al., 2009: Global Signatures and Dynamical Origins of the Little Ice Age and Medieval Climate Anomaly. *Science*, **326**, 1256–1260.

McGregor, H. V., M. J. Fischer, M. K. Gagan, D. Fink, and C. D. Woodroffe, 2011: Environmental control of the oxygen isotope composition of *Porites* coral microatolls. *Geochimica et Cosmochimica Acta*, in press.

Nurhati, I., K. Cobb, C. Charles, and R. Dunbar, 2009: Late 20th century warming and freshening in the central tropical Pacific. *Geophysical Research Letters*, **36**, L21 606, doi:10.1029/2009GL040270.

Packard, N. H., J. P. Crutchfield, J. D. Farmer, and R. S. Shaw, 1980: Geometry from a time series. *Phys. Rev. Lett.*, **45 (9)**, 712–716.

Quinn, T. M., T. J. Crowley, F. W. Taylor, C. Henin, P. Joannot, and Y. Join, 1998: A multicentury stable isotope record from a New Caledonia coral: interannual and decadal SST variability in the southwest Pacific since 1657. *Paleoceanography*, **13**, 412–426.

Rayner, N., P.Brohan, D.E.Parker, C.F.Folland, J.J.Kennedy, M.Vanicek, T.Ansell, and S. Tett, 2006: Improved analyses of changes and uncertainties in sea surface temperature measured in situ since the mid-nineteenth century: the HadSST2 data set. *Journal of Climate*, **19 (3)**, 446–469.

Sangoyomi, T. B., U. Lall, and H. D. I. Abarbanel, 1996: Nonlinear dynamics of the Great Salt Lake: Dimension estimation. *Water Resources Research*, **32 (1)**, 149–159.

Schneider, T., 2001: Analysis of Incomplete Climate Data: Estimation of Mean Values and Covariance Matrices and Imputation of Missing Values. *Journal of Climate*, **14**, 853–871.

Takens, F., 1981: Detecting strange attractors in turbulence. *Dynamical Systems and Turbulence*, D. R. A. L. S. Young, Ed., Springer-Verlag, New York, 366–381.

Tikhonov, A. N. and V. Y. Arsenin, 1977: *Solution of Ill-Posed Problems*. Scripta Series in Mathematics, V. H. Winston and Sons, 258 pp.

Tudhope, A. W. e. a., 2001: Variability in the el niño/southern oscillation through a glacial-interglacial cycle. *Science*, **291**, 1511–1517.

Urban, F., J. Cole, and J. Overpeck, 2000: Inuence of mean climate change on climate variability from a 155- year tropical Pacic coral record. *Nature*, **407**, 989–993.

Venables, W. N. and B. D. Ripley, 2002: *Modern Applied Statistics with S*. New York: Springer (4th ed.).

Woodroffe, C. D. and M. K. Gagan, 2000: Coral microatolls from the central Pacific record late Holocene El Niño. *Geophysical Research Letters*, **27**, 1511–1514.

Woodroffe, C. D., B. M. R., and G. M. K., 2003: Mid-late Holocene El Nio variability in the equatorial Pacific from coral microatolls. *Geophysical Research Letters*, **30**, 1358, doi:10.1029/2002GL015868.

Appendix B

This paper has been published in the Journal of Climate [Stevenson 2010]. The full text may be found at:

http://dx.doi.org/10.1175/2010JCLI3609.1

Appendix C

This paper has been published in the Journal of Climate [Stevenson 2011a]. The full text may be found at:

http://dx.doi.org/10.1175/JCLI-D-11-00252.1

Appendix D

This appendix contains the text of [Stevenson 2011b], which was submitted to the Journal of Climate. The text is current as of November 22, 2011.

Understanding the ENSO-CO_2 Link Using Stabilized Climate Simulations

Samantha Stevenson [1] and Baylor Fox-Kemper
Department of Atmospheric and Oceanic Sciences, University of Colorado, Boulder, CO USA &
Markus Jochum
National Center for Atmospheric Research, Boulder, Colorado, USA

[1] *Corresponding author address:* Samantha Stevenson, CIRES, 216 UCB, Boulder, CO 80303
E-mail: samantha.stevenson@colorado.edu

Abstract

The influence of changing atmospheric CO_2 concentration on ENSO is explored using 800-year integrations of the NCAR Community Climate System Model (CCSM3.5), representing stablilized climates with CO_2 at AD 1850, 1990 and 2050 levels. The amplitude of tropical SST variability increases with CO_2 in both the annual and ENSO bands: however, ENSO changes are significant at annual and 2-4 year periods only. The atmosphere/ocean mean state response includes: preferential SST warming in the eastern equatorial Pacific, a weakening of the equatorial trade winds, increased vertical ocean stratification, increased surface heat flux forcing and a contraction of the atmospheric Hadley and oceanic subtropical overturning circulations. The delayed-oscillator framework alone cannot explain the observed hemispheric asymmetry: Southern (Northern) Hemisphere SST and subsurface temperature variability strengthens (weakens) with CO_2. This asymmetry results from excitation of Rossby waves by seasonal wind stress curl anomalies along the eastern edges of the subtropical gyres. Finally, shorter, higher-resolution stabilized control simulations with the CCSM4 show that ENSO weakens rather than strengthens with CO_2. The difference in ENSO climate sensitivity is not readily explainable, but may potentially be related to changes to high-frequency wind stress variability.

1 Introduction

Understanding how the behavior of the El Niño/Southern Oscillation (ENSO) may change in the future is critical to a variety of social and economic systems (Ropelewski and Halpert, 1996; Rajagopalan and Lall, 1998; Whetton et al., 1990). However, ENSO's complex and chaotic nature makes future projections difficult (Collins et al., 2010; Stevenson et al., 2011a). The major limiting factors in diagnosing future ENSO changes using climate models may be simply summarized: the record length required to obtain robust ENSO statistics, the dynamical timescale of ENSO adjustment to changing CO_2, and the accuracy of ENSO-relevant model physics. To date, no modeling experiment has been constructed which can isolate the influence of CO_2 changes in the absence of other effects; this study is an attempt to provide such an experiment.

Although ENSO has been recognized for many years (Hildebrandsson, 1897; Walker and Bliss, 1932, 1937), accurate observations are available on the required spatial scale only for the past few decades. Basinwide real-time monitoring of Pacific ocean conditions began with the Tropical Atmosphere Ocean (TAO) buoy array (McPhaden et al., 1998), developed as part of the Tropical Ocean-Global Atmosphere (TOGA) program in the 1980s. Observations were more sparse before TOGA/TAO began, though reconstructions of SST from the available observations have been extended back to the 19th century (Smith and Reynolds, 2004; Rayner et al., 2006).

The wide variations in ENSO strength during the 20th century have been a topic of interest for quite some time (Ropelewski and Halpert, 1986; Trenberth and Hurrell, 1994), particularly with respect to the extremely strong events of the 1990s (Trenberth and Hoar, 1996). The 1970s in particular are thought to represent a 'regime shift' in which the dominant ENSO dynamics were fundamentally altered (Miller et al., 1994); but the statistical significance of claims of 20th century ENSO changes have been called into question (Rajagopalan et al., 1997).

How long must one observe the system to be sure of seeing the full range of ENSO characteristics? General circulation model (GCM) simulations carried out by Wittenberg (2009) using the GFDL model have shown that far from being a definitive indicator of climate change, centennial variations in ENSO amplitude of a factor of 2 or more are possible simply due to natural variability, and that several centuries of model output are required for the system to 'converge' to stable statistics. Stevenson et al. (2010) performed a similar analysis using a wavelet-based technique, and found that roughly 240 years of *observations* would be needed to constrain the real ENSO, assuming that the background climate was stable. There is much interest in using the paleoclimate record to extend the baseline for ENSO observations (Emile-Geay et al., 2011a,b), but some issues remain with accurate validation of model ENSO against paleoclimatic proxies (Stevenson et al., 2011b).

The multi-century averaging time required for robust ENSO statistics may explain a great deal of the uncertainties associated with 21st century projections. Multi-model studies of the ENSO climate change response are notorious for their disagreement (AchutaRao and Sperber, 2006; Guilyardi, 2006; Collins et al., 2010), but typically use only a few ensemble members for each climate projection. But attributing the disagreement to the small sample size does not appear completely satisfactory: an analysis of the 20th and 21st century CCSM4 ensembles, each containing 5-6 simulations for a total of > 500 model years, showed no significant ENSO amplitude response to CO_2 (Stevenson et al., 2011a). This seems to be due to the fact that the ocean is continually adjusting to rapidly changing CO_2 forcing over the course of the 21st century.

If slow ocean adjustment to changing radiative forcing explains the insignificant ENSO response to climate change, then disagreement between transient 20th/21st century model projections is not surprising. But this also implies that the overall ENSO climate sensitivity remains an unknown: very long equilibrated simulations at varying CO_2 concentrations are necessary to determine whether the ENSO sensitivity indeed differs between models. Since model ENSO climate sensitivity may be dependent on small changes to resolution and/or physical parameterizations (Guilyardi, 2006), looking at long integrations of a single climate model can thus provide a unique understanding of these effects in the absence of complicating factors.

2 Experimental Setup

The numerical experiments are performed using the National Center for Atmospheric Research (NCAR) Community Climate System Model version 3.5 (CCSM3.5), in the fully coupled configuration (atmosphere, ocean, land and sea ice). The ocean model has a zonal resolution that varies from 340 km at the equator to 40 km around Greenland, and a meridional resolution that varies from 70 km at the equator to 40 km around Greenland and 350 km in the North Pacific. This spatially varying resolution is achieved by placing the north pole of the grid over Greenland, and reflects the different relevant length scales of the 2 processes that are most important in maintaining a stable global climate: deep convection around Greenland and in the Arctic, and oceanic heat uptake at the equator. In the vertical there are 25 depth levels; the uppermost layer has a thickness of 8 m, the deepest layer has a thickness of 500 m. The atmospheric model uses T31 spectral truncation in the horizontal (about 3.75° resolution) with 26 vertical levels. The sea ice model shares the same horizontal grid as the ocean model, and the land model is on the same horizontal grid as the atmosphere. This setup (called T31x3) has been developed specifically for long paleoclimate and biogeochemistry integrations, and its performance is described in detail by Yeager et al. (2006). The most significant difference between the present model setup (CCSM3.5) and the one described in Yeager et al. (2006) is the new atmospheric convection scheme, which leads to significant improvements in the simulation of ENSO in the high resolution (Neale et al., 2008) and the present coarse resolution configuration (Jochum et al., 2010). Changes to the OGCM are a stratification dependent thickness diffusivity (Danabasoglu and Marshall, 2007), which improves the equatorial thermocline; a reduced viscosity (Jochum et al., 2008) which improves the equatorial surface currents; and an increased background diapycnal diffusivity (Jochum, 2009), which stabilizes the meridional overturning circulation.

Three integrations of the T31x3 CCSM3.5 have been carried out, each of which cover 1000 model years. The three model simulations were initialized from the climatology of Levitus (1998), and subsequently run without external forcing: each reached equilibrium after roughly 200 model years[2]. The equilibrium solution is therefore considered to consist of model years 200-1000 for each simulation. The only parameter which changes between the simulations is the atmospheric CO_2 concentration; values of 255, 355, and 455 ppm are adopted to sample the range of concentrations expected over the time period 1850-2050. Hereafter, the simulations are referred to as the 'pre-industrial' (PI; 255 ppm), 'present day' (PD; 355 ppm) and 'high-CO_2' (HC; 455ppm) simulations.

[2]Some residual spin-up effects remain in the deep ($\geq$ 1000 m) ocean, but are not expected to greatly impact ENSO dynamics.

3 ENSO Amplitude Response

The fundamental preliminary question to answer, first, is whether changes to ENSO amplitude between PI, PD and HC are statistically significant. Here the NINO indices NINO3 (5°S-5°N, 90-150°W), NINO4 (5°S-5°N, 160°E-150°W) and NINO3.4 (5°S-5°N, 120-170°W) are adopted as a proxy for ENSO, although of course other indices could easily be used (Gergis and Fowler, 2005; Wolter, 1989; Brown et al., 2008).

The spectral range of NINO3 and NINO4 SST, generated from 100-year subintervals of each simulation, is shown in Figure 1. Spectra are calculated using the wavelet toolkit of Torrence and Compo (1998), with the bias correction of Liu et al. (2007) applied to prevent artificial enhancement at long periods. There is a large degree of overlap between the 'envelopes' in Figure 1, but there is a distinct trend towards high amplitude with CO_2 in the eastern Pacific, which is especially apparent in NINO3 SST. No notable changes in the overall ENSO period are visible in Figure 1, given the broad spectral peak. However, the increase in seasonal cycle amplitude with CO_2 is substantial, consistent with previous coupled model studies (Timmermann et al., 2004).

Much attention has been focused on the CP/EP types of ENSO events (Yu and Kao, 2007; Kao and Yu, 2009). It has been speculated that CP ('Modoki') events are more sensitive to CO_2 than EP events, based on a few strong EP events near the end of the 20th century (Yeh et al., 2009). The distinction between event types is not a primary focus of this work, as the goal is understanding overall dynamical changes rather than event classification. That said, NINO3 and NINO4 can be in some sense regarded as 'proxies' for the EP and CP centers of action. If this were to hold true in a more detailed examination of individual events, based on Figure 1 one would expect that the EP type of ENSO might be more sensitive to CO_2 than the CP/Modoki.

The bandpassed[3] variance constitutes a good first-order diagnostic for the significance of ENSO changes. Previous results (Wittenberg, 2009; Stevenson et al., 2010) showed that several hundred years of data are required for convergence to a stable 'background' ENSO state, and this is upheld in the variance plots in Figure 2. 90% confidence intervals are constructed by selecting random subsamples of a specified length - when 30 years is used, the 2-4 year confidence intervals overlap for all simulations. Confidence interval width decreases with sampling length, and the PI/HC offset becomes significant at record lengths of ≈300-400 years. Strikingly, even at 400 years the variance of PD and HC remain indistinguishable, an indication of the importance of the *degree* of CO_2 increase for ENSO changes on long timescales.

[3]All bandpassing was conducted using a 10th order Butterworth filter; filter start and end points correspond to the 3dB half-power interval boundaries.

The behavior of the 5-7 year bandpass filtered variance differs greatly from the 2-4 year. Rather than a monotonic increase with CO_2, this band shows an enhancement in PD relative to *both* PI and HC. A case could be made for interesting nonlinear dynamical shifts in the western Pacific at longer periods, where modulations by the Pacific Decadal Oscillation (PDO) or coupling with the Indian Ocean might be expected to appear (Saji et al., 1999; Deser et al., 2004; Mantua et al., 1997). Also interesting is the larger decadal modulation of the 5-7 year variance in PD, as demonstrated by its much larger 90% confidence intervals at both 30 and 400-year sampling intervals. However, given the fact that the change is not monotonic with CO_2 and that the PI/HC comparison yields insignificant results, the 5-7 year band is not the focus here.

The probability distribution functions (PDFs) for NINO3.4 scale-averaged wavelet power (SAWP) are shown in Figure 2b for the 2-4 and 5-7 year bands. Here SAWP is calculated following Torrence and Compo (1998):

$$SAWP = \frac{\delta j \delta t}{C_\delta} \sum_{j=j_1}^{j_2} \frac{|W_n(s_j)|^2}{s_j} \tag{1}$$

Changes to the PDF shape are clearly visible in both bands: this changing shape shows up as a positive result when a Kolmogorov-Smirnov (K-S) test is applied (not pictured). However, the K-S test can only measure changes to the distribution, not whether those changes could have arisen from internal ENSO variations. As shown by Stevenson et al. (2011a), the K-S test yields significant differences even between members of a single ensemble, making a less sensitive test essential.

The statistical significance of differences between model NINO3.4 spectra are identified using the wavelet probability analysis (WPA) toolkit developed by Stevenson et al. (2010) and available over the Web[4]. The idea behind WPA is that if a single process is responsible for generating two time series, then their wavelet power PDFs should be roughly the same. Constructing wavelet PDFs from subsamples of a time series then creates a measure of natural variability: the degree to which PDFs of subintervals overlap indicates the expected internal scatter (Stevenson et al., 2010). The significance of differences between two time series may then be measured via hypothesis testing: the spectral overlap between the wavelet decomposition of a reference time series (here HadSST NINO3.4) and that of the CCSM3.5 runs is computed, and the resulting distributions compared. The significance level at which the confidence intervals on the distributions overlap is then the minimum significance at which they differ. Full details of the procedure are available in Stevenson et al. (2010).

Results from WPA testing are shown in Table 1, calculated using a Morlet wavelet at subsampling length 250 years. Here the numerical convention is to provide the significance of

[4]http://atoc.colorado.edu/~slsteven/wpi/

differences between simulations, where a change significant at the 90% level has a test value of 0.9. These results are consistent with the variance plots in Figure 2: NINO3 SST variability is significantly stronger in the 2-4 year band in HC relative to PI. It should be noted that although the overall shift in NINO3 2-4 year power is toward stronger variability with CO_2, the change between PD and HC is insignificant. At longer periods (5-7 year band), NINO3 variability is statistically identical between all simulations, as is the case with NINO4 2-4 year variability. This provides additional justification for the exclusion of the 5-7 year period range from further analysis.

4 Mean Circulation Changes

The assessment of statistical significance in Section 3 provides a strong motivation for understanding the physical mechanisms by which ENSO changes take place. Linkages between the mean state of the atmosphere and ocean and ENSO dynamics are a common way of understanding such changes (Fedorov and Philander, 2000, 2001), although there is still some debate over whether ENSO should be more properly understood in terms of a modulation of the mean state, rather than an oscillation about a stable mean (Sun, 2003; Sun and Zhang, 2006). Here, both the mean state and the general circulation of the atmosphere and ocean are examined.

In the atmosphere, the relevant mean state variables are the wind stress, precipitation and vertical pressure velocity ω: changes between PD vs. PI and HC vs. PD are shown in Figure 3. The wind stress shift between simulations is consistent with results from Vecchi and Soden (2007) and Held and Soden (2006), who suggested that the strength of the Hadley and Walker cells should decrease in a warmer climate due to the decrease in convective exchange between the boundary layer and free troposphere required by the slower increase in precipitation relative to humidity. Indeed, a weakening of the equatorial trade winds is seen with CO_2 in Figure 3: westerly anomalies dominate along the equator, which reflects a decrease in the Walker circulation strength. An eastward shift of the Walker cell is also reflected in the precipitation and ω panels of Figure 3: larger precipitation and ascending velocities are seen in the eastern Pacific at higher CO_2.

Subtropical meridional wind stress changes are consistent with a weakening of the Hadley cell (Figure 3b,c): southerly (northerly) anomalies dominate in the Northern (Southern) Hemispheres. But do these changes truly reflect a shift in the circulation? To answer this question, the atmospheric overturning streamfunction is calculated and plotted in Figure 4. The formulation of the streamfunction follows Döös and Nilsson (2011): in pressure coordinates,

$$\Phi(y,P) = \frac{1}{t-t_0}\int_{t_0}^{t}\oint\int_{0}^{P}\frac{v(x,y,P',t)}{g}dP'dxdt \tag{2}$$

The circulation is plotted separately for DJF and JJA to allow for ease of interpretation. During JJA, the northern Hadley cell weakens slightly (≈10% of the PI value) and shifts to the south, as indicated by the position of the zero contour in Figure 4c. Negative anomalies in Figure 4d also show the weakening of the Southern Hemisphere branch of the circulation. The changes during DJF are smaller, only 1-2% percent of the PI streamfunction, and show less spatial coherence than the JJA anomalies. A small tendency towards poleward contraction may be evident in both branches (Figure 4d,h), but the dominant influence is the boreal summer shift (Figure 4a-d).

A weakening of the Hadley circulation, even during the summer months alone, has several implications. First, the associated reduction in the zonal trade winds will tend to be larger at higher latitudes, since the Coriolis force on the surface flow is stronger farther from the equator. This in turn leads to a reduction in the subtropical wind stress curl, which can be seen in Figure 3b,c. A weaker wind stress curl will then slow subduction and affect circulation in the subtropical cell, and therefore be felt by the equatorial ocean.

To directly assess changes to the subtropical cell in relation to Ekman pumping, a summary of both quantities is provided in Figure 5. The oceanic meridional overturning streamfunction is derived in the appendix; the formulation used in Figure 5 is

$$\Phi = \int_{z_0}^{z} v(y,z)dz - \int_{y_0}^{y} w(y,z_0)dy \tag{3}$$

since now depth coordinates, rather than pressure coordinates, are used. Figure 5 indicates the reduction in equatorial upwelling, which shrinks by 5-10% in HC relative to PI (Figure 5f). Circulation along the poleward edges of the STC also decreases with CO_2 by 10-20% (Figure 5b,c), which may be interpreted as a contraction of the overturning circulation due to the reduction in off-equatorial wind stress curl near 10°N/S (Figure 5e,f). It should also be noted that there is a small (5-10%) increase in circulation in the core of the STC in HC and PD relative to PI, near 5°N/S. This increase is likely related to a change in the source region for water transported to the tropics along subsurface isopycnals, where the region of maximum Ekman downwelling has moved closer to the equator (Figure 5c-d).

The change to the oceanic mean state is shown in Figure 6, and reveals two crucial features: the enhanced SST warming in the eastern Pacific (*i.e.*, the weakened cold tongue; Figure 5b,c), and the increase in equatorial stratification (Figure 5h,i). The enhanced eastern Pacific warming can be understood as a consequence of the reduction in the zonal trade winds due to the Bjerknes feedback (Collins et al., 2005). The stratification increase is related to the

change in the Hadley circulation through its connection with the subtropical cell. A decrease in heat flux divergence from the equatorial region as the climate warms is a known feature of coupled GCMs (Collins et al., 2010; Vecchi and Soden, 2007), and should be expected to lead to an enhanced warming along the equator relative to higher latitudes. Likewise, Liu and Philander (1995) showed that a weaker subtropical wind stress curl leads to less warm water being transported to the lower equatorial thermocline, increasing equatorial stratification. Thus, Figure 5 serves as a confirmation of well-understood dynamical changes.

The increase in vertical stratification and reduction in subtropical wind stress curl seen in Figures 3 and 6 is expected to be accompanied by a shoaling of the mean thermocline. Is the expected degree of shoaling sufficient to explain the changes in Figure 6e-f? The scaling relationship developed by Luyten et al. (1983) and reproduced in Pedlosky (1996) (hereafter the LPS scaling) is applied to these simulations, to assess whether any further exploration of the thermocline shift is necessary. The LPS scaling relationship is given by

$$H = \sqrt{\frac{\tau_0 L}{\gamma_2 \rho_0}} \tag{4}$$

where τ_0 is the mean subtropical wind stress, L the size of the basin, ρ_0 the mean density of seawater, and γ_2 the scaled difference in density for water above and below the thermocline ($\gamma_2 = \frac{\rho_2 - \rho_1}{\rho_0} g$). Here τ_0 and γ_0 have been calculated from the CCSM3.5 output and are provided in Table 2, along with the other constants used in Equation 4. When the mean thermocline is calculated using this relationship, the result ranges from 120-106m, values which are remarkably consistent with the climatological mean thermocline depth in the ocean model. The equatorial thermocline is somewhat shallower (Table 2) but changes in depth with CO_2 are similar to those in the extratropics.

Thermocline changes from Equation 4 are next compared with the thermocline depths measured directly in the CCSM3.5. Here the thermocline in the NINO3.4 region has been calculated based on the position of the maximum vertical temperature gradient, and the result averaged in time and space. Values are generally shallower than the H values from Equation 4, ranging from 92-74m. The percentage change from PI to PD is somewhat larger than the 6% predicted by the LPS scaling, but the PD/HC shoaling is nearly identical. The thermocline is therefore presumed to be set primarily by nondissipative processes, and thermocline changes a straightforward consequence of shifts in the general circulation.

5 Changes to Interannual Variability

Changes to the mean state in CCSM3.5 are consistent with the multi-model results from AR4 (Guilyardi et al., 2009; AchutaRao and Sperber, 2006; Collins et al., 2010). Note that no consistency in the sensitivity of ENSO variability to CO_2 was found among the AR4 models (Collins et al., 2010); this study is thus a first step towards identification of ENSO climate sensitivities in this model. The dynamics of the 2-4 year variability is next examined, in both the atmosphere and ocean.

Figure 7 shows thermocline, SST and subsurface temperature variability calculated using the standard deviation of the 2-4 year bandpassed time series. SST variability clearly appears ENSO-like, with the canonical 'horseshoe' El Niño pattern visible in the equatorial region. Signatures of Rossby and Kelvin wave pathways appear in thermocline depth (Figure 7d-f), with excitation of equatorial Kelvin waves strengthening as CO_2 increases.

It should be noted here that the thermocline definition used in Figure 7d-f differs from that in Section 3. The depth of the maximum temperature gradient does not always match the depth of the main thermocline, especially in the warm pool polewards of 10° where mixed layer effects seem to dominate. A temperature-based definition seems more appropriate in this case, and the effects of overall climate change are offset to first order by adding the mean 0-500m warming to the 20°C thermocline temperature in PI, in PD and HC. This leads to a 20°C thermocline in PI, 20.5° in PD, and 21°C in HC.

The increase in subsurface variability is clearly not an artifact of the choice of thermocline definition - this is demonstrated in Figure 7g-i. These panels show the standard deviation of temperature as a vertical profile, averaged over latitudes 2°S-2°N. Enhanced variability is seen at the surface and at depth, spread over a depth range much larger than the equivalent of an 0.5°C temperature change (≈15m for a mean stratification of -0.02°C/m).

Interestingly, there seem to be several distinct 'centers' of large variance, rather than a uniform region of variability; all 'centers' strengthen with CO_2. The surface SST variability is relatively straightforward to explain, as a larger stratification necessarily leads to larger temperature signals for a given thermocline anomaly. Indeed, the locations where stratification increases most dramatically in Figure 7e-f are collocated with the "centers" of increased activity in Figure 7g-i. The western Pacific signal near 100-150m depth is likely due to Rossby wave activity, since the generation region for Rossby waves seen in Figure 7d-f is quite near these longitudes.

From Figure 7 alone, it is tempting to conclude that an increase in delayed oscillator-like wave activity (Zebiak and Cane, 1987; Battisti and Hirst, 1989), combined with the increased equatorial stratification, provides the entire explanation for enhanced ENSO amplitude. Such an increase in oscillator activity would likely be tied to an increase in the stochastic forcing

due to westerly wind bursts (Gebbie et al., 2007). However, there still remains the question of hemispheric asymmetry. The thermocline standard deviation maps in Figure 7d-f show that the Rossby wave signature grows stronger (weaker) in the Southern (Northern) Hemisphere - this is again borne out in subsurface temperature variability, and is not readily explained by a simple oscillator model. Figure 8 shows similar standard deviation maps equivalent to those in Figure 7g-i, averaged over 10-20°S, 5°S-5°N and 10-20°N: overall subsurface temperature variability strengthens in southern latitudes and weakens in northern latitudes.

Subannual wind stress variability is one possible forcing mechanism, and is therefore examined in Figure 9 using a 2 month to 2 year bandpass filter. Anomalies in the wind stress are enhanced at higher CO_2, along pathways nearly coincident with the anomalous convergence/divergence observed in the wind stress maps of Figure 3b,c. These pathways, it should be noted, are strikingly similar to the pathways typical of the 'seasonal footprinting mechanism' (SFM) of Vimont et al. (2003) and Alexander et al. (2010). In the SFM picture, a subtropical signal generated during the previous (boreal) spring triggers an El Niño event: the features in Figure 9 seem to indicate a similar mechanism at work. As CO_2 increases, not only does the overall strength of Northern (Southern) Hemisphere variability decrease (increase), but the pathways of variability seem to move toward the equator. This is most likely a consequence of the decreased meridional flow in both hemispheres.

Why should this meridional asymmetry in wind stress variability be enhanced with CO_2? The eastern Pacific SST seasonal cycle increases in amplitude with CO_2, as shown in Figure 1. This leads to a larger meridional temperature gradient in the eastern Pacific which reaches a maximum during boreal summer. The cross-equatorial atmospheric flow will then be enhanced during boreal summer, which tends to strengthen trade winds in the Southern Hemisphere and weaken them in the Northern (Xie and Philander, 1994; Xie, 1996), with the same impact on the wind stress curl in the two hemispheres. This should then be expected to lead to a larger (smaller) Ekman pumping signal in the Southern (Northern) Hemisphere.

The increase in variability in Figure 9 is suggestive, but not conclusive: it remains to be shown that wind stress variations really are connected with larger ENSO amplitudes. In the coupled model framework, a definitive mechanistic proof would require additional numerical experiments with varying forcings (*e.g.*, Alexander et al. (2010)); but the necessary dynamical 'steps' can be investigated nonetheless. The correlation between wind stress curl and thermocline depth is shown in Figure 10 for a lag of 1 month (wind stress curl leading). Seasonal footprinting-like pathways appear once more, with correlations consistent with an Ekman pumping signal. Once again, the signal strengthens in the Southern and weakens in the Northern Hemisphere as CO_2 increases: additional circumstantial evidence for a causal relationship between changes in wind stress curl and wave propagation. Ekman pumping is becoming more efficient at exciting waves along the SFM pathways in the Southern Hemi-

sphere, and less efficient in the Northern, as CO_2 increases.

The next step in the logical 'chain' is to demonstrate a connection between Ekman pumping along these pathways and initiation/termination of events in the CCSM3.5. The life cycle of an El Niño event is therefore examined in more detail, using lag-correlations between thermocline depth/zonal wind stress and the NINO3.4 SST (Figures 10, 11,12). Before the peak of the El Niño phase, a negative thermocline anomaly forms in the western Pacific, and sets up across the central portion of the basin (panels a,b). Roughly 3 months before peak El Niño, a positive thermocline signal propagates in from the north and continues along the equator as a Kelvin wave before reaching the eastern Pacific and setting up the fully developed El Niño (panel c). After this point the Southern Hemisphere appears to play a larger role. 3-6 months after peak El Niño, a negative thermocline anomaly forms in the eastern Pacific near 15°S, 250°E then propagates northwest to the equator (panels d,e). This anomaly reflects off the western boundary and propagates east as a Kelvin wave to terminate the event (panel f).

To complete the puzzle, Figures 11 and 12 clearly indicate that the lag-correlations after peak El Niño strengthen in the Southern Hemisphere (panels e-f), and those before the peak weaken in the Northern Hemisphere (panels a-b). This is consistent with the changes in subsurface variability seen in Figure 8, and provides evidence that the Ekman pumping-induced thermocline activity in Figure 10 is in fact related to ENSO dynamics. In effect, what seems to occur is the oceanic manifestation of changes to the seasonal footprinting mechanism: a shift in the seasonal cycle in the eastern Pacific leads to changes in Rossby wave activity along the pathways previously identified as important for transmission of the seasonal signal. The novel result here is the role played by the Southern Hemisphere: the SFM is able to create forcing in *both* hemispheres, which have opposing influences on El Niño events.

6 Preliminary Comparison with CCSM4: Implications for CMIP

The results of the previous sections paint a dynamically consistent picture of the connection between atmospheric CO_2 and ENSO activity. But the oscillation is known to be highly sensitive to changes in model physics (Guilyardi, 2006; Philip and van Oldenborgh, 2006), meaning that any single-model result is not conclusive in and of itself. In fact, the CCSM is itself an excellent case study for model physics' influence on ENSO, as the CCSM4 21st century projections show a slight (though statistically insignificant) *decrease* in ENSO amplitude with CO_2 (Stevenson et al., 2011a). Unfortunately, there are very few model experiments which permit robust detection of dynamical changes in the CCSM4 or other

current-generation coupled models; for example, the CMIP5 simulation suite does not include stabilized, high-CO_2 integrations long enough to provide stable ENSO statistics (see Taylor et al. (2011) for a description of the CMIP5 experimental design).

Taken in conjunction with Stevenson et al. (2011a), these results present an argument for additional long climate model simulations at varying CO_2 concentrations. Stevenson et al. (2011a) showed that trends in tropical thermocline depth persist for decades in climate-change simulations, which is likely part of the reason for the insignificance of the 21st century ENSO weakening. An experiment like the one presented here, therefore, is the only way to be sure that the dynamical changes observed are truly due to CO_2 influences and are not biased by a too-short sampling length.

An illustration of the need for long stabilized simulations with additional CMIP-class models is provided, using the CCSM4 1° Representative Concentration Pathway (RCP) 'extension' simulations for 2100-2300 (Meinshausen, 2011) as a rough comparison case. It is important to note that a 'clean' comparison with CCSM4 is not possible given the short extent of the available simulations: the extension simulations are the closest equivalents to a high-CO_2 control currently available, being stabilization scenarios from 2100-2300 for each of the 21st century projection suites. One of the mid-range extension runs, RCP4.5 (hereafter RCP4.5E), is adopted as a representative example to illustrate potential ENSO-relevant differences: here only the last 50 years are used (AD 2250-2299) to minimize ramp-up effects.

The mean-state response of CCSM4 to CO_2 increases was documented by Stevenson et al. (2011a): mean-state changes are qualitatively similar to the T31x3 CCSM3.5. The equatorial zonal SST gradient and trade winds decrease, ocean stratification increases, and the Walker circulation shifts eastward: all consistent with the T31x3 CCSM3.5 results. Yet the ENSO amplitude response appears quite different; the changes from CCSM3.5 to CCSM4 clearly impact the ENSO climate sensitivity, but why? The answer is probably *not* a mechanism like the seasonal SFM activity described above. Preliminary analysis of the CCSM4 simulations shows similar behavior in thermocline depth correlations with NINO3.4 SST (not pictured), meaning that an explanation for the ENSO climate sensitivity difference must lie elsewhere.

The most obvious difference between the T31x3 CCSM3.5 and 1° CCSM4 is resolution, which increases threefold between the CCSM3.5 T31x3 and CCSM4 1° configurations. This in turn has a dramatic impact on convection and therefore on the level of westerly wind burst (WWB) activity in the model (Neale et al., 2008, 2011). WWBs are weak in the T31x3 configuration of the CCSM3.5 (Figure 13), but are known to initiate ENSO activity in the real world (Harrison and Vecchi, 1997; McPhaden, 2004; Lengaigne et al., 2004), often in conjunction with the Madden-Julian Oscillation (MJO; Madden and Julian (1994); Yu and Rienecker (1998); Lengaigne et al. (2004)). Perhaps high-frequency wind stress variability is an important control on ENSO climate sensitivity?

Here the sub-monthly zonal wind stress variance is used as a rough proxy for WWB activity, and is mapped over the tropical Pacific (Figure 13). The sub-monthly variance was chosen as a computationally inexpensive method of measuring the combined influences of WWBs (which take place a few times per year and last 5-20 days; Harrison and Vecchi (1997)) and synoptic weather activity. Some MJO-related variability may also be captured by this metric; identifying the proportions of variance associated with each process are beyond the scope of this section, which aims only to show that high-frequency variance may play a role in model ENSO sensitivity to climate change.

Figure 13 shows that the patterns of CO_2 response are clearly distinct between models; in particular, the western Pacific warm pool stands out as a region with markedly different behavior in CCSM3.5 and CCSM4. In CCSM3.5, the total variance off the Papua New Guinea coast increases by roughly 20%, while a decrease of the same magnitude takes place over the entire warm pool in CCSM4. This seems in conflict with previous studies (Gebbie et al., 2007), which find that WWB activity increases with warm pool temperature and longitudinal extent. Is this an indication that MJO triggering of WWBs (and possibly, therefore El Niño events) does not occur in the CCSM4? If not, are there other competing processes which 'damp out' the MJO influence on developing ENSO events? How are these processes represented in other climate models? The present study cannot answer these questions; however, Figure 13 should serve as ample evidence for changes which affect the simulated convective influence on ENSO within a single model family. It should also be noted that high-frequency wind stress variability is only a single example of ENSO-relevant dynamical changes between models; others doubtless exist.

A complete understanding of the dynamical sensitivities of ENSO with CO_2 in coupled general circulation models requires stabilized simulations at several different CO_2 levels, conducted with a wide variety of models. If CCSM can be considered representative in terms of ENSO CO_2 sensitivity (which question is as yet unanswered), then potentially one might not detect CO_2-induced ENSO changes unless an additional control at $CO_2 \geq 450$ppm were run. However, it is clear that whatever the desired CO_2 level, quantifying changes to ENSO dynamics in a statistically robust manner requires multiple centuries at a stable forcing level, which should be considered during future model intercomparison efforts.

7 Conclusions

This study has provided the first millennial-scale look at ENSO-CO_2 linkages in equilibrated climate model simulations, relying primarily on three T31x3 CCSM3.5 simulations conducted at 255, 355 and 455 ppm CO_2 with otherwise identical model configurations. Changes to the atmosphere/ocean mean state with increased CO_2 are similar to those found in previous

multi-model studies: enhanced SST warming is seen in the eastern Pacific, reducing the zonal SST gradient. An overall weakening of the overturning circulations in the atmosphere and ocean are seen, consistent with the Vecchi and Soden (2007); Held and Soden (2006) picture of a weakening boundary layer/free atmosphere exchange of moisture. In the atmosphere, the strongest effect on circulation is seen during boreal summer, when the Hadley cell is at its northernmost position.

In the ocean, vertical thermal stratification increases, most likely through a combination of increased surface heat flux, decreased equatorial upwelling and reduced subtropical cell strength. The thermocline shoals accordingly, by a percentage remarkably consistent with the scaling relationship derived by Luyten et al. (1983) and presented in detail in Pedlosky (1996). This indicates that the major processes controlling the climatological mean thermocline depth are nondissipative: cross-isopycnal mixing may be neglected at equilibrium.

The ENSO variance response to CO_2 in the CCSM3.5 is a strengthening which is statistically significant at 2-4 year periods. Longer-period (5-7 year) oscillations differ between simulations, but the direction of change is nonmonotonic. The physics controlling such changes is likely complex, and is beyond the scope of this study. However, the change to the SST seasonal cycle is substantial, with statistically significant strengthening occurring in both the NINO3 and NINO4 regions.

It is tempting to ascribe the increase in ENSO amplitude to the stratification alone, but this cannot explain some of the changes to oceanic variability. In particular, there is a pronounced hemispheric asymmetry in the changes to subsurface temperature variability observed between simulations. Variability near 10°N weakens with CO_2, and a corresponding strengthening is seen near 10°S. These changes occur near the climatological-mean edges of the subtropical gyres, which are expected to be quite sensitive to changes in the structure of the wind stress. When the correlation of the Ekman pumping strength and thermocline depth is calculated, wave generation along the SFM pathways is indeed found to be more (less) efficient in the Southern (Northern) Hemispheres with CO_2. This represents an extension of the SFM framework to include seasonal forcing from both hemispheres.

The sensitivity of these results to model physics is expected to be quite large, but multi-century equilibrated simulations with other CMIP5 models are not currently available. As a first cut, the CMIP5 CCSM4 extension run for RCP 4.5 is adopted as a comparison case for the CCSM3.5. Substantial differences in the wind stress response to increased CO_2 are observed, although the mean state response to CO_2 is the same in both models. A good illustration of model differences is submonthly wind stress variability, which decreases with CO_2 over the western Pacific warm pool in the CCSM4; perhaps stochastic ENSO forcing is highly sensitive to the modeled atmospheric convection.

These results show that it is indeed possible to diagnose dynamical influences when ENSO

changes are statistically significant; however, the mechanism identified here may not be robust across all models. Even within the same model family, there are large differences to ENSO climate sensitivity; millennial-scale integrations at varying CO_2 levels are necessary to ensure that sampling bias does not contaminate the results. Improving experimental design for intermodel comparisons is a challenge to the climate modeling community as a whole, but is nonetheless an essential step towards understanding the controls on ENSO dynamics in future climates.

Derivation of the meridional overturning streamfunction.

In the ocean, the meridional overturning streamfunction can be derived in the y-z plane using the 2-D continuity equation for the zonally averaged flow:

$$\frac{\partial v}{\partial y} + \frac{\partial w}{\partial z} = 0 \tag{5}$$

(Note that the same relationship holds in the atmosphere if pressure coordinates are used; then $\frac{\partial w}{\partial z}$ is replaced with $\frac{\partial \omega}{\partial P}$.)

The definition for streamfunction used here is

$$v = \frac{\partial \Phi}{\partial z}; w = -\frac{\partial \Phi}{\partial y} \tag{6}$$

This implies that

$$\Phi = \int_{z_0}^{z} -\frac{\partial w}{\partial z} dz + a(y) \tag{7}$$

where a(y) is an arbitrary function of y alone. Then taking the derivative with respect to y,

$$\frac{\partial \Phi}{\partial y} = \int_{z_0}^{z} \frac{\partial v}{\partial y} dz + \frac{\partial a}{\partial y} \tag{8}$$

Using the continuity equation and the definition of the streamfunction in terms of w,

$$\frac{\partial \Phi}{\partial y} = \int_{z_0}^{z} -\frac{\partial w}{\partial z} dz + \frac{\partial a}{\partial y} = -w(y, z) \tag{9}$$

Then integrate from y_0 to y:

$$-w(y,z) = -(w(y,z) - w(y,z_0) + \frac{\partial a}{\partial y} \tag{10}$$

$$\frac{\partial a}{\partial y} = -w(y,z_0) \tag{11}$$

$$\Phi = \int_{z_0}^{z} v(y,z)dz - \int_{y_0}^{y} w(y,z_0)dy \tag{12}$$

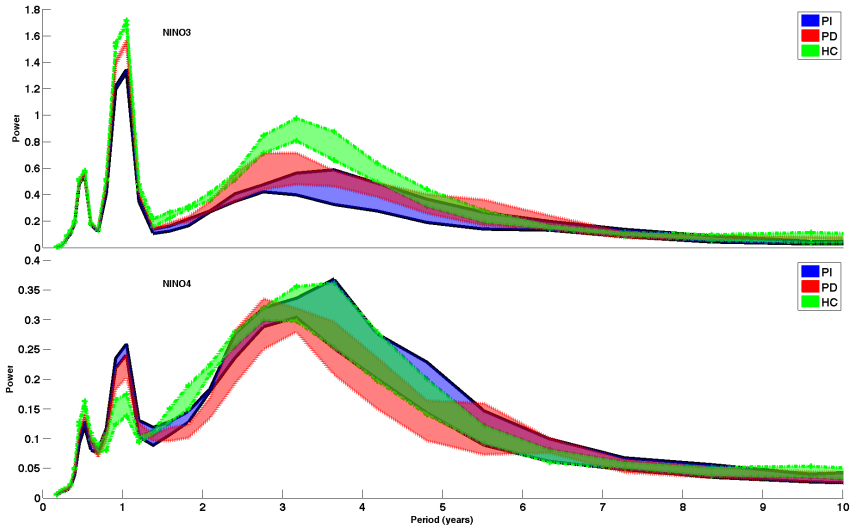

Figure 1: Spectral range for 100-year subintervals taken from each of the three equilibrated CCSM3.5 simulations. PI: pre-industrial (255 ppm CO_2). PD: present day (355 ppm CO_2). HC: high CO_2 (455 ppm CO_2). Top panel: NINO3 SST. Bottom panel: NINO4 SST. All wavelet power values are given in $°C^2$.

References

AchutaRao, K. and K. R. Sperber, 2006: ENSO simulation in coupled ocean-atmosphere models: are the current models better? *Climate Dynamics*, **27 (1)**, 1–15.

Alexander, M. A., D. J. Vimont, P. Chang, and J. D. Scott, 2010: The Impact of Extratropical Atmospheric Variability on ENSO: Testing the Seasonal Footprinting Mechanism Using Coupled Model Experiments. *Journal of Climate*, **23**, 2885–2901.

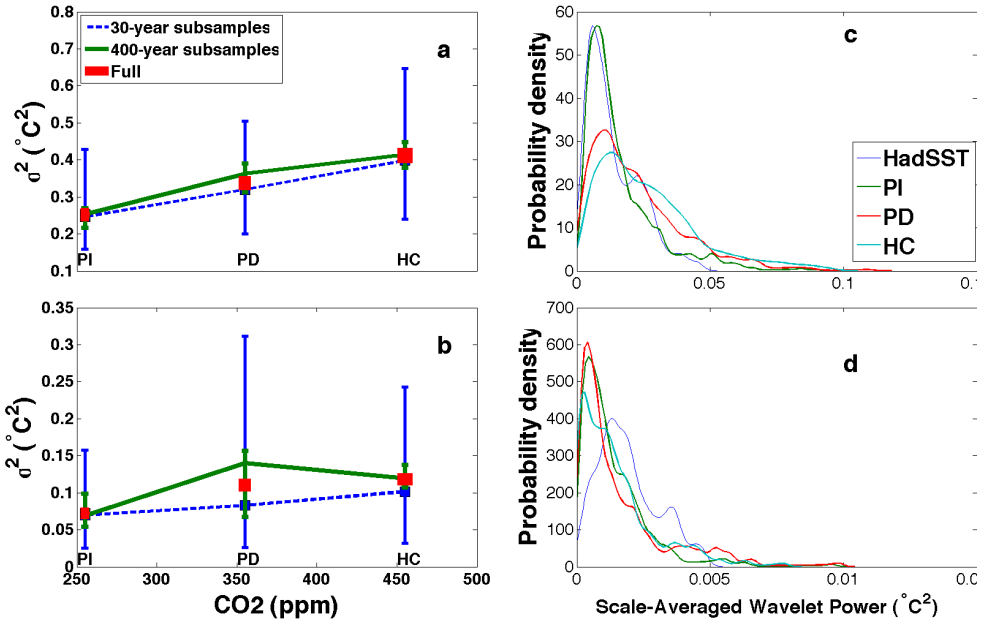

Figure 2: Illustration of the significance of differences between CCSM3.5 simulations. a,b: NINO3 SST variance subsampled at 30-year (blue; dashed line) and 400-year (green; solid line) intervals. c,d: Probability distribution functions of scale-averaged wavelet power. Top row uses a 2-4 year bandpass filter, bottom row a 5-7 year filter. Bandpass filters used are 10th order Butterworth filters, and filter endpoints specified as the 3dB half-power points.

Table 1: Significance of differences in NINO3 and NINO4 spectral power between the CCSM3.5 simulations. Values are calculated using the wavelet probability analysis toolbox of Stevenson et al. (2010) and presented using a '1 - p' convention. Here a p-value of 0.1 indicates 90% confidence that spectra differ, and is reported in Table 1 as a value of 0.9. Entries less than 0.9 indicate that spectra are indistinguishable at 90% significance. All calculations use the Morlet wavelet and subsampling length 250 years.

Comparison	NINO3	NINO4
PI/PD 2-4 yr	**0.90**	0.45
PD/HC 2-4 yr	0.49	0.35
PI/HC 2-4 yr	**1.00**	0.02
PI/PD 5-7 yr	0.46	**0.93**
PD/HC 5-7 yr	0.43	0.72
PI/HC 5-7 yr	0.02	0.48

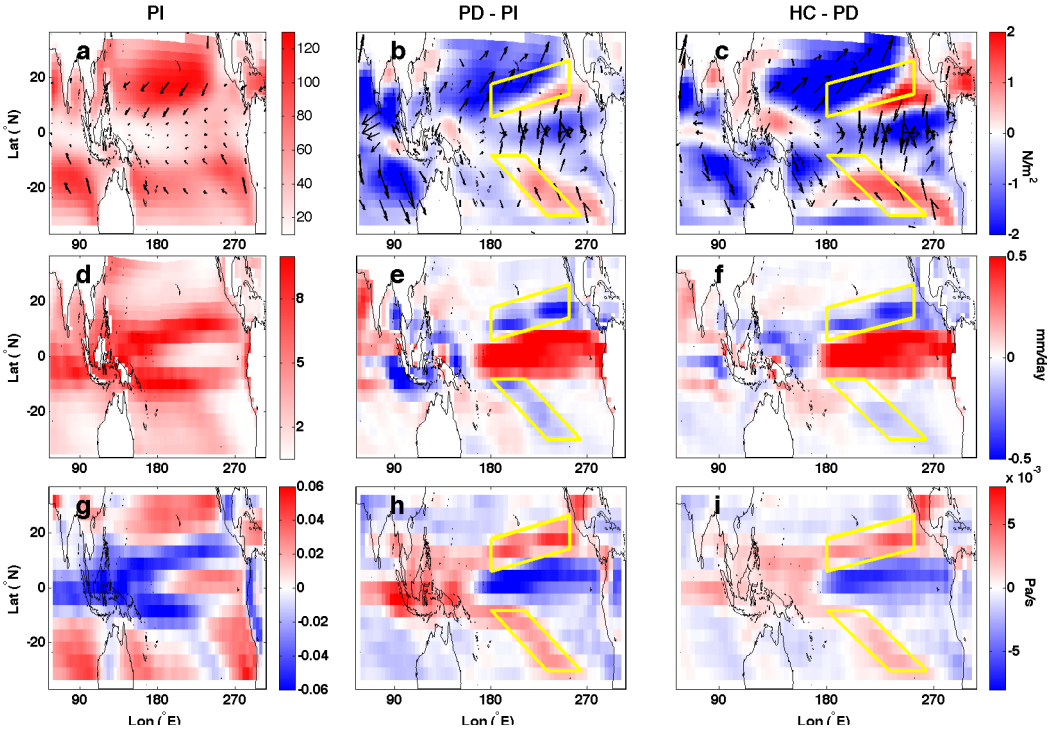

Figure 3: Changes to the mean state of the atmosphere. Left-hand column: mean state for PI. Middle column: differences between PD and PI. Right-hand column: differences between HC - PD. Top row (a-c): differences in wind stress (arrows show direction, colors the magnitude of the wind stress difference). Middle row (d-f): differences in precipitation. Bottom row (g-i): Differences in ω, vertical pressure velocity at 500 mb. In the middle and right-hand columns, the yellow boxes show the approximate positions of the pathways active in the SFM-like mechanism.

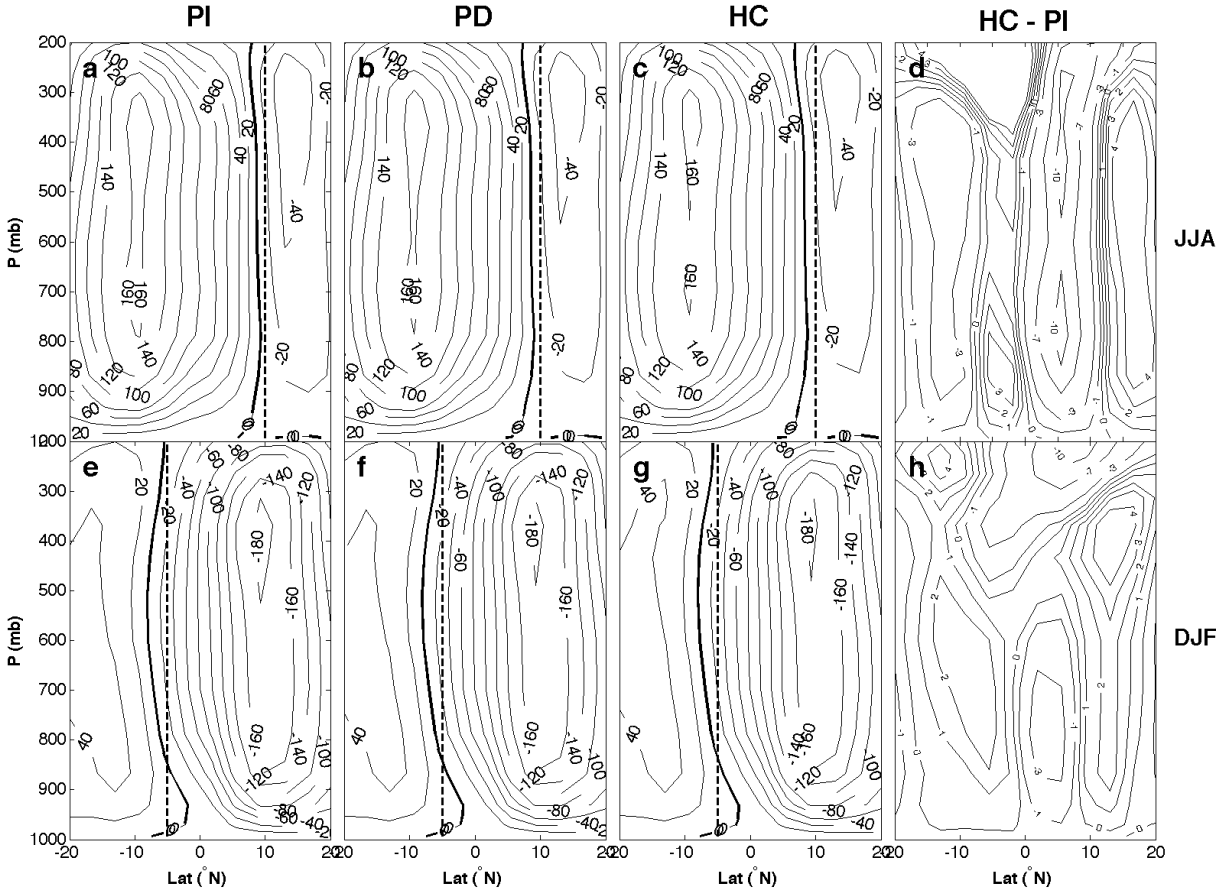

Figure 4: Changes to the atmospheric overturning streamfunction (units of Sv = 10^9 kg/s), corresponding to the strength of the Hadley cell. Here positive values correspond to a counterclockwise circulation, negative values to clockwise circulation. The position of the zero contour is shown in boldface. Vertical dashed lines are included to provide visual context only. a-c: JJA mean for PI, PD and HC respectively. d: Difference between JJA means for HC and PI. e-h: same as a-d for DJF.

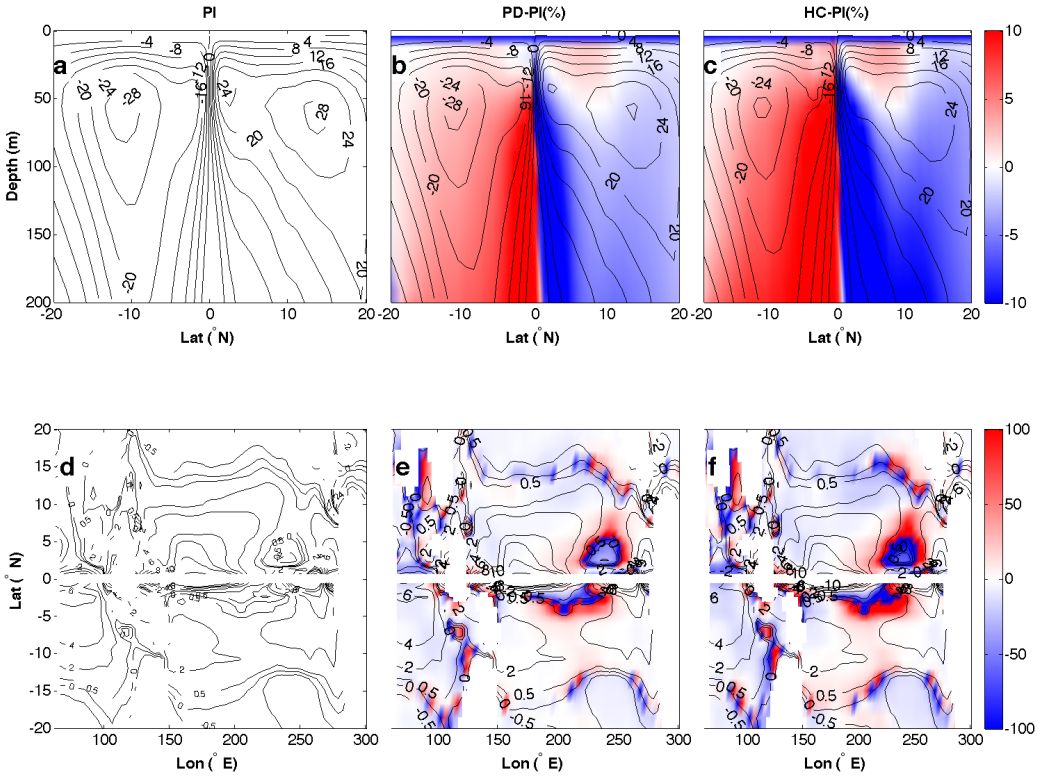

Figure 5: Summary of the circulation of the tropical Pacific. Upper panels: overturning streamfunction for the subtropical cell (units of Sv). Lower panels: strength of the Ekman pumping $\frac{\nabla \times \tau}{\rho_o f}$(values x 10^6). The contours indicate the magnitude of the relevant quantity (in PI for panels a/d, PD for panels b/e and HC for panels c/f), while the colors show the percentage change relative to PI (*i.e.* for HC, colors show (HC - PI)/—PI— x 100%).

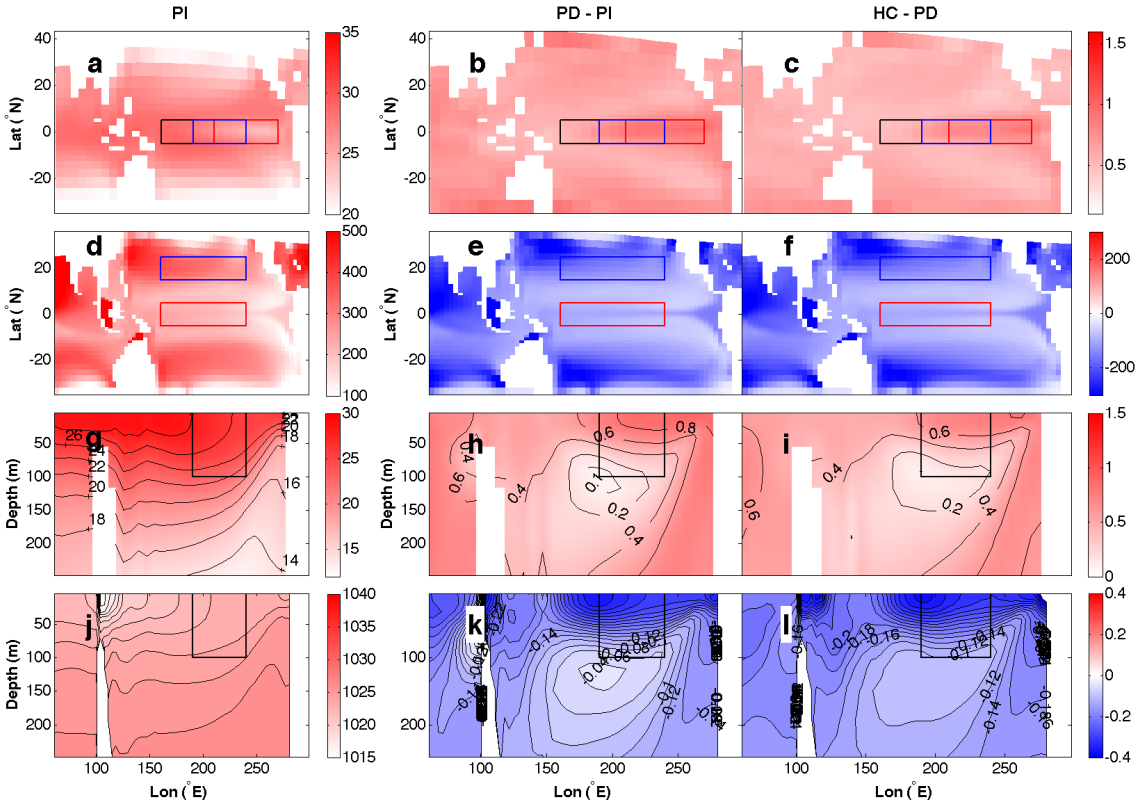

Figure 6: Changes to the mean state of the ocean. Left-hand column gives differences between PD and PI, right-hand column HC - PD. a,b: Differences in SST (°C). c,d: Differences in thermocline depth (m). e,f: Differences in subsurface temperature (°C). g,h: Differences in subsurface potential density (kg/m^3 x -1).

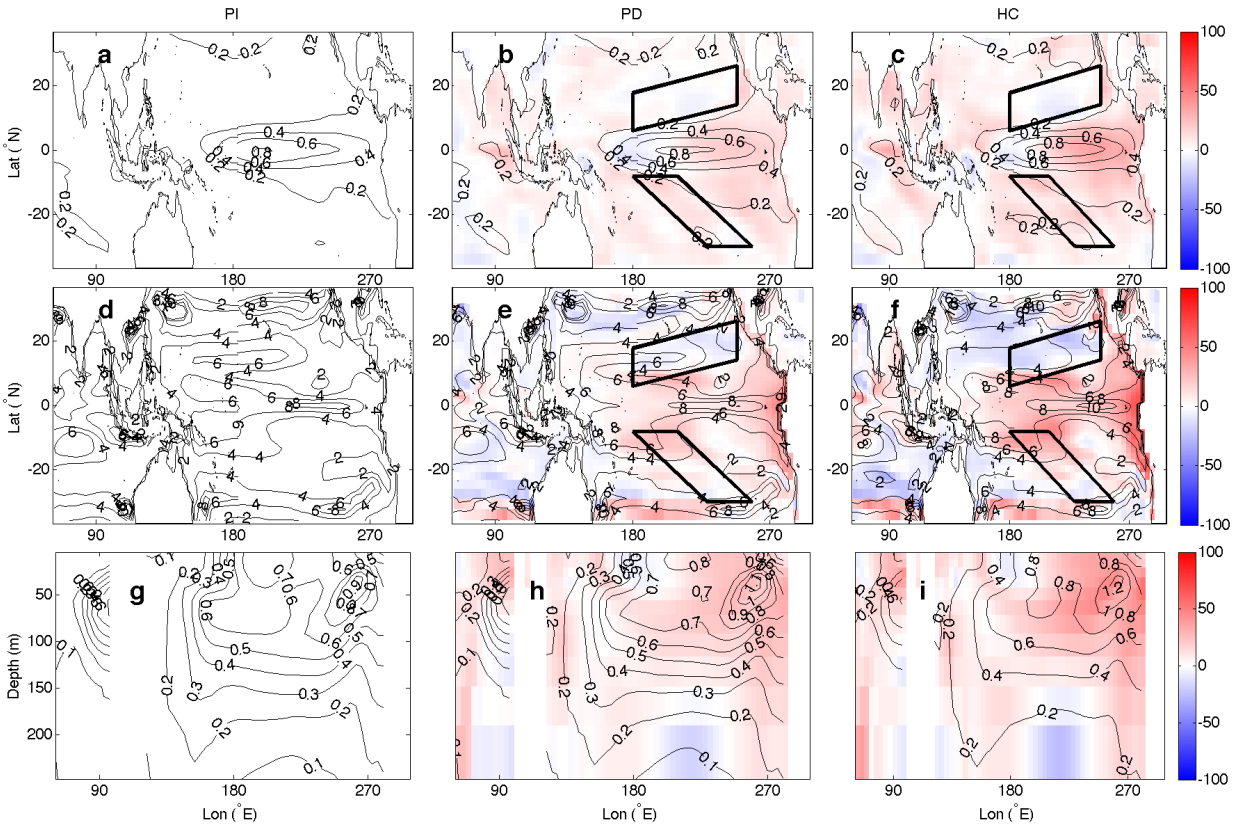

Figure 7: Oceanic variability (bandpass filtered with 3dB points at 2 and 4 years). Each panel shows the variance of the relevant quantity. Top panels: SST ($°C^2$). Middle panels: thermocline depth (m^2). Bottom panels: Subsurface temperature ($°C^2$).

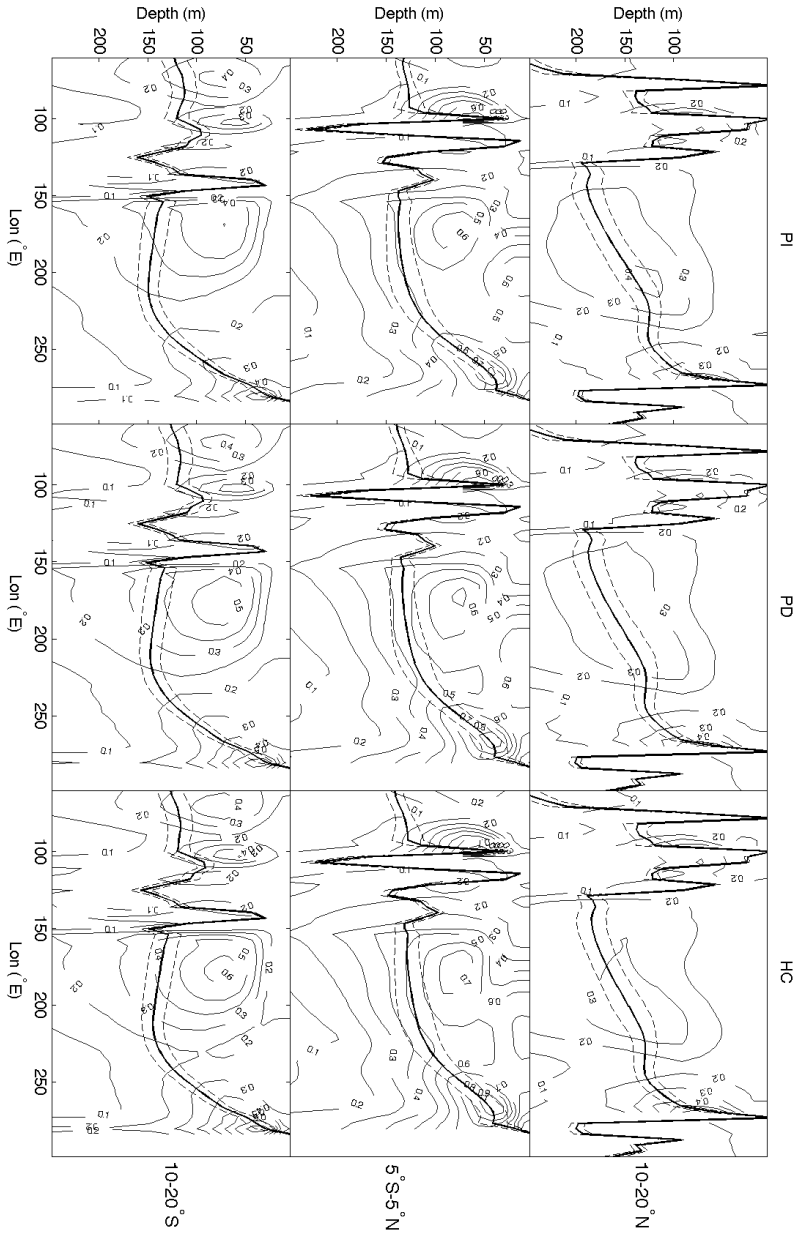

Figure 8: Variability in subsurface ocean temperature (variance of gridpoint time series, bandpass filtered with 3dB points at 2 and 4 years). Thick solid lines indicate the mean position of the thermocline; dashed lines show the $\pm 1\sigma$ uncertainty on the mean thermocline position.

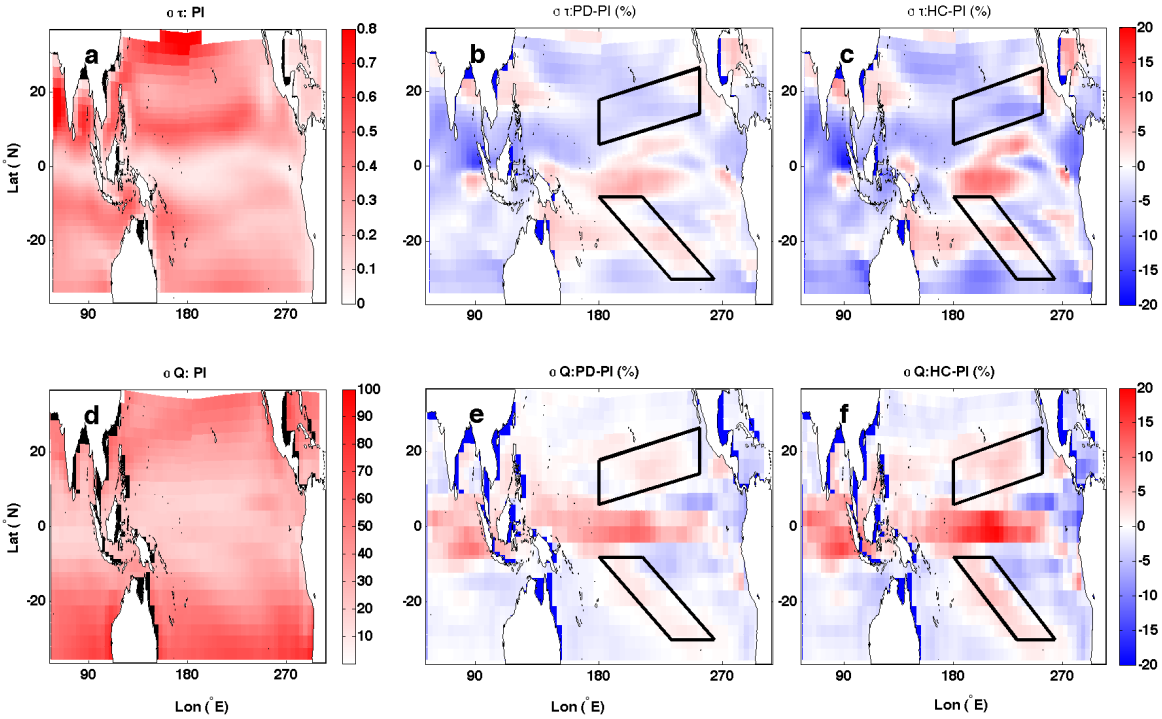

Figure 9: Changes to atmospheric variance, bandpass filtered with 3dB points at 2 months and 2 years. Boxes indicate the positions of anomalous convergence/divergence from Figure 3. a) Surface heat flux variance σ_Q for PI (W^2/m^4). b) % change in σ_Q between PD and PI. c) % change in σ_Q between HC and PI. d) Zonal wind stress variance σ_τ for PI (N^2/m^4). e) % change in σ_τ between PD and PI. f) % change in σ_τ between HC and PI. Black boxes indicate the position of the SFM-like pathways, and are identical to the regions defined in Figure 3.

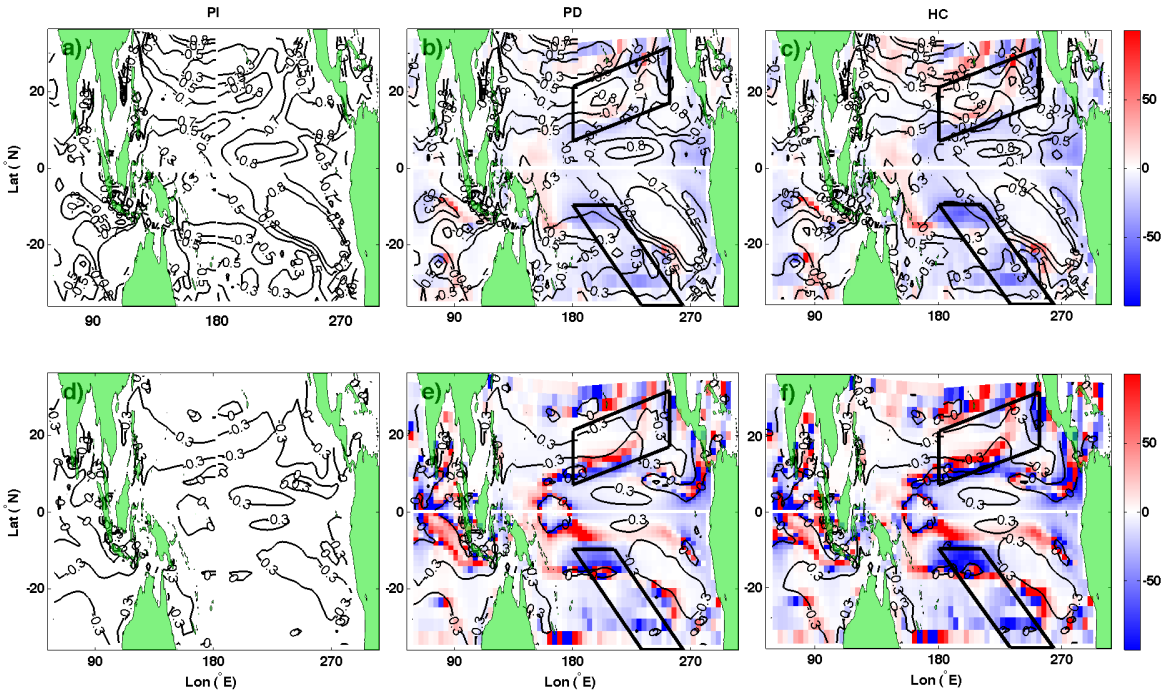

Figure 10: Lag-correlations between the curl of the wind stress and thermocline depth, for all simulations. Top panels (a-c) show the zero-lag correlation for PI-HC; bottom panels (d-f) show correlations at lag 2 months (wind stress leading). Correlations for PI are shown as contours in panels a) and d); in panels b-c and e-f contours indicate the values of the lag-correlations, while colors show the percentage change from PI. Black boxes are identical to those in Figure 3.

Table 2: Estimates of thermocline depth for the CCSM3.5 simulations. H indicates the thermocline depth calculated from the scaling relationships of Pedlosky (1996), using the state variables obtained from each simulation. Z_{mn} is the thermocline depth calculated directly from the CCSM3.5, using the depth at which the vertical temperature gradient is at a maximum. Zonal wind stress is averaged over the so-called 'matching' region in the subtropics, here defined as 10-20°N, 190-240°E. γ_2 is calculated using potential densities above and below the main pycnocline in the NINO3.4 region: averaging depths are 0-50m for the upper layer and 100-150m for the lower layer. Z_{mn} is calculated over the NINO3.4 region.

Simulation	L (km)	τ_x (N/m^2)	γ_2 (kg/m^3)	ρ_0 (kg/m^3)	H (m)	Z_{mn} (m)
PI	3000	-0.0963	-0.0193	1025	120.8	92.3
PD	3000	-0.0947	-0.0218	1025	112.8	79.3
HC	3000	-0.0929	-0.0240	1025	106.5	74.5

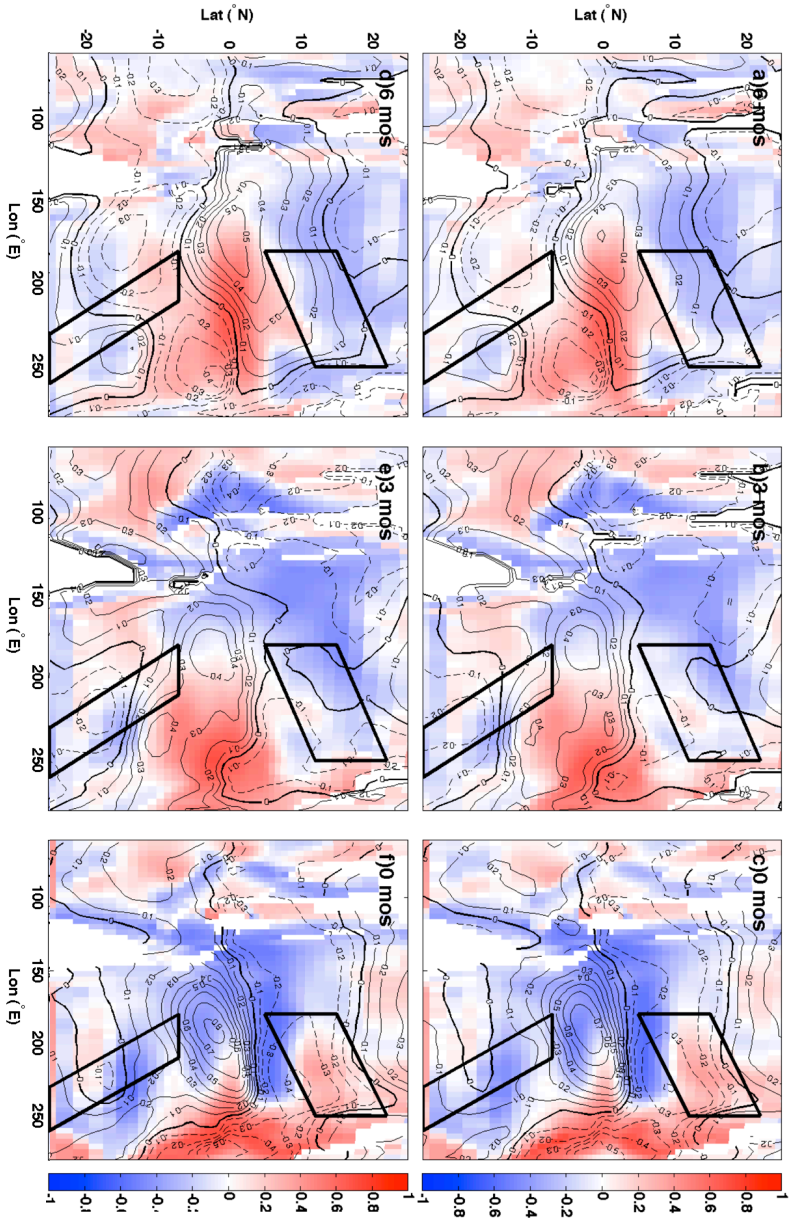

Figure 11: Lag-correlation plot for the 6 months before peak El Niño. PI is shown in the top row (panels a-c), HC in the bottom (panels d-f). Colors show the correlation coefficient between NINO3.4 index and thermocline depth at each grid point, with negative correlations in blue and positive in red. Contours show the correlation coefficient between NINO3.4 index and zonal wind stress. Zero correlation with wind stress is shown as the thick solid black line; positive NINO3.4/wind correlations are thin solid lines, negative correlations are dashed lines. a) 6 months before peak El Niño. b) 3 months before. c) Zero lag: peak El Niño. Black boxes are identical to those in Figure 3.

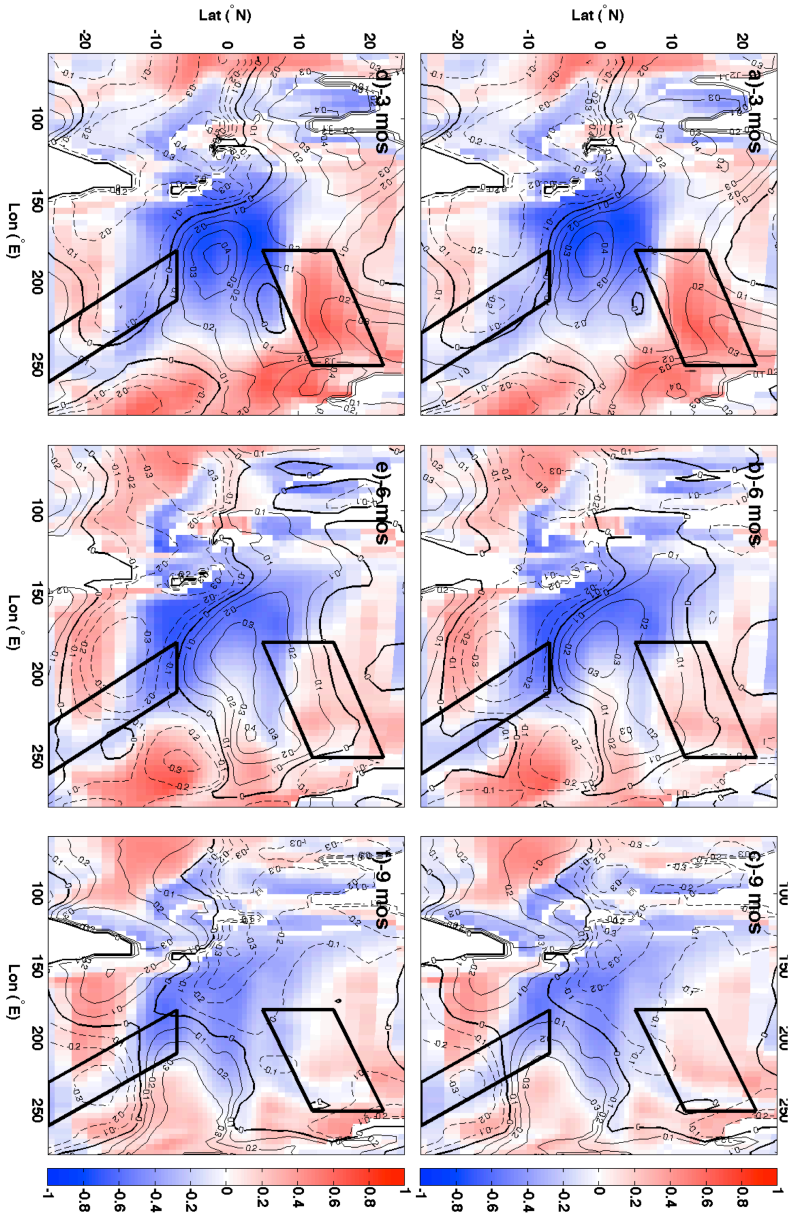

Figure 12: Same as Figure 11, for lags of 3, 6 and 9 months after peak El NIño.

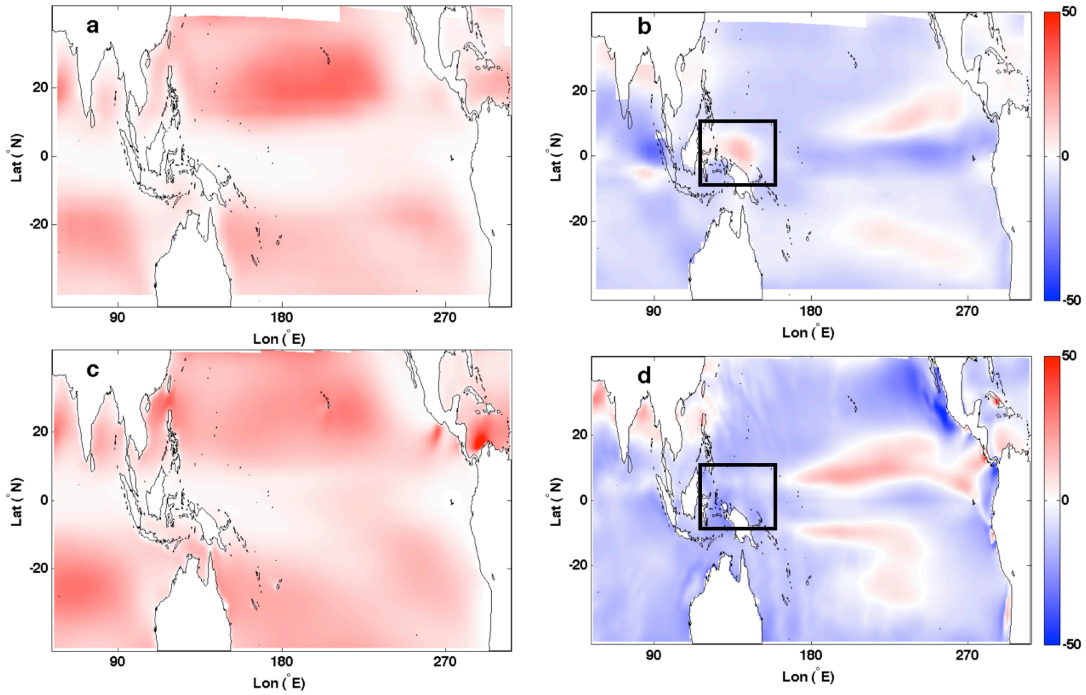

Figure 13: Sub-monthly zonal wind stress variance (N^2/m^{-4}). a: Mean variance for PI (CCSM3.5), years 200-1000. b: Difference between HC and PI (CCSM3.5), years 200-1000 for both. c: Mean variance for RCP 4.5 (CCSM4), years 2250-2299. d: Difference between RCP4.5 and the CCSM4 1850 control (years 800-1299). Note that in panels b,d, the units are % (given relative to PI for panel b, CCSM4 1850 control for panel d).

Battisti, D. S. and A. C. Hirst, 1989: Interannual variability in a tropical atmosphere ocean model: Influence of the basic state, ocean geometry and nonlinearity. *Journal of the Atmospheric Sciences*, **46**, 1687 1712.

Brown, J., A. W. Tudhope, M. Collins, and H. V. McGregor, 2008: Mid-Holocene ENSO: Issues in quantitatve model-proxy data comparisons. *Paleoceanography*, **23**, PA3202.

Collins, M., et al., 2005: El Niño- or La Niña-like climate change? *Climate Dynamics*, **24**, 89–104, dOI:10.1007/s00382-004-0478-x.

Collins, M., et al., 2010: The impact of global warming on the tropical Pacific Ocean and El Niño. *Nature Geoscience*, **3**, 391–397, doi:10.1038/NGEO868.

Danabasoglu, G. and J. Marshall, 2007: Effects of vertical variations of thickness diffusivity in an ocean general circulation model. *Ocean Modelling*, **18**, 122–141.

Deser, C., A. S. Phillips, and J. W. Hurrell, 2004: Pacific Interdecadal Climate Variability: Linkages between the Tropics and the North Pacific during Boreal Winter since 1900. *Journal of Climate*, **17**, 3109–3124.

Döös, K. and J. Nilsson, 2011: Analysis if the Meridional Energy Transport by Atmospheric Overturning Circulations. *Journal of the Atmospheric Sciences*, **68**, 1806–1820.

Emile-Geay, J., K. M. Cobb, M. E. Mann, and A. Wittenberg, 2011a: Estimating Tropical Pacific SST variability over the Past Millennium. Part 1: Methodology and Validation. *Journal of Climate*, submitted.

Emile-Geay, J., K. M. Cobb, M. E. Mann, and A. Wittenberg, 2011b: Estimating Tropical Pacific SST variability over the Past Millennium. Part 2: Reconstructions and Uncertainties. *Journal of Climate*, submitted.

Fedorov, A. V. and S. G. Philander, 2000: Is El Niño changing? *Science*, **288**, 1997–2002.

Fedorov, A. V. and S. G. Philander, 2001: A stability analysis of tropical ocean-atmosphere interactions: Bridging measurements and theory for El Niño. *Journal of Climate*, **14**, 3086–3101.

Gebbie, G., I. Eisenman, A. Wittenberg, and E. Tziperman, 2007: Modulation of westerly wind bursts by sea surface temperature: A semi-stochastic feedback for enso. *Journal of the Atmospheric Sciences*, **64**, 3281–3295.

Gergis, J. L. and A. M. Fowler, 2005: Classification of Synchronous Oceanic and Atmospheric El Niño-Southern Oscillation (ENSO) Events for Palaeoclimate Reconstruction. *International Journal of Climatology*, **25**, 1541–1565.

Guilyardi, E., 2006: El Niño-mean state-seasonal cycle interactions in a multi-model ensemble. *Climate Dynamics*, **26**, 329–348.

Guilyardi, E., A. Wittenberg, A. Fedorov, M. Collins, C. Wang, A. Capotondi, G. Jan van Oldenborgh, and T. Stockdale, 2009: Understanding El Niño in Ocean-Atmosphere General Circulation Models: Progress and Challenges. *BAMS*, 325–340.

Harrison, D. E. and G. A. Vecchi, 1997: Westerly wind events in the tropical pacific, 1986-95. *Journal of Climate*, **10**, 3131–3156.

Held, I. and B. Soden, 2006: Robust Responses of the Hydrological Cycle to Global Warming. *Journal of Climate*, **19**, 5686–5699.

Hildebrandsson, H. H., 1897: Quelques recherches sur les centres d'action de l'atmosphere. I-IV. *Kongl. Svenska Vetenskaps-Akademiens Handlingar*, **29 (3)**, 36 pp.

Jochum, M., 2009: Impact of latitudinal variations in vertical diffusivity on climate simulations. *Journal of Geophysical Research - Oceans*, **114**, C01 010.

Jochum, M., G. Danabasoglu, M. Holland, Kwon, and W. Large, 2008: Ocean Viscosity and Climate. *Journal of Geophysical Research*, **113**, C06 017, doi:10.1029/2007JC004515.

Jochum, M., S. Yeager, K. Lindsay, K. Moore, and R. Murtugudde, 2010: Quantification of the feedback between phytoplankton and ENSO in the Community Climate System Model. *Journal of Climate*, **23 (11)**, 2916–2925.

Kao, H.-Y. and J.-Y. Yu, 2009: Contrasting Eastern-Pacific and Central-Pacific Types of ENSO. *Journal of Climate*, **22**, 615–632, doi:10.1175:/2008JCLI2309.1.

Lengaigne, M., E. Guilyardi, J.-P. Boulanger, C. Menkes, P. Delecluse, P. Inness, J. Cole, and J. Slingo, 2004: Triggering of el niño by westerly wind events in a coupled general circulation model. *Climate Dynamics*, **23**, 601–620.

Levitus, S., 1998: *World Ocean Data- base 1998, vol. 1, Introduction*. NOAA Atlas NESDIS, vol. 18, NOAA, Silver Spring, Md.

Liu, Y., X. S. Lian, and R. H. Weisberg, 2007: Rectification of the bias in the wavelet power spectrum. *Journal of Atmospheric and Oceanic Technology*, **24**, 2093–2102.

Liu, Z. and S. Philander, 1995: How different wind stress patterns affect the tropical-subtropical circulations of the upper ocean. *Journal of Physical Oceanography*, **25**, 449–462.

Luyten, J. R., J. Pedlosky, and H. M. Stommel, 1983: The ventilated thermocline. *Journal of Physical Oceanography*, **13**, 292–309.

Madden, R. A. and P. R. Julian, 1994: Observations of the 4050-day tropical oscillation: a review. *Monthly Weather Review*, **122**, 814–837.

Mantua, N. J., S. R. Hare, Y. Zhang, J. M. Wallace, and R. C. Francis, 1997: A Pacific interdecadal climate oscillation with impacts on salmon production. *Bull. Amer. Meteor. Soc.*, **78**, 1069–1079.

McPhaden, M., et al., 1998: The tropical ocean-global atmosphere observing system: A decade of progress. *Journal of Geophysical Research*, **103**, 14 169–14 240.

McPhaden, M. J., 2004: Evolution of the 2002/03 El Niño. *Bulletin of the American Meteorological Society*, **85**, 677695.

Meinshausen, M. e. a., 2011: The RCP Greenhouse Gas Concentrations and their extension from 1765 to 2500. *Climatic Change*, in prep.

Miller, A., D. Cayan, T. Barnett, N. Graham, and J. Oberhuber, 1994: The 197677 climate shift of the Pacific Ocean. *Oceanography*, **7**, 2126.

Neale, R. B., J. H. Richter, and M. Jochum, 2008: The impact of convection on ENSO: From a delayed oscillator to a series of events. *Journal of Climate*, **21**, 5904–5924.

Neale, R. B., J. H. Richter, A. Park, S. J. Vavrus, P. J. Rasch, and M. Zhang, 2011: The mean atmospheric climate of the Community Atmosphere Model, version (CAM4) in forced SST and coupled experiments. *Journal of Climate*, to be submitted.

Pedlosky, J., 1996: *Ocean Circulation Theory*. Springer, Berlin, 453 pp.

Philip, S. and G. van Oldenborgh, 2006: Shifts in ENSO coupling processes under global warming. *Geophysical Research Letters*, **33**, L11 704.

Rajagopalan, B. and U. Lall, 1998: Interannual variability in western US precipitation. *Journal of Hydrology*, **210**, 51–67.

Rajagopalan, B., U. Lall, and M. A. Cane, 1997: Anomalous enso occurrences: An alternate view. *Journal of Climate*, **10**, 2351–2357.

Rayner, N., P.Brohan, D.E.Parker, C.F.Folland, J.J.Kennedy, M.Vanicek, T.Ansell, and S. Tett, 2006: Improved analyses of changes and uncertainties in sea surface temperature measured in situ since the mid-nineteenth century: the HadSST2 data set. *Journal of Climate*, **19 (3)**, 446–469.

Ropelewski, C. F. and M. S. Halpert, 1986: North American precipitation and temperature patterns associated with the El Niño/Southern Oscillation. *Monthly Weather Review*, **114**, 2352 2362.

Ropelewski, C. F. and M. S. Halpert, 1996: Quantifying Southern Oscillation-precipitation relationships. *Journal of Climate*, **9**, 1043 1059.

Saji, N. H., B. N. Goswami, P. N. Vinayachandran, and T. Yamagata, 1999: A dipole mode in the tropical Indian Ocean. *Nature*, **401**, 360–363.

Smith, T. and R. Reynolds, 2004: Improved extended reconstruction of sst (1854-1997). *Journal of Climate*, **17**, 2466–2477.

Stevenson, S., B. Fox-Kemper, M. Jochum, R. Neale, C. Deser, and G. Meehl, 2011a: Will there be a significant change to El Niño in the 21st century? *Journal of Climate*, in press: CCSM4 special issue. doi:10.1175/JCLI-D-11-00252.1.

Stevenson, S., B. Fox-Kemper, M. Jochum, B. Rajagopalan, and S. Yeager, 2010: Model ENSO Validation Using Wavelet Probability Analysis. *Journal of Climate*, **23**, 5540–5547.

Stevenson, S., H. V. McGregor, S. Phipps, and B. Fox-Kemper, 2011b: Quantifying the Limitations of Paleo-ENSO Model Validation. *Geophysical Research Letters*, in preparation.

Sun, D.-Z., 2003: A Possible Effect of an Increase in the Warm-Pool SST on the Magnitude of El Niño Warming. *Journal of Climate*, **16 (2)**, 185–205.

Sun, D.-Z. and T. Zhang, 2006: A regulatory effect of ENSO on the time-mean thermal stratification of the equatorial upper ocean. *Geophysical Research Letters*, **33**, L07 710, doi:10.1029/2005GL025296.

Taylor, K. E., R. J. Stouffer, and G. A. Meehl, 2011: The CMIP5 Experiment Design. *Bulletin of the American Meteorological Society*, submitted.

Timmermann, A., F.-F. Jin, and M. Collins, 2004: Intensification of the annual cycle in the tropical Pacific due to greenhouse warming. *Geophysical Research Letters*, **31**, L12 208.

Torrence, C. and G. Compo, 1998: A practical guide to wavelet analysis. *Bull. Amer. Meteor. Soc.*, **79**, 61–78.

Trenberth, K. and T. J. Hoar, 1996: The 1990-1995 El Niño-Southern Oscillation event: Longest on record. *Geophys. Res. Lett.*, submitted.

Trenberth, K. and J. W. Hurrell, 1994: Decadal atmosphere-ocean variations in the Pacific. *Clim. Dyn.*, **9**, 303–319.

Vecchi, G. and B. Soden, 2007: Global Warming and the Weakening of the Tropical Circulation. *Journal of Climate*, **20**, 4316–4340, doi:10.1175/JCLI4258.1.

Vimont, D. J., J. M. Wallace, and D. S. Battisti, 2003: The Seasonal Footprinting Mechanism in the Pacific: Implications for ENSO. *Journal of Climate*, 2668–2675.

Walker, G. and E. Bliss, 1932: World Weather V. *Mem. R. Meteorol. Soc.*, **4 (36)**, 53–84.

Walker, G. and E. Bliss, 1937: World Weather VI. *Mem. R. Meteorol. Soc.*, **4 (39)**, 119–139.

Whetton, P., D. Adamson, and M. Williams, 1990: Rainfall and river flow variability in Africa, Australia and east Asia linked to El Niño Southern Oscillation. *Geological Society of Australia Symposium Proceedings*, **1**, 71–82.

Wittenberg, A. T., 2009: Are historical records sufficient to constrain ENSO simulations? *Geophysical Research Letters*, **36**, L12 702.

Wolter, K., 1989: Modes of tropical circulation, Southern Oscillation, and Sahel rainfall anomalies. *Journal of Climate*, **8**, 149–172.

Xie, S.-P., 1996: Westward propagation of latitudinal asymmetry in a coupled oceanatmosphere model. *Journal of the Atmospheric Sciences*, **53**, 3236–3250.

Xie, S.-P. and S. Philander, 1994: A coupled ocean-atmosphere model of relevance to the ITCZ in the eastern Pacific. *Tellus*, **46A**, 340–350.

Yeager, S. G., C. A. Shields, W. G. Large, and J. J. Hack, 2006: The low-resolution CCSM3. *Journal of Climate*, **19**, 2545–2566.

Yeh, S.-W., J.-S. Kug, B. Dewitte, M.-H. Kwon, B. P. Kirtman, and F.-F. Jin, 2009: El Niño in a changing climate. *Nature*, **461**, 511–514, doi:10.1038/nature08316.

Yu, J.-Y. and H.-Y. Kao, 2007: Decadal changes of ENSO persistence barrier in SST and ocean heat content indices: 1958-2001. *Journal of Geophysical Research*, **112**, D13 106, doi:10.1029/2006JD007654.

Yu, L. and M. Rienecker, 1998: Evidence of an extratropical atmospheric influence during the onset of the 19978 El Niño. *Geophysical Research Letters*, **25**, 3537–3540.

Zebiak, S. E. and M. A. Cane, 1987: A model El Niño-Southern Oscillation. *Monthly Weather Review*, **115**, 2262–2278.

Appendix E

This appendix contains the text of [Stevenson 2012b], current as of November 22, 2011.

ENSO Characteristics in the CCSM4 21st Century Projections

Samantha Stevenson and Balaji Rajagopalan

1 Abstract

The influence of climate change on the statistics of El Niño and La Niña events is examined using the 20th and 21st century CMIP5 ensembles run with the NCAR Community Climate System Model version 4 (CCSM4). The effective ensemble size is increased using a combined Markov chain/generalized linear model (Markov GLM), which allows the creation of NINO3.4 time series having the same statistical properties as the CCSM4 ensembles. The Markov GLM performs extremely well in reproducing the 20th century NINO3.4 SST. correctly capturing El Niño/La Niña events, seasonal variances and event magnitude PDFs. Predictor variables required by the Markov GLM are chosen based on the structure of correlations with NINO3.4 SST in several climate variables, and the set of best predictors changes between ensembles. Wind stress and wind stress variance appear to become less important at higher CO_2, as does the seasonal cycle: this may be related to the overall weakening observed with CO_2 in the CCSM4. The overall statistics of El Niño and La Niña also change between ensembles, with La Niña events weakening at higher CO_2 and El Niño experiencing only minimal changes. The persistence of both warm and cold events decreases with CO_2, which leads to a longer return period for long ($geq5$ years in duration) El Niño and La Niñas. However, the 90% confidence intervals overlap for the 5-year event return periods, suggesting that any change in the mean return period will be imperceptible over the course of the 21st century.

2 Introduction

The El Niño/Southern Oscillation (ENSO) is a subject of intense study at the moment, due to its complexity and the variety of impacts it has on societies around the world (*Ropelewski and Halpert*, 1986). Of particular interest are ENSO-related drought and flooding events, which are felt acutely in Australia (*Nicholls*, 1992) and the Southwestern United States (*Cole and Cook*, 1998; *Cayan et al.*, 1999), among other places. The Southwestern US is particularly sensitive to ENSO activity, since streamflow is tightly linked to ENSO dynamics (*Dettinger et al.*, 2000; *Kiladis and Diaz*, 1989; *Cayan and Webb*, 1992). As the overall streamflow in the Colorado River Basin decreases due to anthropogenic climate change (*McCabe and Wolock*, 2007; *Ray*; *Seager et al.*, 2007), understanding ENSO behavior may therefore become more and more important in the future. However, the precise extent of the risk to the Southwestern US' water supply from climate change is not well known at the moment, and most likely will depend strongly on the management choices made in response to the changing climate (*Rajagopalan et al.*, 2009; *Barnett and Pierce*, 2008).

Given the large changes to climate expected in the next few decades, it is important to understand how those changes will impact the properties of El Niño and La Niña events. Although internal variability makes it extremely difficult to identify significant changes to the overall strength of ENSO (*Wittenberg*, 2009; *Stevenson et al.*, 2011b), the characteristics of individual events may change on much shorter timescales (*Fedorov et al.*, 2003; *Kao and Yu*, 2009). This becomes important when one considers the differences in Southwest US teleconnections between different types of events. Rainfall in the region is highly sensitive to the mean position of the jet stream, which leads to large event-to-event changes. Some of the observed variability may relate to coupling between ENSO and the Pacific Decadal Oscillation (PDO; *McCabe and Dettinger* (1999)), while some shifts in teleconnections are also expected due to climate change (*Meehl et al.*, 2007).

In this study, we week to understand changes to event statistics in a single model, the NCAR Community

Climate System Model version 4 (CCSM4; *Gent et al.* (2011)). Since the overall ENSO response in this model was previously shown to be insignificant on 50-100 year timescales (*Stevenson et al.*, 2011b), looking at event statistics illustrates the potential for changes to ENSO characteristics in the absence of a change in ENSO amplitude. Can one diagnose changes to El Niño persistence, for example, before the ENSO amplitude changes significantly?

Unfortunately, the small ensemble size used in the CMIP5 simulations (*Taylor et al.*, 2011) makes obtaining robust event statistics impossible. We therefore use a statistical model to increase the effective ensemble size while retaining the overall characteristics of the simulated time series. The particular model chosen for this analysis is a combined Markov chain/generalized linear model (GLM) (hereafter MGLM). Use of the MGLM approach allows one to predict the ENSO amplitude based both on covariates (*i.e.* wind stress and thermocline depth) and on the system state during previous seasons (*i.e.* to account for the increased probability of an El Niño or La Niña event persisting throughout the course of several months).

3 Modeling Framework

The model is based on the GLM framework used in the stochastic weather generator of *Kim et al.* (2009), where a GLM was used to predict the probability of precipitation occurring on a given day, and the distribution of precipitation then modeled with a gamma distribution. Here the Markov GLM is applied to input data from the CCSM4 CMIP5 simulations, and seasonally averaged to reduce month-to-month noise. Ensembles consist of the 20th century (6 simulations) and three of the so-called 'Representative Concentration Pathway', or RCP, 21st century projection ensembles (*Moss et al.*, 2010). The RCPs replace the previously-used IPCC scenarios, and correspond to various levels of top-of-atmosphere radiative forcing at 2100AD. Here, we make use of the RCP2.6, RCP4.5, and RCP8.5 ensembles, spanning the range of potential climate stabilization outcomes. The ensemble properties are summarized in Table 1.

The model framework here differs from *Kim et al.* (2009) in two respects:

1. The NINO3.4 SST is predicted directly from the GLM, rather than employing a two-step process where the system state is modeled independently from the value of the predictand.

2. The lagged system state is computed using a three-state Markov chain rather than a two-state: El Niño, La Niña, and neutral conditions are allowed. Here values of 1, -1 and 0 are assigned to the three states, respectively.

The mathematical description of the model is slightly different from that in *Kim et al.* (2009): as is standard in linear regressions, the NINO3.4 SST T_{N34} estimate has the form

$$T_{N34} = \mathbf{x^T}\beta \tag{1}$$

where β estimates are created for the system state variables *via* maximum-likelihood estimation. The independent variable matrix $\mathbf{x^T}$ is made up of time series for both continuous and categorical covariates: the continuous covariates are box-averaged time series of field variables (see Section 5) and two sinusoidal functions which simulate the seasonal cycle. The sinusoids are given by $sin(\frac{2\pi t}{4})$ and $cos(\frac{2\pi t}{4})$, respectively.

β values for the categorical system state variables are calculated using the logit function for a multinomial distribution. If there are N_j system state variables, then this leads to the following expression for the transition probabilities:

$$p = \frac{exp(\mathbf{x^T}\beta_\mathbf{j})}{1 + \sum_{j=1}^{N_j} \mathbf{x_j^T}\beta_\mathbf{j}} \tag{2}$$

The *glm* package in R was used to perform all fitting.

Table 1: Simulations used in this study. For the RCPs, the CO_2 value quoted is the approximate value at the end of the simulation period.

Simulation	Length (years)	Ensemble size	CO_2 (ppm)
20th century	156	6	350
RCP 2.6	95	5	450
RCP 4.5	95	5	550
RCP 8.5	95	1	1300

4 Event Statistics

Figure 1 summarizes the statistics of El Niño and La Niña events simulated from the CCSM4 20th century ensemble. To verify that the model correctly reproduces the gross properties of the input time series, we test the NINO3.4 time series (Figure 1a), seasonal variance (Figure 1b), and the PDF of both warm and cold events (Figure 1c,d). Overall simulation of individual events is quite good; with the exception of some extremely large events, the model is able to correctly reproduce the magnitude of the NINO3.4 anomaly extremely well. (Note that the full 20th century time series is not shown in Figure 1 due to space constraints). The simulation of seasonal variance is good as well: there is a slight underprediction of variance in the fall (season 4 in Figure 1b), but the CCSM4 input value is well within the simulated interquartile range.

The magnitudes of El Niño and La Niña events show a large degree of scatter in the simulated values. In Figure 1c,d the red line shows the ensemble-mean PDF for both, with the black boxes representing simulated values; the space between outliers is large compared with the probability values from the 20th century ensemble. Consistent with the time series results in Figure 1a, there seems to be increased error in representing very large El Niño and La Niña events. However, there is a tendency towards overestimation of the likelihood of large events; the red line in Figure 1c,d falls below the median of the simulated distributions for both El Niño and La Niña for anomalies larger than $\approx 2.5°C$. However, the overall performance is reasonable; we therefore have reasonable confidence in the results of simulated statistics for the RCP ensembles. A summary of the simulated RCP statistics is shown in Figure 2.

The magnitudes of El Niño and La Niña events are shown for the 21st century ensembles in the top row of Figure 2. Changes to the El Niño PDF are minimal even in the higher RCPs, as shown by the similarity of the 20th century (solid line) and 21st century (boxplot) distributions. There appears to be a tendency towards weaker El Niños, but the effect seems to be relatively small. La Niñas, in contrast, experience a more pronounced shift: the PDF narrows in the RCP ensembles relative to the 20th century, and the frequency of strong La Niñas decreases dramatically.

Persistence statistics are shown separately in Figure 2 for El Niño (panels d-f) and La Niña (panels g-i). For both phases, long (multi-year) events become less common at high CO_2, although the simulated values in Figure 2 show that the interquartile range brackets the 20th century PDF for the majority of event lengths. The exceptions are long ($\geq$ 7 season) El Niño events and short ($\leq$ 4 seasons) La Niña events in RCP4.5 and 8.5.

The question of event persistence is extremely important for resource management applications, including the aforementioned Southwestern US water management. This has led to a high degree of interest in multi-year El Niño and La Niña events (*Trenberth and Hoar*, 1996; *Rajagopalan et al.*, 1997). Here we revisit the question, calculating the return period of 5-year El Niño and La Niña events for all of the simulated time series. Calculations are performed using the transition probabilities determined from the simulated NINO3.4 index:

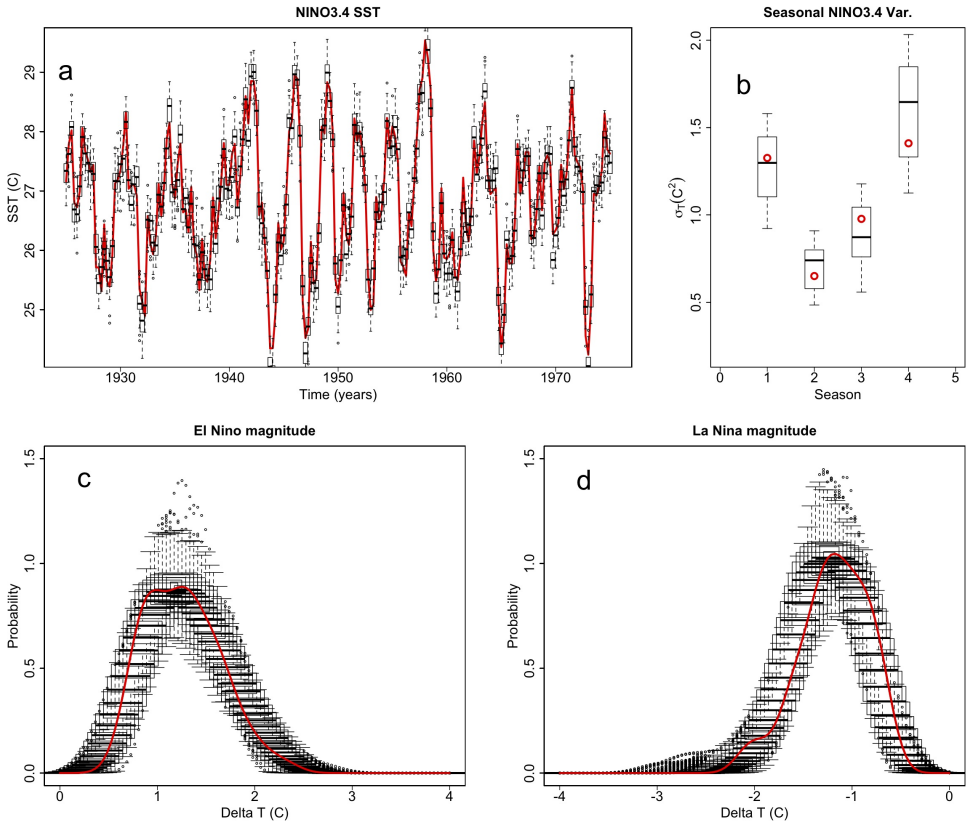

Figure 1: Model validation for the 20th century CCSM4 ensemble. a) NINO3.4 SST time series. b) Seasonal NINO3.4 variance. c) El Niño PDF. d) La Niña PDF. In all panels, the 20th century ensemble is shown as the red solid line (red circles in panel b), simulated values boxplotted in black.

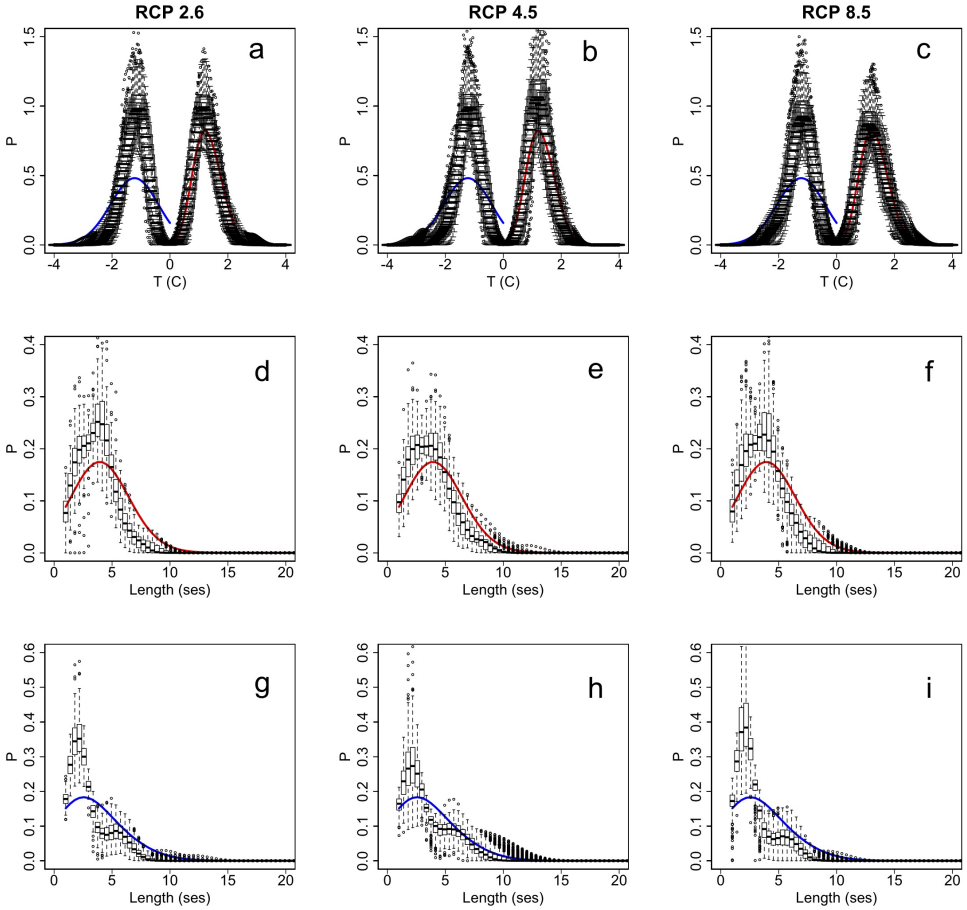

Figure 2: El Niño/La Niña statistics for the 21st century ensembles, simulated using the Markov GLM. Solid lines indicate the PDF for the 20th century, with red and blue indicating El Niño and La Niña, respectively. Event magnitudes appear in panels a-c; El Niño persistence in d-f; and La Niña persistence in g-i.

$$R_{5yr} = p^{-N} \tag{3}$$

where p represents the (El Niño - El Niño) or (La Niña - La Niña) transition probability and N = (4 seasons/year) x (5 years) = 20. The results are shown in Table 2: the 90% confidence intervals for 5-year return periods overlap between all ensembles.

Table 2: Return periods for 5-year El Niño and La Niña events.

Ensemble	10%, EN	Median, EN	90%, EN	10%, LN	Median, LN	90%, LN
20th c.	1,078	3,325	41,337	3,905	7,718	17,388
RCP 4.5	6,041	20,872	104,388	827	5,449	21,938
RCP 8.5	9,504	34,872	155,864	12,870	55,475	342,005

5 Best ENSO Predictors

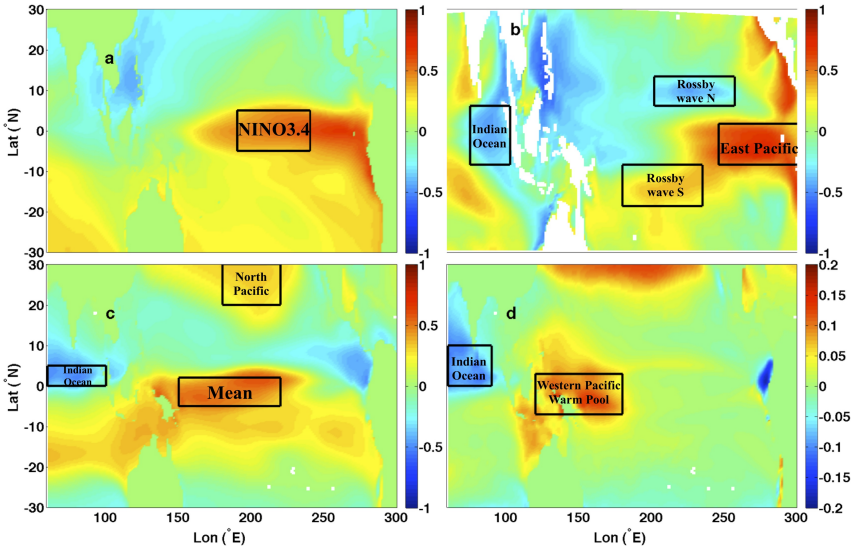

Figure 3: Lag-correlation maps with NINO3.4 SST, lag 3 months. a) SST, b) thermocline depth, c) zonal wind stress, d) submonthly zonal wind stress variance. Note that panel d uses a different color scale from panels a-c, for clarity. Black boxes indicate the positions of the averaging regions used to generate the Markov GLM predictors, which are labeled according to the naming conventions in Table 3. Note that panel d uses a different color scale than panels a-c, owing to the much smaller correlations with wind stress variance.

The next question is whether the most important ENSO covariates change with CO_2. As noted in Section 3, the lagged system state and lagged NINO3.4 SST are included in the model (Table 3). Also included are

box-averaged values for SST, thermocline depth, zonal wind stress and zonal wind stress variance at zero lag. The averaging regions for predictors are chosen to maximize the correlation of the time series with NINO3.4 SST, which is shown in Figure 3. This allows for the inclusion of both surface-driven and subsurface-driven dynamics in the model; both are thought to be active in the real world, and their relative importance may change under global warming (*Fedorov and Philander*, 2000; *Guilyardi*, 2006).

In thermocline depth, averages are taken over: the Indian Ocean, the eastern Pacific, and the 'Rossby wave North' and 'Rossby wave South' regions (Table 3). The eastern Pacific, of course, is one of the primary regions active in ENSO variability (*Zebiak and Cane*, 1987). The Rossby wave pathway regions are chosen as their names imply: previous studies (*Vimont et al.*, 2003; *Alexander et al.*, 2002, 2010) have shown the importance of these locations for seasonally driven Rossby waves. In the CCSM3.5, *Stevenson et al.* (2011a) showed that these pathways indeed play an active role in the generation of El Niño/La Niña events.

The zonal wind stress predictors chosen are averaged over the central equatorial Pacific, over the Indian Ocean and over the north central Pacific. The Indian Ocean shows a strong negative correlation between zonal wind stress and NINO3.4 SST (Figure 3c): this is consistent with the eastward (westward) movement of the convective center in the western Pacific warm pool during El Niño (La Niña). In the central equatorial Pacific, the high correlation is created by the *Bjerknes* (1969) feedback, where weaker trade winds are associated with slackening zonal SST gradients and therefore the development of El NIño events. Finally, the connection with wind stress in the subtropical central Pacific is important since this is what sets the Sverdrup transport in/out of the tropics. Changes in mean Sverdrup transport, in turn, lead to shifts in mean ocean heat content which drive the 'recharge oscillator'-type ENSO (*Jin*, 1997).

Table 3: Set of best predictors for the CCSM4 ensembles. Numbers indicate the value of regression coefficients for each ensemble/variable combination.

Predictor	20th c.	RCP 4.5	RCP 8.5
Lag-1 state	-0.119	-0.133	-0.117
Lag-2 state	0.587	0.588	0.527
Lag-3 state	-0.227	-0.256	-0.165
Lag-1 value	0.114	0.149	0.108
RW path Z (N)	-8.99×10^{-5}	-1.03×10^{-4}	-6.58×10^{-5}
RW path Z (S)	9.24×10^{-5}	1.48×10^{-4}	4.83×10^{-5}
Ind. Ocn. Z	1.12×10^{-4}	4.84×10^{-5}	2.86×10^{-4}
E. Pac. Z	2.06×10^{4}	6.59×10^{-5}	3.49×10^{-4}
Mean Taux	3.90	4.96	3.34
Ind. Ocn. Taux	-0.208	-0.899	
N. Pac. Taux	0.0826		
WPWP Taux var.	-1.86	-1.55	-1.37
Ind. Ocn. Taux var	-0.325	-0.496	
Sin	1.270e-01	0.105	
Cos	-1.532e-01	-0.0706	-0.0817

After the predictors were input into the model, the 'best' predictor set for each CCSM4 ensemble was chosen according to a stepwise regression which minimizes the BIC criterion (*Sakamoto et al.*, 1986). The model was initialized with NINO3.4 values and system states for the past 4 seasons, but the value of NINO3.4 does not appear in the best predictor set for any ensemble at lags greater than 1. The system state is more important, being retained for the previous 3 seasons. The complete set of best predictors for all ensembles is shown in Table 3.

The set of predictors which minimize BIC does not generally differ greatly between ensembles, although there does appear to be some tendency towards wind stress becoming less important with higher CO_2 (based on the absence of the Indian Ocean and North Pacific τ_x in RCP 4.5 and 8.5). RCP 8.5 is particularly striking, as the mean zonal wind stress and the warm pool variance are the only wind predictors appearing in the best-fit variable set. The off-equatorial wind appears only for the 20th century; the decreased importance of the subtropical wind stress may reflect a shift away from 'remotely influenced' ENSO dynamics. Another possibility is that anomalies in wind stress variance become less effective at triggering El Niño events as CO_2 increases. This has been examined in the CCSM3.5 and CCSM4 (*Stevenson et al.*, 2011a), and the high-frequency component of wind variance does seem to decrease with CO_2.

The decreased importance of wind stress and wind stress variance in the western Pacific and Indian Oceans may possibly relate to the position of the Walker cell. Convection migrates eastward with CO_2 as the mean equatorial trades weaken (*Stevenson et al.*, 2011b), which is a robust feature of IPCC-class models (*Collins et al.*, 2010). The dynamical connection between these factors, however, remains unclear and is a subject more properly left for future investigations.

Some conclusions may be drawn from the magnitudes of the regression coefficients in Table 3: for example, the seasonal cycle becomes less important in determining El Niño/La Niña magnitude with CO_2. This is consistent with the overall weakening of the SST seasonal cycle identified by *Stevenson et al.* (2011b), which has been previously linked to the amplitude of El Niño events (*Timmermann et al.*, 2004). If a mechanism related to seasonally forced Rossby waves is a dominant factor in model ENSO dynamics (*i.e. Stevenson et al.* (2011a)), then this would explain the weaker regression slope in the RCP ensembles. However, the thermocline depth regression coefficients themselves do not change monotonically with CO_2, suggesting that the situation may be more complex.

6 Summary and Conclusions

This work has both documented the changes to ENSO event statistics under climate change in the CCSM4, and demonstrated the use of the combined Markov chain/generalized linear model as a simulation technique for increasing effective ensemble size. Validation results for the 20th century simulations from the CCSM4 show that the model performs well at simulating the NINO3.4 time series, in terms of both event simulation and replication of the seasonal variance. The overall PDF of El Niño and La Niña events is likewise reproduced relatively well.

The sets of best predictors using the Markov GLM are remarkably similar between ensembles. The value of NINO3.4 SST does not appear to be important as a predictor at lags greater than 1 season, although the state of the system (El Niño/neutral/La Niña) does remain important for up to three seasons. The wind stress and its variance appear in the set of best predictors for the 20th century, but become progressively less important as CO_2 increases. Some of this may be related to the eastward migration of the Pacific Walker circulation; some may relate to changes in coupling with the Indian Ocean. Likewise, the seasonal cycle becomes less important as a predictor at high CO_2, and is known to weaken in the RCP ensembles (*Stevenson et al.*, 2011b). This may become important for seasonally forced wave propagation.

ENSO event magnitudes show a greater change during the La Niña phase; strong La Niña events become much less common at high CO_2. The magnitudes of El Niño events show a PDF which remains more or less stable with CO_2. However, the persistence of both warm and cold events drops off dramatically in the RCP ensembles; this is likely responsible for much of the weakening of ENSO amplitude seen in previous work on these ensembles.

The implications of this work for changes in the return period of 5-year events are somewhat unclear. The return period increases with CO_2, but large internal variability leads to a 90% confidence interval on the return period which is indistinguishable between ensembles. We conclude that long El Niño/La Niña

events should indeed become more rare as CO_2 increases, but that it will be nearly impossible to distinguish the changes based on observing ENSO evolution during the 21st century.

References

Alexander, M. A., I. Bladé, M. Newman, J. R. Lanzante, N.-C. Lau, and J. D. Scott, The atmospheric bridge: The influence of ENSO teleconnections on air sea interaction over the global oceans, *Journal of Climate*, *15*, 2205–2231, 2002.

Alexander, M. A., D. J. Vimont, P. Chang, and J. D. Scott, The Impact of Extratropical Atmospheric Variability on ENSO: Testing the Seasonal Footprinting Mechanism Using Coupled Model Experiments, *Journal of Climate*, *23*, 2885–2901, 2010.

Barnett, T. P., and D. W. Pierce, Sustainable water deliveries from the Colorado River in a changing climate, *Proceedings of the National Academy of Sciences*, *106*, 73347338, doi:10.1073/pnas.0812762106, 2008.

Bjerknes, J., Atmospheric teleconnections from the equatorial Pacific, *Monthly Weather Review*, *97*, 163–72, 1969.

Cayan, D. R., and R. H. Webb, El Niño-Southern Oscillation and streamflow in the western United States, in *El Niño: Historical and Paleoclimatic Aspects of the Southern Oscillation*, edited by H. F. Diaz and V. Markgraf, pp. 29–68, Cambridge University Press, 1992.

Cayan, D. R., K. T. Redmond, and L. G. Riddle, ENSO and Hydrologic Extremes in the Western United States, *Journal of Climate*, *12*, 2881–2893, 1999.

Cole, J. E., and E. Cook, The changing relationship between ENSO variability and moisture balance in the continental United States, *Geophysical Research Letters*, *25*, 4529–4532, 1998.

Collins, M., S.-I. An, W. Cai, A. Ganachaud, E. Guilyardi, F.-F. Jin, M. Jochum, M. Lengaigne, S. Power, A. Timmermann, G. Vecchi, and A. Wittenberg, The impact of global warming on the tropical Pacific Ocean and El Niño, *Nature Geoscience*, *3*, 391–397, doi:10.1038/NGEO868, 2010.

Dettinger, M. D., D. R. Cayan, G. J. McCabe, and J. M. Marengo, Multiscale streamflow variability associated with El Niño/Southern Oscillation, in *El Niño and the Southern Oscillation: Multiscale Variability and Global and Regional Impacts*, edited by H. F. Diaz and V. Markgraf, pp. 113–147, Cambridge University Press, 2000.

Fedorov, A. V., and S. G. Philander, Is El Niño changing?, *Science*, *288*, 1997–2002, 2000.

Fedorov, A. V., S. L. Harper, S. G. Philander, B. Winter, and A. Wittenberg, How predictable is El Niño?, *Bulletin of the American Meteorological Society*, pp. 911–919, doi:10.1175/CAMS-84-7-911, 2003.

Gent, P. R., G. Danabasoglu, L. J. Donner, M. M. Holland, E. C. Hunke, S. R. Jayne, D. M. Lawrence, R. B. Neale, P. J. Rasch, M. Vertenstein, P. H. Worley, Z. L. Yang, and M. Zhang, The Community Climate System Model version 4 , *Journal of Climate*, submitted, 2011.

Guilyardi, E., El Niño-mean state-seasonal cycle interactions in a multi-model ensemble, *Climate Dynamics*, *26*, 329–348, 2006.

Jin, F.-F., A theory of interdecadal climate variability of the North Pacific Ocean-Atmosphere system, *Journal of Climate*, *10*, 1821–1835, 1997.

Kao, H.-Y., and J.-Y. Yu, Contrasting Eastern-Pacific and Central-Pacific Types of ENSO, *Journal of Climate*, *22*, 615–632, doi:10.1175:/2008JCLI2309.1, 2009.

Kiladis, G. N., and H. F. Diaz, Global climatic anomalies associated with extremes in the southern oscillation, *Journal of Climate*, *2*, 1069–1090, 1989.

Kim, Y., R. W. Katz, B. Rajagopalan, and G. P. Podesta, Reduced overdispersion in stochastic weather generators for statistical downscaling of seasonal forecasts and climate change scenarios, *Journal of Climate*, under review, 2009.

McCabe, G. J., and M. D. Dettinger, Decadal variations in the strength of ENSO teleconnections with precipitation in the western United States, *International Journal of Climatology*, *19*, 8847–8850, 1999.

McCabe, G. J., and D. M. Wolock, Warming may create substantial water supply shortages in the Colorado River basin, *Geophysical Research Letters*, *34*, L22,708, doi:10.1029/2007GL031764, 2007.

Meehl, G. A., C. Tebaldi, H. Teng, and T. C. Peterson, Current and future U.S. weather extremes and El Niño, *Geophysical Research Letters*, *34*, L20,704, doi:10.1029/2007GL031027, 2007.

Moss, R., J. Edmonds, K. Hibbard, M. Manning, S. Rose, D. van Vuuren, T. Carter, S. Emori, M. Kainuma, T. Kram, G. Meehl, J. Mitchell, N. Nakicenovic, K. Riahi, S. Smith, R. Stouffer, A. Thomson, J. Weyant, and T. Wilbanks, The next generation of scenarios for climate change research and assessment, *Nature*, pp. 747–756, Perspectives, 2010.

Nicholls, N., Historical El Niño-Southern Oscillation variability in the Australasian region, in *El Niño: Historical and Paleoclimatic Aspects of the Southern Oscillation*, edited by H. F. Diaz and V. Markgraf, pp. 151–173, Cambridge University Press, 1992.

Rajagopalan, B., U. Lall, and M. A. Cane, Anomalous enso occurrences: An alternate view, *Journal of Climate*, *10*, 2351–2357, 1997.

Rajagopalan, B., K. Nowak, J. Prairie, M. Hoerling, B. Harding, J. Barsugli, A. Ray, and B. Udall, Water supply risk on the Colorado River: Can management mitigate?, *Water Resources Research*, *45*, W08,201, doi:10.1029/2008WR007652, 2009.

Ray, A. J. e. a., *Climate Change in Colorado; A Synthesis to Support Water Resources Management and Adaptation*, Western Water Assessment, Boulder, CO.

Ropelewski, C. F., and M. S. Halpert, North American precipitation and temperature patterns associated with the El Niño/Southern Oscillation, *Monthly Weather Review*, *114*, 2352 2362, 1986.

Sakamoto, Y., M. Ishiguro, and G. Kitagawa, *Akaike Information Criterion Statistics.*, D. Reidel Publishing Company, 1986.

Seager, R., M. Ting, I. Held, Y. Kushnir, J. Lu, G. Vecchi, H.-P. Huang, N. Harnik, A. Leetmaa, N.-C. Lau, C. Li, J. Velez, and N. Naik, Model projections of an imminent transition to a more arid climate in southwestern North America, *Science*, *316*, 1181–1184, doi:10.1126/science.1139601, 2007.

Stevenson, S., B. Fox-Kemper, and M. Jochum, Understanding the ENSO-CO_2 Link Using Stabilized Climate Simulations , *Journal of Climate*, submitted, 2011a.

Stevenson, S., B. Fox-Kemper, M. Jochum, R. Neale, C. Deser, and G. Meehl, Will there be a significant change to El Niño in the 21st century?, *Journal of Climate*, in press: CCSM4 special issue. doi:10.1175/JCLI-D-11-00252.1, 2011b.

Taylor, K. E., R. J. Stouffer, and G. A. Meehl, The CMIP5 Experiment Design, *Bulletin of the American Meteorological Society*, submitted, 2011.

Timmermann, A., F.-F. Jin, and M. Collins, Intensification of the annual cycle in the tropical Pacific due to greenhouse warming, *Geophysical Research Letters*, *31*, L12,208, 2004.

Trenberth, K., and T. J. Hoar, The 1990-1995 El Niño-Southern Oscillation event: Longest on record, *Geophys. Res. Lett.*, submitted, 1996.

Vimont, D. J., J. M. Wallace, and D. S. Battisti, The Seasonal Footprinting Mechanism in the Pacific: Implications for ENSO, *Journal of Climate*, pp. 2668–2675, 2003.

Wittenberg, A. T., Are historical records sufficient to constrain ENSO simulations?, *Geophysical Research Letters*, *36*, L12,702, 2009.

Zebiak, S. E., and M. A. Cane, A model El Niño-Southern Oscillation, *Monthly Weather Review*, *115*, 2262–2278, 1987.

Appendix F

This appendix contains the text of [Stevenson 2012a], current as of November 22, 2011.

Decarbonization Assumptions in the IPCC AR5

Samantha Stevenson

Department of Atmospheric and Oceanic Sciences, University of Colorado/CIRES, Boulder, CO

US

and Roger Pielke, Jr.

Center for Science and Technology Policy Research, University of Colorado/CIRES, Boulder,

Colorado, USA

Abstract

Projections of future climate change depend upon scenarios of future anthropogenic greenhouse gas emissions. In preparation for its Fifth Assessment Report, the Intergovernmental Panel on Climate Change developed a new approach to the generation of emissions scenarios, called 'Representative Concentration Pathways' (RCPs). The RCPs were designed to provide a range of emissions outcomes consistent with a particular radiative imbalance. However for the 'baseline' simulations used to generate the RCPs, the older scenario methodologies were often used as a starting point, meaning that 'built in' to the RCPs are some of the same implicit assumptions found in earlier emissions scenarios. Although energy intensity has dropped dramatically over 2006-2010, the RCPs' predicted decreases in carbon intensity surpass the SRES scenarios for near-term and long-term projections alike. Addressing the carbon emissions challenge may thus require more aggressive policy action than is currently being projected by the IPCC.

1. Introduction

The Intergovernmental Panel on Climate Change (IPCC) assesses the science, impacts and mitigation of climate change in periodic "Assessment Reports," the most recent of which is the Fourth Assessment Report, or AR4 (Pachauri and Reisinger, 2007). The results put out by the IPCC are unique in that they are formally approved by participating governments, and thus have an authoritative status in international policymaking. A central element of the IPCC is the construction of emissions scenarios for projections of future climate changes and associated impacts: these scenarios are then used for the evaluation of various mitigation alternatives. The generation of such scenarios requires modeling the behavior of social, economic, technological and political systems (Fisher et al., 2007; Schneider, 2001).

Until recently, the state of the art in emissions scenarios was the set of projections described in the 2000 'Special Report on Emissions Scenarios', or SRES (Nakicenovic, 2000). The SRES were designed to represent a very broad range of possible future emission paths, taking into account changes in land use, energy consumption and production, and a number of other factors. SRES scenarios were used in the Third and Fourth IPCC Assessment Reports, and these scenarios currently inform most climate projections found in the scientific literature.

The IPCC has altered their approach to scenario construction for the Fifth Assessment Report (AR5; Moss et al. (2010)). Instead of working 'forward' from economic, social, and

technological assumptions to generate scenarios, a 'backward' approach is used: radiative forcing is specified, then scenarios consistent with that forcing profile are created. This allows multiple sets of policy assumptions to be put forward, and in principle should lead to greater flexibility in the construction of scenarios for future emissions. However, in practice we find that significant technological advances are built into the baseline RCP plans, just as was the case for the SRES scenarios. This review discusses the spontaneous technological advance – and commensurate decarbonization – built into the RCPs.

2. Scenario/Pathway Development

2.1 SRES

The AR4 SRES scenarios are divided into four major groups, hereafter referred to as 'families', which differ in their philosophies regarding the future rates of population and economic growth, as well as in their energy usage predictions. The SRES families are referred to by a letter and a number designation, and are summarized in Table 1. Within each family, subgroupings of scenarios were constructed based on differing assumptions (e.g. use of fossil fuels vs. nuclear energy, etc.) in order to span as wide a range of expected futures as possible. After the scenarios were completed, the associated inputs (land use changes, aerosol and GHG emissions, etc.) were used as input forcings for a variety of coupled climate models, to yield climate projections through the 21st century.

Family	Economic Growth	Population Growth	Technological Development
A1	rapid	peaks in mid-century, then declines	rapid introduction of new, efficient technologies
A2	fragmented, slow	continuous slow increase	
B1	transition to service/ information economy	same as A1	clean, resource-driven
B2	intermediate	continuous increase (slower than A2)	diverse, slower development

Table 1: SRES families and associated patterns of economic, population, and technological growth.

The SRES B families are generally known as being 'optimistic' estimates of future growth (Nakicenovic, 2000). In contrast, the A families, particularly A1, are typically used in the literature as examples of 'business as usual' growth (e.g., Schneider (2001); Stroeve et al. (2007)). However, the past 10 years have surpassed the A1B scenarios in greenhouse gas emissions. Demographic trends appear relatively well represented in the SRES (van Vuuren and O'Neill, 2006), which indicates that the SRES underestimates have a different source: energy use and associated carbon emissions are constant or increasing in both the developed and developing world (Raupach et al., 2007). Generally speaking, the more aggressive climate stabilization pathways (RCPs 2.6 and 4.5) are most similar to the SRES B families, and the less stringent pathways (RCPs 6.0 and 8.5) more closely resemble SRES A groups (Section 2.2).

2.2 RCP Development

The RCPs specify a radiative imbalance at which the atmosphere will stabilize, and use that information to determine social, technological and economic factors consistent with that imbalance. The RCPs are designed to provide 'two-way' communication between physical scientists and decision-oriented researchers; in particular, the impacts, assessment and vulnerability (IAV) and integrated assessment and modeling (IAM) communities. In the words of Moss et al. (2008), "...this parallel approach should provide better integration, consistency, and consideration of feedbacks, and more time to assess impacts and responses".

Figure 1 provides an overview of the use of the RCPs in the IPCC AR5 analysis. First, the climate modeling community takes the specified radiative forcing in the RCP baseline simulations to generate profiles of expected changes to the climate system over the appropriate time horizon. Next, the IAM community uses a variety of policy, economic and other assumptions to generate a suite of new scenarios based around each RCP. These scenarios may then be used by the IAV researchers to find the best policy options on local and regional scales.

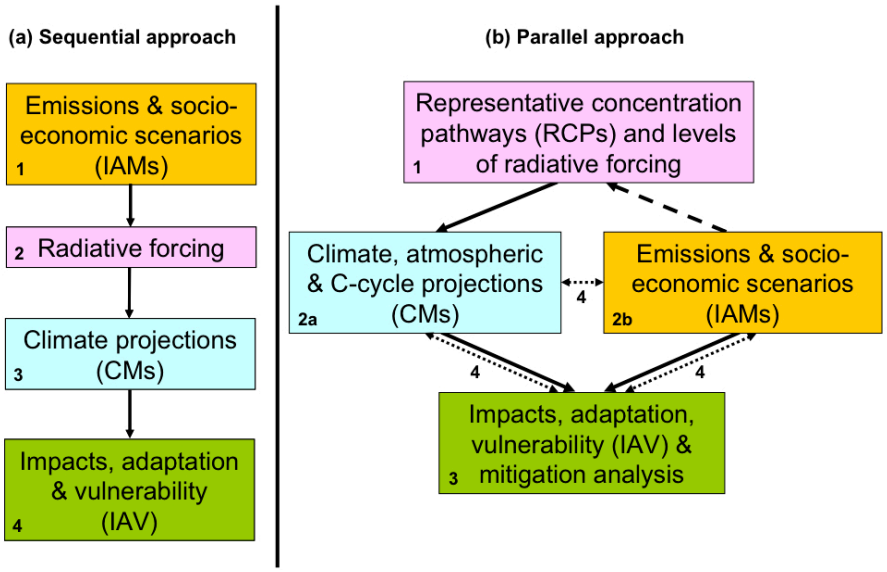

Figure 1: Figure 1 from Moss et !al. (2008), showing a schematic of (a) 'sequential' (linear) and (b) 'parallel' scenario development processes.

Moss et al. (2008) discuss four primary RCP candidates, constructed with four different integrated assessment models, which were selected from the peer-reviewed literature to span a range of potential climate outcomes. The RCPs were each tested with multiple models to ensure replicability (Weyant et al. 2009) The models' general approach is to use representations of the economy, climate policies, and the agricultural sector combined with a simplified climate system model to yield an optimal emissions pathway to achieve the desired stabilization level. Each pathway is designated by the level of radiation above the present value which will be absorbed by the atmosphere at steady state: pathways are summarized in Table 2.

Table 2: RCPs recommended for use in AR5. Modeling groups are: the Asia-Pacific Integrated Model (AIM), the Model for Energy Supply Strategy Alternatives and their General Environmental Impact (MESSAGE), the Mini-Climate Assessment Model (MiniCAM), and the Integrated Model to Assess the Global Environment (IMAGE).

Name	Forcing (W/m^2)	CO_2 level	Modeling group	Country/region
RCP8.5	8.5	≥1370	MESSAGE	Austria
RCP6	6.0	850	AIM	Japan
RCP4.5	4.5	650	MiniCAM	USA
RCP2.6	3.0	490	IMAGE	Netherlands

• RCP2.6: IMAGE

RCP2.6 (van Vuuren et al., 2007; Van Vuuren et al., 2006) is the most stringent pathway. The baseline emissions used in RCP2.6 were specified using the SRES B2 scenarios (Weyant et al., 2009), as envisioned for integrated model applications by van Vuuren et al. (2007) who modified the demographic assumptions to better fit the observed trends from 2000-2010. The input baseline emissions are used by the climate policy model to derive an emissions pathway leading to climate stabilization (van Vuuren et al., 2007; Weyant et al., 2009).

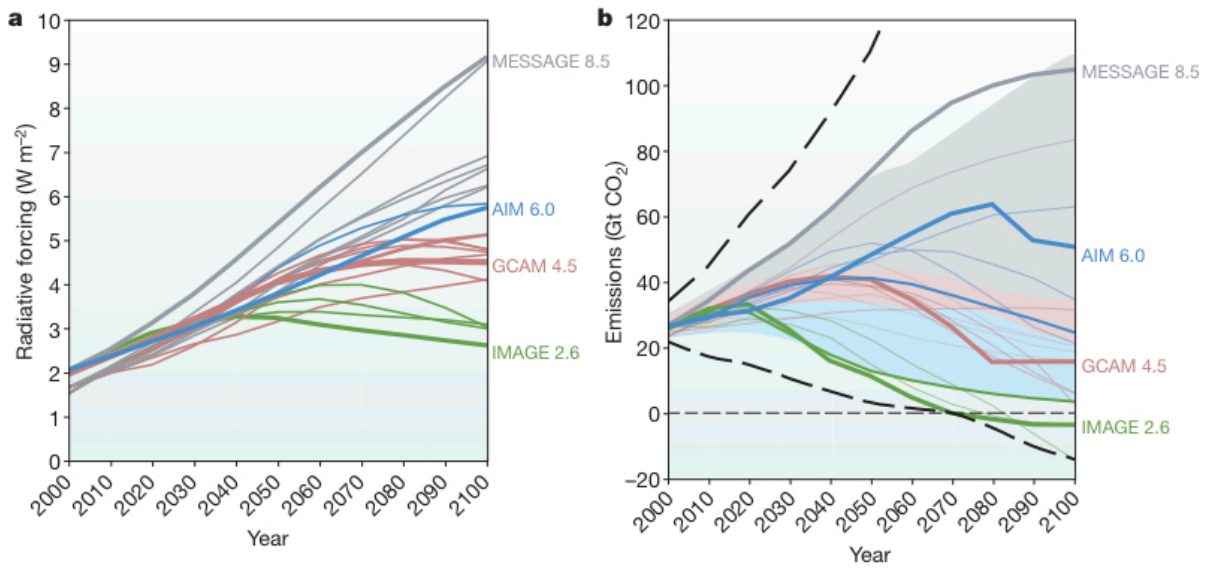

Figure 2: Figure 5 from Moss et al. (2010). MESSAGE is shown in gray, AIM in blue, GCAM/ MiniCAM in pink and IMAGE in green. (a) Radiative forcing, W/m^2. (b) CO_2 emissions in gigatons. Bold curves indicate the RCP baseline simulations: replicates are shown as thin lines.

Heavy emissions cuts are required by RCP2.6; as seen in Figure 2b (green curve), the pathway actually requires negative emissions by 2100. Emissions cuts are applied optimally across 17 world regions, with non-CO_2 gases priced according to their global warming potentials. Notably, even with such steep cuts the RCP2.6 pathway still overshoots the target before declining to the correct forcing level, with peak radiative forcing near 2020.

• RCP4.5: GCAM

RCP4.5 is an intermediate emissions pathway, derived based on simulations with the GCAM (previously MiniCAM) model. Global emissions peak later in RCP4.5 than in RCP2.6, with a maximum near 2040 (Figure 2, pink lines).

The RCP4.5 pathway is derived from the 'Level 3' stabilization scenario of Clarke et al. (2007), developed independently by the MiniCAM group. Population projections came from the UN database, and future energy use is predicted to shift gradually from fossil fuels to renewables. Although the reference scenario for RCP4.5 is not derived directly from SRES, technological improvements yield similar rates of efficiency improvement: each dollar of 2100 US GDP is produced with 25% as much energy as the equivalent in 2000 dollars (Clarke et al., 2007). Also interesting is that the stabilization goals targeted by RCP4.5 were achieved in the model by adopting so-called 'idealized emissions reduction methods', which assume that reductions take place wherever and whenever possible, using the most cost-effective GHG available (Clarke et al., 2007).

• RCP6.0: AIM

RCP6.0 is the second intermediate emissions pathway. Like RCP4.5, RCP6.0 is a 'stabilization without overshoot' situation, which eventually stabilizes at a concentration of about 850ppm CO_2. The model used to develop this pathway is AIM, which models the economy based on its division into 13 economic sectors. The AIM team developed their scenarios independently (Fujino et al., 2006), using energy statistics from the International Energy Association.

• RCP8.5: MESSAGE

RCP8.5 is the highest forcing pathway, with emissions continuing to trend upwards past 2100. The development of RCP8.5 (Rao and Riahi, 2006; Riahi et al., 2007) used baseline emission scenarios derived from the SRES A2 family. Riahi et al. (2007) describes revisions to the A2 used in RCP8.5: population estimates were revised downwards for better agreement with UN projections, and slow economic growth assumed to delay the spread of energy-efficient technologies. Most fuel-use assumptions are carried over from the A2, and used as input to the agriculture, forest and energy models.

3. Decarbonization of Economic Activity Via Reductions in Carbon and Energy Intensities

The widespread adoption of less carbon-intensive energy technologies is fundamental to all stabilization scenarios that have positive rates of economic growth (Hibbard et al., 2007; Hoffert et al., 1998, 2002). In the literature this is referred to as the decarbonization of the economy: the rate at which the carbon emission per unit of gross domestic product decreases with time. The decarbonization rate is the product of two quantities from the Kaya Identity (the other two are per capita wealth and population): carbon intensity (CI) and energy intensity (EI) as a function of time. CI is a measure of the carbon emission required per unit of energy generated, while EI measures the amount of energy required to produce a unit of GDP. Reductions in both CI and EI will be required to achieve the necessary levels of decarbonization described in all four RCPs.

Estimates of carbon intensity were made by Nakicenovic et al. (1996) as part of the AR4; those authors found that historically, CI had decreased by about 0.3%/year. This, however, appears to be substantially slower than the projected decreases in the Third and Fourth IPCC assessment reports, which are closer to 0.6-0.9%/year (Green and Lightfoot, 2002). The upper limit on EI decline was calculated by Lightfoot and Green (2001), who found that theoretically a 1.1% decline would be achievable over the 21st century.

Pielke et al. (2008) look into the projected decarbonization rates generated from AR4 data. Using a 'frozen technology' baseline simulation, they show that the decarbonization in the AR4 simulations relies on 'automatic' efficiency improvements which are inconsistent with advances in energy efficiency to date. In fact, those built-in improvements account for the vast majority of CO_2 emissions reductions to 2100 (see Figure 3). Are the same assumptions built into AR5? This is a bit more difficult to evaluate in the RCPs than the SRES scenarios, since the RCPs were designed to provide a degree of autonomy between the emissions and climate warming projections for AR5.

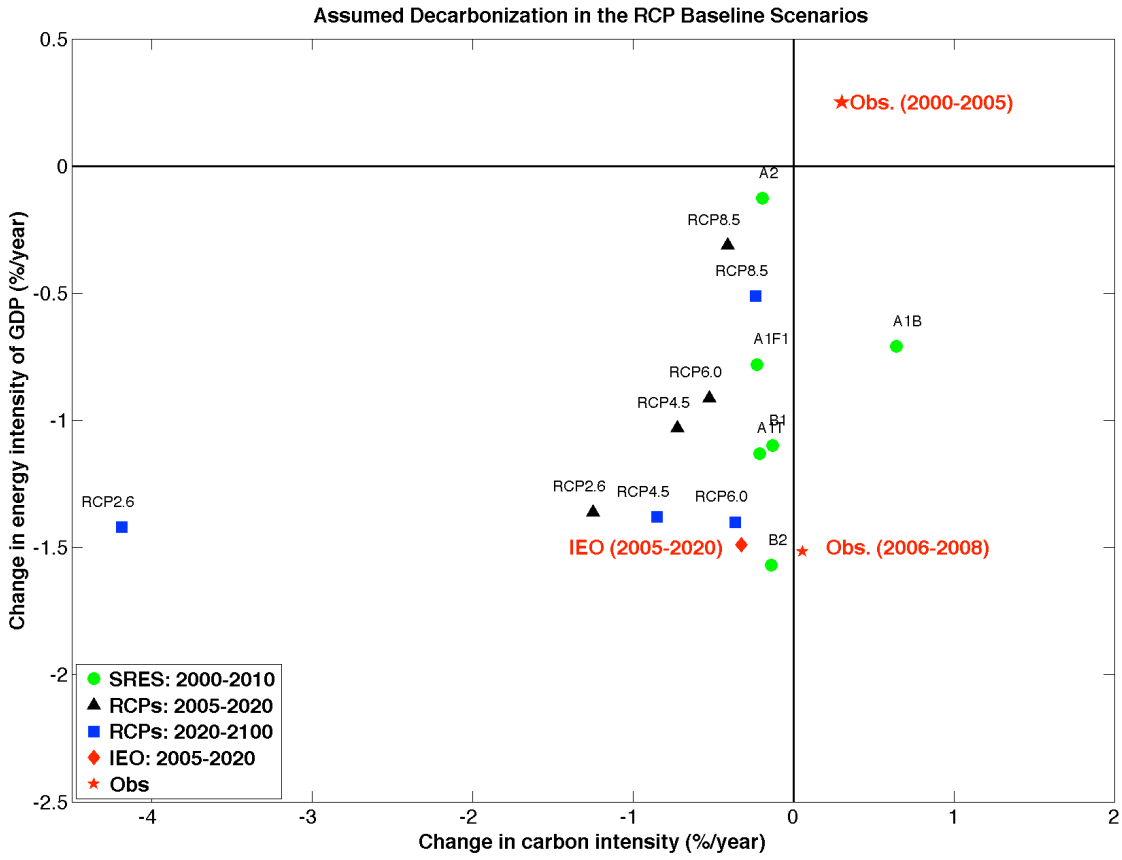

Figure 3: Rates of technological decarbonization in the IPCC SRES scenarios as compared with the observed rate. This figure is modeled after Figure 2 from Pielke et al. (2008).

A ballpark estimate of the required CI and EI reductions can be made using the baseline simulations for the RCPs. Scenarios consistent with the appropriate radiative forcing targets may be expected to have comparable CI and EI values. We have obtained data for the IIASA A2r simulation[1], which is the simulation upon which the RCP8.5 was based. For RCP4.5, we have

[1] http://www.iiasa.ac.at/web-apps/ggi/GgiDb/

used the GCAM baseline scenario from which the RCP was derived[2]. At the time of this writing, online data for RCP2.6 and 6.0 is not available. As a best estimate, we therefore use data taken from the GCAM 'replicates' of the RCP2.6 and 6.0 baseline scenarios.

Changes in carbon and energy intensities are calculated over the periods 2000-2010 and 2010-2100 for the SRES. The former (green circles in Figure 3) is intended to provide a direct comparison to observations, and is analogous to the calculation in Pielke Jr. et al. (2008). Calculations for the RCPs cover 2005-2020 (black triangles) and 2020-2100 (blue squares), to give a sense of the sustained improvements which will be required over the course of the 21st century to achieve stabilization targets. Comparison of the SRES and RCP results leads immediately to the conclusion that required improvements in the baseline scenarios are at least as ambitious as their predecessors. RCP2.6 in particular requires aggressive reductions in carbon intensity out to 2100, up to 7-8x larger than the other scenarios.

The logical counter-argument to the analysis in Figure 3 is that the construction of the RCPs does not assume a particular evolution of GDP, and thus the decarbonization rate might change with the use of a different scenario consistent with that radiative forcing pathway. Socioeconomic conditions could align in multiple ways to produce the same emissions trajectory. However, very high decarbonization rates will still be required to meet the goals of all four RCPs. As a comparison with the RCP baseline scenarios, we use the GDP, CO_2 emissions, and energy consumption projections for 2010-2030 from the U.S. Energy Information

---

[2] http://www.globalchange.umd.edu/gcamrcp/

Administration's International Energy Outlook for 2011 (Energy Information Administration, 2011). These numbers (the 'IEO Reference case'[3]) are derived independently from the RCP calculations, using the EIA's World Energy Projections Plus (WEPS+) model (Energy Information Administration, 2011). WEPS+ is a system of sectoral energy models which derives energy consumption projections given GDP growth and fuel price as input: the results can thus serve as an independent comparison with the RCP baselines.

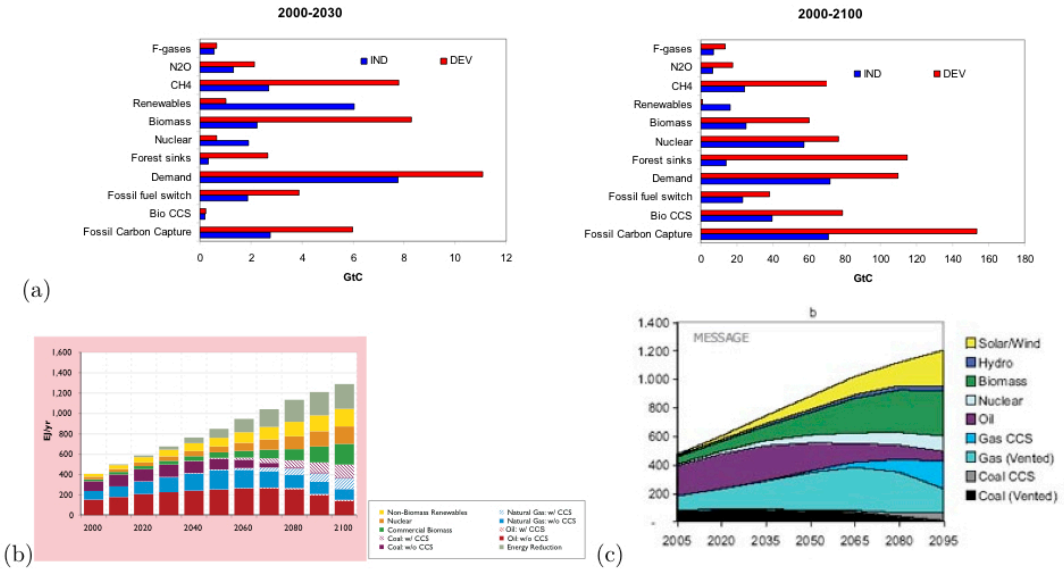

Figure 4: (a) Figure 3.7 from Weyant et al. (2009), showing the contribution to emissions reductions by fuel type for RCP2.6. (b) Figure 4.11 from Clarke et al. (2007), showing projected global energy emissions by fuel type for RCP4.5. Values shown are the differences between the RCP4.5 pathway and the GCAM 'reference' scenario. (c) Figure from the IPCC Special Report on Carbon Capture & Storage, showing energy use by fuel type for RCP8.5.

[3] http://205.254.135.24/forecasts/ieo/ieo tables.cfm

Results from the IEO projections are shown as the red diamonds in Figure 3: overall energy intensity improvements are substantial, with projected 2005-2020 reductions greater than in any of the RCPs. Much of this reduction is driven by a switch to renewables, motivated by rising world oil prices. Notably, however, the reduction in carbon intensity is minimal: the annual reduction is 0.3%/year, comparable to RCP6 and RCP8.5. Meeting the goals of the more stringent RCPs will require not only maintaining the recent (2006-2008) EI reduction rate, but also aggressive measures to decrease the CO_2 emissions associated with energy production.

3.1 Energy Policy in the RCPs

Why are the reductions in carbon and energy intensities so much higher in the RCPs than the EIA projections? The answer likely lies in a combination of factors. One consideration is energy efficiency, which is expected to play a major role in future climate mitigation efforts. In fact, van Vuuren et al. (2007) describe energy efficiency improvements in the RCP 2.6 as one of the largest sources of uncertainty in future CO_2 projections. Rates for the 21st century overall range from 0.8%/year (western Europe) to 1.8%/year (India): van Vuuren et al. (2007) speculate that the action of climate policies could increase those numbers to 1.0-2.1%/year. On the other end of the RCP spectrum, MESSAGE graphics developed by Riahi et al. (2007) for the 670 ppm CO2 RCP8.5 simulations show efficiency measures making up roughly 15-20% of total greenhouse gas reductions, depending on the choice of baseline scenario[4]. Over the 2005-2100 period, this implies an annual improvement of 0.10-0.21%/year.

---

[4] Estimates were made using Figure 11 from Riahi et al. (2007), and are intended only as rough indications of the magnitude of efficiency contributions. For the A2r baseline scenario, efficiency contributes close to 20% of energy use reductions over 2040-2100.

A full review of the energy literature is beyond the scope of this analysis. However, some impressions may be gained from Figure 4, which shows the proportion of energy sources in use in each RCP. The growth in renewable and nuclear energy use is substantial in all RCPs, as is the increase in use of carbon capture and sequestration techniques (CCS). Deployment of CCS in particular on a large scale may be problematic, as the technology is currently quite immature (Litynski et al. 2008, Hawkins et al. 2009). Rates of renewable development may also require international cooperation to maintain at sufficient levels (refs); this may potentially be achievable in practice, but certainly will require concerted effort by governments and should not be regarded as 'automatic'.

4. Conclusions

A comparison of the carbon and energy intensity reductions in the RCP baseline scenarios for 2005-2100 shows that decarbonization rates are similar to the results from the SRES, and when averaged over the entire 21st century rates are substantially higher. This implies that we may still be skewing 21st century climate projections using overly optimistic predictions of mitigation efforts; a comparison with independent projections from the International Energy Outlook shows much slower projected decreases, particularly in carbon intensity.

The projected 21st century changes to the various energy sources included in the RCPs are explored qualitatively using the available literature: improvements to the efficiency of end-user consumption is a significant effect in all projections The RCPs overall find that efficiency must

improve by up to 0.2%/year, with the net impact being a reduction of 10-20% in GHG emissions. However, achieving this result in the real world requires carefully coordinated efforts on the national and international levels to reach people in all sectors of society. Carbon and energy intensity improvements sufficient to meet RCP targets are therefore not a 'sure thing'.

References

Archer, C., and M. Jacobson, Evaluation of global wind power, Journal of Geophysical Research - Atmospheres, 110(D12), D12,110, 2005.

Arvizu, D., P. Balaya, L. Cabeza, T. Hollands, A. J¨ager-Waldau, M. Kondo, C. Konseibo, V. Meleshko, W. Stein, Y. Tamaura, H. Xu, and R. Zilles, Direct Solar Energy, in IPCC Special Report on Renewable Energy Sources and Climate Change Mitigation, Cambridge University Press, Cambridge, United Kingdom and New York, NY USA, 2011.

Athienitis, A., and M. Santamouris, Thermal Analysis and Design of Passive Solar Buildings. , 288 pp., James & James, London, UK, 2002.

AWEA, Wind Energy Assessment 2010, Australian Wind Energy Association, 2010a.

AWEA, AWEA Wind Power Value Chain: Building Links to a Cleaner Future, American Wind Energy Association, 2010b.

Bartis, J., Oil shale development in the United States: prospects and policy issues, RAND corporation, 2005a.

Bartis, J. e. a., Oil Shale Development in the United States: Prospects and Policy Issues, Report prepared for the National Energy Technology Laboratory of the U.S. Department of Energy, Washington, D.C.: RAND corporation, 2005b.

CBO, The Impact of Ethanol Use on Food Prices and Greenhouse Gas Emissions (online), US Congress, Congressional Budget Office, http://www.cbo.gov/ftpdocs/100xx/doc10057/04-08-Ethanol.pdf, 2009.

Chapman, N., and I. McKinley, The geological disposal of nuclear waste, John Wiley & Sons, Inc., New York, N.Y., 1987.

Chen, W., and R. Xu, Clean coal technology development in China, Energy Policy, 38, 2123–2130, 2010.

Christodouleas, J. P., R. D. Forrest, C. G. Ainsley, Z. Tochner, S. M. Hahn, and E. Glatstein, Short-Term and Long-Term Health Risks of Nuclear-Power-Plant Accidents, The New England Journal of Medicine, 364, 2334–2341, doi:10.1056/NEJMra1103676, 2011.

Clarke, L., J. Edmonds, H. Jacoby, H. Pitcher, J. Reilly, and R. Richels, Scenarios of greenhouse gas emissions and atmospheric concentrations, in Sub-report 2.1A of Synthesis and Assessment Product 2.1 by the U.S. Climate Change Science Program and the Subcommittee on Global Change Research, p. 154 pp., Department of Energy, Office of Biological & Environmental Research, Washington, DC., 2007.

Denholm, P., E. Drury, R. Margolis, and M. Mehos, Solar Energy: The Largest Energy Resource, Generating Electricity in a Carbon Constrained World., Elsevier, Paris, France, 2009.

DESA, U., World Population Projections to 2300, United Nations, p. 254, 2004.

EIA, Electric Power Monthly: April 2010 edition, U.S. Energy Information Administration, 2010.

Energy Information Administration, U. S., International Energy Outlook 2011, U.S. Department of Energy, available at http://www.eia.govieopdf/0484(2011).pdf., 2011.

EWEA, Oceans of Opportunity: Harnessing Europe's largest domestic energy source, European Wind Energy Association, 2009.

Fawer, M., and B. Magyar, Solar Industry Entering New Dimensions: Comparison of Technologies, Markets and Industries., 56 pp., Solar Energy 2010. Sustainable Investment Division, Bank Sarasin, Basel, Switzerland, available at www.esocialsciences.comdataarticlesDocument110122010400.3811609.pdf, 2010.

Figueroa, J., Summary of phase I capture and separation activities of the regional carbon sequestration partnerships program, Proceedings of the Fourth Annual Conference on Carbon Sequestration, Alexandria, VA (May 2-5, 2005), 2005.

Fisher, B., N. Nakicenovic, K. Alfsen, J. C. Morlot, F. de la Chesnaye, J.-C. Hourcade, K. Jiang, M. Kainuma, E. La Rovere, A. Matysek, A. Rana, K. Riahi, R. Richels, S. Rose, D. van Vuuren, and R. Warren, Issues related to mitigation in the long-term context, in Climate Change 2007: Mitigation. Contribution of Working Group III to the Fourth Assessment Report of the Inter-governmental Panel on Climate Change, edited by Metz., B. and Davidson, O.R. and Bosch, P.R. and Dave, R. and Meyer, L.A. [eds], Cambridge University Press, Cambridge, U.K., 2007.

Fujino, J., R. Nair, M. Kainuma, T. Masui, and M. Matsuoka, Multigas mitigation analysis on stabilization scenarios using AIM global model, Multigas Mitigation and Climate Policy: The Energy Journal Special Issue, pp. 343–354, 2006.

Green, C., and H. Lightfoot, Making climate stabilization easier than it will be: The report of IPCC WGIII, C2GCR Quarterly, McGill University, 1, 6–13, 2002.

Greenpeace, Concentrating Solar Power Global Outlook 09: Why Renewable Energy is Hot, Greenpeace International, Amsterdam, the Netherlands; SolarPACES, Tabernas, Spain; ESTELA, Brussels, Belgium, 2009.

GWEC, Global Wind Energy Outlook 2008, Global Wind Energy Council/Greenpeace, 2008. 14

Hawkins, D., G. Peridas, and J. Steelman, Twelve years after Sleipner: moving CCS from hype to pipe, Energy Procedia, 1, 4)40,003?0404,010, 2009.

Hendriks, C., W. Graus, and F. van Bergen, GLOBAL CARBON DIOXIDE STORAGE POTENTIAL AND COSTS, Ecofys, Utrecht, 2002.

Hibbard, K., G. Meehl, P. Cox, and P. Friedlingstein, A strategy for climate change stabilization experiments, Eos, 88(20), 217,219,221, 2007.

Hoffert, M., K. Caldeira, A. Jain, E. Haites, L. Danny Harvey, S. Potter, M. Schlesinger, S. Schneider, R. Watts, T. Wigley, and D. Wuebbles, Energy implications of future stabilization of atmospheric CO_2 content, Nature, 395, 881–884, 1998.

Hoffert, M., K. Caldeira, G. Benford, D. Criswell, C. Green, H. Herzong, A. Jain, H. Kheshgi, K. Leckner, J. Lewis, H. Lightfoot, W. Manheimer, J. Mankins, M. Mauel, J. Perkins, M. Schlesinger, T. Volk, and T. Wigley, Advanced technology paths to global climate stability: Energy for a greenhouse planet, Science, 298, 981–987, 2002.

IEA, Energy Balances of Non-OECD Countries 20042005, International Energy Agency, Paris, France, 2007.

IEA, Towards A Sustainable Energy Future, International Energy Association, 2008.

IEA, Energy Technology Perspectives 2010: Scenarios & Strategies to 2050, International Energy Agency, Paris, France, 2010.

IHS, ”Clouds Gather Over Indias Solar Power Plans (November 12, 2009), IHS Global Insight, website www.ihsglobalinsight.com (subscription site), 2009.

Intergovernmental Panel on Climate Change, Statement on Himalayan glacier melt, , www.ipcc.ch/pdf/presentations/himalaya-statement-20january2010.pdf, 2010.

Jollands, N., P. Waide, M. Ellis, T. Onoda, J. Laustsen, K. Tanaka, P. de T’Serclaes, I. Barnsley, R. Bradley, and A. Meier, The 25 IEA energy efficiency policy recommendations to the G8 Gleneagles Plan of Action, Energy Policy, 38, 6409–6418, 2010.

Klara, S., and R. Srivastava, Integrated collaborative technology development program for CO_2 separation and capture - U.S. Department of Energy R&D, Environ. Prog., 21, 247, 2002.

Klara, S., R. Srivastava, and H. McIlvried, Integrated collaborative technology development program for CO_2 sequestration in geologic formations - United States Department of Energy R&D, Energy Conversion & Management, 44, 2699–2712, 2003.

Klessmann, C., W. Graus, M. Harmelink, and F. Geurts, Making Energy- Efficiency Happen: From Potential to Reality., WWF International, Utrecht, The Netherlands., 2007.

Lightfoot, H., and C. Green, Energy intensity decline implications for stabilization of atmospheric CO_2 content, Centre for Climate and Global Change Research Report 2001-7, McGill University, October, 2001.

Litynski, J. T., S. Plasynski, H. McIlvried, C. Mahoney, and R. Srivastava, The United States Department of Energy's Regional Carbon Sequestration Partnerships Program Validation Phase, Environment international, 34, 127–138, 2008.

Lu, X., M. McElroy, and J. Kiviluoma, Global potential for wind-generated electricity, Proceedings of the National Academy of Sciences, 106(27), 10,933–10,938, 2009.

Metz, B., O. Davidson, H. de Coninck, M. Loos, and L. Meyer, Carbon Dioxide Capture and Storage, 431 pp., Cambridge University Press, UK., 2005.

Mitchell, D., A note on rising food prices, Policy Research Working Paper 4682, The World Bank, Development Prospects Group, April, 2008.

Moss, R., M. Babiker, S. Brinkman, E. Calvo, T. Carter, J. Edmonds, I. Elgizouli, S. Emori, L. Erda, K. Hibbard, R. Jones, M. Kainuma, J. Kelleher, J. Lamarque, M. Manning, B. Matthews, G. Meehl, L. Meyer, J. Mitchell, N. Nakicenovic, B. O'Neill, R. Pichs, K. Riahi, S. Rose, P. Runci, R. Stouffer, D. van Vuuren, J. Weyant, T. Wilbanks, J. van Ypersele, and M. e. a. Zurek, Further Work on Scenarios, in Report from the IPCC Expert Meeting: Towards New Scenarios for Analysis of Emissions, Climate Change, Impacts, and Response Strategies, Intergovernmental Panel on Climate Change, 2008.

Moss, R., J. Edmonds, K. Hibbard, M. Manning, S. Rose, D. van Vuuren, T. Carter, S. Emori, M. Kainuma, T. Kram, G. Meehl, J. Mitchell, N. Nakicenovic, K. Riahi, S. Smith, R. Stouffer, A. Thomson, J. Weyant, and T. Wilbanks, The next generation of scenarios for climate change research and assessment, Nature, pp. 747–756, Perspectives, 2010.

Murphy, L., and P. Edwards, Bridging the Valley of Death: Transitioning from Public to Private Sector Financing, 58 pp., NREL/MP-720-34036, 2008.

Nakicenovic, N., Freeing energy from carbon, Daedalus, 125(3), 95–112, 1996.

Nakicenovic, N. e. a., Special Report on Emissions Scenarios: A Special Report of Working Group III of the Intergovernmental Panel on Climate Change, p. 599 pp., Cambridge University Press, Cambridge, U.K., 2000.

NAS, Electricity from Renewable Sources: Status, Prospects, and Impediments, The National Academies, 2010.

Obersteiner, M., C. Azar, K. Mollersten, K. Riahi, J. Moreira, S. Nilsson, P. Read, L. Schrattenholzer, Y. Yamagata, and J. Yan, Biomass Energy, Carbon Removal and Permanent Sequestration - A 'Real Option' for Managing Climate Risk, International Institute for Applied Systems Analysis, Interim Report IF-02-042, 2002.

on Energy Efficiency, E. G., Realizing the Potential of Energy Efficiency: Targets, Policies, and Measures for G8 Countries., United Nations Foundation, Washington, DC., 2007.

Pachauri, R., and A. e. Reisinger, Contribution of Working Groups I, II and III to the Fourth Assessment Report of the Intergovernmental Panel on Climate Change, 104 pp., Intergovernmental Panel on Climate Change, Geneva, Switzerland, 2007.

Parson, E., and D. Keith, Fossil Fuels Without CO_2 Emissions: Progress, Prospects, and Policy Implications., Science, 282, 1053–1054, 1998.

Partnership, G. B., A review of the current state of bioenergy development in G8+5 Countries, Food and Agriculture Organisation, 2009.

Petroleum, B., BP Statistical Review of World Energy 2006., British Petroleum, http://www.bp.com/centres/energyS., 2006.

Pielke Jr., R., T. Wigley, and C. Green, Dangerous Assumptions, Nature, 452, commentary, 2008.

Platts, Chinese Solar Projects in New Surge, Platts Power in Asia (September 17, 2009), 536, 4, 2009.

Rao, S., and K. Riahi, The role of non-CO_2 greenhouse gases in climate change mitigation: Long-term scenarios for the 21st century, The Energy Journal, pp. 177–200, 2006.

Raupach, M. R., G. Marland, P. Clais, C. Le Quere, J. G. Canadell, G. Klepper, and C. B. Field, Global and regional drivers of accelerating CO_2 emissions, Proceedings of the National Academy of Sciences, 104 (24), 10,28810,293, 2007.

REN21, Renewables 2010 Global Status Report., 80 pp., Renewable Energy Policy Network for the 21st Century Secretariat, Paris, France, 2010.

Riahi, K., A. Grubler, and N. Nakicenovic, Scenarios of long-term socio-economic and environmental development under climate stabilization, Technological Forecasting & Social Change, 74, 887–935, 2007.

Steenblik, R., Biofuelsat what cost? Government support for ethanol and biodiesel in selected OECD coun- tries., International Institute for Sustainable Development, Winniped., 2007.

Stroeve, J., M. Holland, W. Meier, T. Scambos, and M. Serreze, Arctic sea ice decline: Faster than forecast, Geophysical Research Letters, 34(L09501), 2007.

SWERA, Solar and Wind Energy Resource Assessment, United Nations Environment Programme, http://www.swera.unep.net, 2011.

Trostle, R., Global agricultural supply and demand: factors contributing to the recent increase in food commodity prices, Outlook Report No. WRS-0801 (Washington, DC: US Department of Agriculture Economic Research Service) May, 2008.

U.S. Dept of Energy, Emissions of Greenhouse Gases in the United States 1985-1990, DOE/EIA-0573, U.S. Energy Information Administration, Washington, DC, 1993.

U.S. Dept. of Energy, Annual energy outlook 2009, report no. DOE/EIA-0383, U.S. Energy Information Administration, Washington, DC, 2010.

van Alphen, K., P. M. Noothout, M. Hekkert, and W. Turkenburg, Evaluating the development of carbon capture and storage technologies in the United States, Renewable and Sustainable Energy Reviews, 14, 971986, 2010.

Van Vuuren, D., B. Eickhout, P. Lucas, and M. den Elzen, Long-term multi-gas scenarios to stabilize radiative forcing - Exploring costs and benefits within an integrated assessment framework, The Energy Journal, pp. 201–233, 2006.

van Vuuren, D., M. den Elzen, P. Lucas, B. Eickhout, B. Strengers, B. van Ruijven, S. Wonink, and R. van Houdt, Stabilizing greenhouse gas concentrations at low levels: an assessment of reduction strategies and costs, Climatic Change, 81, 119–159, 2007.

van Vuuren, D. P., and B. C. O'Neill, The consistency of IPCC's SRES scenarios to recent literature and recent projections, Climatic Change, 75, 9–46, 2006.

WEO, World Energy Outlook 2009, International Energy Agency, 2009.

Weyant, J., C. Azar, M. Kainuma, J. Kejun, N. Nakicenovic, P. Shukla, E. La Rovere, and G. Yohe, Future IPCC Activities: New Scenarios, Intergovernmental Panel on Climate Change, Thirtieth Session: Antalya, 21-23 April 2009, 1, 1–48, 2009.

Wiser, R., Z. Yang, M. Hand, O. Hohmeyer, D. Infield, P. H. Jensen, V. Nikolaev, M. O'Malley, G. Sinden, and A. Zervos, Wind Energy, in IPCC Special Report on Renewable Energy: Sources and Climate Change Mitigation, edited by O. Edenhofer, R. Pichs-Madruga, Y.

Sokona, K. Seyboth, P. Matschoss, S. Kadner, T. Zwickel, P. Eickemeier, G. Hansen, S. Schl¨omer, and C. von Stechow, Cambridge University Press, Cambridge, United Kingdom and New York, NY USA, 2011.

Wyman, C., What is (and is not) vital to advancing cellulosic ethanol, Trends in Biotechnology, 25(4), 153–157, 2007.

Yao, T., J. Pu, A. Lu, Y. Wang, and W. Yu, Recent glacial retreat and its effect on hydrological processes on the Tibetan Plateau, China, and surrounding regions, Arctic, Antarctic, and Alpine Research, 39(4), 642–650, 2007.

Zarvos, A., Developing Wind Energy to meet the Kyoto Targets in the European Union, Wind Energy, 6, 309–319, 2003.